REPORT SERIES IN AEROSOL SCIENCE
N:o 193 (2016)

MISAPPLICATIONS AND GENERALISATIONS OF NUCLEATION THEOREMS
WITH A SPECIAL REFERENCE TO ATMOSPHERIC NEW PARTICLE FORMATION

JUSSI MALILA

Department of Applied Physics
Faculty of Science and Forestry
University of Eastern Finland

Academic dissertation
To be presented, with the permission of the Faculty of Science and Forestry of the University of Eastern Finland, for public criticism in auditorium SN201, Yliopistonranta 1, on Thursday December 8th, 2016, at 12 o'clock noon.

Kuopio 2016

Author's address Department of Applied Physics
University of Eastern Finland
P. O. Box 1627, FI-70211 Kuopio

Supervisors Professor Ari Laaksonen, Ph.D.
Department of Applied Physics
University of Eastern Finland
and
Climate Research
Finnish Meteorological Institute

Senior researcher Robert McGraw, Ph.D.
Environmental and Climate Sciences Department
Brookhaven National Laboratory

Docent Ismo Napari, Ph.D.
Department of Physics
University of Helsinki

Reviewers Senior researcher Madis Noppel, C.Sc.
Institute of Physics
University of Tartu

University lecturer Theo Kurtén, Ph.D.
Department of Chemistry
University of Helsinki

Opponent Professor David Reguera, Ph.D.
Department of Fundamental Physics
University of Barcelona

ISBN 978-952-7091-69-2 (printed version)
ISBN 978-952-7091-70-8 (pdf version)
ISSN 0784-3496
http://atm.helsinki.fi/FAAR/
Unigrafia oy
Helsinki 2016

Foreword

Here we are, finally. The process of writing this thesis has taken up a decade, and consequently there are number of people who I am indebted to for their help, guidance, or company during this period. The actual work has taken place at the Department of Applied Physics, University of Eastern Finland (which, when I began this work, was still the Department of Physics at the University of Kuopio). I thank the various heads of the department during this period, as well rest of the staff, for pleasant years in an inspiring working environment.

It was Professor Ari Laaksonen, my main supervisor, who first introduced me to nucleation theory and later provided the general topic for this thesis. Although the outcome is something different than what we were anticipating back then, I am quite happy what we have achieved here. These thanks naturally extent also to my other supervisors, Dr. Robert McGraw and Docent Ismo Napari, who both have through discussions enlightened me on the various aspects of nucleation theory and shown the ways of theoretical research in general. I am also indebted to Professor Kari Lehtinen on his various comments during the later part of this work, as well as my pre-examiners, Dr. Madis Noppel and Docent Theo Kurtén, for their very detailed reading of the thesis and resulting constructive comments—I certainly got what I was looking for with you two.

I am also grateful to all my coauthors for the work we have done together and things that we have learned. Also other members of the Aerosol Physics group at the Department of Applied Physics (and by an extension also several people at the Finnish Meteorological Institute) deserve my thanks due to all things related to work (and badminton) during these years. I have also enjoyed on discussions with various members—all too many to be listed here, but most notably Dr. Jan Hrubý—of the international nucleation community considering various aspect of vapour-to-liquid nucleation; I am very grateful to Professor David Reguera for kindly accepting the invitation to serve as an opponent in the public examination of this thesis.

In retrospect it seems that most of the time during the past ten years I have either been teaching or doing things related to study administration, so I also thank all my fellow teachers and students during these years. Especially I would like to thank Dr. Antti Lauri for our collaboration.

Last, but not least, I want to warmly thank my family and friends for their continuous encouragement during this work.

For funding of this thesis, Finnish Doctoral Programme in Atmospheric Composition and Climate Change: From Molecular Processes to Global Observations and Models (ACCC) and the Centre-of-Excellence Programme of the Academy of Finland are acknowledged.

Kuopio, Nov. 25th 2016
Jussi Malila

Misapplications and generalisations of nucleation theorems

Malila, Jussi Tapani
University of Eastern Finland, 2016

Abstract

Nucleation is the general mechanism of first-order phase transitions, for example the formation of the first liquid-like clusters in the on-set of condensation from vapour. In Earth's atmosphere, nucleation processes are assumed to cause observed new particle formation, while liquid–solid nucleation initiates the freezing of cloud droplets. As atmospheric aerosol particles affect Earth's radiative balance both via direct scattering of radiation and acting as cloud condensation nuclei, changes in the new particle formation rate can have a direct effect on climate.

Nucleation theorems are relations describing how the nucleation rate—or the nucleation work—depends on environmental conditions: supersaturation, temperature, ... The first nucleation theorem describes how the nucleation rate depends on the saturation ratio of precursor(s), and under certain assumptions this dependence results in the number of molecules in the critical cluster that forms the bottleneck for the nucleation process. Such results have been extensively used to identify the molecular-level mechanism of nucleation, when applied to both laboratory and field measurements. However, it turns out that the often implicit assumptions required for this identification break down in the real world non-ideal conditions: In this thesis, I have reviewed the existing work suggesting corrections or amendments to nucleation theorems to overcome these effects. Furthermore, I have extended the previous treatments of nucleation in the presence of cluster losses to produce an explicit form of the first nucleation theorem under such conditions. Overview of studies applying the first nucleation theorem to atmospheric measurements now suggests that in general it is not possible to apply nucleation theorems to infer the mechanism of atmospheric new particle formation.

In a more general level, the science philosophical implications of nucleation theorems are profound, as nucleation theorems seem to provide a direct molecular insight based on macroscopic observations. Taking into account the overlooked assumptions needed for the application of nucleation theorems provide a less positivistic interpretation.

PACS: 64.60.Q-, 82.60.Nh, 92.60.Mt

MSC: 80A99, 82B26, 30B70

Keywords: nucleation, nucleation theorem, new particle formation

So then physicists will replace the models with newer mathematical models because mathematical terms can be stretch to fit any data. And then physicists will end up saying that "because we can't observe it, we can't measure it. So the position might be this and the energy is probably that."

– attributed to Ernst Mach by anonymous[1]

[1]This quote can be found from the internet, though its origins are questionable. Although most likely not Mach, the author of this statement has certainly taken some stylistic influences from his work, [e.g. E. Mach. Die Leitgedanken meiner naturwissenschaftlichen Erkenntnislehre und ihre Aufnahme durch die Zeitgenossen. *Scientia* 7 (1910), 225–240]. And though the obvious reference is made to quantum mechanics, it is at least an equally apt notion when concerning nucleation (theorems).

Nomenclature

Functions, variables and operators	
A	surface area
	surface area density (Chap. 5)
A, B	non-linear fitting parameters for (D, t) (Chap. 4)
	canonical nominator and denominator (Appendix)
a, b	linear fitting parameters for (D, t) (Chap. 4)
	continued fraction elements (Chap. 5, Appendix)
a	mass accommodation coefficient
α	evaporation rate coefficient
B	second virial coefficient (Chap. 3)
	disk in $\mathbb{C}^2$ (Appendix)
$\mathbf{B}$	rate coefficient matrix
β	condensation/coagulation rate coefficient
C	constant of integration
CoagS	coagulation sink
CS	condensation sink
$\hat{\mathbb{C}}$	Riemann sphere
c	normalised loss rate coefficient (Chap. 5)
	(molecular) specific heat
D	diffusion coefficient
	displacement barrier height (Chap. 4)
Δ	(generalised) difference
δ	Kronecker delta function
E	(activation) energy
ϵ	remainder in the first nucleation theorem ($\sum_i \epsilon_i = 1$)
Φ	grand potential
f	actual concentration, an arbitrary function
ϕ	potential energy
G	Gibbs free energy, a large integer
	domain in $\hat{\mathbb{C}}^2$ (Appendix)
g	number of molecules
	a $\mathbb{C}^2 \to \mathbb{C}^2$ function (Appendix)
γ	surface tension
H	enthalpy
h	molecular enthalpy
η	entropy
I, J	sets of integers smaller than some N (Appendix)
J	net formation rate, nucleation rate

Functions, variables and operators (cont.)	
$\mathbf{J}$	net formation rate vector
K	kinetic prefactor, equilibrium constant
k	number of molecules (Chap. 6)
	reaction-rate coefficient
L	loss rate, dimensionless loss parameter
λ	ratio of heat carried by vapour and carrier gas molecules
M	number of molecular species
m	mass
μ	chemical potential
	dipole moment (Chap. 4)
$\mu_{\mathcal{N}}$	"chemical potential" of replicas
N	number of molecules (Chaps. 2 and 3)
	number of data points (Chap. 4)
	aerosol number concentration (Chap. 6)
N, ℓ, n	integers ($N \geq \ell \geq n$; Appendix)
$\mathcal{N}$	number of replicas
n	constrained equilibrium concentration
	amount of molecules
P	nucleation exponent (Chaps. 1, 3, and 6)
	total pressure (Chap. 3)
	probability (Chap. 3)
	normalised $1/p_g$ distribution (Chap. 5)
	induction step (Appendix)
$\mathbf{p}$	forward rate coefficient matrix
p	pressure
	normalised forward rate coefficient (Chap. 5)
Q	cumulative of P (Chap. 5)
	excess latent heat (Chap. 3)
	canonical partition function (Chap. 3)
q	loss rate coefficient
R	radius
r	position vector
ρ	density
S	saturation ratio
σ	scattering cross section
	Lennard-Jones size parameter
T	temperature
t	time
	reduced temperature (Chap. 4)
U	internal energy

Functions, variables and operators (cont.)	
$\mathbf{U}$	normalised concentration vector
u	normalised concentration
V	volume
v	molecular volume
W	work of formation
X	Hill free energy ($= -k_\mathrm{B}T \ln \Upsilon$)
Ξ	grand canonical partition function
Υ	great grand canonical partition function
y	(gas phase) mole fraction
Z	Zel'dovich factor
z, ζ	complex number
Ψ, Ω	open domain in $\hat{\mathbb{C}}$ (Appendix)
Ω	surface entropy parameter (Chap. 4)
ω	acentric factor
$\mathbf{1}$	unit vector
$\langle \cdot \rangle$	ensemble average

Super- and subscripts	
$*$	at (thermodynamic) critical size
$-$	at kinetic critical size
	complex conjugate (Appendix)
$\wedge$	at ostensible critical size (Chap. 5)
	normalised (Chap. 3)
$\sim$	at apparent critical size
	extended (for $\mathbf{U}$)
$1, 2, \ldots$	number of molecules
	projection to a given coordinate (Appendix)
app	apparent
B	Boyle (temperature)
CNT	classical nucleation theory
c	critical (temperature)
d	droplet
	diameter of the cluster as in $J_{1.5}$, which denotes the formation rate of 1.5 nm clusters
E	equimolecular dividing surface
e	equilibrium (vapour pressure)
G	Szilárd limit
g	(inert) carrier gas
g, k	size of the cluster
ICT	internally consistent theory

Super- and subscripts (cont.)	
i, m	type of the molecule
id	ideal
NPF	new particle formation
p	pore
S	scavenged (Chap. 5)
	surface of tension (Chap. 2)
SC	simple correction
sm	statistical mechanic
t	total
td	thermodynamic
v	vapour
$\rightarrow$	extend of composition
0	initial
∞	limiting value (Appendix)
	plane surface
$+$	forward
$-$	backward
Constant	
k_B	Boltzmann constant

Contents

1 Introduction **1**

1.1 A short history of nucleation studies with emphasis on atmospheric science 4

1.1.1 First scientific ideas 5

1.1.2 From natural philosophy to experimental science . . 7

1.1.3 From laboratory to outdoors 9

1.1.4 Formation of the classical nucleation theory 9

1.1.5 Ignorance was amiss 12

1.2 Nucleation theorem and NPF 13

2 Nucleation phenomena **35**

2.1 Classical nucleation theory 35

2.1.1 Thermodynamics of a phase transition 36

2.1.2 Nucleation kinetics 42

2.2 Computational models for nucleation 46

2.3 Nucleation experiments 50

3 Nucleation theorems **59**

3.1 Background 59

3.2 First nucleation theorem 63

3.2.1 Scaling of nucleation rates based on the first nucleation theorem and the Kelvin equation 63

3.3 Second nucleation theorem 65

3.4 Other nucleation theorems 66

3.5 Corrections and amendments of nucleation theorems 67

3.5.1 Nonequilibrium corrections 67

3.5.2 Compressibility and nonideality corrections 69

3.6 Critique of nucleation theorems . . . 73
3.A Appendix . . . 76
3.A.1 Derivation of the first nucleation theorem using statistical mechanics . . . 76
3.A.2 On slope analysis . . . 78

4 Displacement barrier heights from the experimental nucleation rate data 89
4.1 Motivation . . . 90
4.2 Theory . . . 90
4.2.1 Classical nucleation theory . . . 90
4.2.2 Displacement barrier height . . . 91
4.3 Data analysis . . . 93
4.3.1 Thermodynamic properties . . . 93
4.3.2 Experimental nucleation rate data . . . 94
4.3.3 Pressure effects . . . 96
4.4 Results . . . 98
4.4.1 Comparison of different measurement devices . . . 98
4.4.2 Waters and n-alkanols . . . 100
4.4.3 n-Alkanes . . . 103
4.4.4 Correlation of the coefficients a and b with molecular properties . . . 105
4.5 Discussion . . . 106
4.5.1 On the universality of $D(T)$ . . . 106
4.5.2 Comparison with other measurements and scaled and phenomenological models . . . 107
4.6 Conclusions . . . 109
4.A Addendum: $D(T)$-scaling for metals . . . 109

5 Losses of sub-critical clusters and the first nucleation theorem 123
5.1 Introduction . . . 124
5.2 Theory . . . 124
5.3 Results and discussion . . . 129
5.4 Concluding remarks . . . 133
5.A Appendix . . . 134
5.A.1 Calculation of J_g and $\partial \ln J_g / \partial \ln n_1$ . . . 134
5.A.2 On the kinetic critical size $\hat{g}$ . . . 140
5.A.3 Flux weighting and sum rules for loss rates . . . 141

5.A.4 Model system 142
5.B Addendum: Comparison with results from Ref. [21] 144

6 Critical cluster size cannot in practice be determined by slope analysis in atmospherically relevant applications 153
6.1 Introduction 154
6.2 The first nucleation theorem 157
6.3 Methods 164
6.3.1 ACDC 164
6.3.2 UHMA 166
6.4 Case studies 167
6.4.1 The critical cluster size depends on conditions (assumptions A, D and H) 168
6.4.2 Cluster-cluster collisions (assumptions A and B) . . . 169
6.4.3 External losses (assumption C) 171
6.4.4 Definition of the precursor concentration (assumptions E and H) 175
6.4.5 Presence of ions (assumptions B, D and G) 177
6.4.6 Experiments where concentrations are not constant (assumption F) 178
6.4.7 Practical problems related to analyzing field observations of particle formation events (assumptions E, G and H) 180
6.5 Summary and conclusions 183
6.A Appendix 186
6.A.1 Validity of the multicomponent nucleation theorem Eq. (6.9) 186
6.A.2 Cluster concentrations in the sulphuric acid–DMA system 186
6.A.3 Ion concentrations when the ion production rate is fixed 188

7 Discussion and reflections 197
7.1 How to interpret the first nucleation theorem? 198
7.2 Kelvin equation and the first nucleation theorem 202
7.3 Implications and perspectives 203
7.A Translation–rotation correction 205

Appendix: On continued fractions **215**
A.1 Continued fractions 215
A.2 Applications to nucleation studies 217
A.3 Derivative of a continued fraction 218
A.3.1 Introduction 218
A.3.2 Preliminaries and the main result 219
A.3.3 Partial derivatives with respect to a_ℓ and b_ℓ 222
A.3.4 Concluding remarks 225

Original publications

The main results of this thesis have been published in following original publications:

I J. Malila, A.-P. Hyvärinen, Y. Viisanen and A. Laaksonen. Displacement barrier heights from experimental nucleation rate data. *Atmospheric Research* 90 (2008), 303–312,

II O. Kupiainen-Määttä, T. Olenius, H. Korhonen, J. Malila, M. Dal Maso, K. E. J. Lehtinen and H. Vehkamäki. Critical cluster size cannot in practice be determined by slope analysis in atmospherically relevant applications. *Journal of Aerosol Science* 77 (2014), 127–144,

III J. Malila, R. McGraw, A. Laaksonen and K. E. J. Lehtinen. Communication: Kinetics of scavenging of small, nucleating clusters: First nucleation theorem and sum rules. *Journal of Chemical Physics* 142 (2015), 011102, and

IV J. Malila. The derivative of a finite continued fraction. *Applied Mathematics E-Notes* 14 (2014), 13–19.

Of these publications, I, II and III have been included into this thesis as Chapters 4, 6 and 5, respectively, and the publication IV has been included as a part of the Appendix.[2] Besides these, this thesis contains also previ-

[2]Minor changes have been made to ensure uniformity in presentation and as a response to comments made by reviewers. Notes that were already part of published versions have been included as endnotes, while footnotes are reserved for commentary and chapter specific acknowledgments. Copyrights of the previously published versions of articles are owned by Elsevier B.V. (articles I and II), American Institute of Physics (article III), and Applied Mathematics E-Notes (article IV), and articles are reproduced here with an implicit permission from the publisher(s).

ously unpublished results.

In publication I, I did the data collection together with Dr. Hyvärinen, analysed the data and wrote the manuscript with inputs from other authors. In publication II, my contributions were mainly in the literature survey[3] and in the interpretation of computational results and commenting the various versions of the manuscript. Publication III was instigated by Profs. Laaksonen and Lehtinen, while most of the theoretical work was done with Dr. McGraw while I visited the Brookhaven National Laboratory 2013; I also wrote the manuscript together with Dr. McGraw with comments from other authors. I am the sole responsible for publication IV.

The progress in research is rarely, if ever, straightforward, and while working this thesis it feels that for each step forward I must have taken a corresponding amount of leaps backwards, or at least sideways. Some of the explored tracks have been documented in the following conference papers that are not included into this thesis (with the exception of some results from publication V), in some cases because during further work the results have been found dubious or even straightforwardly erroneous.

V J. Malila, A.-P. Hyvärinen, Y. Viisanen and A. Laaksonen. Displacement barrier heights from experimental nucleation rate data: Scaling and universality. In: *Nucleation and Atmospheric Aerosols: 17th International Conference*. Ed. by C. D. O'Dowd and P. E. Wagner. Dordrecht: Springer, 2007, 139–143,

VI J. Malila and A. Laaksonen. Properties of supercooled water clusters from nucleation rate data with the effect of non-ideal vapour phase. In: *Water, Steam and Aqueous Solutions*. Ed. by R. Span and I. Weber. Düsseldorf: VDI/GET, 2008,

VII J. Malila, A. Laaksonen and I. Napari. Densities of critical clusters from nucleation experiments. In: *Nucleation and Atmospheric Aerosols*. Ed. by J. Smolík and C. D. O'Dowd. Prague: Institute of Chemical Process Fundamentals ASCR, v.v.i. and Czech Aerosol Society, 2009, 619–622, and

[3]This article grows from multiple roots, including publication IX as well as the talk "Application of nucleation theorems to atmospheric new particle formation" that I gave back in 2010 at the Workshop of Atmospheric Nucleation in Hyytiälä.

VIII J. Malila, R. McGraw, A. Laaksonen and K. E. J. Lehtinen. Repairing the first nucleation theorem: Precritical cluster losses. *AIP Conference Proceedings* 1527 (2013), 31–34.[4]

Furthermore, some immature conclusions on the effect of losses on the first nucleation theorem when applied to atmospheric new particle formation were also presented at

IX H. Korhonen, J. Malila, H. Vehkamäki, V.-M. Kerminen and K. E. J. Lehtinen. Log-log slope analyses of simulated particle formation events at different conditions. *AIP Conference Proceedings* 1527 (2013), 234–237.

[4]See also J. Malila, K. Lehtinen, I. Napari, R. McGraw and A. Laaksonen. Coagulation scavenging of precritical clusters and the first nucleation theorem. In: *European Aerosol Conference 2011*. Manchester, abstract 4P59.

1 Introduction

> Nunc id vides, nunc ne vides.
>
> – motto of the Unseen University

This thesis is about nucleation theorems. Especially, this work concentrates on the applicability of nucleation theorems into non-ideal (in wide sense) cases of nucleation of liquid droplets—or solid particles, the difference is anyhow often ambiguous for the smallest clusters—from vapour.[1] Such nucleation processes are encountered in various systems, including, for example, formation of new aerosol particles in planetary atmospheres [12, 13] and nanomaterial production [14, 15]. To discuss nucleation theorems, one needs first to define *nucleation*, which is the process of first-order phase transformations, where a metastable state relaxes by lowering its chemical potential in a process, where the first derivatives of the suitable free energy become discontinuous and can be used as order parameters

[1] This choice of model system is dictated by the tradition of nucleation studies and—to a greater extent—by the background research on atmospheric aerosols and atmospheric new particle formation. Would this thesis be written in different circumstances, the results and general conclusions could have retained similar form, but the applications would have been different: Examples of other important nucleation processes include liquid–vapour nucleation or cavitation, relevant for biological systems [1, 2], brewing of beer [3], and vulcanology [4]; extensions of nucleation theorems into cavitation problems have been discussed in Refs. [5] and [6]. Liquid–solid nucleation or crystallisation is perhaps the oldest known example of a phase transition, with first quantitative studies dating back to Fahrenheit [7]; again, nucleation theorems have found wide use in studies of crystallisation [e.g. 8, 9]—the original application of the first nucleation theorem [10]. Besides crystallisation, some proteins can also undergo phase transitions between different conformers that gives, for example, a molecular basis of several diseases, and nucleation theorems have also been applied for such systems with a variable success, one interesting example being an application to the onset of sickle-cell disease [11].

for this process. This process, however, requires a creation of an interface between old, metastable and new, stable (at least less metastable than the old one) phases, which comes with an energetic cost, rendering the process to proceed at finite rate. In our special case, molecules in supersaturated vapour can minimize the free energy of the system forming a liquid phase. To achieve this, random fluctuations in vapour are required to form a large enough aggregate, a critical cluster, that the energetic cost for the creation of an interface can be compensated by the decrease of free energy due to condensation. This stochastic process is known as (*homogeneous*) nucleation, and its finite rate explains the relative ubiquity of metastable states in our environment. However, in the vicinity of gradients of external fields, such as the dispersion forces accompanying a solid surface or the gradient of the electric potential of an ion, the energetic cost related to the creation of the interface can be alleviated by decrease of the potential energy of molecules in this field, resulting in an enhanced probability for nucleation. This *heterogeneous* (or ion-induced) *nucleation* explains, why supersaturation with respect to liquid water seldom exceeds few percent in the atmosphere.

Although the air in which we live is usually said to consist of main gasses—nitrogen and oxygen—together with various trace gasses, such as water vapour, argon, carbon dioxide, etc., it is actually an *aerosol*. That is, there are myriad particles, both liquid and solid, embedded in the air that we breath. The size range of these particles varies from clusters of few molecules to dust grains visible with naked eye, spanning more than six orders of magnitude in radius. These particles can originate from primary sources, i.e. they are emitted directly to the air, or form in the air due to chemical reactions creating low-volatility vapours. Aerosol particles have a huge influence on life on Earth: First and foremost, they provide surface for the condensation of atmospheric moisture, facilitating cloud formation and the whole hydrological cycle;[2] some aerosol particles can also initiate ice nucleation in supercooled cloud droplets [16]. Aerosol particles are also vital for aerobiology and biogeochemical cycling [17]. On the other hand, exposure to atmospheric aerosol particles can deteriorate plant and animal health [18, 19], and is estimated to contribute over three million premature human deaths annually [20]. A significant, but relatively small portion of

[2]Traditionally, cloud droplets, ice crystals and other hydrometeors are not counted into atmospheric aerosol particles.

atmospheric aerosol particles that can act as cloud condensation nuclei are formed in the atmosphere [21]: This *new particle formation* (NPF) is assumed to be due to homogeneous and/or ion-induced heteromolecular condensation of various vapours [22]. According to the current knowledge, highly hygroscopic sulphuric acid is the most important vapour initiating NPF in Earth's (and also in Venerian) atmosphere [12]. In the planetary boundary layer, ammonia and organic bases, mainly amines, are known to strongly enchance this process [23]. Also highly oxidised, mainly biogenic but also anthropogenic organic compounds [24, 25] are potential precursors for freshly formed particles. In coastal areas and over oceans, methanesulphonic acid and iodine oxides, formed via gas-phase oxidation of organic sulphur and iodine compounds emitted by algae, respectively, are known to produce new particles [26].[3] Once formed, particles continue to grow via condensation of predominantly organic vapours and coagulation with other particles. As changes in the amount of particles large enough to act as cloud condensation nuclei has a strong influence on radiative forcing, together with direct scattering of radiation by such particles [32], changes in the processes affecting the formation and growth of new particles in the atmosphere induce several feedbacks in the climate system [33].[4]

The first steps towards quantitative description of the nucleation problem were taken by thermodynamic works of William Thomson (Lord Kelvin) [35] and J. W. Gibbs (Jr.) [36] (see sections 1.1 and 2.1.1 for further discussion), whose treatment extended the macroscopic notion of a droplet to describe what later become known as a critical cluster—an unstable nanosize object corresponding to the bottleneck of nucleation process. This image has since underpinned our view of nucleation phenomena, and notably the interpretation of nucleation theorems that, to put it short, are relations giving the extensive properties attributed to a such droplet in terms of measurable quantities. However, such a positivistic approach is likely to

[3] A distinct process—homogeneous nucleation of pure water vapour—has been suggested as the source of new particles in the Earth's mesosphere [27] (first proposed in Ref. [28]). As the occurrence of noctilucent clouds is largely dictated by the amount of particles and water vapour in the upper mesosphere—where the dominant source of H_2O is the oxidation of upwelled methane, such process would be a climate canary [29]. For NPF at the planetary boundary layer, also some more exotic compounds have been proposed to initiate the process [30, 31].

[4] Also in case of other planets, for example Jupiter [34], atmospheric NPF has been proposed to significantly influence the planetary radiative balance.

fall short when the critical cluster consists only of few molecules: First, as we are discussing tiny, tiny clusters [37], we need to take into account that cluster properties differ from those of bulk matter, most obviously due to larger surface-to-volume ratio leading to enhanced reactivity and blurring the distinction between intensive and extensive properties. Further deviations from macroscopic behaviour arise because such clusters are inherently smaller than the mean free path of the surrounding gas, have a discrete structure consisting of a finite number of molecules, and, last but maybe not least, due to quantum effects.[5] Secondly, critical clusters are seldom surrounded by isothermal and isobaric perfect gas, instead, citing Smirnov [40], we need to consider processes involving clusters and small particles in a buffer gas, where temperature and concentration gradients may take place and which may not be ideal. Despite these limitations, nucleation theorems, especially the so-called first nucleation theorem—relating the size of the critical cluster g^*, expressed in terms of number of molecules, to the relative sensitivity of the observed nucleation rate J on saturation ratio—have been shown to reproduce the predictions of classical thermodynamics for certain systems, e.g. water [41, 42]. In this thesis, the following questions have been attributed: i) To what extent can we rely on nucleation theorems? ii) What effects do various nonideal factors listed above have on nucleation theorems? iii) Can we derive generalised forms of nucleation theorems that account for these factors? and iv) Can we apply nucleation theorems to atmospheric NPF?

1.1 A short history of nucleation studies with emphasis on atmospheric science

Humankind has been aware of aerosols throughout its existence via common phenomena like dust and smoke. The properties of atmospheric fine particles also captured the scientific interest already at the classical era,

[5] In this context, it is good to remind that the wave–particle duality has been experimental verified to objects such as buckminsterfullerene (C_{60}) [38] and organic molecules with masses larger than 10000 amu [39], well in or above the size range critical clusters. Although constant interactions of a critical cluster with the mother phase lead to a rapid decoherence...

as vividly demonstrated by Lucretius' *De rerum natura* (ca. 58 BCE) that summed up the Epicurean physics and was found again in high medieval times.[6] It is therefore not surprising that over one and half millennia later, the existence and effects of atmospheric aerosols were largely recognised. For example, the effect of atmospheric aerosol particles[7] on the resolving power of telescopes was well known and discussed by Auzout [43] in a letter to Charles Abbe in 1666, i.e. only 56 years after the publication of Galileo's *Sidereus nuncius*! However, sources of these particles and their formation mechanisms remained unclear, excluding the obvious counter-examples such as coarse dust.

1.1.1 First scientific ideas

In the wake of the Lisbon 1755 earthquake, Immanuel Kant wrote a series of essays describing his theory of earthquakes. According to him, exothermic underground reactions of sulphates and water (forming sulphuric acid) and iron minerals were the driving force behind tectonic and volcanic action. Although this line of reasoning failed, in two essays he also made a connection between the formation of haze and release of inorganic acid vapours from the ground: In the first essay [44], he pointed out that the speculated reactions could lead to emanations of sulphuric and nitric acids, and correctly pointed the enhancing effect that the hygroscopicity of these substances could have to the formation and growth of haze particles.[8] In the second essay [47], he made a connection between a haze event observed in Locarno on October 14—two weeks before the Lisbon earthquake—and the assumed emissions of sulphuric acid fumes.[9] This made Kant the first

[6] Full-text is publicly available e.g. at `http://www.thelatinlibrary.com/lucretius.html`.

[7] "[L]es vapeurs, la poussiere & les autres petits corps dont l'air est tous jours [sic.] plein..."

[8] It should be noted that Kant was not the first to suggest connection between earthquakes and meteorological phenomena: Aristotle, citing Democritus, linked earthquakes with the evaporation of (water) vapour from soil and commented that haze is created in such a process. Both Aristotle and Pliny the Elder (Part 9 of Book 2 and Chap. 84 of Book 2 in eprints [45] and [46], respectively) also wrote on peculiar clouds preceding earthquakes. It is likely that Kant was influenced by these writings.

[9] Husar [48] has proposed that what Kant actually reported was a Saharan dust episode.

to propose the connection between sulphuric acid and atmospheric NPF. It should be noted, though, that Kant later started to doubt his own theory of earthquakes as there might not be enough sulphur available in the Earth's crust to explain the amount of released energy [49, §51].[10]

Followed by the eruption of Laki starting June 8, 1783, widespread and persistent fog covered most of the Europe [51]. This led to a number of published observations together with theoretical speculations [for examples, see 48].[11] Although some observers noted sulphurous smell in connection to the fog [52], anachronistically the most interesting theory was presented by Marcorelle [53], who concluded that condensing fermentation products of fumes from plants and soil, together with salt-like and "bituminous" compounds were a major source of haze droplets, and that evaporation of such droplet would leave a small, solid particle. Considering the lack of relevant measurements, these thoughts are not far from the current understanding of the role of secondary organic compounds in the formation and growth of new particles [cf. 54, 55].

Neither Kant, Marcorelle, nor their contemporaries made any clear distinction between primary and secondary particles. Indeed, even the concept of vapour was still vague until mid-19th century, when the kinetic theory of heat finally superseded the caloric one. However, Patrin [56] and Rafinesque [57] clearly stated that some part of atmospheric dust is formed from chemical reaction products of gasses. In a subsequent publication [58], Rafinesque made a statement that already sounds quite modern:[12]

> The insight given us by modern chemistry into the gaseous formations of solid substances, will be amply sufficient to account for this spontaneous formation. We know that. . . sulphur, muriate of ammoniae, &c. can be formed by sublimation of gases. . . &c. may be spontaneously combined by a casual meeting or mixture of gaseous emanations. It is not therefore diffi-

[10] However, a particle formation method, similar to the one originally described by Kant, has been recently observed in nature [50].

[11] It should be noted that there are some inaccuracies in the references in [48], probably due to their secondary nature.

[12] One should note, though, that the first—and only—issue of the journal where this article was published, edited (and to a large extent authored) by Rafinesque himself, was censored immediately after printing due to rather obscure reasons and did not see public release until 1949.

> cult to conceive how dusty particles may be formed in the great chemical laboratory of our atmosphere.

Besides the role of chemical transformation on the dynamics of atmospheric aerosols, Rafinesque [57] also clearly expressed the importance of the processes of wet and dry deposition on the evolution of the atmospheric aerosol population.

1.1.2 From natural philosophy to experimental science

Almost all of the work done on atmospheric aerosols until early 20th century could be classified as natural philosophy, as it was based on conclusions drawn from mostly unsystematic observations. First systematic studies on the formation and growth of aerosol particles were undertaken by John Tyndall. In 1868 he reported results from a series of experiments [59], where vapours of volatile liquids were exposed to light in a glass tube, forming clouds inside. Varying carrier gas from purified air to oxygen and hydrogen, he further showed that the observed reactions were due to photolytic decomposition of vapour molecules, not by oxidation. Yet, the selection of substances he used has some intriguing implications when considering current knowledge of atmospheric new particle formation: nitrite of amyl, allyl and isopropyl iodides, and hydrobromic, -chloric and -iodic acids. In a subsequent paper [60], results of further experiments with various mixtures of organic compounds and CS_2 with nitric acid were reported. Tyndall noted that minute impurities had a strong effect on particle formation, and without thorough cleaning, trace amounts of vapours emanating from glassware and metallic parts of the experimental setup were enough to produce a visible cloud of particles in otherwise pure air (as Tyndall passed filtered air through potassium hydroxide and sulphuric acid, in this order, to dry it, a small amount of sulphuric acid must have also been present). One can say that these experiments mark the beginning of both photochemistry and aerosol research as scientific disciplines. Tyndall in fact gave the first proper definition of an aerosol [61, footnote on p. 27]:

> As regards size, there is probably no sharp line between molecules and particles; the one gradually shades into the other. But the distinction that I draw is this: the atom or the molecule,

> if free, is always part of a gas, the particle is never so. A particle is a bit of liquid or solid matter, formed by the aggregation of atoms or molecules.

This statement also implies the existence of a barrier—kinetic or thermodynamic—for new particle formation. Although Tyndall was not using the term *(chemical) potential* here, he apparently[13] had been on Gibbs' mailing list and consequently was aware of his work on phase equilibrium.

Following the demonstration of Coulier [63] that there is something in unfiltered air allowing water to condense at moderate supersaturations, in contrary to filtered air, other researchers became interested on the condensation of water vapour, using adiabatic expansion and cooling as the method to achieve supersaturation. Aitken [64] and Kiessling [65] developed expansion chambers while Robert von Helmholtz [66] performed the first studies with nozzles: All of them observed that when sulphuric acid was added to the gas, condensation was strongly enhanced. Aitken and von Helmholtz, however, reached opposite conclusions on the relative strengths of sulphuric and hydrochloric acids enhancement: Aitken found hydrochloric acid being the less effective, while von Helmholtz listed the relative effect of various acidic compounds as HCl > H_2SO_4 > SO_2 > HNO_3 > CO_2. All three authors considered the formation of ammonium chloride as a reason for the observed effects with HCl, but only Aitken paid special attention on the reaction of sulphuric acid and ammonia in air. He further noted that these reactions can actually result in condensation without external nucleus, i.e. via homogeneous nucleation. The possibility of homogeneous nucleation of water vapour was proposed soon after by Carl Barus [67] on the basis of his own work with condensation of steam.

The role of ions on condensation was first demonstrated by von Helmholtz [68]. At the end of the 19th century, the nature of electric charge was a hot topic in science, and consequently the ion-induced nucleation soon become the dominating topic of nucleation studies [69], not least by the work done at the Cavendish laboratory [70, Chap. 7 and references therein]. The apex of this work was the cloud chamber, developed by C. T. R. Wilson [71], who not only quantified the effect of ions on the critical supersaturation to form droplets, but also demonstrated the chemistry-mediated effect of UV-

[13] This is documented by a marking on his copy of Ref. [62], which is available at `https://archive.org/details/Onequilibriumhe00Gibb`.

radiation on new particle formation and also performed the first controlled experiments on the homogeneous nucleation of water vapour, confirming the conclusions of Barus.

1.1.3 From laboratory to outdoors

The first atmospheric observations of new particle formation by Aitken [72] were soon followed by the first continuous measurements due to Barus, who, using a fog chamber of his own design, reported time series from both urban [73, 74] and remote [75] environments. These measurements together with meteorological observations led Barus to notice the inverse correlation between new particle formation rate and relative humidity [cf. 76]. Based on his lab experiments and field studies, he was also opposing the current view at the beginning of century that ion-induced nucleation could explain atmospheric NPF, and instead considered sulphuric acid as an extremely potential nucleator in air [74].

In 1912, Aitken [77] proposed that atmospheric NPF essentially follows from photolytic reactions (referring to Tyndall's work here), leading to gas-phase oxidation of SO_2 to H_2SO_4, which then together with ammonia and water vapour forms new particles. Further proof on the role of sulphuric acid was provided by Hogg [78], who noticed that the intermediate air ions in Kew Observatory, London were composed of what seemed to be aggregates of sulphuric acid droplets with a diameter of 3.6 nm.

1.1.4 Formation of the classical nucleation theory

The origin of the theoretical description of nucleation can be traced back to the seminal work on capillarity by Young [79] and Laplace [80, Suppl. to book X]. Building on their work, Thomson [35] derived his famous equation, showing that due to the action of surface tension, a tiny droplet can only be stable in supersaturated vapour, quantifying the relationship between droplet size and saturation ratio, in modern notation [cf. 66]

$$\ln S = \frac{2\gamma_\infty v_l}{k_\mathrm{B} T R}, \tag{1.1}$$

where S is the saturation ratio, i.e. ratio of the actual partial pressure of vapour p_v to the equilibrium vapour pressure p_e at the same temperature, R the radius of the droplet coexisting with vapour with surface tension (of plane surface) γ_∞ and molecular volume v_l, and k_B and T have their usual meanings of the Boltzmann constant and temperature.

Clarification of the concepts of reaction rate and the law of mass action by Guldberg and Waage [81, 82] were also important steps towards a quantitative understanding of nucleation phenomena, though those did not contribute directly to the actual development of the description that is known as the classical nucleation theory (CNT). CNT was initiated by Volmer and Weber [83], who were the first to give an expression for the nucleation rate, combining the thermodynamic expression of Gibbs [36] for the work of formation of the critical cluster with the Smoluchowski–Einstein [84, 85] relation for the probability of a critical fluctuation, originally devised to describe the second-order phase transformation leading to critical opalescence.[14] Soon after, Farkas [88] sketched the first kinetic treatment of homogeneous nucleation: Following the suggestion of Szilárd, he treated the formation of a g-mer as a chain of reactions involving addition or evaporation of a monomer from a cluster. This description has since dominated our understanding of nucleation phenomena. Farkas, however, was not able to give completely closed form expression for the nucleation rate J, which was obtained by Becker and Döring in 1935 [89], who gave both the discrete treatment and an approximating continuum form, where the number of molecules in the cluster g is treated as a continuous variable, obtaining an expression that was essentially of same form than that of Volmer and Weber,

$$J = Kn_{g^*} = Kn_1 \exp(-W^*/k_\mathrm{B}T). \tag{1.2}$$

Here K is the kinetic prefactor, describing the net rate of attachment of a monomer (concentration n_1[15]) into a critical cluster with (constrained) equilibrium concentration n_{g^*}, i.e. concentration following the Boltzmann statistics with energy $\Delta W(g)$, and the reversible work of formation W^*.

[14] Much of the early development in nucleation studies focused on crystallisation, and is not discussed here. For a more detailed exposition, reader is referred to reviews [86, 87] and references therein.

[15] If one assumes ideal gas behaviour, as it is (too) often done, this translates into $Sp_e/k_\mathrm{B}T$, where p_e is the equilibrium vapour pressure of the condensing liquid.

Approximations used by Becker and Döring to obtain the continuum approximation were refined by Frenkel [90], Zel'dovich [91] and Goodrich [92].[16] The continuum theory was then extended to describe the thermodynamic part of the problem already by Volmer on his monograph [96], while the kinetic part of the binary case by studied in detail b Reiss [97] and Stauffer [98], with a further extension to multicomponent systems by Hirschfelder [99] and Trinkaus [100]. Theory of ion-induced nucleation was refined by Tohmfor and Volmer [101] and Rusanov and Kuni [102], and extended to multicomponent systems by Noppel et al. [103].[17] From the kinetic viewpoint, the important $1/S$-correction to expression (1.2)—i.e. division of the right-hand-side of Eq. (1.2) by $S \propto n_1$—was first proposed by Courtney [113]: this correction is needed to make the nucleation rate satisfy the law of mass action, and has been since deduced also via different arguments [e.g. 114–116], and it emerges naturally from thermodynamically more consistent treatment of the Becker–Döring kinetics that was proposed by Katz and coauthors [e.g. 117]—and extended for multicomponent systems by Flagan [118]—placing CNT into firmer theoretical

[16] A more fundamental approach based on field-theoretic description was put forth by Langer [93, 94]; however, it has been shown that both Langer's approach and CNT result in a practically equivalent formulation for J [95].

[17] With the exception of some results in Chap. 6, multicomponent or ion-induced nucleation are not discussed in this thesis. The reason is not that multicomponent or ion-induced pathways would be negligible for the atmospheric new particle formation, vice versa. However, in most cases that have been studied so far, one can treat multicomponent nucleation as quasiunary one, as the dynamics of cluster population are determined by large of the collision and evaporation rates of a single dominating component from the gas phase. A classical example is the binary water–sulphuric acid nucleation [104], where the cluster evolution can be mapped with the number of sulphuric acid molecules with reasonable accuracy for most purposes (at least when considering Earth's atmosphere) [105]. A second, more practical, excuse to omit multicomponent theory in this work stems from the fact that one cannot derive nucleation theorems for a truly multicomponent case, at least in closed form, without making the continuum assumption (or other approximations [106], see also Chap. 6), effectively rendering the differences between various treatments into small variations of term relative to the derivative of $\ln K$ respect to the monomer concentrations, which are typically close to unity. When it comes to ion-induced nucleation, most evidence suggest that it gives only a modest background contribution to the atmospheric NPF rate at most occasions [for a review, see 107]—a conclusion that is also supported by more recent state-of-the-art measurements [108–111] reporting competitive enhancement of the stabilisation of sulphuric acid containing clusters by ions, bases, and oxidised organic compounds—and complications induced to nucleation theorems have already been discussed in literature [112].

basis.

1.1.5 Ignorance was amiss

Despite aerosol research becoming largely acknowledged as a separate scientific discipline after the Second World War, results concerning atmospheric NPF started to fade into oblivion. Development of CNT and related experiments showed that it is extremely unlikely for any pure vapour to nucleate homogeneously in tropospheric conditions, and since the seminal work of Köhler [119] and general advancement of meteorology, the scientific focus moved more towards understanding the nature and role of cloud condensation nuclei [120]. Although Byers still mentioned in 1965 gas-phase chemical reactions among potential sources of new condensation nuclei in the atmosphere [121], in the following decade reviews of the subject generally considered NPF in the atmosphere unlikely: Montefinale et al. [122] note, after discussing activation of Aitken nuclei, that

> Supersaturations required are considerably higher in the case of small ions [8–10] or for homogeneous nucleation [8–10], and the practical occurrence of those last two processes, in the free atmosphere, thus appears to be very unlikely.

Textbooks of that era were not more optimistic on the possibility of homogeneous nucleation in the atmosphere [123, p. 159]:

> The importance of homogeneous nucleation in the atmosphere is unknown at this juncture, but is probably important in only a few rare instances, possibly in the nearly dust-free upper atmosphere, or at points of emission to the atmosphere where the supersaturation is extremely high.

There were, however, also other opinions:[18] A world-wide layer of stratospheric aerosol particles was found by Junge et al. [124] in the early sixties, and the origin of these particles was generally assumed to be homogeneous nucleation [125]. Meanwhile, laboratory studies on the formation of urban

[18] An anecdotal example is the "man sniffer" device that the General Electric company developed for U.S. military during the Vietnam War, which relied on the detection of particles formed inside the instrument when ammonia emitted by humans reacted with ionised hydrochloric acid [120].

smog pointed out that mixtures of anthropogenic organics, sulphur dioxide and oxides of nitrogen produced new particles under irradiation [e.g. 126, 127]. These findings led Doyle [128] to perform theoretical calculations on the possibility of binary H_2O–H_2SO_4 nucleation in the atmosphere.[19] The formation of the blue haze in forested areas was studied by Went [131, 132], who proposed that the condensation of the oxidation products of plant-emitted terpenes could cause NPF. However, although all of these mechanisms found some experimental support, the idea of widespread NPF in the atmosphere did not become accepted until the development of aerosol measurement technology allowed determination of under 10-nm particle concentration in field conditions, revealing new particle formation events in various locations (for an overview, see Table 1 in [133], and for the stratospheric aerosol Ref. [134]).

1.2 The first nucleation theorem and atmospheric new particle formation

The first nucleation theorem, in its commonly used form, reads as

$$\left(\frac{\partial \ln J}{\partial \ln n_1}\right)_T \approx \left(\frac{\partial \ln J}{\partial \ln S}\right)_T \approx \Delta g^*(+1). \tag{1.3}$$

Here Δg^* is the excess number of molecules in the critical cluster, that is, the number of molecules in the critical cluster minus the average number of vapour molecules that would occupy the same space if there would be no cluster; for nucleation from vapour it is often assumed that $\Delta g^* \approx g^*$. Factor +1 in Eq. (1.3) stems from the kinetic prefactor K, when the $1/S$-correction is accounted for. In given form, the first nucleation theorem provides what seems to be a direct relation between properties that can be measured in a laboratory (J, S, T) and nanoscopic information on the critical cluster.

[19] It is a historical curiosity that Doyle [128], as well as Kiang al. [129]—who were first to apply CNT for ternary nucleation in the atmosphere—used wrong equation(s) to calculate the molecular composition of the critical cluster, neglecting the Gibbs–Duhem equation. The correct equation for the binary case was already presented by Volmer [96, Eq. (51)], who, however, continued his derivation with an equation that contained the erroneous surface term. For a more detailed discussion and later perspective, see [130].

This fact together with its simple form has led to a widespread (mis)use of the first nucleation theorem when interpreting data from new particle formation measurements, both in lab settings and outdoors.

The first nucleation theorem in the form of Eq. (1.3) was first derived by Nielsen using CNT [10, p. 18], who used it to interpret data of nucleation from solutions. He also pointed out the analogue between the first nucleation theorem and chemical reaction-order analysis, noticing that if one can locally express the nucleation rate in power-law form $J = kn_1^P$, where the kinetic factor k does not depend on the monomer concentration n_1, the nucleation exponent P should match the number of molecules in critical cluster, g^* (see Sec. 3.A.2). One can argue that this gives a more general justification for the first nucleation theorem as a manifestation of the law of mass action [135]. This view was already expressed by Volmer [96, p. 127], who concluded that $J \propto S^{g^*}$ (*not* S^{g^*+1}). He, however, most likely due to lack of experimental (J, S) data at that time, did not take the final step to express the first nucleation theorem in form of Eq. (1.3).

Analysis based on CNT was also applied to measurements of homogeneous vapour-to-liquid nucleation by Allen and Kassner in 1969 [136].[20] While several other authors have provided similar derivations for the first nucleation theorem since then [see 137, Chap. 5], Kashchiev [138] was the first to propose that relation (1.3) could be more general than CNT, thus coining the term *nucleation theorem*. Kashchiev's phenomenological proof was put on a firmer thermodynamic basis by Oxtoby and Kashchiev [139], who also extended the derivation into multicomponent systems.[21] Work of Oxtoby and Kashchiev, together with the statistical mechanic derivation of the first nucleation theorem by Reiss [140], soon led to widespread use of the first nucleation theorem when analysing experimental nucleation rate data, often in parallel with the scaling analysis of Hale [141].

The first application of the first nucleation theorem on a study with atmospheric relevance is due to Marvin and Reiss [142], who, while using a cloud chamber to interpret data of the photo-oxidation of sulphur di-

[20] "It is seen that the slope of the curve of ln J vs. S [sic.] for constant temperature will give the number of molecules in the critical clusters,..."

[21] Actually, Kashchiev [138]—as well as Oxtoby and Kashchiev [139]—were expressing their results in terms of $\partial W^*/\partial \Delta\mu$, where $\Delta\mu$ is the difference between vapour and condensed phase chemical potentials. For a more detailed description, see Chap. 3.

oxide, used the reaction-rate analysis (a.k.a. slope analysis) to interpret the obtained nucleation rate in form $J = 6.85 \cdot 10^{-35}$ cm^9 s^{-1} [H_2SO_4]^4. A more detailed analysis based on CNT was provided in the theoretical work of McGraw and Saunders [143], who found that $(\partial \ln J / \partial \ln n_1)_T = g^* + 2$, neglecting the $1/S$-correction. However, it was not until 1996 when Weber et al. [133] first applied slope-analysis into field measurements of J vs. [H_2SO_4].

Nucleation theorems in Kashchiev's sense were first mentioned together with atmospheric NPF—though no relation between these two were made—in a review by Laaksonen et al. [144]. However, it soon became a standard practice to discuss nucleation theorems and their implications applied into atmospheric new particle formation, as witnessed by various reviews [13, 145–152], and laboratory [e.g. 153–159] and field studies [e.g. 160–163]. In most cases the derivative in Eq. (1.3) with respect to sulphuric acid concentration was again of main interest. Majority of this work did not pay attention to the limitations of nucleation theorems when applied to non-ideal conditions, although there were some exceptions: Kulmala et al. [160] and Metzger et al. [154] pointed out that the effect of losses was both variable and unaccounted for both in applications to field and smog chamber measurements, and that the same was true also for other conditions, i.e. temperature and concentrations of other species. When comparing sulphuric acid nucleation exponents from various studies, a disagreement between field (typically $P \approx 1$ or 2) and some laboratory experiments (P = 4–20) was found. To explain this discrepancy, several reasons have been suggested: Role of other oxidation products of SO_2 than H_2SO_4 in NPF was studied both experimentally [164] and computationally [165, 166], as were uncertainties related to the measurements gas-phase H_2SO_4 concentration [167, 168]. The role of residence time in laboratory experiments on P was first noted by Young et al. [153], and later confirmed by Sipilä et al. [169], who pointed out the crucial role played by detection sensitivity of the smallest clusters. More recently, issues related to the assumptions of nucleation theorems have been noted to be able to explain most of this variation, as discussed in Chaps. 5 and 6 [see also 112, 170].

The reason why the nucleation exponent with respect to [H_2SO_4] has drawn such attention are the implementations concerning the physical mechanism of NPF: Case $P = 1$, i.e. $J = k_1$[H_2SO_4], has been considered to imply "activation"-type new particle formation, where clusters containing

one sulphuric acid molecule are beyond the critical size with respect to addition of more sulphuric acid into cluster, but generally under the nucleation limit with respect to other condensable vapours [160].[22] Case $P = 2$ ($J = k_2[H_2SO_4]^2$) has been interpreted as kinetically limited NPF, where collisions of two (clusters containing one) sulphuric acid molecules lead to formation of a thermodynamically stable cluster [172, 173]. In this case, the kinetic factor k_2 can be interpreted as sticking/reaction probability. Although it is well-known that coefficient k_1 and k_2 are not constants but do depend on concentrations of other vapours participating NPF as well as other environmental conditions [174], in climate and process models these are often taken as constants, causing potentially drastic errors in the description of the smallest particles.[23] Finally, if $P \sim 5$ or larger (the exact number depends ultimately on the researcher at hand), NPF is generally assumed to proceed according to the liquid droplet model described by CNT.

References

Please note that, for the sake of simplicity, all references that could have been treated as articles in a journal/series are treated so.

[22] The term *activation* originates from an analogue with cloud droplet activation described by Köhler's theory; in other contexts it, however, implies the existence of thermodynamic barrier. To describe similar process in transitions between condensed phases, a potentially more appropriate term *athermal nucleation* has also been used [171].

[23] It is possible to augment these descriptions considering multilinear dependence of $\ln J$ from the logarithms of concentrations of various precursors [cf. 106] as done for example in Refs. [110, 159, 175]. A further uncertainty in models stems from the fact that the given formula for J is used to describe formation of new particles at some preset critical size, typically at diameter of 1.5 nm, although in reality the critical size does depend on conditions. If such chosen "formation size" is larger than the "true" critical size in the model, this description may give a physically consistent presentation, but only if vapours responsible for the growth of freshly formed particles—or their presentation in the model—are the same than those responsible for the nucleation. In some studies it has been acknowledged that activation and kinetic mechanisms are only parameterisations to used to describe the net formation rate of particles at some larger size [e.g. 176], in which case the three parameters—size d, rate constant k_d, and exponent P—can be interpreted as fitting parameters for $J_d = k_d[H_2SO_4]^P$.

[1] H. Cochard. Cavitation in trees. *Comptes Rendus Physique* 7 (2006), 1018–1026.

[2] C. C. Coussios and R. A. Roy. Applications of acoustics and cavitation to noninvasive therapy and drug delivery. *Annual Reviews of Fluid Mechanics* 40 (2008), 395–420.

[3] D. M. Lynch and C. W. Bamforth. Measurement and characterization of bubble nucleation in beer. *Journal of Food Science* 67 (2002), 2696–2701.

[4] O. Navon and V. Lyakhovsky. Vesiculation processes in silicic magmas. *Geological Society, London, Special Publications* 145 (1998), 27–50.

[5] G. Wilemski. Volumes of critical bubbles from the nucleation theorem. *Journal of Chemical Physics* 125 (2006), 114507.

[6] M. El Mekki Azouzi, C. Ramboz, J.-F. Lenain and F. Caupin. A coherent picture of water at extreme negative pressures. *Nature Physics* 9 (2013), 38–41.

[7] D. G. Fahrenheit. Experimenta & observationes de congelatione aqua in vacuo factae. *Philosophical Transactions* 33 (1724), 78–84.

[8] I. J. Ford. Properties of ice clusters from an analysis of freezing nucleation. *Journal of Physical Chemistry B* 105 (2001), 11649–11655.

[9] O. Galkin and P. G. Vekilov. Nucleation of protein crystals: critical nuclei, phase behavior, and control pathways. *Journal of Crystal Growth* 232 (2001), 63–76.

[10] A. E. Nielsen. *Kinetics of Precipitation*. Oxford: Pergamon, 1964.

[11] P. G. Vekilov. Sickle-cell haemoglobin polymerization: is it the primary pathogenic event of sickle-cell anaemia? *British Journal of Haematology* 139 (2007), 173–184.

[12] K. McGouldrick, O. B. Toon and D. H. Grinspoon. Sulfuric acid aerosols in the atmospheres of the terrestrial planets. *Planetary and Space Science* 59 (2011), 934–941.

[13] R. Zhang, A. Khalizov, L. Wang, M. Hu and W. Xu. Nucleation and growth of nanoparticles in the atmosphere. *Chemical Reviews* 112 (2012), 1957–2011.

[14] B. Buesser and S. E. Pratsinis. Desing of nanomaterial synthesis by aerosol processes. *Annual Review of Chemical and Biomolecular Engineering* 3 (2012), 103–127.

[15] N. E. Motl, A. K. P. Mann and S. E. Skrabalak. Aerosol-assisted synthesis and assembly of nanoscale building blocks. *Journal of Materials Chemistry A* 1 (2013), 5193–5202.

[16] M. O. Andreae and D. Rosenfeld. Aerosol–cloud–precipitation interactions. Part 1. The nature and sources of cloud-active aerosols. *Earth-Science Reviews* 89 (2008), 13–41.

[17] N. Mahowald, D. S. Ward, S. Kloster, M. G. Flanner, C. L. Heald, N. G. Heavens, P. G. Hess, J.-F. Lamarque and P. Y. Chuang. Aerosol impacts on climate and biogeochemistry. *Annual Review of Environment and Resources* 36 (2011), 45–74.

[18] D. A. Grantz, J. B. Garner and D. W. Johnson. Ecological effects of particulate matter. *Environment International* 29 (2003), 213–239.

[19] P. Goodman and O. Hänninen. Air pollution and health and the role of aerosols. In: *Aerosol Science: Technology and Applications*. Ed. by I. Colbeck and M. Lazaridis. Chichester: Wiley, 2014. Chap. 9.

[20] J. Lelieveld, J. S. Evans, M. Fnais, D. Giannadaki and A. Pozer. The contribution of outdoor air pollution sources to premature mortality on a global scale. *Nature (London)* 525 (2015), 367–371.

[21] V.-M. Kerminen, M. Paramonov, T. Anttila, I. Riipinen, C. Fountoukis, H. Korhonen, E. Asmi, L. Laakso, H. Lihavainen, E. Swietlicki, B. Svenningsson, A. Asmi, S. N. Pandis, M. Kulmala and T. Petäjä. Cloud condensation nuclei production associated with atmospheric nucleation: a synthesis based on existing literature and new results. *Atmospheric Chemistry and Physics* 12 (2012), 12037–12059.

[22] H. Vehkamäki and I. Riipinen. Thermodynamics and kinetics of atmospheric aerosol particle formation and growth. *Chemical Society Reviews* 41 (2012), 5160–5173.

[23] M. Kulmala, J. Kontkanen, H. Junninen, K. Lehtipalo, H. E. Manninen, T. Nieminen, T. Petäjä, M. Sipilä, S. Schobesberger, P. Rantala, A. Franchin, T. Jokinen, E. Järvinen, M. Äijälä, J. Kangasluoma, J. Hakala, P. P. Aalto, P. Paasonen, J. Mikkilä, J. Vanhanen, J. Aalto, H. Hakola, U. Makkonen, T. Ruuskanen, R. L. Mauldin III, J. Duplissy,

H. Vehkamäki, J. Bäck, A. Kortelainen, I. Riipinen, T. Kurtén, M. V. Johnston, J. N. Smith, M. Ehn, T. F. Mentel, K. E. J. Lehtinen, A. Laaksonen, V.-M. Kerminen and D. R. Worsnop. Direct observations of atmospheric aerosol nucleation. *Science* 339 (2013), 943–946.

[24] R. Zhang, I. Suh, J. Zhao, D. Zhang, E. C. Fortner, X. Tie, L. T. Molina and M. J. Molina. Atmospheric new particle formation enhanced by organic acids. *Science* 304 (2004), 1487–1490.

[25] R. Zhang, L. Wang, A. Khalizov, J. Zhao, J. Zheng, R. L. McGraw and L. T. Molina. Formation of nanoparticles of blue haze enhanced by anthropogenic pollution. *Proceedings of the National Academy of Sciences U.S.A.* 106 (2009), 17650–17654.

[26] C. D. O'Dowd and T. Hoffmann. Coastal new particle formation: a review of the current state-of-the-art. *Environmental Chemistry* 2 (2005), 245–255.

[27] B. J. Murray and E. J. Jensen. Homogeneous nucleation of amorphous solid water particles in the upper mesosphere. *Journal of Atmospheric and Solar–Terrestial Physics* 72 (2010), 51–61.

[28] A. Wegener. Die Erforschung der oberstern Atmosphärenschichten. *Zeitschrift für anorganische Chemie* 75 (1912), 107–131.

[29] G. E. Thomas. Is the polar mesosphere the miner's canary of global change? *Advances in Space Research* 18 (1996), 149–158.

[30] R. S. Humphries, R. Schofield, M. Keywood, J. Ward, J. R. Pierce, C. M. Gionfriddo, M. Tate, D. Krabbenhoft, I. E. Galbally, S. B. Molloy, A. Klekociuk, P. V. Johnston, K. Kreher, A. J. Thomas, A. D. Robinson, N. R. P. Harris, R. Johnson and S. R. Wilson. Boundary layer new particle formation over East Antarctic sea ice—possible Hg driven nucleation? *Atmospheric Chemistry and Physics* 15 (2015), 13339–13364.

[31] Y. Liu, Z. Wang, S. Wang, H. Fang and D. Wang. Soot nanoparticles could partake in nucleation of biogenic particles in the atmosphere: using fullerene as a model compound. *Atmosphere* 7 (2016), 45.

[32] O. Boucher, D. Randall, P. Artaxo, C. Bretherton, G. Feingold, P. Forster, V.-M. Kerminen, Y. Kondo, H. Liao, U. Lohmann, P. Rasch, S. K. Satheesh, S. Sherwood, B. Stevens and X. Zhan. Clouds and aerosols. In: *Climate Change 2013: The Physical Science Basis. Contribution of Working Group I to the Fifth Assessment Report of the Intergovernmental Panel on Climate Change*. Ed. by T. F. Stocker, D. Qin, G.-K. Plattner, M. Tignor, S. K. Allen, J. Boschung, A. Nauels, Y. Xia, V. Bex and P. M. Midgley. Cambridge and New York: Cambridge University Press, 2013. Chap. 7.

[33] K. S. Carslaw, O. Boucher, D. V. Spracklen, G. W. Mann, J. G. L. Rae, S. Woodward and M. Kulmala. A review of natural aerosol interactions and feedbacks within the Earth system. *Atmospheric Chemistry and Physics* 10 (2010), 1701–1737.

[34] X. Zhang, R. A. West, P. G. J. Irwin, C. A. Nixon and Y. L. Yung. Aerosol influence on the energy balance of the middle atmosphere of Jupiter. *Nature Communications* 6 (2015), 10231.

[35] W. Thomson. On the equilibrium of vapour at a curved surface of liquid. *Philosophical Magazine* 42 (1871), 448–452.

[36] J. W. Gibbs. On the equilibrium of heterogeneous substances (concluded). *Transactions of the Connecticut Academy of Arts and Sciences* 3 (1878), 343–524.

[37] O. Preining. The physical nature of very, very small particles and its impact on their behaviour. *Journal of Aerosol Science* 29 (1998), 481–495.

[38] M. Arndt, O. Nairz, J. Vos-Andreae, C. Keller, G. van der Zouw and A. Zeilinger. Wave-particle duality of C_{60} molecules. *Nature (London)* 401 (1999), 680–682.

[39] S. Gerlich, S. Eibenberger, M. Tomandl, S. Nimmrichter, K. Hornberger, P. J. Fagan, J. Tüxen, M. Mayor and M. Arndt. Quantum interference of large organic molecules. *Nature Communications* 2 (2011), 263.

[40] B. M. Smirnov. Processes involving clusters and small particles in a buffer gas. *Physics – Usphekhi* 54 (2011), 691–721.

[41] R. Strey, P. E. Wagner and Y. Viisanen. The problem of measuring homogeneous nucleation rates and the molecular contents of nuclei: Progress in the form of nucleation pulse measurements. *Journal of Physical Chemistry* 98 (1994), 7748–7758.

[42] Y. J. Kim, B. E. Wyslouzil, G. Wilemski, J. Wölk and R. Strey. Isothermal nucleation rates in supersonic nozzles and the properties of small water clusters. *Journal of Physical Chemistry A* 108 (2004), 4365–4377.

[43] A. Auzout. Lettre a Monsieur l'Abbe Charles. *Journal des Sçavans* 2 (1666), 21–24.

[44] I. Kant. Von den Ursachen der Erderschütterungen bei Gelegenheit des Unglücks, welches die westliche Länder von Europa gegen das Ende des vorigen Jahres betroffen hat. *Wöchentliche Königsbergische Frag- und Anzeigungs-Nachrichten* (1756). 4 (24th Jan. 1756), 5 (31st Jan. 1756).

[45] Aristotle. *Meteorology*. Trans. by E. W. Webster. 350 BCE. URL: `https://ebooks.adelaide.edu.au/a/aristotle/meteorology/`.

[46] Pliny the Elder. *Naturalis historia*. Ed. by K. F. T. Mayhoff. 77. URL: `http://www.perseus.tufts.edu/hopper/text?doc=Perseus:text:1999.02.0138`.

[47] I. Kant. *Geschichte und Naturbeschreibung der merkwürdigsten Vorfälle des Erdbebens, welches an dem Ende des 1755sten Jahres einen großen Theil der Erde erschüttert hat*. Königsberg: J. H. Hartung, 1756.

[48] R. B. Husar. Atmospheric aerosol science before 1900. In: *History of Aerosol Science*. Ed. by O. Preining and E. J. Davis. Vienna: Verlag der Österreichischen Akademie der Wissenschaften, 2000. Chap. 2.

[49] I. Kant. *Physische Geographie*. Comp. by F. T. Rink. Band 1. Königsberg: Göbbelns und Unzer, 1802.

[50] J. J. Cao, Y. K. Li, T. Jiang and G. Hu. Sulfur-containing particles emitted by concealed sulfide ore deposits: an unknown source of sulfur-containing particles in the atmosphere. *Atmospheric Chemistry and Physics* 15 (2015), 6959–6969.

[51] R. B. Stothers. The great dry fog of 1783. *Climatic Change* 32 (1996), 79–89.

[52] J. Senebier. Sur la vapeur qui a régné pendant l'eté de 1783. *Observations sur la Physique, sur l'Histoire Naturelle et sur les Arts* 24 (1784), 401–411.

[53] Baron d'Escalle. Marcorelle. Description d'un brouillard extraordinaire qui a paru fur la fin du mois de Juin, & au commencement de celui de Juillet 1783. *Observations sur la Physique, sur l'Histoire Naturelle et sur les Arts* 24 (1784), 18–23.

[54] J. L. Jimenez, M. R. Canagaratna, N. M. Donahue, A. S. H. Prevot, Q. Zhang, J. H. Kroll, P. F. DeCarlo, J. D. Allan, H. Coe, N. L. Ng, A. C. Aiken, K. S. Docherty, I. M. Ulbrich, A. P. Grieshop, A. L. Robinson, J. Duplissy, J. D. Smith, K. R. Wilson, V. A. Lanz, C. Hueglin, Y. L. Sun, J. Tian, A. Laaksonen, T. Raatikainen, J. Rautiainen, P. Vaattovaara, M. Ehn, M. Kulmala, J. M. Tomlinson, D. R. Collins, M. J. Cubison, E. J. Dunlea, J. A. Huffman, T. B. Onasch, M. R. Alfarra, P. I. Williams, K. Bower, Y. Kondo, J. Schneider, F. Drewnick, S. Borrmann, S. Weimer, K. Demerjian, D. Salcedo, L. Cottrell, R. Griffin, A. Takami, T. Miyoshi, S. Hatakeyama, A. Shimono, J. Y. Sun, Y. M. Zhang, K. Dzepina, J. R. Kimmel, D. Sueper, J. T. Jayne, S. C. Herndon, A. M. Trimborn, L. R. Williams, E. C. Wood, A. M. Middlebrook, C. E. Kolb, U. Baltensperger and D. R. Worsnop. Evolution of organic aerosols in the atmosphere. *Science* 326 (2009), 1525–1529.

[55] M. Kulmala, T. Petäjä, M. Ehn, J. Thornton, M. Sipilä, D. R. Worsnop and V.-M. Kerminen. Chemistry of atmospheric nucleation: On the recent advances on precursor characterization and atmospheric clusters composition in connection with atmospheric new particle formation. *Annual Review of Physical Chemistry* 65 (2014), 21–37.

[56] E. M. L. Patrin. A l'occasion des pierres météoriques ou météorilites. *Journal de Physique, de Chimie, d'Histoire Naturelle et des Arts* 68 (1809), 401–408.

[57] C. S. Rafinesque. Thoughts on atmospheric dust. *American Journal of Science* 1 (1819), 397–400.

[58] C. S. Rafinesque. Letters on atmospheric dust. *Western Minerva* 1 (1821), 27–29.

[59] J. Tyndall. On a new series of chemical reactions produced by light. *Proceedings of the Royal Society of London* 17 (1868), 92–102.

[60] J. Tyndall. On the action of rays of high refrangibility upon gaseous matter. *Philosophical Transactions of the Royal Society of London* 160 (1870), 333–365.

[61] J. Tyndall. *Essays on the Floating-Matter of the Air, in Relation to Putrefaction and Infection*. London: Longmans, Green, and Co., 1881.

[62] J. W. Gibbs. On the equilibrium of heterogeneous substances. First part. *Transactions of the Connecticut Academy of Arts and Sciences* 3 (1875), 108–248.

[63] P. J. Coulier. Note sur une nouvelle propriété de l'air. *Journal de Pharmacie et de Chimie* 22 (1875), 165–178.

[64] J. Aitken. On dust, fogs and clouds. *Transactions of the Royal Society of Edinburgh* 30 (1881), 337–368.

[65] J. Kiessling. Nebelglüh-Apparat. *Abhandlungen aus dem Gebiete der Naturwissenschaften herausgegeben vom Naturwissenschaftligen Verein in Hamburg* 8 (1884), 147–154.

[66] R. von Helmholtz. Untersuchungen über Dämpfe und Nebel, besonders über solche von Lösungen. *Annalen der Physik und Chemie* 27 (1886), 508–543.

[67] C. Barus. Colored cloudy condensation as depending on air temperature and dust-contents, with a view to dust counting. *American Meteorological Journal* 10 (1893), 12–34.

[68] R. von Helmholtz. Versuche mit einem Dampfstrahl. *Annalen der Physik und Chemie* 268 (1887), 1–19.

[69] W. Schröder and K. H. Wiederkehr. Geophysics contributed to the radical change from classical to modern physics 100 years ago. *Eos, Transactions of the American Geophysical Union* 79 (1998), 559–562.

[70] J. J. Thomson. *Conduction of Electricity through Gases*. 2nd ed. Cambridge University Press, 1906.

[71] C. T. R. Wilson. Condensation of water vapour in the presence of dust-free air and other gases. *Philosophical Transactions of the Royal Society of London, Series A* 189 (1897), 265–307.

[72] J. Aitken. On some nuclei of cloudy condensation. *Transactions of the Royal Society of Edinburgh* 39 (1900), 15–25.

[73] C. Barus. Nucleation during cold weather. *Physical Review* 16 (1903), 193–198.

[74] C. Barus. A continuous record on atmospheric nucleation. *Smithsonian Contributions to Knowledge* 34 (1905), i–226.

[75] C. Barus. The nucleation of the uncontaminated atmosphere. *Carnegie Publications* 40 (1906), iii–152.

[76] A. Hamed, H. Korhonen, S.-L. Sihto, J. Joutsensaari, H. Järvinen, T. Petäjä, F. Arnold, T. Nieminen, M. Kulmala, J. N. Smith, K. E. J. Lehtinen and A. Laaksonen. The role of relative humidity in continental new particle formation. *Journal of Geophysical Research: Atmospheres* 116 (2011), D03202.

[77] J. Aitken. The Sun as a fog producer. *Proceedings of the Royal Society of Edinburgh* 32 (1912), 183–215.

[78] A. R. Hogg. The intermediate ions of the atmosphere. *Proceedings of the Physical Society* 51 (1939), 1014–1026.

[79] T. Young. An essay on the cohesion of fluids. *Philosophical Transactions of the Royal Society of London* 95 (1805), 65–87.

[80] P.-S. Laplace. *Traité de Méchanique Céleste*. Vol. 4. Paris: Courcier, 1806.

[81] C. M. Guldberg and P. Waage. Studier over Affiniteten. *Forhandlinger i Videnskabs-Selskabet i Christiania* (1865), 35–45.

[82] C. M. Guldberg. Om Tidens Inflydelse. *Forhandlinger i Videnskabs-Selskabet i Christiania* (1865), 111–120.

[83] M. Volmer and A. Weber. Keimbildung in übersättigten Gebilden. *Zeitschrift für physikalische Chemie* 119 (1926), 277–301.

[84] M. Smoluchowski. Molekular-kinetische Theorie der Opaleszenz von Gasen im kritischen Zustande, sowie einiger verwandter Erscheinungen. *Annalen der Physik* 25 (1908), 205–225.

[85] A. Einstein. Theorie der Opaleszenz von homogenen Flüssigkeiten und Flüssigkeitsgemischen in der Nähe der kritischen Zustandes. *Annalen der Physik* 33 (1910), 1275–1298.

[86] V. K. La Mer. Nucleation in phase transitions. *Industrial and Engineering Chemistry* 44 (1952), 1270–1277.

[87] S. M. Kathmann. Understanding the chemical physics of nucleation. *Theoretical Chemistry Accounts* 116 (2006), 169–182.

[88] L. Farkas. Keimbildungsgeschwindigket in übersättigten Dämpfen. *Zeitschrift für physikalische Chemie* 175 (1927), 236–242.

[89] R. Becker and W. Döring. Kinetische Behandlung der Keimbildung in übersättigten Dämpfen. *Annalen der Physik* 416 (1935), 719–752.

[90] J. Frenkel. Statistical theory of condensation phenomena. *Journal of Chemical Physics* 7 (1939), 200–201.

[91] Ya. B. Zel'dovich. [Theory of the formation of new phase, cavitation]. *Zhurnal Eksperimental'noi i Teoreticheskoi Fiziki* 12 (1942), 525–538.

[92] F. C. Goodrich. Nucleation rates and the kinetics of particle growth. II. The birth and death equations. *Proceedings of the Royal Society of London A* 277 (1964), 167–182.

[93] J. S. Langer. Theory of the condensation point. *Annals of Physics* 41 (1967), 108–157.

[94] J. S. Langer. Theory of nucleation rates. *Physical Review Letters* 21 (1968), 973–976.

[95] L. V. Bravina and E. E. Zabrodin. Homogeneous nucleation: Comparison between two theories. *Physics Letters A* 233 (1997), 423–429.

[96] M. Volmer. *Kinetik der Phasenbildung*. Dresden und Leipzig: Verlag von Theodor Steinkopff, 1939.

[97] H. Reiss. The kinetics of phase transitions in binary systems. *Journal of Chemical Physics* 18 (1950), 840–848.

[98] D. Stauffer. Kinetic theory of two-component ("hetero-molecular") nucleation and condensation. *Journal of Aerosol Science* 7 (1976), 319–333.

[99] J. O. Hirschfelder. Kinetics of homogeneous nucleation on many-component systems. *Journal of Chemical Physics* 61 (1974), 2690–2694.

[100] H. Trinkaus. Theory of nucleation of multicomponent precipitates. *Physical Review B* 27 (1983), 7372–7378.

[101] G. Tohmfor and M. Volmer. Die Keimbildung unter dem Einfluß-elektrischer Ladungen. *Annalen der Physik* 425 (1938), 109–131.

[102] A. I. Rusanov and F. M. Kuni. Reformulation of the thermodynamic theory of nucleation on charged particles. *Journal of Colloid and Interface Science* 100 (1984), 264–277.

[103] M. Noppel, H. Vehkamäki, P. M. Winkler, M. Kulmala and P. E. Wagner. Heterogeneous nucleation in multi-component vapor on a partially wettable charged conducting particle. II. The generalized Laplace, Gibbs–Kelvin, and Young equations and application to nucleation. *Journal of Chemical Physics* 139 (2013), 134108.

[104] W. J. Shugard, R. H. Heist and H. Reiss. Theory of vapor phase nucleation in binary mixtures of water and sulfuric acid. *Journal of Chemical Physics* 61 (1974), 5298–5305.

[105] R. McGraw. Two-dimensional kinetics of binary nucleation in sulfuric acid–water mixtures. *Journal of Chemical Physics* 102 (1995), 2098–2108.

[106] R. McGraw and R. Zhang. Multivariate analysis of homogeneous nucleation rate measurements. Nucleation in the *p*-toluic acid/ sulfuric acid/water system. *Journal of Chemical Physics* 128 (2008), 064508.

[107] A. Hirsikko, T. Nieminen, S. Gagné, K. Lehtipalo, H. E. Manninen, M. Ehn, U. Hõrrak, V.-M. Kerminen, L. Laakso, P. H. McMurry, A. Mirme, S. Mirme, T. Petäjä, H. Tammet, V. Vakkari, M. Vana and M. Kulmala. Atmospheric ions and nucleation: a review of observations. *Atmospheric Chemistry and Physics* 11 (2011), 767–798.

[108] J. Kirkby, J. Curtius, J. Almeida, E. Dunne, J. Duplissy, S. Ehrhart, A. Franchin, S. Gagné, L. Ickes, A. Kürten, A. Kupc, A. Metzger, F. Riccobono, L. Rondo, S. Schobesberger, G. Tsagkogeorgas, D. Wimmer, A. Amorim, F. Bianchi, M. Breitenlechner, A. David, J. Dommen, A. Downard, M. Ehn, R. C. Flagan, S. Haider, A. Hansel, D. Hauser, W. Jud, H. Junninen, F. Kreissl, A. Kvashin, A. Laaksonen, K. Lehtipalo, J. Lima, E. R. Lovejoy, V. Makhmutov, S. Mathot, J. Mikkilä, P. Minginette, S. Mogo, T. Nieminen, A. Onnela, P. Pereira, T. Petäjä, R. Schnitzhofer, J. H. Seinfeld, M. Sipilä, Y. Stozhkov, F. Stratmann, A. Tomé, J. Vanhanen, Y. Viisanen, A. Vrtala, P. E. Wagner, H. Walther, E. Weingartner, H. Wex, P. M. Winkler, K. S. Carslaw, D. R. Worsnop, U. Baltensperger and M. Kulmala. Role of sulphuric acid, ammonia

and galactic cosmic rays in atmospheric aerosol nucleation. *Nature (London)* 476 (2011), 429–433.

[109] J. Almeida, S. Schobesberger, A. Kürten, I. K. Ortega, O. Kupiainen-Määttä, A. P. Praplan, A. Adamov, A. Amorim, F. Bianchi, M. Breitenlechner, A. David, J. Dommen, N. M. Donahue, A. Downard, E. Dunne, J. Duplissy, S. Ehrhart, R. C. Flagan, A. Franchin, R. Guida, J. Hakala, A. Hansel, M. Heinritzi, H. Henschel, T. Jokinen, H. Junninen, M. Kajos, J. Kangasluoma, H. Keskinen, A. Kupc, T. Kurtén, A. N. Kvashin, A. Laaksonen, K. Lehtipalo, M. Leiminger, J. Leppä, V. Loukonen, V. Makhmutov, S. Mathot, M. J. McGrath, T. Nieminen, T. Olenius, A. Onnela, T. Petäjä, F. Riccobono, I. Riipinen, M. Rissanen, L. Rondo, T. Ruuskanen, F. D. Santos, N. Sarnela, S. Schallhart, R. Schnitzhofer, J. H. Seinfeld, M. Simon, M. Sipilä, Y. Stozhkov, F. Stratmann, A. Tomé, J. Tröstl, G. Tsagkogeorgas, P. Vaattovaara, Y. Viisanen, A. Virtanen, A. Vrtala, P. E. Wagner, E. Weingartner, H. Wex, C. Williamson, D. Wimmer, P. Ye, T. Yli-Juuti, K. S. Carslaw, M. Kulmala, J. Curtius, U. Baltensperger, D. R. Worsnop, H. Vehkamäki and J. Kirkby. Molecular understanding of sulphuric acid-amine particle nucleation in the atmosphere. *Nature (London)* 502 (2013), 359–363.

[110] F. Riccobono, S. Schobesberger, C. E. Scott, J. Dommen, I. K. Ortega, L. Rondo, J. Almeida, A. Amorim, F. Bianchi, M. Breitenlechner, A. David, A. Downard, E. M. Dunne, J. Duplissy, S. Ehrhart, R. C. Flagan, A. Franchin, A. Hansel, H. Junninen, M. Kajos, H. Keskinen, A. Kupc, A. Kürten, A. N. Kvashin, A. Laaksonen, K. Lehtipalo, V. Makhmutov, S. Mathot, T. Nieminen, A. Onnela, T. Petäjä, A. P. Praplan, F. D. Santos, S. Schallhart, J. H. Seinfeld, M. Sipilä, D. V. Spracklen, Y. Stotzhkov, F. Stratmann, A. Tomé, G. Tsagkogeorgas, P. Vaattovaara, Y. Viisanen, A. Vrtala, P. E. Wagner, E. Weingartner, H. Wex, D. Wimmer, K. S. Carslaw, J. Curtius, N. M. Donahue, J. Kirkby, M. Kulmala, D. R. Worsnop and U. Baltensperger. Oxidation products of biogenic emissions contribute to nucleation of atmospheric particles. *Science* 344 (2014), 717–721.

[111] J. Kirkby, J. Duplissy, K. Sengupta, C. Frege, H. Gordon, C. Williamson, M. Heinritzi, M. Simon, C. Yan, J. Almeida, J. Tröstl, T. Nieminen, I. K. Ortega, R. Wagner, A. Adamov, A. Amorim, A.-K. Bernhammer, F. Bianchi, M. Breitenlechner, S. Brilke, X. Chen, J.

Craven, A. Dias, S. Ehrhart, R. C. Flagan, A. Franchin, C. Fuchs, R. Guida, J. Hakala, C. R. Hoyle, T. Jokinen, H. Junninen, J. Kangasluoma, J. Kim, M. Krapf, A. Kürten, A. Laaksonen, K. Lehtipalo, V. Makhmutov, S. Mathot, U. Molteni, A. Onnela, O. Peräkylä, F. Piel, T. Petäjä, A. P. Praplan, K. Pringle, A. Rap, N. A. D. Richards, I. Riipinen, M. P. Rissanen, L. Rondo, N. Sarnela, S. Schobesberger, C. E. Scott, J. H. Seinfeld, M. Sipilä, G. Steiner, Y. Stozhkov, F. Stratmann, A. Tomé, A. Virtanen, A. L. Vogel, A. C. Wagner, P. E. Wagner, E. Weingartner, D. Wimmer, P. M. Winkler, P. Ye, X. Zhang, A. Hansel, J. Dommen, N. M. Donahue, D. R. Worsnop, U. Baltensperger, M. Kulmala, K. S. Carslaw and J. Curtius. Ion-induced nucleation of pure biogenic particles. *Nature (London)* 533 (2016), 521–526.

[112] H. Vehkamäki, M. J. McGrath, T. Kurtén, J. Julin, K. E. J. Lehtinen and M. Kulmala. Rethinking the application of the first nucleation theorem to particle formation. *Journal of Chemical Physics* 136 (2012), 094107.

[113] W. G. Courtney. Remarks on homogeneous nucleation. *Journal of Chemical Physics* 35 (1961), 2249–2250.

[114] S. L. Girshick and C.-P. Chiu. Kinetic nucleation theory: A new expression for the rate of homogeneous nucleation from ideal supersaturated vapor. *Journal of Chemical Physics* 93 (1990), 1273–1277.

[115] S. L. Girshick. Comment on: "Self-consistency correction to homogeneous nucleation theory". *Journal of Chemical Physics* 94 (1991), 826–827.

[116] H. Reiss, W. K. Kegel and J. L. Katz. Resolution of the problems of replacement free energy, $1/S$, and internal consistency in nucleation theory by consideration of the length scale for mixing entropy. *Physical Review Letters* 78 (1997), 4506–4509.

[117] J. L. Katz and M. C. Donohue. A kinetic approach to homogeneous nucleation theory. *Advances in Chemical Physics* 40 (1979), 137–155.

[118] R. C. Flagan. A thermodynamically consistent kinetic framework for binary nucleation. *Journal of Chemical Physics* 127 (2007), 214503.

[119] H. Köhler. Zur Thermodynamik der Kondensation an hygroskopischen Kernen und Bemerkungen über das Zusammenfliessen der Tropfen. *Meddelanden från Statens meteorologisk-hydrografiska anstalt* 3 (1926), 1–16.

[120] V. A. Mohnen and G. M. Hidy. Atmospheric nanoparticles: Early metrology and observations (1875–1980). In: *Aerosol Science and Technology: History and Reviews*. Ed. by D. S. Ensor. Research Triangle Park: RTI Press, 2011. Chap. 16.

[121] H. R. Byers. Nucleation in the atmosphere. *Industrial and Engineering Chemistry* 67 (1965), 32–40.

[122] A. C. Montefinale, T. Montefinale and H. M. Papée. Recent advances in the chemistry and properties of atmospheric nucleants: A review. *Pure and Applied Geophysics* 91 (1971), 171–210.

[123] S. S. Butcher and R. J. Charlson. *An Introduction to Air Chemistry*. New York and London: Academic Press, 1972.

[124] C. E. Junge, C. W. Chagnon and J. E. Manson. A world-wide stratospheric aerosol layer. *Science* 133 (1961), 1478–1479.

[125] A. W. Castleman, Jr. Nucleation processes and aerosol chemistry. *Space Science Reviews* 15 (1974), 547–589.

[126] M. J. Prager, E. R. Stephens and W. E. Scott. Aerosol formation from gaseous air pollutants. *Industrial and Engineering Chemistry* 52 (1960), 521–524.

[127] N. A. Renzetti and G. J. Doyle. Photochemical aerosol formation in sulfur dioxide–hydrocarbon systems. *International Journal of Air Pollution* 2 (1960), 327–345.

[128] G. J. Doyle. Self-nucleation in the sulfuric acid–water system. *Journal of Chemical Physics* 35 (1961), 795–799.

[129] C. S. Kiang, R. D. Cadle, P. Hamill, V. A. Mohnen and G. K. Yue. Ternary nucleation applied to gas to particle conversion. *Journal of Aerosol Science* 6 (1975), 465–474.

[130] A. Laaksonen, R. McGraw and H. Vehkamäki. Liquid-drop formalism and free-energy surfaces in binary homogeneous nucleation theory. *Journal of Chemical Physics* 111 (1999), 2019–2027.

[131] F. W. Went. Organic matter in the atmosphere, and its possible relation to petroleum formation. *Proceedings of the National Academy of Sciences U.S.A.* 46 (1960), 212–221.

[132] F. W. Went. On the nature on Aitken condensation nuclei. *Tellus* 18 (1966), 549–556.

[133] R. J. Weber, J. J. Marti, P. H. McMurry, F. L. Eisele, D. J. Tanner and A. Jefferson. Measured atmospheric new particle formation rates: Implications for nucleation mechanisms. *Chemical Engineering Communications* 151 (1996), 53–64.

[134] C. A. Brock, P. Hamill, J. C. Wilson, H. H. Johnson and K. R. Chan. Particle formation in the upper tropical troposphere: A source of nuclei for the stratospheric aerosol. *Science* 270 (1995), 1650–1653.

[135] R. K. Bowles, R. McGraw, P. Schaaf, B. Senger, J.-C. Voegel and H. Reiss. A molecular based derivation of the nucleation theorem. *Journal of Chemical Physics* 113 (2000), 4524–4532.

[136] L. B. Allen and J. L. Kassner, Jr. The nucleation of water vapor in the absence of particulate matter and ions. *Journal of Colloid and Interface Science* 30 (1969), 81–93.

[137] D. Kashchiev. *Nucleation: Basic Theory with Applications*. Oxford: Butterworth–Heinemann, 2000.

[138] D. Kashchiev. On the relation between nucleation work, nucleus size, and nucleation rate. *Journal of Chemical Physics* 76 (1982), 5098–5102.

[139] D. W. Oxtoby and D. Kashchiev. A general relation between the nucleation work and the size of the nucleus in multicomponent nucleation. *Journal of Chemical Physics* 100 (1994), 7665–7671.

[140] Y. Viisanen, R. Strey and H. Reiss. Homogeneous nucleation rates for water. *Journal of Chemical Physics* 99 (1993), 4680–4692.

[141] B. N. Hale. Application of scaled homogeneous nucleation-rate formalism to experimental data at $T << T_c$. *Physical Review A* 33 (1986), 4156–4163.

[142] D. C. Marvin and H. Reiss. Cloud chamber study of the gas phase photooxidation of sulfur dioxide. *Journal of Chemical Physics* 69 (1978), 1897–1918.

[143] R. McGraw and J. H. Saunders. A condensation feedback mechanism for oscillatory nucleation and growth. *Aerosol Science and Technology* 3 (1984), 367–380.

[144] A. Laaksonen, V. Talanquer and D. W. Oxtoby. Nucleation: Measurements, theory and atmospheric applications. *Annual Review of Physical Chemistry* 46 (1995), 489–524.

[145] A. Laaksonen. Application of nucleation theories to atmospheric new particle formation. *AIP Conference Proceedings* 534 (2000), 711–723.

[146] M. Kulmala, T. Vesala and A. Laaksonen. Physical chemistry of aerosol formation. In: *Aerosol Chemical Processes in the Environment*. Ed. by K. R. Spurny. Boca Raton, Florida: CRC Press, 2000. Chap. 2.

[147] C. Anastasio and S. T. Martin. Atmospheric nanoparticles. *Reviews in Mineralogy and Geochemistry* 44 (2001), 293–349.

[148] J. Curtius. Nucleation of atmospheric aerosol particles. *Comptes Rendus Physique* 7 (2006), 1027–1045.

[149] M. Kulmala and V.-M. Kerminen. On the formation and growth of atmospheric nanoparticles. *Atmospheric Research* 90 (2008), 132–150.

[150] J. N. Smith. Atmospheric nanoparticles. In: *Dekker Encyclopedia of Nanoscience and Nanotehcnology*. Ed. by S. E. Lyshevski, C. I. Contescu and K. Putyera. 2nd ed. Boca Raton, Florida: CRC Press, 2008. Chap. 19.

[151] A. Laaksonen and K. E. J. Lehtinen. Nucleation. In: *Environmental Chemistry of Aerosols*. Ed. by I. Colbeck. Oxford: Blackwell, 2008. Chap. 2.

[152] R. Zhang. Getting to the critical nucleus of aerosol formation. *Science* 328 (2010), 1366–1367.

[153] L. H. Young, D. R. Benson, F. R. Kameel, J. R. Pierce, H. Junninen, M. Kulmala and S.-H. Lee. Laboratory studies of H_2SO_4/H_2O binary homogeneous nucleation from the SO_2 + OH reaction: evaluation of the experimental setup and preliminary results. *Atmospheric Chemistry and Physics* 8 (2008), 4997–5016.

[154] A. Metzger, B. Verheggen, J. Dommen, J. Duplissy, A. S. H. Prevot, E. Weingartner, I. Riipinen, M. Kulmala, D. V. Spracklen, K. S. Carslaw and U. Baltensperger. Evidence for the role of organics in aerosol particle formation under atmospheric conditions. *Proceedings of the National Academy of Sciences U. S. A.* 107 (2010), 6646–6651.

[155] M. E. Erupe, A. A. Viggiano and S.-H. Lee. The effect of trimethylamine on atmospheric nucleation involving H_2SO_4. *Atmospheric Chemistry and Physics* 11 (2011), 4767–4775.

[156] D. Brus, K. Neitola, A.-P. Hyvärinen, T. Petäjä, J. Vanhanen, M. Sipilä, P. Paasonen, M. Kulmala and H. Lihavainen. Homogenous nucleation of sulfuric acid and water at close to atmospherically relevant conditions. *Atmospheric Chemistry and Physics* 11 (2011), 5277–5287.

[157] J. H. Zollner, W. A. Glasoe, B. Panta, K. K. Carlson, P. H. McMurry and D. R. Hanson. Sulfuric acid nucleation: Power dependencies, variation with relative humidity, and effect of bases. *Atmospheric Chemistry and Physics* 12 (2012), 4399–4411.

[158] W. A. Glasoe, K. Volz, B. Panta, N. Freshour, R. Bachman, D. R. Hanson, P. H. McMurry and C. Jen. Sulfuric acid nucleation: An experimental study of the effect of seven bases. *Journal of Geophysical Research: Atmospheres* 120 (2015), 1933–1950.

[159] M. Olin, T. Rönkkö and M. Dal Maso. CFD modeling of a vehicle exhaust laboratory sampling system: sulfur-driven nucleation and growth in diluting diesel exhaust. *Atmospheric Chemistry and Physics* 15 (2015), 5305–5323.

[160] M. Kulmala, K. E. J. Lehtinen and A. Laaksonen. Cluster activation theory as an explanation of the linear dependence between formation rate of 3 nm particles and sulphuric acid concentration. *Atmospheric Chemistry and Physics* 6 (2006), 787–793.

[161] S.-L. Sihto, M. Kulmala, V.-M. Kerminen, M. Dal Maso, T. Petäjä, I. Riipinen, H. Korhonen, F. Arnold, R. Janson, M. Boy, A. Laaksonen and K. E. J. Lehtinen. Atmospheric sulphuric acid and aerosol formation: Implications from atmospheric measurements for nucleation and early growth mechanisms. *Atmospheric Chemistry and Physics* 6 (2006), 4079–4091.

[162] I. Riipinen, S.-L. Sihto, M. Kulmala, F. Arnold, M. Dal Maso, W. Birmili, K. Saarnio, K. Teinilä, V.-M. Kerminen, A. Laaksonen and K. E. J. Lehtinen. Connections between atmospheric sulphuric acid and new particle formation during QUEST III-IV campaigns in Heidelberg and Hyytiälä. *Atmospheric Chemistry and Physics* 7 (2007), 1899–1914.

[163] C. Kuang, P. H. McMurry, A. V. McCormick and F. L. Eisele. Dependence of nucleation rates on sulfuric acid vapor concentration in diverse atmospheric locations. *Journal of Geophysical Research: Atmospheres* 113 (2008), D10209.

[164] A. Laaksonen, M. Kulmala, T. Berndt, F. Stratmann, S. Mikkonen, A. Ruuskanen, K. E. J. Lehtinen, M. Dal Maso, P. Aalto, T. Petäjä, I. Riipinen, S.-L. Sihto, R. Janson, F. Arnold, M. Hanke, J. Ücker, B. Umann, K. Sellegri, C. D. O'Dowd and Y. Viisanen. SO_2 oxidation products other than H_2SO_4 as a trigger of new particle formation. Part 2: Comparison of ambient and laboratory measurements, and atmospheric implications. *Atmospheric Chemistry and Physics* 8 (2008), 7255–7264.

[165] M. Salonen, T. Kurtén, H. Vehkamäki, T. Berndt and M. Kulmala. Computational investigation of the possible role of some intermediate products of SO_2 oxidation in sulfuric acid–water nucleation. *Atmospheric Research* 91 (2009), 47–52.

[166] M. Toivola, T. Kurtén, I. K. Ortega, M. Sundberg, V. Loukonen, A. Pádua and H. Vehkamäki. Quantum chemical studies on peroxodisulfuric acid–sulfuric acid–water clusters. *Computational and Theoretical Chemistry* 967 (2011), 219–225.

[167] O. Kupiainen-Määttä, T. Olenius, T. Kurtén and H. Vehkamäki. CIMS sulfuric acid detection efficiency enhanced by amines due to higher dipole moments—a computational study. *Journal of Physical Chemistry A* 117 (2013), 14109–14119.

[168] K. Neitola, D. Brus, U. Makkonen, M. Sipilä, U. Makkonen, R. L. Mauldin, III, N. Sarnela, T. Jokinen, H. Lihavainen and M. Kulmala. Total sulfate vs. sulfuric acid monomer concenterations in nucleation studies. *Atmospheric Chemistry and Physics* 15 (2015), 3429–3443.

[169] M. Sipilä, T. Berndt, T. Petäjä, D. Brus, J. Vanhanen, F. Stratmann, J. Patokoski, R. L. Mauldin, III, A.-P. Hyvärinen, H. Lihavainen and M. Kulmala. The role of sulfuric acid in atmospheric nucleation. *Science* 327 (2010), 1243–1246.

[170] S. Ehrhart and J. Curtius. Influence of aerosol lifetime on the interpretation of nucleation experiments with respect to the first nucleation theorem. *Atmospheric Chemistry and Physics* 13 (2013), 11465–11471.

[171] J. C. Fisher, J. H. Hollomon and D. Turnbull. Nucleation. *Journal of Applied Physics* 19 (1948), 775–784.

[172] P. H. McMurry and S. K. Friedlander. New particle formation in the presence of an aerosol. *Atmospheric Environment* 13 (1979), 1635–1651.

[173] A. A. Lushnikov and M. Kulmala. Dimers in nucleating vapors. *Physical Review E* 58 (1998), 3157–3167.

[174] P. Paasonen, T. Olenius, O. Kupiainen, T. Kurtén, T. Petäjä, W. Birmili, A. Hamed, M. Hu, L. G. Huey, C. Plass-Duelmer, J. N. Smith, A. Wiedensohler, V. Loukonen, M. J. McGrath, I. K. Ortega, A. Laaksonen, H. Vehkamäki, V.-M. Kerminen and M. Kulmala. On the formation of sulphuric acid–amine clusters in varying atmospheric conditions and its influence on atmospheric new particle formation. *Atmospheric Chemistry and Physics* 12 (2012), 9113–9133.

[175] T. Bergman, A. Laaksonen, H. Korhonen, J. Malila, E. Dunne, T. Mielonen, K. Lehtinen, T. Kühn, A. Arola and H. Kokkola. Geographical and diurnal features of amine-enhanced boundary layer nucleation. *Journal of Geophysical Research: Atmospheres* 120 (2015), 9606–9624.

[176] J.-P. Pietikäinen, S. Mikkonen, A. Hamed, A. I. Hienola, W. Birmili, M. Kulmala and A. Laaksonen. Analysis of nucleation events in the European boundary layer using the regional aerosol-climate model REMO-HAM with a solar radiation-driven OH proxy. *Atmospheric Chemistry and Physics* 14 (2014), 11711–11729.

2 Nucleation phenomena

Theoretical understanding of the first order phase transformations is underpinned by the classical liquid droplet model, especially so in the case of vapour–liquid transition: Here the new phase embryo is depicted as a drop of liquid, and its dynamics are given in terms of condensation and evaporation fluxes of vapour phase monomers. Although this approach is questionable, especially in cases where the critical cluster consists only of few molecules, it also gives a theoretical background for much of the work on nucleation theorems, and is shortly described in this chapter.

From a theoretical viewpoint, the most important feature of CNT is that it allows a closed-form expression for the nucleation rate, thus making the physical interpretation of the effect of various factors transparent. A complementary picture follows, when nucleation is studied using methods of computational physics, ranging from molecular dynamics simulations based on Newtonian mechanics to quantum-chemical evaluation of cluster energetics. At the end, both of these approaches can only be validated via comparison with nucleation experiments.

2.1 Classical nucleation theory

Although the classical nucleation theory (CNT) is generally referenced as a single theory, it is actually a group of theories developed from the combination of the Gibbsian liquid drop model and the Szilárd–Farkas kinet-

ics, describing growth and decay of such droplets via collision with and evaporation of vapour monomers. With respect to both of these aspects—thermodynamics and kinetics of droplet formation—there are several refinements proposed in the literature during the past ninety years: curiously, most such refinements tend to make the accuracy of CNT predictions poorer in comparison to rougher treatments when the theory is compared with experiments. The basic assumptions of CNT can be summarised as follows:

- clusters grow only by addition or removal of a single monomer at a time,
- the height of the energy barrier for the nucleation process is given by the free energy difference of g^* vapour molecules and a spherical droplet treated as a macroscopic object consisting of the same amount of molecules and being in unstable equilibrium with the old (vapour) phase,
- there is only one rate limiting step, i.e. the free energy maximum or saddle point, in the growth path of the cluster.

In most cases only isothermal steady-state nucleation rates are considered, which means that the short induction period before the net flux reaches sizes larger than the critical one after a change in saturation ratio, together with the effect of latent heat release and evaporative cooling due to exchange of monomers with the old phase, are neglected. Yet another simplifying assumption of constant monomer number density (saturation ratio), i.e. clusters making up only a negligible fraction of the vapour, is often done; in kinetic treatment this is rationalised by imposing the McDonald's daemon [1] that breaks up clusters reaching some post-critical size G back into monomers. Furthermore, cluster coagulation, fission and loss are also assumed to be negligible. For a more detailed exposition, recent monographs [2–4, see also 5, Chap. 3] are referred to.

2.1.1 Thermodynamics of a phase transition

One can obviously construct the free energy of a droplet in various ensembles, though the most common one is probably that with constant T

and p, and consequently the free energy is that of Gibbs. However, integration of $\mathrm{d}G = V\mathrm{d}p - \eta\mathrm{d}T + \mu\mathrm{d}N$ from the metastable vapour phase to liquid phase does not simply give the correct result for the work of formation, as the droplet presenting critical cluster is in unstable equilibrium with the vapour phase instead of stable one.[1] (We only consider here unary case in detail; for most parts, the extension to multicomponent systems is trivial when it comes to the thermodynamic part of the problem, although the treatment of surface terms requires some care [6].) Thus, we must study the change of internal energy during the formation of a droplet [5, Sec. A.2.],[3, Chap. 3]: Following Gibbs' treatment of thermodynamics, we divide the internal energy of the system into vapour, liquid and surface components, $U = U_v + U_l + U_s$. Here the surface term U_s is a correction to bulk liquid properties due to existence of a sharp interface, which we assume to have zero thickness and such energy, entropy and amount of molecules N_s that the sum of all extensive variables over vapour, liquid and surface terms corresponds to the properties of a real system with non-sharp interface. The internal energy of a homogeneous vapour in volume V is

$$U_v^0 = -p_v^0 V + \eta_v^0 T + N_v \mu_v^0,$$

where p_v^0, η_v^0 and μ_v^0 are the partial pressure, entropy and chemical potential of vapour at the initial state. When a cluster (droplet) is created into vapour, similar equations hold for the liquid and remaining vapour in volume V:

$$\begin{aligned} U_l &= -p_l V_l + \eta_l T + N_l \mu_l, \\ U_v &= -p_v V_v + \eta_v T + N_v \mu_v. \end{aligned}$$

We now assume that the volume of the forming droplet V_l is negligible in comparison to V, and we can assume the same values for η_v, p_v and μ_v before and after the formation of the droplet and drop the superscript 0.[2] The internal energy of the surface separating the liquid and the vapour is

$$U_s = \gamma A + \eta_s T + N_s \mu_s,$$

[1] Symbol η is used for the entropy, as was originally done by Gibbs, throughout this thesis instead of the more common S to avoid confusion between entropy and saturation ratio.

[2] It can be shown [3, Sec. 3.4.] that under such conditions, one can alternatively present the work of formation W^* of the critical cluster as a change in Gibbs (as done here) or Helmholtz free energy or Landau grand potential.

where γ is the surface tension and A the surface area. The total internal energy of the system is now

$$U = T\eta - p_l V_l - p_v V_v + N_l \mu_l + N_v \mu_v + N_s \mu_s + \gamma A. \tag{2.1}$$

The Gibbs free energy change for the formation is now obtained subtracting the initial Gibbs free energy of the whole system G_v^0 from that of a system containing the droplet, giving[3]

$$\Delta G = (p_v - p_l)V_l + N_l(\mu_l - \mu_v) + N_s(\mu_s - \mu_v) + \gamma A. \tag{2.2}$$

The free energy of the system does not depend on the position of the dividing surface, but volume V_l and surface area A do. Let us set the derivative of Eq. (2.2) with respect to V_l to zero:

$$\left[\frac{\partial \Delta G}{\partial V_l}\right]_{N_l,N_s;T,p_v} = 0, \tag{2.3}$$

where brackets indicate that the derivative is understood as variation with respect to the position of the dividing surface while keeping physical properties of the system intact. Evaluation of Eq. (2.3) gives the generalised Young–Laplace equation,

$$p_l - p_v = \frac{2\gamma}{R^*} + \left[\frac{\partial \gamma}{\partial R^*}\right]. \tag{2.4}$$

We can now choose the dividing surface and the corresponding radius R^* in a such way that the second term at the right-hand-side becomes zero. Such a dividing surface is know as the *surface of tension* and its radius is R_S (we drop the superscript $*$ for simplicity): $p_l - p_v = 2\gamma/R_S$. Correspondingly we also set the derivatives of ΔG with respect to N_l and N_s zero that gives the equilibrium condition for chemical potentials,

$$\mu_l = \mu_v = \mu_s. \tag{2.5}$$

[3]Here we effectively neglect the cluster's contribution to the entropy of the vapour–cluster system. Although this is a reasonable assumption, entropy due to cluster movement in laboratory coordinates has been found both to introduce uncertainties to the proper evaluation of the free energy of the cluster and also to provide a non-negligible contribution for nucleation theorems. For further discussion see Chap. 3.

Using Eqs. (2.4) and (2.5) we get the formation free energy of a critical cluster as[4]

$$\Delta G^* = (p_v - p_l)V_l^* + \gamma^* A^* = \frac{4\pi\gamma(R_S)R_S^2}{3}. \tag{2.6}$$

The derivation above is completely general. However, the value of the surface tension of a small droplet is generally not known, and chemical potentials are not directly measurable quantities either. Thus several approximations are needed to transform Eq. (2.6) into a form that can be evaluated based on measured vapour-phase properties. First, integrating Maxwell's relation $\mathrm{d}\mu_l = v_l \mathrm{d}p$, where v is the (partial) molecular volume, from p_l to p_v gives

$$\begin{aligned} \mu_l(p_l) - \mu_l(p_v) &= \mu_v(p_v) - \mu_l(p_v) \\ &= \int_{p_v}^{p_l} v_l(p)\mathrm{d}p \\ &\approx v_l(p_l - p_v), \end{aligned} \tag{2.7}$$

where the last expression follows if an incompressible liquid phase is assumed. Denoting the chemical potential difference[5] $\Delta\mu = \mu_l(p_v) - \mu_v(p_v)$ and multiplying both sides of Eq. (2.7) by N_l^* (for one-component systems $V^* = V_l^* + V_s^* = V_l^* \approx N_l^* v_l$, where the approximative form is again valid for an incompressible liquid phase) results in

$$\Delta G^* \approx N_l^* \Delta\mu + \gamma(R_S)A^*. \tag{2.8}$$

Let us denote the total number of molecules in the critical cluster $g^* := N_l^* + N_s^*$. Equation (2.8) suggests now writing

$$\Delta G^* = g^* \Delta\mu + \gamma A^*. \tag{2.9}$$

Obviously, this corresponds to setting $n_s^* = 0$. The resulting dividing surface is known as the *equimolecular (*or equimolar*) surface* with radius R_E. It can be shown [8] that surface tension is independent of radius—and thus has the value corresponding to plane surface, γ_∞—if $R_S = R_E$. Making

[4]This equation was first presented by Gibbs [Eq. (560) in Ref. 7].

[5]Some authors, most notably Kashchiev [e.g. 2, Chap. 2], traditionally define this difference vice versa.

this *capillarity assumption* results in the often quoted CNT expression for the work of formation

$$W^*_{\mathrm{CNT}} = g^*\Delta\mu + \gamma_\infty A^{*2} \tag{2.10}$$

$$\approx -g^* k_\mathrm{B} T \ln S + \gamma_\infty 4\pi R_E^2. \tag{2.11}$$

The second form follows after using $\mathrm{d}\mu = v\mathrm{d}p$ to express both $\mu_l(p_v)$ and $\mu_v(p_v)$ as deviations from corresponding values for coexisting phases ($p = p_e$):

$$\begin{aligned}\mu_l(p_v) &= \mu_l(p_e) + \int_{p_e}^{p_v} v_l \mathrm{d}p \\ &\approx \mu_l(p_e) + v_l(p_v - p_e)\end{aligned}$$

and

$$\begin{aligned}\mu_v(p_v) &= \mu_v(p_e) + \int_{p_e}^{p_v} v_v \mathrm{d}p \\ &\approx \mu_v(p_e) + k_\mathrm{B} T \ln \frac{p_v}{p_e},\end{aligned}$$

where incompressible liquid phase is again assumed and ideal gas law $pv_v = k_\mathrm{B}T$ is used for the vapour. By definition, $\mu_l(p_e) = \mu_v(p_e)$, so that $\Delta\mu \approx -k_\mathrm{B}T \ln S + v_l(p_v - p_e)$, where the second term is usually negligible.

Equations (2.6), (2.8) and (2.9) have a direct physical interpretation, when extended also for non-critical clusters: $\Delta G(g)$ can be decomposed into bulk term $\propto -g$ and surface term $\propto g^{2/3}$, i.e. there is a free energy benefit for forming the new phase, but this is accompanied by an energetic cost due to formation of interphase between old and new phases. Thermodynamic critical size g^* is given by the point, where either addition of a monomer into, or removal of monomer from the cluster decreases ΔG (Fig. 2.1)

Searching for the maximum of ΔG (cf. Fig. 2.1) gives

$$\left(\frac{\partial \Delta G}{\partial g}\right)_{T,p_v;g=g^*} = \Delta\mu + \left(\frac{\partial \gamma^*}{\partial g}\right)_{T,p_v} A^* + \gamma^* \left(\frac{\partial A^*}{\partial g}\right)_{T,p_v} = 0.$$

Making the capillarity approximation and assuming ideal vapour phase

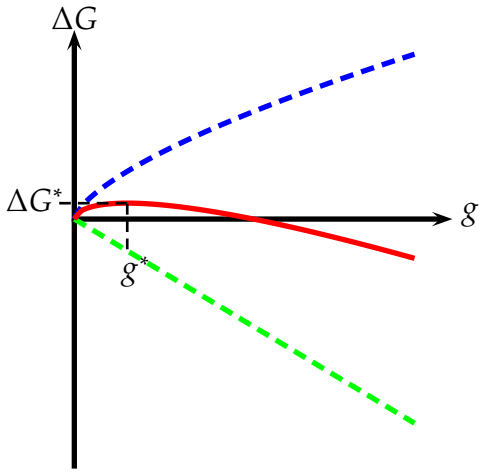

Fig. 2.1. Schematic presentation of the free energy ΔG of cluster formation as function of the total number of molecules g in the cluster: blue and green dashed lines, respectively, give the surface and bulk contributions to the total free energy difference (red) between cluster and vapour.

results in

$$\begin{aligned} 0 &= -k_{\mathrm{B}}T \ln S + \gamma_\infty \left(\frac{\partial A^*}{\partial R^*}\right)_{T,p_v;g=g^*} \left(\frac{\partial R^*}{\partial V^*}\right)_{T,p_v;g=g^*} \left(\frac{\partial V^*}{\partial g}\right)_{T,p_v;g=g^*} \\ &= -k_{\mathrm{B}}T \ln S + \frac{2v_l\gamma_\infty}{R_E}. \end{aligned} \tag{2.12}$$

Reorganising Eq. (2.12) gives the Kelvin equation. For further reference we note that to derive Eq. (1.1), the following assumptions are mandatory:

- vapour phase follows ideal gas law
- liquid phase is incompressible
- surface tension does not depend on droplet radius.

These assumptions are more obvious when mechanical arguments are used to derive the Kelvin equation [9].[6]

[6]Powles [10] has argued, based on data from molecular dynamic simulations of truncated Lennard-Jones fluid, that if vapour phase nonideality (up to the second virial

There have been several attempts to modify classical expressions for ΔG^* to include the size-dependence of surface tension, rotation and translation of the cluster, etc.; for a systematic overview, see [11]. Some more recent approaches have been discussed by Kalikmanov [4, Chaps. 3, 6, and 7].

2.1.2 Nucleation kinetics

A full kinetic treatment of vapour phase nucleation process—excluding cluster loss processes—is given by the Smoluchowski [12] coagulation equation supplemented with terms describing cluster fission, i.e. the birth–death equations for g-mers. These equations give the time derivatives of various cluster concentrations f_g as

$$\begin{aligned}\frac{\partial f_g}{\partial t} =& \frac{1}{2}\sum_{i=1}^{g-1}\beta(g-i,i)f_{g-i}(t)f_g(t) - \sum_{i=1}^{\infty}\beta(g,i)f_i(t)f_g(t) \\ &+ \sum_{i=g+1}^{\infty}\alpha(i,g)f_i(t) - \sum_{i=1}^{g-1}\alpha(g,i)f_g(t).\end{aligned} \tag{2.13}$$

Here $\beta(i,j)$ is the coagulation kernel for collision between an i-mer and a j-mer and $\alpha(i,j)$ the fission rate coefficient for the breakage of an i-mer to an $(i-j)$-mer and a j-mer; obviously $\alpha(i,i) = 0$. The factor $1/2$ at the first term in the right-hand-side is required to avoid overcounting of collisions between indistinguishable g-mers [cf. 13, pp. 551–553]. For solution of Eqs. (2.13), a boundary condition for the monomer concentration f_1 must be specified. For homogeneous nucleation from vapour, though, collisions encountered by a g-mer, $g > 1$, are assumed to be dominated by collisions with vapour phase monomers and clusters are assumed to evaporate monomers only, which leads to the Szilárd–Farkas model [14],

$$\frac{\partial f_g}{\partial t} = \beta_{g-1}f_1(t)f_{g-1}(t) - \beta_g f_1(t)f_g(t) - \alpha_g f_g(t) + \alpha_{g+1}f_{g+1}(t). \tag{2.14}$$

coefficient) and cluster compressibility are taken into account in the derivation of the Kelvin equation, contributions from these factors nearly cancel each other out. However, lennard-jonesium is a notoriously compressible substance, and further evidence is required to extend this assertion for other systems.

Here $\beta_g := \beta(g,1)$ and $\alpha_g := \alpha(g,1)$ are the condensation and evaporation rate coefficients for a g-mer, respectively. For $g > 1$, Eqs. (2.14) can be written in terms of net fluxes from size g to size $g+1$, $J_g = \beta_g f_1 f_g - \alpha_{g+1} f_{g+1}$, as

$$\frac{\partial f_g}{\partial t} = J_{g-1} - J_g. \tag{2.15}$$

The Becker–Döring [15] model consists of equations (2.14) or (2.15) together with the boundary condition of constant monomer concentration f_1.

To obtain an analytic solution for the Becker–Döring model at steady-state conditions ($\partial f_g/\partial t = 0$), the local equilibrium assumption

$$\beta_g f_1 n_g = \alpha_{g+1} n_{g+1}, \tag{2.16}$$

is invoked. Here $n_g = n_1 e^{-\Delta G_g/k_B T}$ for $g > 1$ is the so-called constrained equilibrium concentration of a g-mer and $n_1 = f_1$. This assumption derives from the microscopic reversibility condition and implies the principle of detailed balance, customarily used in physical kinetics [for a detailed discussion, see 16, Chap. 5]. Application of Eq. (2.16) to the net formation rate of $(g+1)$-mers gives

$$J_g = \beta_g n_1 n_g \left(\frac{f_g}{n_g} - \frac{f_{g+1}}{n_{g+1}} \right), \tag{2.17}$$

where the term in parenthesis is the Zel'dovich factor Z, which effectively describes the decrease of the net flux towards larger sizes due to backward flux, for the discrete case. Without this term, Eq. (2.17) applied at the critical size g^* would be formally identical to that of the transition state theory of chemical kinetics, i.e. concentration of the activated complex (here critical cluster) n_{g^*} times the forward rate constant (monomer number collision frequency). At steady-state $J_{g-1} = J_g \equiv J$, and rearrangement and summing up Eqs. (2.17) gives

$$J \left(\sum_{g=1}^{\infty} \frac{1}{\beta_g n_1 n_g} \right) = \frac{f_1}{n_1} - \frac{f_2}{n_2} + \frac{f_2}{n_2} - \frac{f_3}{n_3} + \dots$$

Invoking the boundary condition $f_G/n_G = 0$ for some G sufficiently larger than g^* terminates the telescoping sum at the right-hand-side of the

previous expression, resulting in the Becker–Döring sum for J:

$$J = \left(\sum_{g=1}^{G-1} \frac{1}{\beta_g n_1 n_g} \right)^{-1} . \tag{2.18}$$

Due to applied boundary conditions, Eq. (2.18) remarkably includes only parameters determined at constrained equilibrium. Condensation rate coefficients can be determined from the kinetic gas theory [12] as

$$\beta_g = \sqrt{8\pi k_\mathrm{B} T \left(\frac{1}{m_g} + \frac{1}{m} \right)} \left(R_g + R_1 \right)^2 . \tag{2.19}$$

Here the sum of g-mer and monomer radii, $R_g + R_i$, is interpreted as the collision radius. Since often $m_g >> m$, mass of a monomer, and $R_g >> R_1$, a resulting approximative form [Eq. (5.37)] that neglects the contribution of the incoming monomer into the scattering cross section σ is often used in practical calculations.

Equation (2.19) as given here only gives the number of collisions between a monomer and a g-mer, and it is possible that not all of these collisions lead to capture of the colliding monomer. One can introduce a size-dependent mass accommodation coefficient a_g to correct this: Formally this coefficient gives the ratio of incorporated monomers to all colliding ones. However, in practice a_g plays the role of a fudge factor to account for deviations from the kinetics described by Eq. (2.19) that can be due to occasional collisions with gas-phase dimers (or higher oligomers) [17], or scattering cross section deviating from the geometrical one based on the equimolecular dividing surface [e.g. 18, 19], which can be due to attractive forces between the cluster and monomer [20]. Usually it is assumed that $a_g \equiv 1$, i.e. $\sigma \approx \pi R_e^2 \approx \pi R_s^2$ in CNT (and consequently in most presented derivations of nucleation theorems).

If g^* is sufficiently large, one can reasonably treat the cluster size as a continuous variable and turn the differential–difference equation (2.15) into a partial differential one:

$$\frac{\partial f_g}{\partial t} = -\frac{\partial J(g,t)}{\partial g} = \frac{\partial}{\partial g} \left[a(g) \beta(g,1) n_1 n(g,t) \frac{\partial}{\partial g} \left(\frac{f(g,t)}{n(g,t)} \right) \right] . \tag{2.20}$$

where the continuum version of the microscopic balance condition has been applied. The boundary condition $f_1/n_1 = 1$ retains its form while the other boundary condition reforms to $f(g)/n(g) \to 0$ for $g \to \infty$. The steady-state solution of Eq. (2.20) with these boundary conditions is

$$J = \left(\int_1^\infty \frac{\mathrm{d}g}{a(g)\beta(g,1)n_1^2 e^{-\Delta G(g)/k_\mathrm{B}T}} \right)^{-1}. \tag{2.21}$$

To evaluate the integral, let us expand $\Delta G(g)$ into Taylor series around $g = g^*$:

$$\Delta G(g) = \Delta G(g^*) + \left.\frac{\partial \Delta G(g)}{\partial g}\right|_{g=g^*} (g - g^*) + \frac{1}{2}\left.\frac{\partial^2 \Delta G(g)}{\partial g^2}\right|_{g=g^*} (g - g^*)^2 + \ldots$$

Now the second summand is zero as $\Delta G(g)$ has a maximum at g^*. Truncating the series after quadratic term and substituting into Eq. (2.21) results in

$$\begin{aligned} J &\approx \left(\int_1^\infty \frac{\mathrm{d}g}{a(g)\beta(g,1)n_1^2 e^{-\frac{\Delta G(g^*)}{k_\mathrm{B}T}} \; e^{-\frac{(g-g^*)^2}{2k_\mathrm{B}T}\left.\frac{\partial^2 \Delta G(g)}{\partial g^2}\right|_{g=g^*}}} \right)^{-1} \\ &\approx \frac{a_{g^*}\beta_{g^*} n_1 n_{g^*}}{\int_1^\infty e^{\frac{(g-g^*)^2}{2k_\mathrm{B}T}\left.\frac{\partial^2 \Delta G(g)}{\partial g^2}\right|_{g=g^*}} \mathrm{d}g}. \end{aligned} \tag{2.22}$$

As the integral peaks strongly near g^*, $a(g)$ and $\beta(g,1)$ have been approximated by their corresponding values for the critical cluster. The remaining integral has a standard Gaussian form,[7] and approximating the lower limit of integration by $-\infty$,[8] and noticing that $\partial^2 \Delta G/\partial g^2 < 0$ in the vicinity of

[7] Physically, this implies that we treat nucleation as diffusion in size space, at least in the vicinity of the critical size g^*. This interpretation is actually more general, as already Eq. (2.17) has the form of the Fick's first law with effective concentration gradient $(f_{g+1}/n_{g+1} - f_g/n_g)$ and diffusion coefficient $D = \beta_g n_1 n_g$.

[8] To get the remaining integral in Eq. (2.22) proportional to the simplest Gaussian form, $\int e^{-g'^2}\mathrm{d}g'$, a change in integration variable from g to $g - g^*$ moves the lower limit of the remaining integration to $1 - g^*$. Now, in these new coordinates the integral peaks strongly at $g' = 0$, so approximation $1 - g^* \approx -\infty$ is reasonable as long as g^* is sufficiently larger than 1.

the critical size, we get

$$J = a_{g^*}\beta_{g^*}n_1 n_{g^*}\sqrt{\frac{1}{2\pi k_\mathrm{B}T}\left|\frac{\partial^2\Delta G(g)}{\partial g^2}\Big|_{g=g^*}\right|} = a_{g^*}\beta_{g^*}n_1 n_{g^*}Z. \tag{2.23}$$

Applying the capillarity approximation [Eq. (2.11)] for $\Delta G(g^*)$, using Eq. (2.19) in an approximative form together with the ideal gas expression $n_1 = Sp_e/k_\mathrm{B}T$ and assuming $a_{g^*} = 1$ finally gives

$$J_\mathrm{CNT} = \sqrt{\frac{2\gamma_\infty}{\pi m}}v_l S\left(\frac{p_e}{k_\mathrm{B}T}\right)^2 e^{-W^*_\mathrm{CNT}/k_\mathrm{B}T}, \tag{2.24}$$

where we have also incorporated the $1/S$-correction [21]. An alternative implementation of the $1/S$-correction is to use the *intensive work of formation*, $\Delta W^*_\mathrm{CNT} = -(g^* - 1)k_\mathrm{B}T\ln S + \gamma_\infty A^*$—or more generally following Eq. (2.8) as

$$\Delta W^* = (g^* - 1)\Delta\mu + \gamma^* A^*, \tag{2.25}$$

which also implies that there is no free energy cost to create a monomer in vapour, solving the inconsistency with the law of mass action, as it is assumed that $\gamma \to 0$ when $g \to 1$, unless capillary approximation is applied. Although the preceding derivation has highlighted several restricting assumptions required to obtain Eq. (2.24), from the viewpoint of nucleation theorems it needs to be reminded that expression with similar form are obtained from all continuum-based approaches [22].

2.2 Computational models for nucleation

There are several numerical methods that have been used to describe nucleation phenomena. One can consider the numerical solution of Eqs. (2.15), which allows inclusion of size-dependent fudge factors, cluster losses—as done in Chap. 5—and studies of non-steady-state nucleation all leading to fluxes J_g varying with the size coordinate g, as simplest computational models for nucleation. A more detailed picture and complicated behaviour follows if one disregards the Szilárd's approximation, and instead solves the full Smoluchowski coagulation equation, allowing coagulations

between all different cluster sizes present in the model. An example of this type of model is the ACDC-model [23] used in Chap. 6.[9] There are also more sophisticated approaches, ranging from classical and quantum density functional calculations for the minimum free energy of the (critical) cluster to molecular dynamics, essentially simulating the nucleation process using Newtonian mechanics to describe movement and interactions of individual molecules.

Phenomenology of *density functional* (DF) methods can traced back to the pioneering work of van der Waals [25] on phase coexistence, and independently to the later work of Ginzburg and Landau [26] on second-order phase transitions in relation to superconductivity. The common thread of various DF formalisms is to treat the density of interest—molecular density in the classical case and and electron density in the quantum case—as a continuous variable of spatial coordinates, and minimise the (free) energy of the system, which itself is a functional of the density. Classical DF calculations were first applied to phase equilibrium and nucleation by Cahn and Hilliard [27, 28], whose technique was motivated by earlier studies on magnetism of materials. In studies of homogeneous nucleation, though, the Cahn–Hilliard approach has been largely superseded by the one presented by Oxtoby and Evans [29], where instead of the original square gradient approximation, i.e. free energy functional containing a term proportional to $\nabla^2\rho$, intermolecular interactions are divided into a repulsive part that is approximated by the repulsion of hard spheres, and attractive interactions which are treated in a mean-field manner [e.g. 30, 31]. In either form, classical DF techniques allow studies of the effects of non-sharp vapour–liquid boundary, absent from the Gibbsian description of thermodynamics, and varying intermolecular pair-potential on ΔG. Most notably, the DF theory predicts the existence of spinodal in contrast to classical thermodynamic treatment. For a more detailed but concise description of the classical DF methods, see [2, Chap. 8] and [4, Chap. 5]. In this thesis, results of classical DF calculations are used—together with results from Monte Carlo

[9] Collisions between all available particle sizes are also featured in aerosol dynamics models: Here, however, clusters/particles are not followed at molecular resolution, but are lumped together into size bins in sectional models or represented by superposition of continuous functions when the modal description is followed; nucleation is usually treated in black box manner, i.e. a prescribed function is used to insert new particles into the smallest size bin or mode. The UHMA-model [24] used in Chap. 6 is a sectional model.

simulations—to motivate the functional form for the displacement barrier height in Chap. 4.

Quantum chemical methods come in two flavours. Both of these methods are based on the numerical solution of the Schrödinger equation for the studied system, but use different numerical approaches. Typically, the Born–Oppenheimer approximation, differentiating the time scales for the motions of electrons and nuclei, allowing to treat the former ones instantaneously adjusted to the later ones, is done. Also relativistic effects are often ignored, especially for the light atoms[10] relevant for the atmospheric NPF. *Ab initio* methods can be roughly described as numerical solutions of the Schrödinger equation using superposition of individual electronic wavefunctions to describe the total electronic wavefunction of the system. Another approach, which has been used in calculations reported in Chap. 6, is the quantum DF treatment of electrons, which follows from the development of the Thomas–Fermi model for the electron gas by Hohenberg and Kohn [32]; for a more detailed description of the methods used in Chap. 6 see Refs. [33, Sec. 2.3] and [34, Chap. 2].

Both classical and quantum density functional methods can be used to solve the minimum-energy configuration of the system (droplet/cluster, respectively). Thus they are static models, and do not give any information on the dynamics of the nucleation process. That is to say that those methods have to be supplemented by a classical description of cluster population dynamics, i.e. Szilárd–Farkas or Smoluchowski model, to obtain actual nucleation rates. The same is also true for *Monte Carlo* (MC) methods: Here, however, the focus is not solely on the thermodynamic properties of the critical cluster, but rather in an efficient sampling of the available phase space for determination of the properties of non-equilibrium clusters. In practice, this is done using a random sampling algorithm [35]; several alternative methods exist for calculating the moves from one state of the vapour–cluster system into another, though generally the probability of each move is weighted by a related Boltzmann-factor. In a sense, MC calculations provide a series of snapshots of the system under constrained (pseudo-)equilibrium. MC methods were first applied to homogeneous nucleation from vapour by Lee et al. [36]. To study truly nonequilibrium dynamics of nucleation, molecular dynamics (MD) calculations can be per-

[10] See, however, footnote 3 on p. 3.

formed. Here the behaviour of the system is modelled solving Newton's (or Hamilton's) equations of motion for each molecule during each time step. Although the MD approach mimics the actual nucleation process in nature, due to computational restrictions only systems with experimentally unrealistic saturation ratios and simplified classical intermolecular potentials[11] have been studied so far; a computationally more feasible alternative, known as indirect nucleation simulation, is to study the stability of a cluster initially present in simulation cell [39]. Further deviations from the physics of real world systems, hindering direct comparisons with nucleation experiments, are due to finite-size effects [40], although a recent study [41] suggests that at least for simple systems, there is a possibility for analytical correction of these effects. For a more detailed description of MC and MD methods in nucleation studies, see [4, Chap. 8].

From the viewpoint of nucleation theorems, there are some restrictions on how MC and MD simulations can be used (in case of DF calculations, the application of the first nucleation theorem is trivial, as it can be derived directly from a density functional theory [e.g. 2, 42, Chap. 8.]): If a consistent comparison with a CNT-type theory is required, properties of bulk phases have to be evaluated using the exactly same conditions concerning e.g. intermolecular potential functions as used in nucleation simulations [43]. For the evaluation of the critical cluster size, the cluster definition used in simulations is also of prior importance: the most used definitions are based on the total energy of the cluster [36] or connectivity [44, 45]. Napari et al. [39] compared the predictions of the first nucleation theorem with the results from both direct and indirect MD calculations for a Lennard-Jones fluid: Although they could not reach definitive conclusions, critical cluster sizes derived using the first nucleation theorem had different temperature dependence than those obtained from direct and indirect simulations. At a lower temperature ($T \approx 0.60T_c$), the critical size from the first nucleation theorem corresponded to reasonably well with both direct and indirect simulations with cluster definitions based on the conditions of a molecule belonging to the cluster if three or four other molecules lay within distance 1.5σ, where σ is the Lennard-Jones size parameter. At a higher temperature ($T \approx 0.74T_c$), critical sizes from the first nucleation theorem corresponded cluster definition with only one or two other molecules within distance

[11] There are, though, emerging attempts for *ab initio* MD calculations for atmospherically relevant systems, see [37] and [38, Chap. 5].

of 1.5σ. In both cases, the results conflict with a previous study [46], although the critical cluster sizes obtained from the first nucleation theorem are consistently larger than those given by the Kelvin equation, but smaller than those estimated from the density profile. Also results from direct simulations suggested denser clusters than indirect simulations. It is thus likely that for more complex systems, the possibilities to use MD or MC simulations to confirm the results obtained using nucleation theorems are quite limited.

2.3 Nucleation experiments

Studying vapour-to-liquid nucleation experimentally requires controlled means to produce supersaturared vapour, and a method to observe forming droplets. The first experiments [47–49] relied on the expansion of vapour to achieve high enough saturation ratios. A notable advancement was achieved by Franck and Hertz [50], who applied the thermal diffusion chamber, originally developed to study ions, on homogeneous nucleation, allowing for the first time continuous measurements of new particle formation in controlled conditions, at least in principle. In both cases, the deducible parameter was so-called critical or on-set saturation ratio S^*, i.e. the degree of supersaturation producing high enough new particle formation rate that the formed mist could be detected visually. Since these pioneering works, most experimental setups can be largely assigned into two groups that are based either on adiabatic expansion—including expansion and nucleation pulse chambers, expansion wave tubes and supersonic nozzles—or a temperature gradient and different temperature dependencies of partial and equilibrium vapour pressures—thermal diffusion chambers and laminar flow tubes. For a concise overview of the operation principles, see Ref. [51]; also setups based e.g. on turbulent mixing have been utilised, but to a lesser extent [52].

Development of photographic techniques enabled first quantitative estimations of the nucleation rate J from expansion chambers [e.g. 53], when the number of formed droplets was counted from photograph plates, and this information was converted into nucleation rate with the estimated length of the nucleation pulse. Knowledge of J as function of S and T then

allowed the first applications of the first nucleation theorem in vapour-to-liquid nucleation. Automated photographic methods are still used for droplet counting, but have been supplemented by methods based on total light attenuation,[12] and in the case of expansion-based devices and higher nucleation rates with those based of x-ray [55], neutron [56], or constant angle Mie scattering [57]. To estimate $J(S,T)$ [or $J(S_1, S_2, \ldots, T, P)$], one also needs to know S and T. These are either calculated from the known expansion rate or—in the case of diffusion based devices—from the flux equations for mass and energy transfer inside the measurement device. In both cases, the properties of carrier gas–vapour mixture are usually assumed to be given by the ideal gas equation of state. For the searched correspondence between S and J, the effect of vapour consumption due to condensation on surfaces and growth of freshly formed particles has to be taken into account or minimise. In expansion based devices, this is usually obtained by separation of nucleation and growth with nucleation pulse techniques [58]. In supersonic nozzles, however, there is no clear-cut separation of nucleation and growth regimes, and static pressure measurement along the flow axis are used to identify the location of the nucleation zone. In diffusion based devices, freshly nucleated particles are transported away from the nucleation zone either via gravitational deposition, thermophoretic movement or flow of the medium.

In laboratory studies miming atmospheric NPF process, as well as in field measurements, both production of sulphuric acid and/or oxidised organics and scavenging of vapour, clusters and particles occur simultaneously with nucleation: Here measurements are typically done using a differential mobility particle sizer (DMPS), consisting of size-classification of charged particles using a differential mobility analyser [59], followed by optical counting of particles using a condensation particle counter [60]. Typically measurements have to be done at a size larger than the critical one, e.g. particles of 3 or 5 nm by (mobility) diameter, and then the formation rate at the estimated critical size J_{d^*} is back-calculated [e.g. 61]. In some cases, particle size magnifiers, i.e. condensation particle counters using two different condensing vapours, are used to retrieve number concentrations down to approximately 1-nm particles [62]. For more detailed description of the measurement protocol, see Ref. [63]. For the detection of nucleating

[12]For a case study comparing photographic and light attenuation based methods, see Ref. [54].

vapours, various novel mass spectrometers have been introduced during last decades [64], most notably chemical ionisation mass spectrometers for detection of sulphuric acid [65], and more recently also for ammonia and amines [66]. However, in several, especially older studies the concentrations of potentially nucleating species are estimated using chemical reaction rate calculations [e.g. 67], off-line techniques [e.g. 68], or statistical proxies [e.g. 69]. When interpreting results obtained from nucleation theorems, uncertainties introduced by indirect determination of the concentration of nucleating species and the actual nucleation rate on the exact value of the derivative need to be considered.

References

[1] J. E. McDonald. Homogeneous nucleation of vapor condensation. II. Kinetic aspects. *American Journal of Physics* 31 (1963), 31–41.

[2] D. Kashchiev. *Nucleation: Basic Theory with Applications*. Oxford: Butterworth–Heinemann, 2000.

[3] H. Vehkamäki. *Classical Nucleation Theory in Multicomponent Systems*. Berlin: Springer, 2006.

[4] V. Kalikmanov. *Nucleation Theory*. Dordrecht: Springer, 2013.

[5] P. G. Debenedetti. *Metastable Liquids: Concepts and Principles*. Princeton, N.J.: Princeton University Press, 1996.

[6] A. Laaksonen, R. McGraw and H. Vehkamäki. Liquid-drop formalism and free-energy surfaces in binary homogeneous nucleation theory. *Journal of Chemical Physics* 111 (1999), 2019–2027.

[7] J. W. Gibbs. On the equilibrium of heterogeneous substances (concluded). *Transactions of the Connecticut Academy of Arts and Sciences* 3 (1878), 343–524.

[8] R. C. Tolman. The effect of droplet size on surface tension. *Journal of Chemical Physics* 17 (1949), 333–337.

[9] K. P. Galvin. A conceptually simple derivation of the Kelvin equation. *Chemical Engineering Science* 60 (2005), 4659–4660.

[10] J. G. Powles. On the validity of the Kelvin equation. *Journal of Physics A* 18 (1985), 1551–1560.

[11] R. B. McClurg and R. C. Flagan. Critical comparison of droplet models in homogeneous nucleation theory. *Journal of Colloid and Interface Science* 201 (1998), 194–199.

[12] M. Smoluchowski. Drei Vorträge über Diffusion, Brownische Molekular Bewgung und Koagulation von Kolloidteilchen. *Physikalische Zeitschrift* 17 (1916), 557–571 and 587–599.

[13] J. H. Seinfeld and S. N. Pandis. *Atmospheric Chemistry and Physics: From Air Pollution to Climate Change*. 3rd ed. Hoboken, N.J.: Wiley, 2016.

[14] L. Farkas. Keimbildungsgeschwindigket in übersättigten Dämpfen. *Zeitschrift für physikalische Chemie* 175 (1927), 236–242.

[15] R. Becker and W. Döring. Kinetische Behandlung der Keimbildung in übersättigten Dämpfen. *Annalen der Physik* 416 (1935), 719–752.

[16] K. Hansen. *Statistical Physics of Nanoparticles in the Gas Phase*. Dordrecht: Springer, 2013.

[17] J. L. Katz, H. Saltsburg and H. Reiss. Nucleation in associated vapors. *Journal of Colloid and Interface Science* 21 (1966), 560–568.

[18] J. Lengyel, J. Kočišek, V. Poterya, A. Pysanenko, P. Svrčková, M. Fárnik, D. K. Zaouris and J. Fedor. Uptake of atmospheric molecules by ice nanoparticles: Pickup cross sections. *Journal of Chemical Physics* 137 (2012), 034304.

[19] I. Braud, J. Boulon, S. Zamith and J.-M. L'Hermite. Attachment of water and alcohol molecules onto water and alcohol clusters. *Journal of Physical Chemistry A* 119 (2015), 6017–6023.

[20] O. V. Vasil'ev and H. Reiss. Effect of the attractive potential of a drop in vapor phase nucleation. *Physical Review E* 54 (1996), 3950–3954.

[21] W. G. Courtney. Remarks on homogeneous nucleation. *Journal of Chemical Physics* 35 (1961), 2249–2250.

[22] D. W. Oxtoby. Homogeneous nucleation: theory and experiment. *Journal of Physics: Condensed Matter* 4 (1992), 7627–7650.

[23] M. J. McGrath, T. Olenius, I. K. Ortega, V. Loukonen, P. Paasonen, T. Kurtén, M. Kulmala and H. Vehkamäki. Atmospheric Cluster Dynamics Code: A flexible method for solution of the birth–death equations. *Atmospheric Chemistry and Physics* 12 (2012), 2345–2355.

[24] H. Korhonen, K. E. J. Lehtinen and M. Kulmala. Multicomponent aerosol dynamics model UHMA: Model development and validation. *Atmospheric Chemistry and Physics* 4 (2004), 757–771.

[25] J. D. van der Waals. Thermodynamische theorie der capillariteit in de onderstelling van continue dichtheidsverandering. *Verhandelingen der Koninklijke Akademie van Wetenschappen, Afdeeling Natuurkunde. Eerste Sectie: Wiskunde, Natuurkunde, Scheikunde, Kristallenleer, Sterrenkunde, Weerkunde, en Ingenieurswetenschappen* 1 (1893), 1–56.

[26] V. I. Ginzburg and L. D. Landau. K teorii sverkhrovodimosti. *Žurnal Eksperimental'noi i Teoreticheskoi Fiziki* 20 (1950), 1064–1082.

[27] J. W. Cahn and J. E. Hilliard. Free energy of a nonuniform system. I. Interfacial free energy. *Journal of Chemical Physics* 28 (1958), 258–267.

[28] J. W. Cahn and J. E. Hilliard. Free energy of a nonuniform system. III. Nucleation in a two-component incompressible fluid. *Journal of Chemical Physics* 31 (1959), 688–699.

[29] D. W. Oxtoby and R. Evans. Nonclassical nucleation theory for the gas–liquid transition. *Journal of Chemical Physics* 89 (1988), 7521–7530.

[30] R. McGraw and A. Laaksonen. Scaling properties of the critical nucleus in classical and molecular-based theories of vapor–liquid nucleation. *Physical Review Letters* 76 (1996), 2754–2757.

[31] V. Talanquer. A new phenomenological approach to gas-liquid nucleation based on the scaling properties of the critical nucleus. *Journal of Chemical Physics* 106 (1997), 9957–9960.

[32] P. Hohenberg and W. Kohn. Inhomogeneous electron gas. *Physical Review* 136 (1964), B864–B871.

[33] T. Olenius. *Cluster Population Simulations as a Tool to Probe Particle Formation Mechanisms*. PhD thesis. Helsingin yliopisto, 2015.

[34] O. Kupiainen-Määttä. *From Cluster Properties to Concentrations and from Concentrations to Cluster Properties*. PhD thesis. Helsingin yliopisto, 2016.

[35] N. Metropolis and S. Ulam. The Monte Carlo method. *Journal of the American Statistical Association* 44 (1949), 335–341.

[36] J. K. Lee, J. A. Barker and F. F. Abraham. Theory and Monte Carlo simulation of physical clusters in the imperfect vapor. *Journal of Chemical Physics* 58 (1973), 3166–3180.

[37] V. Loukonen, I.-F. W. Kuo, M. J. McGrath and H. Vehkamäki. On the stability and dynamics of (sulfuric acid) (ammonia) and (sulfuric acid) (dimethylamine) clusters: A first-principles molecular dynamics investigation. *Chemical Physics* 428 (2014), 164–174.

[38] J. L. Stinson. *Modelling microscopic clusters of sulphuric acid and water relevant to atmospheric nucleation*. PhD thesis. University College London, 2015.

[39] I. Napari, J. Julin and H. Vehkamäki. Cluster size in direct and indirect molecular dynamics simulation of nucleation. *Journal of Chemical Physics* 131 (2009), 244511.

[40] J. Wedekind, D. Reguera and R. Strey. Finite-size effects in simulations of nucleation. *Journal of Chemical Physics* 125 (2006), 214505.

[41] Ø. Wilhelmsen and D. Reguera. Evaluation of finite-size effects in cavitation and droplet formation. *Journal of Chemical Physics* 142 (2015), 064703.

[42] J. W. P. Schmelzer. Comments on the nucleation theorem. *Journal of Colloid and Interface Science* 242 (2001), 354–372.

[43] S. J. Keasler and J. I. Siepmann. Understanding the sensitivity of nucleation free energies: The role of supersaturation and temperature. *Journal of Chemical Physics* 143 (2015), 164516.

[44] F. H. Stillinger. Rigorous basis of the Frenkel–Band theory of association equilibrium. *Journal of Chemical Physics* 38 (1963), 1486–1494.

[45] P. R. ten Wolde and D. Frenkel. Computer simulation study of gas–liquid nucleation in a Lennard-Jones system. *Journal of Chemical Physics* 109 (1998), 9901–9918.

[46] J. Wedekind and D. Reguera. What is the best definition of a liquid cluster at the molecular scale? *Journal of Chemical Physics* 127 (2007), 154516.

[47] R. von Helmholtz. Untersuchungen über Dämpfe und Nebel, besonders über solche von Lösungen. *Annalen der Physik und Chemie* 27 (1886), 508–543.

[48] C. Barus. Colored cloudy condensation as depending on air temperature and dust-contents, with a view to dust counting. *American Meteorological Journal* 10 (1893), 12–34.

[49] C. T. R. Wilson. Condensation of water vapour in the presence of dust-free air and other gases. *Philosophical Transactions of the Royal Society of London, Series A* 189 (1897), 265–307.

[50] J. P. Franck and H. G. Hertz. Messung der kritischen Übersättigung von Dämpfen mit der Diffusionsnebelkammer. *Zeitschrift für Physik* 143 (1956), 559–590.

[51] F. Maršík, T. Němec, J. Hrubý, P. Demo, Z. Kožíšek, V. Petr and M. Kolovratník. Binary homogeneous nucleation in selected aqueous vapor mixtures. *Journal of Solution Chemistry* 37 (2008), 1671–1708.

[52] R. H. Heist and H. He. Review of vapor to liquid homogeneous nucleation experiments from 1968 to 1992. *Journal of Physical and Chemical Reference Data* 23 (1994), 781–804.

[53] L. B. Allen and J. L. Kassner, Jr. The nucleation of water vapor in the absence of particulate matter and ions. *Journal of Colloid and Interface Science* 30 (1969), 81–93.

[54] D. Brus, V. Ždímal and H. Uchtmann. Homogeneous nucleation rate measurements in supersaturated water vapor II. *Journal of Chemical Physics* 131 (2009), 074507.

[55] B. E. Wyslouzil, G. Wilemski, R. Strey, S. Seifert and R. E. Winans. Small angle X-ray scattering measurements probe water nanodroplet evolution under highly non-equilibrium conditions. *Physical Chemistry Chemical Physics* 9 (2007), 5353–5358.

[56] B. E. Wyslouzil, J. L. Cheung, G. Wilemski and R. Strey. Small angle neutron scattering from nanodroplet aerosols. *Physical Review Letters* 79 (1997), 431–434.

[57] P. E. Wagner. A constant-angle Mie scattering method (CAMS) for investigation of particle formation processes. *Journal of Colloid and Interface Science* 105 (1985), 456–467.

[58] R. Strey, P. E. Wagner and Y. Viisanen. The problem of measuring homogeneous nucleation rates and the molecular contents of nuclei: Progress in the form of nucleation pulse measurements. *Journal of Physical Chemistry* 98 (1994), 7748–7758.

[59] R. C. Flagan. Electrical mobility methods for submicrometer particle characterization. In: *Aerosol Measurement: Principles, Techniques, and Applications*. Ed. by P. Kulkarni, P. A. Baron and K. Willeke. 3rd ed. Hoboken, N.J.: Wiley, 2011. Chap. 15.

[60] Y.-S. Cheng. Condensation particle counters. In: *Aerosol Measurement: Principles, Techniques, and Applications*. Ed. by P. Kulkarni, P. A. Baron and K. Willeke. 3rd ed. Hoboken, N.J.: Wiley, 2011. Chap. 17.

[61] K. E. J. Lehtinen, M. Dal Maso, M. Kulmala and V.-M. Kerminen. Estimating nucleation rates from apparent particle formation rates and vice versa: Revised formulation of the Kerminen–Kulmala equation. *Journal of Aerosol Science* 38 (2007), 988–994.

[62] M. Sipilä, T. Berndt, T. Petäjä, D. Brus, J. Vanhanen, F. Stratmann, J. Patokoski, R. L. Mauldin, III, A.-P. Hyvärinen, H. Lihavainen and M. Kulmala. The role of sulfuric acid in atmospheric nucleation. *Science* 327 (2010), 1243–1246.

[63] M. Kulmala, T. Petäjä, T. Nieminen, M. Sipilä, H. E. Manninen, K. Lehtipalo, M. Dal Maso, P. P. Aalto, H. Junninen, P. Paasonen, I. Riipinen, K. E. J. Lehtinen, A. Laaksonen and V.-M. Kerminen. Measurement of the nucleation of atmospheric aerosol particles. *Nature Protocols* 7 (2012), 1651–1667.

[64] M. Kulmala, T. Petäjä, M. Ehn, J. Thornton, M. Sipilä, D. R. Worsnop and V.-M. Kerminen. Chemistry of atmospheric nucleation: On the recent advances on precursor characterization and atmospheric clusters composition in connection with atmospheric new particle formation. *Annual Review of Physical Chemistry* 65 (2014), 21–37.

[65] F. Eisele and D. Tanner. Measurement of the gas phase concentration of H_2SO_4 and methane sulfonic acid and estimates of H_2SO_4 production and loss in the atmosphere. *Journal of Geophysical Research: Atmospheres* 98 (1993), 9001–9010.

[66] Y. You, V. P. Kanawade, J. A. de Gouw, A. B. Guenther, S. Madronich, M. R. Sierra-Hernández, M. Lawler, J. N. Smith, S. Takahama, G. Ruggeri, A. Koss, K. Olson, K. Baumann, R. J. Weber, A. Nenes, H. Guo, E. S. Edgerton, L. Porcelli, W. H. Brune, A. H. Goldstein and S.-H. Lee. Atmospheric amines and ammonia measured with a chemical ionization mass spectrometer (CIMS). *Atmospheric Chemistry and Physics* 14 (2014), 12181–12194.

[67] A. Metzger, B. Verheggen, J. Dommen, J. Duplissy, A. S. H. Prevot, E. Weingartner, I. Riipinen, M. Kulmala, D. V. Spracklen, K. S. Carslaw and U. Baltensperger. Evidence for the role of organics in aerosol particle formation under atmospheric conditions. *Proceedings of the National Academy of Sciences U. S. A.* 107 (2010), 6646–6651.

[68] R. Janson, K. Rosman, A. Karlsson and H.-C. Hansson. Biogenic emissions and gaseous precursors to forest aerosols. *Tellus B* 53 (2001), 423–440.

[69] S. Mikkonen, S. Romakkaniemi, J. N. Smith, H. Korhonen, T. Petäjä, C. Plass-Duelmer, M. Boy, P. H. McMurry, K. E. J. Lehtinen, J. Joutsensaari, A. Hamed, R. L. Mauldin III, W. Birmili, G. Spindler, F. Arnold, M. Kulmala and A. Laaksonen. A statistical proxy for sulphuric acid concentration. *Atmospheric Chemistry and Physics* 11 (2011), 11319–11334.

3 Nucleation theorems

> . . . [P]henomenologically, i.e., without reference to a specified (given by a concrete model, including Gibbs's) cluster excess energy. . . That is what makes the original derivation so general: it is exactly as general as the law of energy conservation.
>
> – D. Kashchiev on the first nucleation theorem, as cited in Ref. [1]

3.1 Background

Classical nucleation theory (CNT) shares common foundations with the other classical rate theories—such as the transition state theory [2], Kramers' reaction rate theory [3], and Marcus' theory of electron transfer [4]—including the quasi-equilibrium (or constrained equilibrium) assumption and reduction of the number of reaction coordinates, which in the case of CNT means that the extent of the process can be given solely in terms of cluster size. The latter property is related to the fact that classical rate theories all make the assumption of a single bottleneck, or a rate-limiting step, for the process. Due to these common foundations, classical rate theories also share the property that it is possible to use these theories "in reverse" to extract the properties of the transition state from experimental data [5]. In case of nucleation, this was already exploited by Barus [6]—who, interestingly though, did not make any explicit reference to Lord Kelvin's work that he was obviously aware of—and Wilson [7], who while reporting their pioneering measurements commented on the size of the critical nucleus for condensation, assuming it to composed of water molecules, based on measured critical supersaturations. There is nothing new, either, in using

nucleation measurements to estimate the size-dependence of the surface tension while resorting to the CNT expressions, although this has been rationalised in terms of nucleation theorems only more recently [8, 9]. It has been pointed out that the term *nucleation theorem* underestimates the validity of these theorems, as such relations hold also for other activated processes described by classical rate theories [10], thus commodifying the above-mentioned "reverse engineering" property. On the other hand, this also implies that nucleation theorems may not be as general as the principle of the conservation of energy, as those may be limited by some of the assumptions of the classical rate theories.

Since the first derivations based on CNT [e.g. 11, p. 18], more general thermodynamic derivations of the first nucleation theorem have been given by Kashchiev and Oxtoby [12, 13], whose main result is[1]

$$\left(\frac{\partial W^*}{\partial \Delta\mu}\right)_T = g^* \tag{3.1}$$

that follows from Eq. (2.9), if $(\partial\gamma_E/\partial\Delta\mu)_T + (\partial\left\{R_E[\partial\gamma/\partial R]_{R=R_E}\right\}/\partial 2\Delta\mu)_T = 0$, i.e. surface contribution to the nucleation barrier does not depend on the supersaturation. (When a more specific designation is required, we denote the *thermodynamic critical size* given by Eq. (3.1) with g^*_{td}.) Alternatively, one can take the derivative with respect to the old phase chemical potential μ_v, in which case

$$\begin{aligned}\left(\frac{\partial W^*}{\partial \mu_v}\right)_T &= \left(\frac{\partial W^*}{\partial \Delta\mu}\right)_T \left(\frac{\partial \Delta\mu}{\partial \mu_v}\right)_T \\ &= \left\{\left(\frac{\partial \mu_l}{\partial \mu_v}\right)_{p=p_v;T} - 1\right\} g^* \\ &= \left(\frac{\rho_v}{\rho_l} - 1\right) g^* =: -\Delta g^*,\end{aligned} \tag{3.2}$$

[1] Again, Kashchiev and Oxtoby defined $\Delta\mu$ in an opposite manner to presented here, so their result actually reads as

$$\left(\frac{\partial W^*}{\partial \Delta\mu}\right)_T = -g^*.$$

Of course, when expressing $\Delta\mu$ in terms of a measurable quantity, i.e. S, the resulting equations do agree.

where the definition $\Delta\mu = \mu_l(p_v) - \mu_v(p_v)$ has been applied together with the Maxwell relation $\mathrm{d}\mu = v\mathrm{d}p$ that holds at constant temperature; $\rho_l = 1/v_l(p_v)$ and $\rho_v = 1/v_v(p_v)$ are the molecular densities of coexisting liquid and gas phases, respectively. The physical interpretation of the term $(1 - \rho_v/\rho_l)$ is the subtraction of the number of vapour-phase molecules occupying the volume corresponding the critical cluster prior nucleation.

Other authors have provided proofs for the first nucleation theorem based on statistical mechanics [14–17], fluctuation theory [18], or physical kinetics [19, 20, see also 15].[2] The last mentioned derivations differ from other proposed ones as no functional relationship in form of Eq. (1.2) is assumed, but instead the nucleation theorems are deduced directly from the Becker–Döring sum (2.18); these results can be described as *kinetic nucleation theorems*, while other derivations produce—for a lack of a better term—*thermodynamic nucleation theorems*. This is to say that the rate-forms of the thermodynamic nucleation theorems are basically differential relations in form

$$k_\mathrm{B}T\left(\frac{\partial \ln J}{\partial \Delta\mu}\right)_T = k_\mathrm{B}T\left(\frac{\partial \ln K}{\partial \Delta\mu}\right)_T - \left(\frac{\partial W^*}{\partial \Delta\mu}\right)_T = -1 - g^*,$$

which follows if one combines Eq. (3.1)—or some corresponding, in principle exact relationship between W^* and $\Delta\mu$, also referred as the first nucleation theorem—with a CNT-type rate expression.

As the distinction between extensive and intensive variables breaks up for small clusters, as demonstrated e.g. by the aforementioned dependence of the surface tension on cluster size, validity of original thermodynamic derivations [12, 13] can be questioned. One possible way to fix this limitation is to resort to Hill's small system thermodynamics [22, 23],[3] where the thermodynamic system is divided into an ensemble of small systems that can act as heat, pressure and particle reservoirs for each other. Derivations based on small system thermodynamics are given below, for derivations

[2]This classification is not unambiguous: for example, Hrubý et al. [21] have given a derivation of the first nucleation theorem loosely based on association–dissociation treatment of vapour-phase clusters that has common features with derivations based on physical and chemical kinetics, though actual results are then obtained using a CNT-type expression for J.

[3]García-Morales et al. [24] have pointed out the correspondence of small system thermodynamics and the non-extensive entropy formulation of Tsallis [25].

based on statistical mechanics and chemical kinetics, please see Appendices 3.A.1 and 3.A.2. The kinetic derivation of the first nucleation theorem is reviewed and extended in Chaps. 5 and 6, see also [26, Sec. 3.2.1].

The first rigorous derivation of the first nucleation theorem (in terms of W^*) was given by Hill using small system thermodynamics [22], though no connection to nucleation was made. The derivation has been repeated by Ford [27] and Kalikmanov [28, Sec. 4.4], see also [29]; Bowles et al. [10] have given an equivalent derivation in terms of constrained equilibrium thermodynamics [30]. In small system thermodynamics, the internal energy of the whole system is given as

$$\begin{aligned} \mathrm{d}U_t &= T\mathrm{d}\eta_t - P\mathrm{d}V_t + \mu_v \mathrm{d}g_t + \mathrm{d}X \\ &= T\mathrm{d}\eta_t - P\mathrm{d}V_t + \mu_v \mathrm{d}g_t + \mu_{\mathcal{N}}\mathrm{d}\mathcal{N}, \end{aligned} \tag{3.3}$$

where $\mathcal{N}$ is the number of subsystems (replicas) and total entropy, volume and number of molecules are given respectively as $\eta_t = \mathcal{N}\eta$, $V_t = \mathcal{N}V$, and $g_t = \mathcal{N}g$ (the surface energy contribution can be implicitly incorporated into U [23, e.g. p. 83], so there is no need to differentiate g and N here). P is the total pressure of the system that for a pure vapour we are considering momentarily to equal the partial pressure p_v. The internal energy of a single subsystem retains the familiar form,

$$\mathrm{d}U = T\mathrm{d}\eta - P\mathrm{d}V + \mu_v \mathrm{d}g. \tag{3.4}$$

Since replicas are free to exchange matter, energy, and volume with each other, small system thermodynamics allows us to consider "completely open" systems [31, 32], for which

$$\mathrm{d}X = -\eta \mathrm{d}T + V\mathrm{d}P - g\mathrm{d}\mu_v \tag{3.5}$$

gives the differential of the free energy for a single subsystem (this is in contrast to classical thermodynamics, where thermodynamic potential describing a completely open system is the zero potential, manifested by the Gibbs–Duhem equation). It is possible to construct the partition function Υ for completely open systems, so that

$$\begin{aligned} X &= -k_\mathrm{B}T \ln \Upsilon \\ &= -k_\mathrm{B}T \ln \sum_V \Xi e^{-PV/k_\mathrm{B}T}, \end{aligned} \tag{3.6}$$

where Ξ is the usual grand canonical partition function.

3.2 First nucleation theorem

From Eq. (3.5) we have $W^* = \Delta X^* = X^* - X_0$, where subscript 0 refers again to initial, homogeneous vapour at given T and P (remember that for a completely open system, one can formally vary T, P, and μ_v independently, see [23, Chap. 10]). Redifferentiating results in

$$\mathrm{d}W^* = \mathrm{d}\Delta X^* = -\Delta\eta^*\mathrm{d}T - \Delta g^*\mathrm{d}\mu_v + \Delta V^*\mathrm{d}P, \tag{3.7}$$

where $\Delta\eta^* = \eta^* - \eta_0$, $\Delta g^* = g^* - g_0$, and $\Delta V^* = V^* - V_0$ give the excess entropy, number of particles, and volume, respectively, due to formation of a critical cluster. Equation (3.7) gives now immediately[4]

$$\left(\frac{\partial\Delta X^*}{\partial\mu_v}\right)_{T,P} = -\Delta g^*. \tag{3.8}$$

Assuming now that the prefactor K is given by Eq. (2.24) results in

$$\begin{aligned}\left(\frac{\partial\ln J}{\partial\ln S}\right)_{T,P} &= -\frac{1}{k_\mathrm{B}T}\left(\frac{\partial W^*}{\partial\ln S}\right)_{T,P} + \left(\frac{\partial\ln K}{\partial\ln S}\right)_{T,P}\\ &\approx g^* + \left(\frac{\partial\ln K}{\partial\ln S}\right)_{T,P}\\ &\approx g^* + 1,\end{aligned} \tag{3.9}$$

where we have again assumed ideal gas behaviour for the supersaturated vapour with a corresponding form for the chemical potential, and identified the contribution due to homogeneous vapour via X_0 with the corresponding term, $(\rho_v/\rho_l)g^*$ in Eq. (3.2).

3.2.1 Scaling of nucleation rates based on the first nucleation theorem and the Kelvin equation

Based on the initial good agreement between predictions of the first nucleation theorem and the Kelvin equation [e.g. 33], McGraw and Laaksonen

[4]Strictly speaking, Eq. (3.8) gives the ensemble average excess number of molecules, or the excess *small system thermodynamic critical size*, $\langle\Delta g\rangle$. Assuming ergodic-type condition, it is not far fetched to identify $\langle g\rangle$ with the kinetic critical size $\bar{g}$ (see Ref. [19] or Sec. 5.2). We shall, however, neglect the difference of Δg^* and $\langle\Delta g\rangle$ for the time being.

[34] proposed simple scaling relations for g^* and W^*. A concise derivation of these, following Koga and Zeng [35], is given below.

From Eqs. (2.6) and (2.9) it follows that if one makes the capillarity approximation,

$$W^*_{\mathrm{CNT}} = -\frac{g^*_{\mathrm{CNT}}\Delta\mu}{2}. \tag{3.10}$$

Let us assume for a moment that the functional dependence of W^* on $\Delta\mu$ is correctly (i.e. beyond CNT) predicted by Eq. (3.10). Differentiating with respect to $\Delta\mu$ at constant T (and P) gives

$$\begin{aligned}\left(\frac{\partial W^*}{\partial\Delta\mu}\right)_T &= -\frac{g^*}{2} - \frac{\Delta\mu}{2}\left(\frac{\partial g^*}{\partial\Delta\mu}\right)_T \\ &= g^*,\end{aligned}$$

where the second equality follows from the first nucleation theorem, e.g. Eq. (3.1). Reorganising gives

$$3g^* + \Delta\mu\left(\frac{\partial g^*}{\partial\Delta\mu}\right)_T = 0,$$

which results in a generalised Kelvin or Gibbs–Thomson equation written in terms g^* and $\Delta\mu$,

$$g^* = \frac{C(T)}{(\Delta\mu)^3}, \tag{3.11}$$

where the coefficient of proportionality is a function of temperature only, and in case of CNT is given as $C(T) = 32\pi\gamma_\infty^3/3\rho_l^2$. Using Eq. (3.1) to integrate (3.11) and substituting the CNT expression for $C(T)$ gives

$$\begin{aligned}W^* &= -\frac{C(T)}{2(\Delta\mu)^2} - D(T) \\ &= W^*_{\mathrm{CNT}} - D(T),\end{aligned} \tag{3.12}$$

where the second constant of integration, D, is a function of temperature (and possibly total pressure) only, and is known as the *displacement barrier height*.

DF calculations [34, 36, 37] have lent further support for the ansatz above, at least for simple liquids. A straightforward physical interpretation of

$D(T)$ is the value of W^*_{CNT} evaluated at the spinodal. Alternatively, $D(T)$ can be expressed in terms related to the size dependence of the surface tension [36] and, in case of a more complete expansion of W^* in powers of $\Delta\mu$ [35], compressibility of the cluster.

3.3 Second nucleation theorem

Similarly to the first nucleation theorem, from Eq. (3.7) it follows that

$$\left(\frac{\partial \Delta X^*}{\partial T}\right)_{\mu_v,P} = -\Delta\eta^*. \tag{3.13}$$

A thermodynamic proof for this result—which was later dubbed as *the second nucleation theorem* by Ford [27]—was given by Oxtoby and Kashchiev [13], with further derivations by ten Wolde [16, Sec. 2.5].

When considering practical measurements, we have to deal with macroscopic systems where it is not possible to treat μ_v, T, and P as completely independent variables. Thus, in practice conditions with constant saturation ratio S, which generalises into a condition of constant activities in case of mixture, of vapours, and total pressure P or inert carrier gas pressure p_g (see Sec. 3.5.2) can be assumed. If one only fixes S and lets P vary freely (i.e. an isochoric process), the second nucleation theorem can be written in form

$$\left(\frac{\partial W^*}{k_{\mathrm{B}}T\partial T}\right)_{S,V} = -\frac{\Delta U^*}{k_{\mathrm{B}}T^2}, \tag{3.14}$$

where ΔU^* is the excess internal energy of the cluster when compared to g^* molecules in bulk liquid [15], see also [38, Sec. 6.4]. Assuming ideal vapour phase and a CNT-type rate expression results in [15][5]

$$\left(\frac{\partial \ln J}{\partial T}\right)_S \approx \frac{h - k_{\mathrm{B}}T + \Delta U^*}{k_{\mathrm{B}}T^2} \approx \frac{\Delta U^*}{k_{\mathrm{B}}T^2}, \tag{3.15}$$

where h is the latent heat of condensation per molecule, and $k_{\mathrm{B}}T$ in numerator—which stems from the temperature dependence of the kinetic prefactor—can be interpreted as the pressure–volume work needed to bring

[5] Again in a similar manner to the first nucleation theorem, corresponding results determined on the basis of CNT can be found from the literature [e.g. 39].

the molecule into constant-volume gas phase; thus the first two terms give the excess internal energy of a vapour molecule in supersaturated vapour. It should be noted that if the preceding derivatives were taken also at constant pressure, a more proper interpretation of the obtainable excess quantity would be that of excess enthalpy with respect to the same cluster in liquid, ΔH^*. In this case, physical interpretation for $k_\mathrm{B}T$ would be related into translation of the cluster as whole [cf. 40].[6]

For the kinetic derivation of the second nucleation theorem, see [19].

3.4 Other nucleation theorems

The dependence of nucleation rate on total (or carrier gas) pressure has been constantly recognised as one of the main open problems in vapour-to-liquid nucleation studies [43]. For recent experimental work, see Refs. [44–46] and references therein. Much of this issue is due to the fact that CNT neglects the role of the total pressure in the nucleation process. The corresponding relative sensitivity of J on the total pressure P is thus of special interest also from a theoretical viewpoint. From Eq. (3.7) it follows that [cf. Eq. (2.2)]

$$\left(\frac{\partial \Delta X^*}{\partial P}\right)_{T,\mu_v} = \Delta V^*, \tag{3.16}$$

where ΔV^* is now the excess volume of the critical nucleus, i.e. the volume occupied by Δg^* molecules at given conditions resulting in the condensed phase the density ρ^*. A similar relation results in from other approaches [e.g. 1, 17, 47] as well. A related result was already obtained by Gibbs [Eq. (576) in Ref. 48] when discussing the stability of a lentil-shaped phase formed at the interface of two fluid phases; when considering the primary role of Eq. (2.6) as the definition of the nucleation work, this form of nucleation theorem can actually be considered as the most fundamental one [cf. 49].

[6] This contribution differs from $3k_\mathrm{B}T/2$, expected on the basis of equipartition, as impinging molecules have a different velocity distribution than all molecules in the gas phase. A somewhat simplified description for this effect is that a non-stationary cluster encounters more head-on collisions, slowing it down, than collisions from behind that would speed up the cluster. For a more detailed treatment, see [41] or [42].

The corresponding equation for the nucleation rate,

$$\left(\frac{\partial \ln J}{\partial P}\right)_T = -\frac{V^*}{k_\mathrm{B}T}, \tag{3.17}$$

was first proposed by Kashchiev for bubble nucleation [50, Chap. 14]; for further development, see [51, 52]. In Eq. (3.17), V^* is the volume of the critical cluster/bubblet defined by the equimolecular dividing surface. In droplet nucleation, such pressure or "third nucleation theorem" [Eq. (3.17)] and its extensions (see Sec. 3.5.2) have mainly been used in integrated form to predict the pressure dependence of J [e.g. 53].

Nucleation theorems are by no means limited to systems that can be described using μPT-, or more conventional NPT- or NVT-ensembles, as similar relations can be derived for other first order phase transitions as well. For example, Vehkamäki and Ford [54] have derived an analogue of the first nucleation theorem for the Ising model.

3.5 Corrections and amendments of nucleation theorems

Nucleation theorems as given above share most of the restrictions of CNT. Various amendments of these forms to incorporate missing physical effects have been proposed in the literature. These can be roughly divided into two categories: nonequilibrium and -ideality corrections.

3.5.1 Nonequilibrium corrections

In CNT, there are two principal equilibrium assumptions. First, it is assumed that nucleation takes place in steady-state regime. However, if there is any change in vapour phase intensive properties, the nucleation rate changes to react this change. Thus, there is a short induction period before the nucleation rate reaches the new steady-state value. Secondly, condensation of vapour phase monomers on growing clusters releases latent heat that warms up the cluster: this excess energy is then dissipated

either via collision of inert carrier gas molecules, providing the heat bath for the cluster, and thermal evaporation of molecules back to the gas phase. The problem of incorporating nonstationary effect into the first nucleation theorem has been tackled by Kashchiev [50, Chap. 16], but in a manner that requires either simultaneous estimation of both the characteristic timescale for reaching steady-state and the steady-state nucleation rate, or making some model-specific assumptions for either of these.

Nonisothermal effects were recognised early on in the development of the nucleation theory [55, Sec. 4.A]. Thus, there exist several studies on how to incorporate these effects into the CNT description of the nucleation rate. Both discrete [41, 56, 57] and continuum [58, 59] treatments result in an essentially a similar correction factor that has been incorporated into the first nucleation theorem by Barrett [60]: Assuming ideal vapour, a zeroth-order approximation for this correction reads as[7]

$$\left(\frac{\partial \ln J}{\partial \ln S}\right)_T = g^*_{\mathrm{td}} + 1 - \frac{2(\hat{Q} + \hat{c}_v)}{\hat{c}_v(1+\lambda) + (\hat{Q} + \hat{c}_V)^2} \frac{\theta \mathrm{d}T}{T \mathrm{d}\theta}, \tag{3.18}$$

where constant T refers now to the constant gas phase temperature only. In Eq. (3.18)

$$\hat{Q} = \frac{h}{k_{\mathrm{B}}T} - \frac{1}{2} - \hat{c}_v + \frac{2T}{3\sqrt[3]{g^*}} \frac{\mathrm{d}\theta}{\mathrm{d}T}$$

is the normalised net heat released by condensation of a vapour-phase monomer with

$$\hat{c}_v = \frac{c_v}{k_{\mathrm{B}}} + \frac{1}{2}$$

as the normalised molecular specific heat of vapour phase monomers, enhanced by addend $k_{\mathrm{B}}/2$ for the increased collision rate of high energy monomers,

$$\lambda = \frac{\hat{c}_g n_g \eta_g}{\hat{c}_v n_1 \eta_v}$$

is the ratio of heat carried by collisions with the carrier gas (subscript g) and vapour molecules with n_i as the molecular density and η_i the mean thermal speed of species i (vapour or carrier gas) in the gas phase, and

[7] Instead of thermodynamic critical size g^*_{td}, a reference could be made to isothermal statistical mechanic critical size g^*_{sm} as well.

$\theta = \gamma A_1/k_\mathrm{B}T$ is the dimensionless surface tension. Numerical calculations for real substances suggest a positive, but negligible correction to the first nucleation theorem (i.e. increase of the critical size with a term corresponding to 0 to 1 molecules), as $\mathrm{d}\theta/\mathrm{d}T$ is generally negative [60]. It should be noted that the above mentioned correction factor does not include radiative heat transfer effects that can be important for nucleation in interplanetary and -stellar environments [61].

3.5.2 Compressibility and nonideality corrections

Slight nonideality of the mixture of vapour and carrier gas can be presented using truncated virial equation of state:

$$P = k_\mathrm{B}T\rho_v\left(1 + B\rho_v\right); \tag{3.19}$$

for a detailed thermodynamic treatment of this system see [62, Chap. 7]. The second virial coefficient is given as

$$B = y_v^2 B_v + 2y_v y_g B_{vg} + y_g^2 B_g,$$

where $y_v = p_v/P$ and y_g are the mole fractions of vapour and carrier gas, which also define the Dalton pressures p_v and p_g, respectively. We shall follow here the convention designating p_v and p_g as partial pressures, although this nomenclature is not exact for nonideal mixtures. The chemical potential of the vapour is now given as

$$\mu_v(p_v, P, T) = k_\mathrm{B}T\ln S + \sum_{i,j\in\{v,g\}}\sum \left(2B_{iv} - B_{ij}\right) y_j y_i P + f_v(T), \tag{3.20}$$

where f_v is a function of temperature only, and one-to-one correspondence of density and pressure second virial coefficients is used. Above we actually have chosen the Gibbs–Dalton law, $P = (y_v + y_g)P = p_v + p_g$, as our constitutive relation, and differentiating now under isothermal conditions yields

$$\begin{aligned}\mathrm{d}\mu_v(p_v, p_g; T) = k_\mathrm{B}T\mathrm{d}\ln S &+ \frac{\left[(p_v + p_g)^2 B_v + p_g^2 B_v - 2p_g^2 B_{vg} + p_g^2 B_g\right]\mathrm{d}p_v}{(p_v + p_g)^2} \\ &+ \frac{\left[p_v^2 B_v + 2p_g(p_g + 2p_v)B_{vg} - 2p_v p_g B_g\right]\mathrm{d}p_g}{(p_v + p_g)^2}.\end{aligned} \tag{3.21}$$

The differential of the condensed phase chemical potential under isothermal conditions and at gaseous phase pressure is again obtained directly from the Maxwell relation $\mathrm{d}\mu_v = v\mathrm{d}P$, where v is the molecular volume of the condensing component (vapour) in the condensed phase. The chemical potential difference between new and old phases of during isothermal condensation can now be expressed as a function of p_v and p_g or P as [cf. 63][8]

$$\begin{aligned}\mathrm{d}\Delta\mu = &\left[v - \frac{k_\mathrm{B}T}{p_v} - \frac{(p_v+p_g)^2B_v + p_g^2(B_v - 2B_{vg} + B_g)}{(p_v+p_g)^2}\right]\mathrm{d}p_v \\ &+ \left[v - \frac{p_v^2B_v + 2p_g(p_g+2p_v)B_{vg} - 2p_vp_gB_g}{(p_v+p_g)^2}\right]\mathrm{d}p_g \qquad (3.22)\end{aligned}$$

$$\begin{aligned}= &\left[v - \frac{k_\mathrm{B}T}{p_v} - \frac{2(P^2-p_v^2)B_v - 4P(P-p_v)B_{vg} + (P^2-p_v^2)B_g}{P^2}\right]\mathrm{d}p_v \\ &+ \left[v - \frac{p_v^2B_v + 2(P^2-p_v^2)B_{vg} - 2p_v(P-p_v)B_g}{P^2}\right]\mathrm{d}P. \qquad (3.23)\end{aligned}$$

[8] Another form of such "effective chemical potential difference" was defined by Wedekind et al. [64], who wrote (applying the sign convention used in this thesis)

$$\Delta\mu = -k_\mathrm{B}T\ln S + v(p_v + p_g - p_e),$$

which was then used to define *pV-corrected work of formation and nucleation rate* via equations similar to Eqs. (2.8) and (2.24). Wedekind et al. continued to show that the effect of carrier gas concentration was to decrease J either due inefficient thermalisation at low p_g or due increased W^* via pressure–volume work at high p_g. They also pointed out that there should also be a corresponding increase in g^* obtained using the first nucleation theorem, and highlighted the need for conditions of constant p_g (or P) when applying the first nucleation theorem. Computational support for this ansatz was provided by MD simulations. Holten [65, p. 62] has however pointed out that when the Poynting correction [66]—i.e. the decrease of p_e due to p_g—is taken into account, such an extra pV-term disappears from W^*, which highlights the need to include such correction into any consistent description from beginning.

Applying Eq. (3.23) to the first nucleation theorem gives now

$$\left(\frac{\partial \ln J}{\partial \ln S}\right)_{T,P} = (g^*_{\mathrm{id}} + 1)\left[1 - \frac{v p_v}{k_\mathrm{B} T} + \frac{(P^2 - p_v^2)(2B_v - B_g) - 4P(P - p_v)B_{vg}}{k_\mathrm{B} T P^2}\right]. \tag{3.24}$$

Here g^*_{id} is the critical size that follows assuming ideal gas behaviour with correction terms given by Eq. (3.24) due to i) mechanical work needed to create the critical cluster, and ii) nonideality of the vapour given in brackets. Under typical experimental conditions, both of these factors are negligible. For nucleation from an ideal vapour, Eq. (3.24) gives $(g^*_{\mathrm{id}} + 1)(1 - \rho_v/\rho_l)$, i.e. it produces a slightly different kinetic correction factor $\epsilon \lesssim 1$. One can find several approaches to both compressibility and nonideality corrections from the literature: differences between various treatments boil down to the applied operational definitions of S and p_v.

- The treatment above defines $S = p_v/p_e$ in a manner that includes the effect of dimers on the vapour pressure p_v via virial coefficients B_v and B_{vg}, which gives a reduction in S when compared to the ideal case.[9]
- Kashchiev [63], Luijten et al. [70], and Holten [65, Sec. 2.9] (and also implicitly Oxtoby and Laaksonen [53]) have applied the definition $S = e^{\Delta\mu/k_\mathrm{B}T}$, also often encountered in molecular simulations. In this case, no correction term appears when the nucleation theorem is presented as a derivative with respect to $\ln S$. From a practical point of view, this approach suggests that the measurable quantity is the fugacity of the vapour, instead of the Dalton or partial pressure, which may also incorporate the Poynting effect [66] on p_e due to p_g [see, e.g., 46].
- In both above-mentioned approaches, contribution from the derivative of the kinetic prefactor K is 1—in a single-component case. Knott

[9] In the analysis of atmospheric NPF, a more significant nonideality is due to clustering of sulphuric acid molecules with water and base molecules in the air (see Ref. [67] and Sec. 6.4.4): not only the appropriate concentration, monomer vs. total, to be used when applying the first nucleation theorem, but also proper detection of the total concentration [68] have been under scrutiny. A correction to the first nucleation theorem to account for the hydration effects has been presented by Zollner et al. [69].

et al. [71], on the other hand, have argued that one should instead define S as p_1/p_e, where p_1 is the partial pressure of vapour-phase monomers. Then, an additional correction due to existence of dimers (and possible higher oligomers) appears in K [72], and consequently on $(\partial \ln K/\partial \ln S)_{T,P}$. Knott et al. [71], however, neglected this contribution together with terms containing vapour–carrier gas interactions and carrier gas nonidealities (i.e. B_{vg} and B_g) when deriving corrections for the first and second nucleation theorems.

Now the nucleation rate J must be some function of the driving force $\Delta\mu$, T, and according to empirical observations, P (or p_g). Using the cyclic relation of derivatives,

$$\left(\frac{\partial P}{\partial \ln J}\right)_{\Delta\mu,T}\left(\frac{\partial \Delta\mu}{\partial P}\right)_{J,T}\left(\frac{\partial \ln J}{\partial \Delta\mu}\right)_{P,T} = -1,$$

we have an extended form of the pressure nucleation theorem,[10]

$$\left(\frac{\partial \ln J}{\partial P}\right)_{T,\Delta\mu} = (g^* + 1) \times \left[v^* - \frac{p_v^2 B_v + 2(P^2 - p_v^2)B_{vg} - 2p_v(P - p_v)B_g}{P^2}\right]. \quad (3.25)$$

Corresponding equations with similar but not identical form, due to slightly different assumptions made, have been provided and applied to nucleation at high pressures by Kashchiev [63], Luijten et al. [70], Kalikmanov and Labetski [73], and Holten [65, Sec. 2.9]; the three last-mentioned studies expressed this nucleation theorem in terms of $(\partial \ln J/\partial \ln P)_{\Delta\mu,T}$. At the limit $P >> p_v$, Eq. (3.25) reduces to the form deduced earlier by Ford [74] using CNT and more generally using binary nucleation theorem by Oxtoby and Laaksonen [53].

Ostensibly no other assumptions besides the validity of the Maxwell relation $\mathrm{d}\mu = v\mathrm{d}P$ and the first nucleation theorem have been made when

[10] Alternatively, a similar nucleation theorem with respect to p_g can be derived:

$$\left(\frac{\partial \ln J}{\partial p_g}\right)_{T,\Delta\mu} = (g^* + 1)\left[v^* - \frac{p_v^2 B_v + 2p_g(p_g + 2p_v)B_{vg} - 2p_v p_g B_g}{P^2}\right].$$

deriving Eq. (3.25). Thus, it is in principle possible to use it to deduce how the density of the critical cluster $\rho^* = 1/v^*$ depends on the ambient conditions.[11] However, the physical identification of this density is not straightforward: various derivations of the first nucleation theorem suggest that one could properly assign the density with that inside an equimolecular surface (cf. Fig. 3.1). Also, due to the restriction of constant J when evaluating $(\partial\Delta\mu/\partial P)$, a peculiar variation of p_v and p_g around the constant nucleation rate conditions is required. Furthermore, as the derivation above assumes unary nucleation, such a formula for v^* holds only when carrier gas molecules do neither adsorb on the cluster surface nor penetrate into it. Based on molecular simulations [e.g. 75–79], only helium (and possibly neon) fulfils this criterion as a carrier gas (and even it may be present in the precritical clusters, only to be squeezed out before the cluster reaches critical size [80]).[12] On the other hand, light helium atoms are not effective in transporting heat away from the growing cluster, thus reducing the nucleation rate due to nonisothermal effects [82].

3.6 Critique of nucleation theorems

Since the first applications to vapour–liquid nucleation, nucleation theorems have received both positive and and negative criticism. Much of the positive criticism has followed from the experimental work using expansion-based setups (cf. Sec. 2.3) and molecular fluids [for an overview, see 33, 83, 84], as here the results from the application of the first and second nucleation theorems have been inline with the expectations based on macroscopic droplet models. There are some exceptions, such as the recent work on homogeneous nucleation of N_2 [85], where it was found that both g^* and U^* estimated using the nucleation theorems were substantially smaller than those predicted by CNT. There has also been some praise of nucleation theorems based on computational work: for example,

[11] Schmelzer [1] has presented a counterargument based on the reference states required by the application of Gibbs' surface thermodynamics, stating that "it makes no sense, in general, to discuss the properties of real critical clusters. . . "

[12] This phenomenon of mixed clusters containing carrier gas molecules that are only slightly soluble to vapour's bulk liquid can be seen as a manifestation of the oversolubility of such gasses into nanoscopic samples [81].

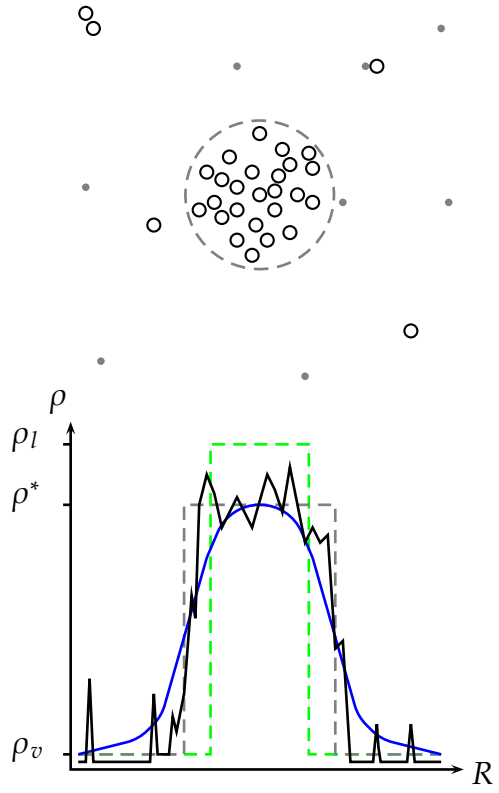

Fig. 3.1. Above: A schematic "snapshot" of a nucleus bounded by the equimolecular dividing surface (EDS). Open symbols present vapour and filled symbols carrier gas molecules, respectively. Below: Density profiles for the "snapshot" (black), a corresponding mean-field fluctuation (blue) and the EDS defined by the mean density at the center of nucleus ρ^* (grey), and bulk liquid density ρ_l (green). For an incompressible cluster the last two coincide, while in other cases both $\rho^* > \rho_l$ and $\rho^* < \rho_l$ are possible.

Kathmann et al. [86] noted that the application of the multicomponent version of the first nucleation theorem was able to predict the composition of critical clusters correctly when compared to indirect MC simulations (see, however, Sec. 2.2).

Thermodynamic derivation of the first nucleation theorem, together with its claimed universality, has encountered negative criticism by Schmelzer [1, 87]: When considering development from Eq. (2.6) to Eq. (2.8), it is obvious that the thermodynamic derivation of the first nucleation theorem [12, cf. Eq. (3.1)] holds only for a stationary, incompressible cluster that is defined by the equimolecular dividing surface. More recently, Mori et al. [88, 89] have arrived with similar conclusions. It is interesting to note that the conditions for the validity of the thermodynamic derivation of the rate-form of the first nucleation theorem agree with those of the Kelvin equation (see p. 41), while the other derivations of the first nucleation theorem have alleviated these restrictions, but typically only one at time; this has also been pointed out by Reiss [90], and the topic will be returned in Sec. 7.1.

Kusaka et al. [91] studied binary sulphuric acid–water nucleation using MC techniques, and found that the rate limiting step was kinetically controlled dimerisation of two hydrated H_2SO_4 molecules, which was contrasted to $g^*_{H_2SO_4} \approx 15$ obtained from experimental data [92] using the first nucleation theorem. Inspired by this perplexity, they argued that the first nucleation theorem "*presumes* that the rate limiting step is nucleation involving a critical cluster in equilibrium with the surrounding vapor", and that it "holds only at equilibrium where the grand potential is stationary with respect to fluctuation in the density profile". Although such a description is indeed a cornerstone for the thermodynamic and statistical mechanic derivations of the first nucleation theorem, neither assumption is required for the kinetic first nucleation theorem to hold. Only under these assumptions, though, we can identify $\bar{g}$ with g^*, and if these assumptions do not hold, the resulting critical size should be interpreted as $\bar{g}$. However, this implies that both the simulated and the experimental critical sizes should be understood as kinetic ones. Now the discrepancy between measured and modelled values can be due to various factors, for example an uncertainty in the simulated free energy of formation that was pointed out in the original article [91].

The negative criticism discussed above focuses on the validity of the work-form of the first nucleation theorem. Another options are due to failure of the kinetic description, i.e. deviation from the Szilárd–Farkas kinetics. Such an issue was brought up by Vehkamäki et al. [93], who pointed out that the existence of stable precritical clusters with an associated local minimum in the free energy, which participation into cluster growth sequence results in the (kinetic) first nucleation theorem to give the difference between sizes corresponding to the maximum and the minimum in the free energy of the cluster formation. During recent years, further issues related to the improper experimental determination of related quantities and the effect of cluster losses on the interpretation of the first nucleation theorem have been brought up and clarified e.g. in Chaps. 5 and 6. It is likely that such contributions explain the recently noted anomaly in the application of the first nucleation theorem into data from diffusion-based measurement setups [e.g. 94] discussed in more detail in Sec. 7.2.

3.A Appendix

3.A.1 Derivation of the first nucleation theorem using statistical mechanics

Statistical mechanic arguments were first applied to the derivation of the first nucleation theorem by Reiss [14], with more detailed derivations provided by Ford [15], Bowles et al. [17], and an essentially identical derivation by ten Wolde and Frenkel [47] and MacDowell [18], which is summarised below.

Let us consider a system characterised by the temperature T, chemical potential μ_v, and volume V. The grand canonical partition function for this system reads as

$$\Xi(\mu_v, V, T) = \sum_{N=0}^{\infty} e^{-\mu_v N/k_\mathrm{B}T} Q(N, V, T), \tag{3.26}$$

where

$$Q(N, V, T) = \frac{\int_V e^{-\phi(r^N)/k_\mathrm{B}T} \mathrm{d}r^N}{\Lambda^{3N} N!}$$

is the N-particle canonical partition function after integration over momenta; ϕ is the potential energy of the configuration with coordinates r^N and Λ the thermal de Broglie wavelength. We now divide the molecules between the vapour and a cluster: $N = N_v + g$. Probability to find exactly g molecules in the system is given by

$$P(g) = \frac{e^{-\mu_v g/k_\mathrm{B}T} Q(g, V, T)}{\Xi(\mu_v, V, T)}. \tag{3.27}$$

The Landau free energy, i.e. a shifted grand potential $\Delta\Phi(g) = -k_\mathrm{B}T \ln P(g) + k_\mathrm{B}T \ln \Xi(\mu_v, V, T)$, can be associated with the probability distribution $P(g)$:

$$\begin{aligned} \Delta\Phi(g) &= -k_\mathrm{B}T \ln \left[e^{\mu_v g/k_\mathrm{B}T} Q(g, V, T) \right] \\ &= -\mu_v g + F(g, V, T), \end{aligned} \tag{3.28}$$

where F is the Helmholtz free energy.[13] The Landau free energy difference between two number of molecules in a restricted system, e.g. a cluster, is now $\Delta\Delta\Phi = \Delta\Phi(g_2) - \Delta\Phi(g_1) = -\mu_v \Delta g + F(g_2, V, T) - F(g_1, V, T)$ that immediately gives

$$\left(\frac{\partial \Delta\Delta\Phi}{\partial \mu_v} \right)_{T,V} = -(g_2 - g_1) \equiv -\Delta g. \tag{3.29}$$

This result holds for any g_1 and g_2, and thus it holds also when we choose $g_2 = g^*_\mathrm{sm}$ and g_1 as the number of homogeneous vapour molecules occupying the same space, which gives us the work-form of the first nucleation theorem. Similarly, we can derive the extension of the first nucleation theorem [93] for cases where some stable precritical clusters are present in volume V.

A more detailed discussion was provided by Bowles et al. [17], who noted that in order to split the potential energy and thus factorise the Landau free energy into cluster and vapour contributions to arrive with Eq. (3.28), one has to assume an ideal vapour phase. Thus, while it seems that the statistical mechanic derivation is completely general, as it apparently holds also for nonstationary and compressible clusters, there are some implicit limitations concerning the validity of Eq. (3.29).

[13] Physical interpretation of $\Delta\Phi(g)$ is the free energy (grand potential) required to create a g-mer into volume V minus the free energy of homogeneous vapour described by μ_v and T occupying the same volume.

3.A.2 On slope analysis

Already Nielsen [11, Chap. 2] noticed that over a limited range of concentrations, it is possibly to express the nucleation rate as $J = k[\mathrm{A}]^P$, where [A] is the concentration of nucleating species A and the nucleation exponent P equals to the number of molecules in the critical cluster g^*. He commented that in this case one can interpret $(\partial \ln J / \partial \ln[\mathrm{A}])_T$ also as the reaction order, as ordinarily done in the studies of chemical kinetics. In the context of atmospheric NPF, conclusions concerning the actual nucleation mechanism based on a such "chemical picture" were first given by Weber et al. [95], who found that J deduced from the field experiments had a second-order dependence of $[H_2SO_4]$, implying that collisions of two clusters, both containing one H_2SO_4 molecule each, were the rate-determining step for NPF.

There exists, in fact, a profound analogue between nucleation and chemical kinetics, as we can always mode unary nucleation as an equilibrium reaction[14]

$$\underbrace{\mathrm{A} + \cdots + \mathrm{A}}_{g \text{ molecules}} \leftrightharpoons \mathrm{A}_g \equiv \mathrm{C}. \tag{3.30}$$

For such reactions, the reaction rate can be defined as

$$J_g = \frac{1}{V}\frac{\partial[\mathrm{C}]}{\partial t} \approx \frac{\partial f_g}{\partial t}, \tag{3.31}$$

where f_g is again the concentration of g-mers in volume V, and the latter form holds if V remains constant [e.g. 96, Chap. 15]. The reaction rate can now be written in terms of concentrations as

$$J_g = k_+[\mathrm{A}]^g - k_-[\mathrm{C}], \tag{3.32}$$

where k_+ and k_- are the forward and backward rate coefficients. If now the forward rate dominates over the backward rate, direct evaluation of the relative rate sensitivity with respect to the precursor concentration at

[14] However, in case of a true equilibrium reaction, forward and backward reaction rates are equal, while for nucleation they are not. Only the probabilities for the critical cluster to grow or decrease are assumed to be equal.

$g = g^*$ results in the first nucleation theorem in form

$$\left(\frac{\partial \ln J_{g^*}}{\partial \ln[\mathrm{A}]}\right)_{T,V} = g^* \tag{3.33}$$

as k_+ and k_- are independent of [A].[15] Equation (3.33) differs now from the thermodynamic and statistical mechanic nucleation theorems in two aspects. First, there is no contribution from the old phase, i.e. $g^* = \Delta g^*$ here. Secondly, there is no kinetic contribution due to prefactor, which follows from the assumption that [C] does not depend on [A], which obviously makes a significant difference if g^* is small. This assumption is common to all approximations leading to irreversible dynamics and those behind transition-state theory, either of these which might have motivated the development of collision-limited nucleation treatments.

Analogue between chemical kinetics and nucleation extends beyond the first nucleation theorem. If we consider E^* as the activation energy for the reaction above, we have

$$\left(\frac{\partial \ln k}{\partial T}\right)_{[\mathrm{A}]} = \frac{E^*}{k_\mathrm{B} T^2}, \tag{3.34}$$

where k is the net reaction-rate constant. Equation (3.34) is obviously a statement of the second nucleation theorem. Chemical kinetics even suggests for a proper identification of E^* either as a difference in the internal energy (ΔU^*), if the reaction-rate constant k refers to a rate expression given in terms of concentrations, or the enthalpy (ΔH^*), if the rate expression is given in terms of partial pressures. Furthermore, a more detailed expression in a manner to Eq. (3.15) follows from the transition-state theory [96, p. 450 and 458]. Consideration of the equilibrium constant K for the vapour–liquid equilibrium results in an analogue of the third or pressure nucleation theorem, a result that bears a close connection to the kinetic derivations of the first and second nucleation theorems [cf. Eq. (8.36) in 96].

[15] In a more general case,

$$\left(\frac{\partial \ln J_g}{\partial \ln[\mathrm{A}]}\right)_{T,V} = \frac{k_+ g[\mathrm{A}]^g - k_-[\mathrm{A}]\left(\frac{\partial[\mathrm{C}]}{\partial[\mathrm{A}]}\right)_{T,V}}{k_+[\mathrm{A}]^g - k_-[\mathrm{C}]},$$

and the direct correspondence with the first nucleation theorem is lost.

References

[1] J. W. P. Schmelzer. Comments on the nucleation theorem. *Journal of Colloid and Interface Science* 242 (2001), 354–372.

[2] H. Eyring. The activated complex and the absolute rate of chemical reactions. *Chemical Reviews* 17 (1935), 65–77.

[3] P. Hänggi, P. Talkner and M. Borkovec. Reaction-rate theory: fifty years after Kramers. *Reviews of Modern Physics* 62 (1990), 251–342.

[4] R. A. Marcus. Chemical and electrochemical electron-transfer theory. *Annual Review of Physical Chemistry* 15 (1964), 155–196.

[5] B. Peters. Common features of extraordinary rate theories. *Journal of Physical Chemistry B* 119 (2015), 6349–6356.

[6] C. Barus. Colored cloudy condensation as depending on air temperature and dust-contents, with a view to dust counting. *American Meteorological Journal* 10 (1893), 12–34.

[7] C. T. R. Wilson. Condensation of water vapour in the presence of dust-free air and other gases. *Philosophical Transactions of the Royal Society of London, Series A* 189 (1897), 265–307.

[8] A. Laaksonen and R. McGraw. Thermodynamics, gas–liquid nucleation, and size-dependent surface tension. *Europhysics Letters* 35 (1996), 367–372.

[9] N. Bruot and F. Caupin. Curvature dependence of the liquid–vapor surface tension beyond the Tolman approximation. *Physical Review Letters* 116 (2016), 056102.

[10] R. K. Bowles, D. Reguera, Y. Djikaev and H. Reiss. A theorem for inhomogeneous systems: The generalization of the nucleation theorem. *Journal of Chemical Physics* 115 (2001), 1853–1866.

[11] A. E. Nielsen. *Kinetics of Precipitation*. Oxford: Pergamon, 1964.

[12] D. Kashchiev. On the relation between nucleation work, nucleus size, and nucleation rate. *Journal of Chemical Physics* 76 (1982), 5098–5102.

[13] D. W. Oxtoby and D. Kashchiev. A general relation between the nucleation work and the size of the nucleus in multicomponent nucleation. *Journal of Chemical Physics* 100 (1994), 7665–7671.

[14] Y. Viisanen, R. Strey and H. Reiss. Homogeneous nucleation rates for water. *Journal of Chemical Physics* 99 (1993), 4680–4692.

[15] I. J. Ford. Nucleation theorems, the statistical mechanics of molecular clusters, and a revision of classical nucleation theory. *Physical Review E* 56 (1997), 5615–5629.

[16] P. R. ten Wolde. *Numerical Study of Pathways for Homogeneous Nucleation*. PhD thesis. Universiteit van Amsterdam, 1998.

[17] R. K. Bowles, R. McGraw, P. Schaaf, B. Senger, J.-C. Voegel and H. Reiss. A molecular based derivation of the nucleation theorem. *Journal of Chemical Physics* 113 (2000), 4524–4532.

[18] L. G. MacDowell. Formal study of nucleation as described by fluctuation theory. *Journal of Chemical Physics* 119 (2003), 453–463.

[19] R. McGraw and D. T. Wu. Kinetic extensions of the nucleation theorem. *Journal of Chemical Physics* 118 (2003), 9337–9347.

[20] R. McGraw and R. Zhang. Multivariate analysis of homogeneous nucleation rate measurements. Nucleation in the *p*-toluic acid/ sulfuric acid/water system. *Journal of Chemical Physics* 128 (2008), 064508.

[21] J. Hrubý, Y. Viisanen and R. Strey. Homogeneous nucleation rates for *n*-pentanol in argon: Determination of the critical cluster size. *Journal of Chemical Physics* 104 (1996), 5181–5187.

[22] T. L. Hill. Thermodynamics of small systems. *Journal of Chemical Physics* 36 (1962), 3182–3197.

[23] T. L. Hill. *Thermodynamics of Small Systems*. Parts I and II. New York: W. A. Benjamin, 1963–1964.

[24] V. García-Morales, J. Cervera and J. Pellicer. Correct thermodynamic forces in Tsallis thermodynamics: Connection with Hill nanothermodynamics. *Physics Letters A* 336 (2005), 82–88.

[25] C. Tsallis. Possible generalization of Boltzmann–Gibbs statistics. *Journal of Statistical Physics* 52 (1988), 479–487.

[26] O. Kupiainen-Määttä. *From Cluster Properties to Concentrations and from Concentrations to Cluster Properties*. PhD thesis. Helsingin yliopisto, 2016.

[27] I. J. Ford. Thermodynamic properties of critical clusters from measurements of vapour–liquid homogeneous nucleation rates. *Journal of Chemical Physics* 105 (1996), 8324–8332.

[28] V. Kalikmanov. *Nucleation Theory*. Dordrecht: Springer, 2013.

[29] D. Reguera. Mesoscopic nonequilibrium kinetics of nucleation processes. *Journal of Non-Equilibrium Thermodynamics* 29 (2004), 327–344.

[30] H. Reiss. *Methods of Thermodynamics*. Mineola, N.Y.: Dover, 1996.

[31] T. L. Hill and R. V. Chamberlin. Extension of the thermodynamics of small systems to open metastable systems: An example. *Proceedings of the National Academy of Sciences U.S.A.* 95 (1998), 12779–12782.

[32] T. L. Hill and R. V. Chamberlin. Fluctuations in energy in completely open small systems. *Nano Letters* 2 (2002), 609–613.

[33] R. Strey, P. E. Wagner and Y. Viisanen. The problem of measuring homogeneous nucleation rates and the molecular contents of nuclei: Progress in the form of nucleation pulse measurements. *Journal of Physical Chemistry* 98 (1994), 7748–7758.

[34] R. McGraw and A. Laaksonen. Scaling properties of the critical nucleus in classical and molecular-based theories of vapor–liquid nucleation. *Physical Review Letters* 76 (1996), 2754–2757.

[35] K. Koga and X. C. Zeng. Thermodynamic expansion of nucleation free-energy barrier and size of critical nucleus near the vapor-liquid coexistence. *Journal of Chemical Physics* 110 (1999), 3466–3471.

[36] R. McGraw and A. Laaksonen. Interfacial curvature free energy, the Kelvin relation, and vapor–liquid nucleation rate. *Journal of Chemical Physics* 106 (1997), 5284–5287.

[37] V. Talanquer. A new phenomenological approach to gas-liquid nucleation based on the scaling properties of the critical nucleus. *Journal of Chemical Physics* 106 (1997), 9957–9960.

[38] H. Vehkamäki. *Classical Nucleation Theory in Multicomponent Systems*. Berlin: Springer, 2006.

[39] M. P. Anisimov and A. G. Cherevko. Gas-flow diffusion chamber for vapour nucleation studies. Relations between nucleation rate, critical nucleus size and entropy of transition from a metastable into a stable state. *Journal of Aerosol Science* 16 (1985), 97–107.

[40] M. P. Anisimov, A. G. Nasibulin, S. D. Shandakov and I. N. Shaidormanov. Experimental determination of the surface energy of critical nuclei during the nucleation of supersaturated vapor. *Colloid Journal* 63 (2001), 131–136.

[41] J. Feder, K. C. Russell, J. Lothe and G. M. Pound. Homogeneous nucleation and growth of droplets in vapours. *Advances in Physics* 15 (1966), 111–178.

[42] J. C. Barrett, C. F. Clement and I. J. Ford. Energy fluctuations in homogeneous nucleation theory of aerosols. *Journal of Physics A* 26 (1993), 529–548.

[43] M. P. Anisimov, E. G. Fominykh, S. V. Akimov and P. K. Hopke. Vapor–gas/liquid nucleation experiments: A review of the challenges. *Journal of Aerosol Science* 40 (2009), 733–746.

[44] A.-P. Hyvärinen, D. Brus, J. Wedekind and H. Lihavainen. How ambient pressure influences water droplet nucleation at tropospheric conditions. *Geophysical Research Letters* 37 (2010), L21802.

[45] H. Görke, K. Neitola, A.-P. Hyvärinen, H. Lihavainen, J. Wölk, R. Strey and D. Brus. Homogeneous nucleation rates of n-propanol measured in the laminar flow diffusion chamber at different pressures. *Journal of Chemical Physics* 140 (2014), 174301.

[46] M. A. L. J. Fransen, J. Hrubý, D. M. J. Smeulders and M. E. H. van Dongen. On the effect of pressure and carrier gas on homogeneous water nucleation. *Journal of Chemical Physics* 142 (2015), 164307.

[47] P. R. ten Wolde and D. Frenkel. Computer simulation study of gas–liquid nucleation in a Lennard-Jones system. *Journal of Chemical Physics* 109 (1998), 9901–9918.

[48] J. W. Gibbs. On the equilibrium of heterogeneous substances (concluded). *Transactions of the Connecticut Academy of Arts and Sciences* 3 (1878), 343–524.

[49] D. Kashchiev. Forms and applications of the nucleation theorem. *Journal of Chemical Physics* 125 (2006), 014502.

[50] D. Kashchiev. *Nucleation: Basic Theory with Applications*. Oxford: Butterworth–Heinemann, 2000.

[51] G. Wilemski. Volumes of critical bubbles from the nucleation theorem. *Journal of Chemical Physics* 125 (2006), 114507.

[52] K. Davitt, A. Arvengas and F. Caupin. Water at the cavitation limit: Density of the metastable liquid and size of the critical bubble. *Europhysics Letters* 90 (2010), 16002.

[53] D. W. Oxtoby and A. Laaksonen. Some consequences of the nucleation theorem for binary fluids. *Journal of Chemical Physics* 102 (1995), 6846–6850.

[54] H. Vehkamäki and I. J. Ford. Nucleation theorems applied to the Ising model. *Physical Review E* 59 (1999), 6483–6488.

[55] M. Volmer. *Kinetik der Phasenbildung*. Dresden und Leipzig: Verlag von Theodor Steinkopff, 1939.

[56] J. C. Barrett. Equilibrium and steady-state distributions of vapour clusters in nucleation theory. *Journal of Physics A* 27 (1994), 5053–5068.

[57] J. H. ter Horst, D. Bedeaux and S. Kjelstrup. The role of temperature in nucleation processes. *Journal of Chemical Physics* 134 (2011), 054703.

[58] N. V. Alekseechkin. Multivariable theory of droplet nucleation in a single-component vapor. *Physica A* 412 (2014), 186–205.

[59] M. Schweizer and L. M. C. Sagis. Nonequilibrium thermodynamics of nucleation. *Journal of Chemical Physics* 141 (2014), 224102.

[60] J. C. Barrett. A stochastic simulation of nonisothermal nucleation. *Journal of Chemical Physics* 128 (2008), 164519.

[61] D. Lazzati. Non-local thermodynamic equilibrium dust nucleation in subsaturated vapours. *Monthly Notes of the Royal Astronomical Society* 384 (2008), 165–172.

[62] S. E. Wood and R. Battino. *Thermodynamics of Chemical Systems*. Cambridge: Cambridge University Press, 1990.

[63] D. Kashchiev. Effect of carrier-gas pressure on nucleation. *Journal of Chemical Physics* 104 (1996), 8671–8677.

[64] J. Wedekind, A.-P. Hyvärinen, D. Brus and D. Reguera. Unravelling the "pressure effect" in nucleation. *Physical Review Letters* 101 (2008), 125703.

[65] V. Holten. *Water Nucleation: Wave Tube Experiments and Theoretical Considerations*. PhD thesis. Technische Universiteit Eindhoven, 2009.

[66] J. H. Poynting. Change of state: solid–liquid. *Philosophical Magazine* 12 (1881), 32–48.

[67] K. Neitola, D. Brus, U. Makkonen, M. Sipilä, U. Makkonen, R. L. Mauldin, III, N. Sarnela, T. Jokinen, H. Lihavainen and M. Kulmala. Total sulfate vs. sulfuric acid monomer concenterations in nucleation studies. *Atmospheric Chemistry and Physics* 15 (2015), 3429–3443.

[68] O. Kupiainen-Määttä, T. Olenius, T. Kurtén and H. Vehkamäki. CIMS sulfuric acid detection efficiency enhanced by amines due to higher dipole moments—a computational study. *Journal of Physical Chemistry A* 117 (2013), 14109–14119.

[69] J. H. Zollner, W. A. Glasoe, B. Panta, K. K. Carlson, P. H. McMurry and D. R. Hanson. Sulfuric acid nucleation: Power dependencies, variation with relative humidity, and effect of bases. *Atmospheric Chemistry and Physics* 12 (2012), 4399–4411.

[70] C. C. M. Luijten, P. Peeters and M. E. H. van Dongen. Nucleation at high pressure. II. Wave tube data and analysis. *Journal of Chemical Physics* 111 (1999), 8535–8544.

[71] M. Knott, H. Vehkamäki and I. J. Ford. Energetics of small *n*-pentanol clusters from droplet nucleation rate data. *Journal of Chemical Physics* 112 (2000), 5393–5398.

[72] J. L. Katz, H. Saltsburg and H. Reiss. Nucleation in associated vapors. *Journal of Colloid and Interface Science* 21 (1966), 560–568.

[73] V. I. Kalikmanov and D. G. Labetski. Theory of anomalous critical-cluster content in high pressure binary nucleation. *Physical Review Letters* 98 (2007), 085701.

[74] I. J. Ford. Imperfect vapour–gas mixtures and homogeneous nucleation. *Journal of Aerosol Science* 23 (1992), 447–455.

[75] H. Y. Tang and I. J. Ford. Microscopic simulations of molecular cluster decay: Does the carrier gas affect evaporation? *Journal of Chemical Physics* 125 (2006), 144316.

[76] K. Yasuoka and X. C. Zeng. Molecular dynamics of homogeneous nucleation in the vapor phase of Lennard-Jones. III. Effect of carrier gas pressure. *Journal of Chemical Physics* 126 (2007), 124320.

[77] S. Braun and T. Kraska. Dynamic structure of methane/*n*-nonane clusters during nucleation and growth. *Journal of Chemical Physics* 136 (2012), 214506.

[78] F. Römer, B. Fischer and T. Kraska. Investigation of the nucleation and growth of methanol clusters from supersaturated vapor by molecular dynamics simulations. *Soft Materials* 10 (2012), 130–152.

[79] S. Braun, V. Kalikmanov and T. Kraska. Molecular dynamics simulation of nucleation in the binary mixture of *n*-nonane/methane. *Journal of Chemical Physics* 140 (2014), 124305.

[80] S. Toxvaerd. Molecular dynamics simulation of nucleation in the presence of carrier gas. *Journal of Chemical Physics* 119 (2003), 10764–10770.

[81] M. Pera-Titus, R. El-Chahal, V. Rakotovao, C. Daniel, S. Miachon and J.-A. Dalmon. Direct volumetric measurement of gas oversolubility in nanoliquids: Beyond Henry's law. *ChemPhysChem* 10 (2009), 2082–2089.

[82] S. Braun, F. Römer and T. Kraska. Influence of the carrier gas molar mass on the particle formation in a vapor phase. *Journal of Chemical Physics* 131 (2009), 064308.

[83] Y. J. Kim, B. E. Wyslouzil, G. Wilemski, J. Wölk and R. Strey. Isothermal nucleation rates in supersonic nozzles and the properties of small water clusters. *Journal of Physical Chemistry A* 108 (2004), 4365–4377.

[84] B. E. Wyslouzil, R. Strey, J. Wölk, G. Wilemski and Y. Kim. Homogeneous nucleation rate measurements and the properties of critical clusters. In: *Nucleation and Atmospheric Aerosols: 17th International Conference*. Ed. by C. D. O'Dowd and P. E. Wagner. Dordrecht: Springer, 2007, 3–13.

[85] A. Bhabhe and B. Wyslouzil. Nitrogen nucleation in a cryogenic supersonic nozzle. *Journal of Chemical Physics* 135 (2011), 244311.

[86] S. M. Kathmann, G. K. Schenter, B. C. Garrett, B. Chen and J. I. Siepmann. Thermodynamics and kinetics of nanoclusters controlling gas-to-particle nucleation. *Journal of Physical Chemistry C* 113 (2009), 10354–10370.

[87] J. W. P. Schmelzer. Some additional comments on the nucleation theorem. *Russian Journal of Physical Chemistry* 77 (2003), S143–S145.

[88] A. Mori and Y. Suzuki. Vanishing linear term in chemical potential difference in volume term of work of critical nucleus formation for phase transition without volume change. *Journal of Crystal Growth* 375 (2013), 16–19.

[89] A. Mori. Volume term of work of critical nucleus formation in terms of chemical potential difference relative to equilibrium one. *Journal of Crystal Growth* 377 (2013), 118–122.

[90] H. Reiss. Critique of molecular theories of nucleation. *AIP Conference Proceedings* 534 (2000), 181–196.

[91] I. Kusaka, Z.-G. Wang and J. H. Seinfeld. Binary nucleation of sulfuric acid and water: Monte Carlo simulation. *Journal of Chemical Physics* 108 (1998), 6829–6848.

[92] B. E. Wyslouzil, J. H. Seinfeld, R. C. Flagan and K. Okuyama. Binary nucleation in acid–water systems. II. Sulfuric acid–water and a comparison with methanesulfonic acid–water. *Journal of Chemical Physics* 94 (1991), 6842–6850.

[93] H. Vehkamäki, M. J. McGrath, T. Kurtén, J. Julin, K. E. J. Lehtinen and M. Kulmala. Rethinking the application of the first nucleation theorem to particle formation. *Journal of Chemical Physics* 136 (2012), 094107.

[94] D. Brus, V. Ždímal and H. Uchtmann. Homogeneous nucleation rate measurements in supersaturated water vapor II. *Journal of Chemical Physics* 131 (2009), 074507.

[95] R. J. Weber, J. J. Marti, P. H. McMurry, F. L. Eisele, D. J. Tanner and A. Jefferson. Measured atmospheric new particle formation rates: Implications for nucleation mechanisms. *Chemical Engineering Communications* 151 (1996), 53–64.

[96] K. Denbigh. *The Principles of Chemical Equilibrium*. 4th ed. Cambridgre: Cambridge University Press, 1981.

4 Displacement barrier heights from the experimental nucleation rate data[1]

Nucleation phenomena have a great importance in many areas of science. However, the main theoretical tool to analyse these phenomena, the classical nucleation theory (CNT), has its known weaknesses. Two decades ago a nucleation theorem based correction to CNT was developed [R. McGraw and A. Laaksonen. Scaling properties of the critical nucleus in classical and molecular-based theories of vapor–liquid nucleation. *Physical Review Letters* 76 (1996), 2754–2757]. We have reanalysed the experimental nucleation rate data of two homologous series of molecular fluids in terms of this scaling relation. Our first results suggest a possible universal functional form for the correction to the temperature dependence of CNT.

[1]This chapter incorporates the article J. Malila, A.-P. Hyvärinen, Y. Viisanen and A. Laaksonen. Displacement barrier heights from experimental nucleation rate data. *Atmospheric Research* 90 (2008), 303–312; see also Ref. [1] for a preliminary analysis. Prof. Mikhail Anisimov, Dr. David Brus, and Dr. Vincent Holten are acknowledged for providing us with their experimental data in electronic form. We also thank Ms. Riikka Annila, Dr. Ismo Napari, and Prof. Hanna Vehkamäki for their help with the collection of the thermodynamic and nucleation rate data.

4.1 Motivation

Nucleation phenomena are ubiquitous in the Nature. For example, in the atmosphere, nucleation processes take place in the formation of new ultrafine particles in the planetary boundary layer and in the free troposphere [2], and in ice crystal formation in cloud droplets [3]. These processes have a potential impact on the radiative forcing of the atmosphere, and thereby on the global climate [4, 5], and they are subject to direct and indirect anthropogenic disturbances. The basic tool to analyse these phenomena is the classical nucleation theory (CNT) [6, 7]. It has been applied to describe nucleation phenomena in different fields of science more or less successfully [e.g. 3, 8–11]. However, vapour-to-liquid homogeneous nucleation experiments have indicated that CNT predicts the saturation ratio dependence of the nucleation rate (i.e. the number of emerging droplets in unit volume and time) rather well, but fails to predict the temperature dependence of the nucleation rate. To overcome this problem, several phenomenological theories have been suggested, which usually can improve CNT predictions for some substances, but fail to describe the nucleation behaviour of others. Here we present results of a nucleation theorem based analysis of the experimental vapour-to-liquid homogeneous nucleation rate data for a variety of substances, and discuss the general nature of corrections needed to bring CNT in unison with the experiments.

4.2 Theory

4.2.1 Classical nucleation theory

According to CNT, the nucleation rate is given by an Arrhenius-type expression,

$$J_{\mathrm{CNT}} = \sqrt{\frac{2\gamma_\infty}{\pi m}} v_l S \left(\frac{p_e}{k_\mathrm{B}T}\right)^2 e^{-W^*_{\mathrm{CNT}}/k_\mathrm{B}T}. \tag{4.1}$$

Here γ_∞ is the surface tension, m molecular mass, v_l molecular volume (of the liquid phase), S the saturation ratio and p_e the equilibrium vapour pressure of the nucleating substance. T is the nucleation temperature and

k_B the Boltzmann constant. The nucleation rate J depends exponentially on the work of formation of the critical nucleus, W^*, which in the case of vapour-to-liquid nucleation in the framework of CNT is given as the free energy cost to create a spherical drop of macroscopic liquid [6, 12], also known as the capillarity approximation,

$$W^*_{\mathrm{CNT}} = \frac{4\pi R^2 \gamma_\infty}{3}, \tag{4.2}$$

where R is the radius that fulfils the Kelvin equation,

$$R = \frac{2\gamma_\infty v_l}{k_B T \ln S}. \tag{4.3}$$

In Eq. (4.1), the $1/S$-correction [13] is included, which makes J_{CNT} satisfy the law of mass action. It is also assumed that the mass accommodation coefficient is unity: according to recent reviews [14, 15], this assumption is valid in the typical case of a liquid droplet nucleating from supersaturated vapour phase. However, in light of some theoretical [see e.g. discussion in 16] and experimental [17] results, this assumption should break down for clusters smaller than roughly 20 molecules, and so it may affect some of the experimental results analysed here.

4.2.2 Displacement barrier height

Based on the model independent[2] first nucleation theorem [for a review, see 18],

$$\left(\frac{\partial(W^*/k_B T)}{\partial \ln S}\right)_T = -g^*, \tag{4.4}$$

where g^* is the excess number of molecules in the critical nucleus, the classical Kelvin relation (4.3), and a homogeneity assumption, a scaling relation was derived to give a correction to the CNT prediction of the work of formation [19]:

$$-D(T) = W^* - W^*_{\mathrm{CNT}}. \tag{4.5}$$

This $D(T)$ is known as the displacement barrier height, and it is a function of temperature only. The displacement barrier height gives the difference

[2] Or supposedly model independent...

between the observed work of formation and the CNT prediction that can be attributed especially to interfacial effects, i.e. the size-dependence of the surface tension [20].

Density functional calculations [19, 21] and Monte Carlo simulations [22] have suggested that the relation (4.5) holds for homogeneous nucleation of simple liquids and that for a fixed temperature, $D(T)$ is a constant. Furthermore, they imply that $D(T)/k_\mathrm{B}T$ is a linear function of the reduced temperature t. In more recent molecular dynamic calculations [23],[3] it has also been found that $D(T)/k_\mathrm{B}T$ is a linear function of t for lennard-jonesium and water for clusters larger than a certain critical size. However, recent density functional calculations of dimeric and trimeric fluids [24] suggest that there is a slight size-dependence in $D(T)$ also for larger clusters, which can be explained by considering $D(T)$ as the dominating term of the polynomial expansion of the free energy difference in Eq. (4.5) [25]. However, it can be assumed that the deviations in experimental results due to measurement inaccuracies yield more significant error than the omission of other terms in the expansion, and Eq. (4.5) will be used to reanalyse the experimental data.

It has been observed that when plotting the experimentally obtained and CNT predictions of J versus T in a log–log-scale, the resulting lines often have different slopes and they cross at some point in the measured range. It seems reasonable that the real nucleation rate is given by an equation having the same form as Eq. (4.1). Considering computational observations, and the fact that the kinetic prefactor in Eq. (4.1) varies only weakly with temperature when compared to the exponential Boltzmann-factor, we suggest that $D(T)/k_\mathrm{B}T$ could be extracted from the experimental data as

$$\frac{D(T)}{k_\mathrm{B}T} \approx \ln \frac{J}{J_\mathrm{CNT}} = a + bt, \tag{4.6}$$

where $t = T/T_c$ and T_c is the critical temperature. Equation (4.6) is now also in agreement with computational studies, as the reduced temperature scales defined by the critical temperature or parameters of intermolecular potential functions used in simulations differ only by a constant factor for any given substance.

[3] Here is a typo in the original article: also Merikanto et al. [23] performed *Monte Carlo simulations*.

Hale [26] has noted that the temperature-dependent correction with a similar magnitude than $D(T)$ may also arise from the kinetic prefactor in cases where it does not vary so weakly with temperature, especially when this variation is either under- or overpredicted by CNT. The temperature dependence of the classical prefactor is given (in leading order) by $e^{f(T)}/T^n$, where now both the exponent $n \sim 2-3$ and the function $f(T)$ depend on the temperature dependence of the thermodynamic properties γ_∞, v_l, and p_e, respectively. So the effect of prefactors on the obtained values of a and b cannot be totally neglected, but in this work the prefactors are assumed to be similar enough in both J and J_{CNT} and for different substances that the obtained coefficients a and b are comparable.[4]

4.3 Data analysis

4.3.1 Thermodynamic properties

To evaluate J_{CNT} at given T and S, Eqs. (4.1)–(4.3), we need to know the thermodynamic properties of the studied substances. In the nucleation experiments, large supersaturations are needed to produce observable nucleation rates. This often leads to a situation in which not only the mother phase, but also the new, nucleating phase is in a metastable state. In the case of vapour-to-liquid nucleation, this means that the clusters of the new phase are supercooled, and the thermodynamic properties are needed at lower temperatures than usually reported in the literature. We have reviewed the published experimental data and the suggested temperature dependent fits for different properties (see Tables 4.1 and 4.2 for the original sources of the used fits or earlier critical evaluations when available). Critical temperatures for H_2O and D_2O were taken from [27], and for n-alkanols, recommendations of [28] were followed. The T_c of i-octane is from [29], and with n-alkanes, we used values taken from the compilation of Ambrose and Tsonopoulos [30].

The estimated error of J_{CNT} is now due to errors in the used fits for the thermodynamic. Errors in the fits, for their part, emerge from possible in-

[4]For the same reason, the vertical axis in Figs. 4.1–4.4 and 4.6 has been labelled as $D(T)/k_{\mathrm{B}}T$ instead of more accurate $\ln(J/J_{\mathrm{CNT}})$.

accuracies in the original measurements, from the suitability of the chosen model for a given property (e.g. the usage of the Antoine equation for the equilibrium vapour pressure), inadequate extrapolations, and also from printing errors. Problems here are illustrated by an example of the density of supercooled D_2O: the fit given by Wölk and Strey [27] follows closely the experimental values of Hare and Sorensen [31], measured in glass capillaries. However, the recent small angle neutron scattering (SANS) measurements of Liu et al. [32] of D_2O confined into nanopores, while extending the measured density values to higher degrees of supercooling, yield notably smaller densities at overlapping temperatures. These measurements were done for a liquid under the Laplace pressure $p_p = \gamma_p / r_p$, where r_p is the radius of the cylindrical nanopore and γ_p the surface tension of supercooled D_2O–pore interface, and so the SANS measurements should give *higher* densities.[5] Another examples are the surface tension and equilibrium vapour pressure of n-nonane [cf. 36, 37], where erroneous extrapolation of measured values to lower temperatures can lead to substantially biased estimates for the nucleation work and rate. Comparing different expressions for different thermodynamic properties for different substances, the error in J_{CNT} was estimated to be approximately one or two orders of magnitude, comparable to that of measured values of J.

4.3.2 Experimental nucleation rate data

Since the pioneering work of Wilson [50], a variety of methods has been developed to measure the nucleation rate J as a function of temperature and saturation ratio. The most popular ones are based on adiabatic expansion (expansion chambers and tubes, supersonic nozzles) or diffusive mixing (static, thermal and laminar flow diffusion chambers) of the mixture of

[5] There has been some controversy regarding density measurements of water and heavy water done in nanopores [e.g. 33]. Besides the curved surface of the nanopore itself, and the effect of hydrogen bonding between hydroxyl groups in the nanoporous silica and water molecules, there is also a concave water meniscus at the end of nanopores, causing a negative Laplace pressure in the longitudinal direction. All these factors make the pressure and density fields inside the nanopore inhomogeneous, complicating the interpretation of the measurements. However, there are some indications that the averaged density over the nanopore should be comparable to that of a bulk liquid [34], although the exact nature of this correspondence remains still open to interpretations [35].

Table 4.1. References for the thermodynamic data used for light and heavy water and n-alkanols. Symbols are as in the main text except for ρ that is used for liquid density.

Substance	p_e	ρ	γ_∞
light water	[38]	[27]	[39]
heavy water	[27]	[27]	[27]
methanol	[40]	[41][a]	[42]
ethanol	[43]	[44]	[42]
n-propanol	[40]	[36]	[36]
n-butanol	[40]	[42]	[42]
n-pentanol	[40]	[45]	[42]
n-hexanol	[40]	[42]	[42]
n-heptanol	[46]	[42]	[42]
n-octanol	[46]	[42]	[42]

[a] Linear fit to tabulated values: also values reported by Mikhail and Kimel [47] follow this fit.

Table 4.2. Same as Table 4.1 for alkanes.

Substance	p_e	ρ	γ_∞
n-heptane	[48]	[48]	[48]
n-octane	[48]	[29]	[29]
i-octane	[29]	[29]	[29]
n-nonane	[43]	[48]	[37]
n-decane	[48]	[48]	[48]
n-dodecane	[49]	[49]	[49]
n-hexadecane	[49]	[49]	[49]
n-octadecane	[49]	[49]	[49]

the studied vapour and an inert carrier gas. A review of experimental methods can be found from the article by Heist and He [51], where also experimental results prior to 1992 have been reviewed. Further information on the different measurement setups can be found from the cited articles.

The majority of newer references, after early 1990's, report the actual measured, nucleation rates with the corresponding temperatures and saturation ratios. Only this full T, S, J-data were used for analysis. To obtain $D(T)$ from these data, basic techniques of discrete least squares were applied to obtain the coefficients a and b in Eq. (4.6).[6] Only molecular fluids are considered in this study. The reason behind this choice is that other fluids used in the experimental vapour-to-liquid nucleation research—metals and noble gasses—have other problems that tend to complicate the analysis: metal-nonmetal phase transitions, poor knowledge of the needed thermodynamic properties, and quantum effects just to mention some. Also, there is a lot of experimental data of the fluids studied here—normal and heavy water, n-alkanols and n-alkanes—with nucleation measurements made by multiple techniques.

4.3.3 Pressure effects

There are two kinds of pressure effects present in nucleation experiments. The first one is merely a computational one, and related to the fitting functions of the equilibrium vapour pressure: due to the exponential dependence of p_e on T, even small deviations in parameterisations can produce large errors in calculated saturation ratios $S = p/p_e(T)$, where p is the measured partial pressure of the nucleating vapour. To overcome this effect, when different equilibrium vapour pressure fits are used by different research groups, we have applied the following correction to all used experimental data:

$$S_{\text{new}} = \frac{p}{p_{e,\text{new}}(T)} = \frac{S_{\text{old}} p_{e,\text{old}}(T)}{p_{e,\text{new}}(T)}. \tag{4.7}$$

[6] Generally, the nucleation temperature is better constrained than the nucleation rate in the experiments. However, as the nucleation temperature is also an estimated quantity, a more proper treatment would have been to use total least squares or some other bi-variate least squares variant for the data analysis [cf. 52].

Here $p_{e,\mathrm{old}}(T)$ is the fit used by the referenced author to calculate the published saturation ratios S_{old}, and $p_{e,\mathrm{new}}(T)$ is the recommended fit that is used in this article. As we have already noted [46], this is only a partial correction, since for the results from diffusion based devices and supersonic nozzles, one should correct equilibrium vapour pressure fits also to the equations determining temperature, saturation and flow profiles.

Another reference to pressure effects is made, when the dependence of the nucleation rate J on the prevailing pressure is discussed. According to CNT, J should depend only on temperature and the partial pressure of the nucleating vapour; the pressure of the carrier gas should not have any effect to the nucleation rate as long as it provides thermalisation for the nucleating clusters. However, some experiments do suggest that the carrier gas affects the nucleation rate even when this condition is fulfilled. Here the main division is between expansion and diffusion based apparatuses. In diffusion based devices, pressure effects can be seen when the carrier gas pressure is lowered [53–55] or the carrier gas is changed to another one with different molecular mass [56]. However, the existence of both upper and lower bound for suitable operation of diffusion based devices has been addressed [57]. On the other hand, in expansion based devices, the observed pressure dependencies are weak and opposite to those observed in diffusion based devices [53], and usually do not depend on the used carrier gas [e.g. 58, 59]. Pressure effects in expansion based devices are usually related to the increasing non-ideality of the mixture of carrier gas and vapour, invalidating some of the assumptions done when deriving Eq. (4.1) or analysing the measured data, or to the adsorption of the carrier gas to the surface of cluster, causing a decrease in the surface tension [54]. As our aim is to study the nucleation of pure substances only, experimental results that describe nucleation where the carrier gas is also participating in the formation of the critical nuclei [e.g. 60, 61] are left out.

To get rid off possible pressure effects and other yet undetermined systematic errors in the measured data, the nucleation rate data from diffusion based devices were used only, when the total pressure of the mixture of vapour and carrier gas in the nucleation chamber has been chosen so high that no significant pressure effects were observed, when possible [e.g. 45, 53, 55, 62, 63], otherwise data from pressures higher than 1 atm were used. For expansion based devices, data from high overpressures were not used. To check the possible existence of the pressure effects, we have compared

all nucleation rate measurement sets for any given substance (or a group of similar substances) with each other. Those data that exhibit different temperature dependence from all other measurements of the same substance or are otherwise inconsistent have been excluded from the further analysis. The most important group of data showing such systematic deviation from other data sets has been obtained using the laminar flow diffusion tube or a similar setup [e.g. 64, 65] at low total pressures. Also some other measurements [66, 67] yield similar results, though reasons for this behaviour are unknown; possible reasons include, for example, the effect of impurities and the subsequent "washing effect" [68].[7]

4.4 Results

4.4.1 Comparison of different measurement devices

In Fig. 4.1 all analysed data for *n*-pentanol, mostly from the Joint Nucleation Experiment [71], are given. Measurements included are those of Brus et al. [54], Gharibeh et al. [72], Hrubý et al. [73], Iland et al. [59], Luijten et al. [74], Rudek et al. [45], Strey et al. [75], Schmitt and Doster [76], and Ždímal and Smoliík [77], and span the largest range of nucleation rates measured and experimental techniques used for any given substance. It can be seen that the different measurement methods are mostly consistent with each others, see also Fig. 6 in the article of Iland et al. [59], or Fig. 8 in the article of Hyvärinen et al. [46], where data left out from this study [64, 66] are also shown. Also, Ferguson et al. [78] have given a similar fit in their Fig. 7, where data of Rudek et al. [45] have been recalculated. These recalculated values are in fact closer to the linear fit given here than the original data of Rudek et al. [45] shown in Fig. 4.1, especially at high

[7] In the case of the flow tube at the Finnish Meteorological Institute it was found that the results are biased due to a flaw in the code used to evaluate the saturation ratio and temperature fields inside the tube [69]; however, the analysis given here is partially based on the revised data [62, 63] available when writing the original article. Further insight into this phenomenon was obtained by Wedekind et al. [70], who pointed out the competing roles of thermalisation and change in W^* due to pressure-work on J as function of pressure (cf. Sec. 3.5).

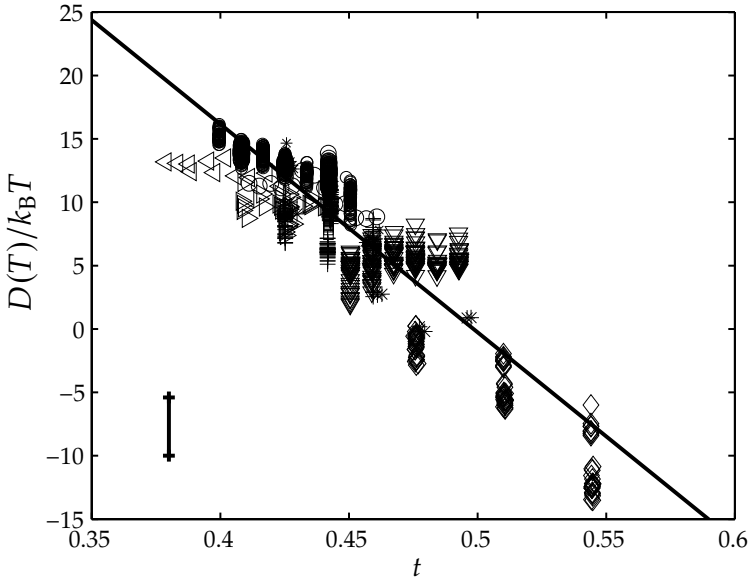

Fig. 4.1. Analysed data of n-pentanol, different symbols refer to different measurement techniques: □ stands for a static diffusion chamber, ◯ for a nucleation pulse chamber, + for a piston-expansion tube, ∗ for an expansion chamber, ◊ for a thermal diffusion chamber, ◁ for a supersonic nozzle combined with SANS, ▷ for ean xpansion wave tube, and ▽ for a laminar flow diffusion chamber. For the coefficients a and b of the fitted line, see Table 4.3. Vertical bar gives the approximate error for all data points (see text for details).

temperatures ($t > 0.45$), suggesting the validity of the proposed fit for the whole temperature range.

In Fig. 4.1 also the estimated average error, two orders of magnitude in J/J_{CNT}, is given. When we compare this to the results of our scaling, Eq. (4.6), we notice that i) all measurements made with the same setup are internally consistent (for the isotherm at $t \approx 0.54$, see [78] as discussed above), and ii) averages of all data sets for each isotherm are within this error from the fitted line $a + bt$.

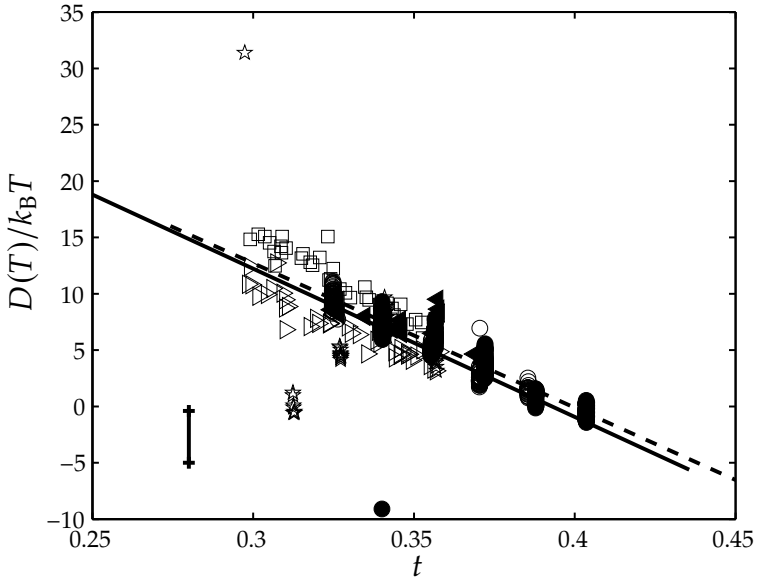

Fig. 4.2. Analysed data of normal (open symbols and solid line) and heavy water (filled symbols and dashed line). For the values of coefficients a and b see Table 4.4; different symbols are as in Fig. 4.1 except for ★ that stands for a laminar flow reaction tube. Vertical bar gives the approximated error for all data points.

4.4.2 Waters and n-alkanols

In Fig. 4.2, results for normal and heavy water are represented: Experimental nucleation rates for water were obtained from the recent measurements of Holten et al. [39], Kim et al. [79], Labetski et al. [80], Mikheev et al. [81], and Wölk and Strey [27]. Results for heavy water are derived from the extensive measurements of Wölk and Strey [27] and from the recent measurements utilising a setup with a supersonic nozzle and a SANS device [79, 82–84]. Older results of Viisanen et al. [58] [see also 85] and Miller et al. [86] for H_2O are not fully consistent with the more recent measurements, and are not included.

Results for different n-alkanols from methanol to n-octanol (excluding n-pentanol) are depicted in Fig. 4.3. These measurements are originally reported by Brus et al. [53, 62], Gharibeh et al. [72], Graßmann and Peters [87], Hyvärinen et al. [46, 63], Lihavainen and Viisanen [64, 88], Strey et

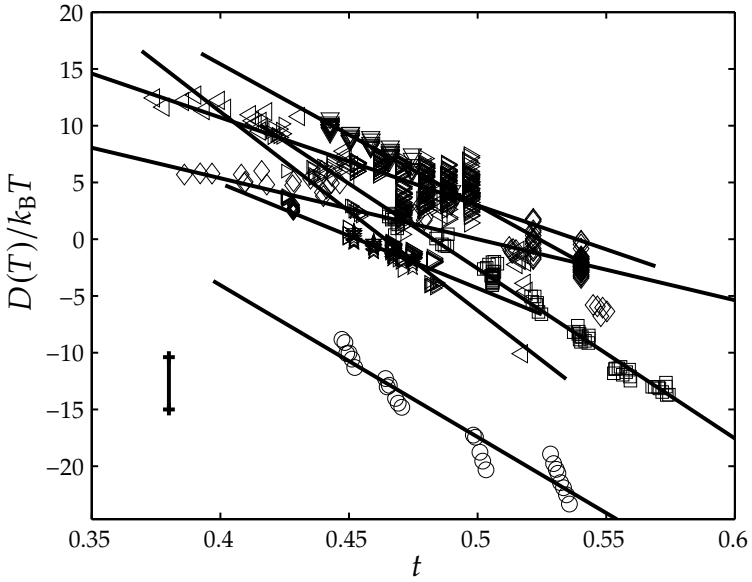

Fig. 4.3. Analysed data of n-alkanols other than n-pentanol. See Table 4.3 for the coefficients a and b of fitted lines, and for a legend. Vertical bar gives the approximated error for all data points.

al. [75, 89], and Viisanen et al. [90, 91]. Coefficients a and b, and the qualities of fits (R^2) with the number of data points used for each fit (N) for the n-alkanols are given in Table 4.3 together with a legend to Fig. 4.3. Despite the variability of the coefficients a and b, all data of n-alcohols are clustered roughly within a distance given by the offset of different measurement setups for any given n-alcohol without significant deviations due to the carbon number, except for methanol, which is closer to the fits of the waters.

Coefficients a and b are given in Tables 4.3 and 4.4 with error estimates corresponding to ± standard deviation. Only some outliers do not fall within these errors. Also it should be noted that the dependence of the correlation of linear fits does not depend so much on the number of data points used for one fit (N), but instead on the number of experimental data sets for one substance, thus also implying that the main reason behind the scatter of data points are differences in experimental setups. For example, if the water laminar flow tube reactor data [81], which are evidently outliers in lower temperatures, are left out from the fit of water, the quality of the

Table 4.3. Coefficients a and b for n-alkanols to fits shown in Figs. 4.1 and 4.3, qualities of linear fits (R^2), the number of data points for each fit (N), and symbols used in Fig. 4.3.

Substance	a	b	R^2	N	symbol
methanol	49.5 ± 3.4	-133.8 ± 7.0	0.969	25	○
ethanol	72.2 ± 1.1	-149.6 ± 2.2	0.992	78	□
n-propanol	26.8 ± 1.3	-53.7 ± 2.5	0.899	108	◊
n-butanol	41.7 ± 2.1	-77.4 ± 4.2	0.687	357	◁
n-pentanol	81.8 ± 1.0	-164.2 ± 2.2	0.897	1344	
n-hexanol	81.3 ± 3.0	-175.2 ± 6.5	0.936	105	▷
n-heptanol	65.2 ± 2.1	-124.6 ± 4.7	0.965	54	▽
n-octanol	41.9 ± 2.7	-92.4 ± 5.9	0.926	42	★

Table 4.4. Coefficients a and b for heavy and normal water from experimental data with the qualities of linear fits (R^2) and the number of experimental data points (N). Predictions of the scaling relations of Hale [26] and Wölk et al. [92], the internally consistent theory (ICT) of Girshick and Chiu [93], and "simple correction" (SC) of Nadykto and Yu [94] for H_2O are also compared to that of CNT: in these cases $D(T) = W^*_{\text{scaled/ICT/SC}} - W^*$.

Substance/scaling	a	b	R^2	N
D_2O	51.2 ± 0.8	-128.2 ± 2.3	0.936	451
H_2O	51.1 ± 2.0	-119.7 ± 5.7	0.725	393
H_2O, Wölk	22.8 ± 2.0	-38.1 ± 5.8		
H_2O, Hale	39.7 ± 2.3	55.7 ± 6.7		
H_2O, ICT	17.7 ± 2.0	-58.7 ± 5.8		
H_2O, SC	7.9 ± 2.0	-38.1 ± 6.0		

Table 4.5. Coefficients a and b for n-alkanes and i-octane, qualities of linear fits (R^2), the number of data points for each fit (N), and the legend to Fig. 4.4.

Substance	a	b	R^2	N	symbol
n-heptane	78.7 ± 2.9	−169.8 ± 5.9	0.989	19	◯
n-octane	91.3 ± 1.9	−172.4 ± 4.3	0.878	465	□
i-octane	34.5 ± 1.2	−47.7 ± 3.0	0.687	265	
n-nonane	71.1 ± 0.9	−150.7 ± 2.1	0.995	50	◊
n-decane	93.1 ± 869.0	−187.9 ± 1627.5	0.057	5	◁
n-dodecane	66.3 ± 5.2	−135.0 ± 11.3	0.934	22	▷
n-hexadecane	98.9 ± 3.0	−196.8 ± 6.6	0.983	33	▽
n-octadecane	97.0 ± 2.6	−195.3 ± 5.9	0.981	44	★

fit, R^2, increases from 0.725 to 0.920. Errors in coefficients a and b for water and n-alcohols also correspond reasonably with estimated average errors in $D(T)$ due to experimental errors in nucleation rate measurements and inaccuracies of the thermodynamic parameterisations, also shown in left lower corners of Figs. 4.2 and 4.3.

4.4.3 n-Alkanes

Results for n-alkanes from n-heptane to n-decane from the measurements of Doster et al. [29], Hung et al. [37], Rudek et al. [48], and Viisanen et al. [91], as well as for n-dodecane, n-hexadecane, and n-octadecane [49], are given in Fig. 4.4 and in Table 4.5, where also the results for i-octane from the measurements of Doster et al. [29] are shown for comparison. It is interesting to note that higher n-alkanes seem to follow the general trend of lower n-alkanes well, although Rusyniak et al. [49] found a poor correlation between the nucleation theorem and the CNT, as the obtained g^* from the first nucleation theorem were significantly larger than predicted by the CNT, implying that the displacement barrier height analysis might not be applicable in this case. Also their total pressures were lower than 1 atm, which may have caused significant pressure effects.

Again, the reported errors of coefficients in Table 4.5 do reproduce the experimental variation and correspond to the estimated error of $D(T)$ due to measurement inaccuracies and uncertainties in the used thermodynamic

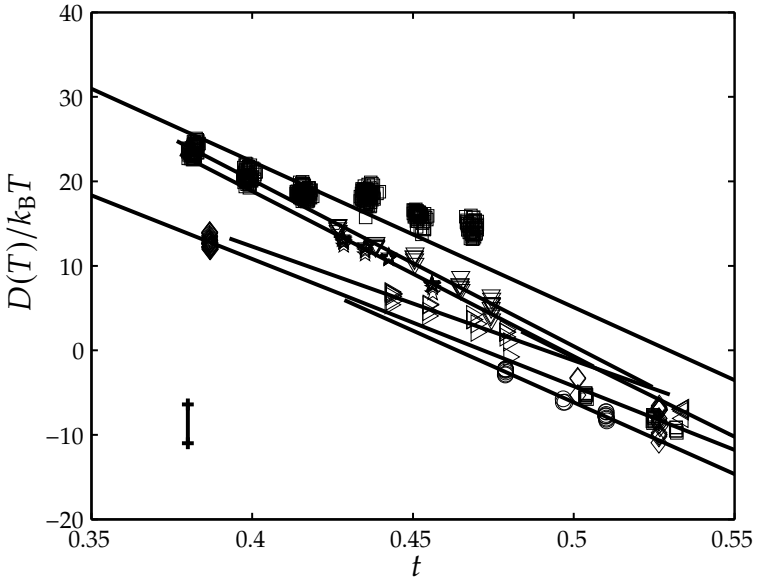

Fig. 4.4. Analysed data of n-alkanes. See Table 4.5 for the coefficients a and b of fitted lines, and for a legend. Vertical bar gives the approximated error for all data points.

data, with the exception of *n*-decane. The very large error estimates of *n*-decane originate from the fact that practically only the measurements of Rudek et al. [48] at a single temperature satisfied the condition that the total pressure wa larger than 1 atm. Comparison of the measurements of *n*-octane using an expansion chamber [29] and a thermal diffusion chamber [48] (black squares in Fig. 4.4) shows that although there is a similar temperature dependence, there is a significant offset of the results, which is comparable to the differences between different alkanes (the results for *i*-octane, which are not shown in Fig. 4.4, agree with *n*-alkanes in the measured temperature range), and forces the coefficient b to have a smaller value than could be deduced from a single dataset.

Rusyniak et al. [49] have also given practically the same correlation than our Eq. (4.6). However, their values for a and b differ somewhat from those proposed here; the most probable reason for this departure is that they have used values J/J_{CNT} in their fit,[8] whereas we have used $\ln(J/J_{\mathrm{CNT}})$.

4.4.4 Correlation of the coefficients a and b with molecular properties

Correlations of the obtained coefficients a and b with molecular mass (m), dipole moment (μ), the acentric factor (ω) [95], and the Boyle temperature (T_B) are given in Fig. 4.5. Molecular masses were calculated assuming a natural isotopic composition, except for D_2O. Molecular gas phase dipole moments were taken from the critical compilations of Mallard [41], Lide [96], and Abboud and Notario [97] for waters, lighter *n*-alkanols, and alkanes, respectively. For *n*-alkanols from *n*-pentanol to *n*-octanol, reliable values of molecular dipole moments in the gas phase were not available from the literature, and the values provided by El-Hefnawy et al. [98] for infinitely dilute solutions were used instead. Boyle temperatures for most substances were obtained from Estrada-Torres et al. [99]. There seems to be no clear correlation between the coefficients and the mass (or carbon number) of the molecule, its dipole moment (which can be used as a rough estimate of hydrogen bonding), acentric factor, nor the Boyle temperature. Neither isotopic composition (H_2O vs D_2O) nor isomerism (*n*-octane vs.

[8] Which is indeed the preferable way to perform least squares fitting, as the distribution of errors remains approximately Gaussian. . .

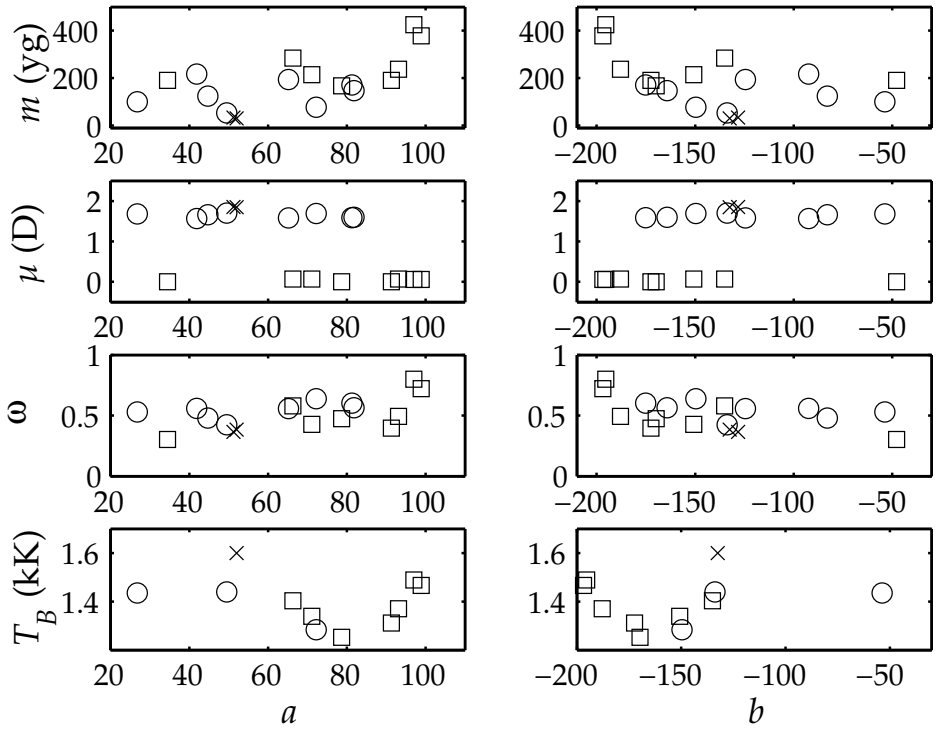

Fig. 4.5. Correlations of coefficients a and b with molecular properties. Waters are marked with ×, homologous series of n-alkanols with ○ and that of n-alkanes and i-octane with □ .

i-octane) seems to differentiate the coefficients a and b either, although subsequent studies of multiple isotopes or isomers would be needed to confirm this claim.

4.5 Discussion

4.5.1 On the universality of $D(T)$

According to the results depicted in Figs. 4.1–4.4 and Tables 4.3–4.5, the experimental nucleation rate data can be reasonably described by a linear

function $a + bt$ when using the reduced variables $D(T)/k_\mathrm{B}T$ and t. For all studied substances, the variation of the parameters of this fit is mainly determined by the experimental method used to measure the nucleation rate, and it is not very sensitive to the molecular mass of the studied substance nor even to the degree of hydrophobicity or the nature of bonding between molecules (van der Waals or hydrogen bonds). However, it is possible to classify the waters and methanol into one group, and other n-alkanols and alkanes to another one, suggesting the importance of the release of latent heat to the nucleation process [75]. In fact, the given data can be presented by a function

$$\frac{D(T)}{k_\mathrm{B}T} = 75 - (160 \pm 30)t, \tag{4.8}$$

where the ±30 variation in b corresponds now twice to the maximum deviations between different measurement setups for one given substance. The above correlation, together with the fact that all individual correlations yield negative values for b, implies that the temperature dependence of CNT is generally overpredicted, at least for molecular fluids (and metals) studied here.

The found values for a and b give now the possibility to estimate the nucleation rate using only thermodynamic parameters from laboratory measurements in form

$$\ln J = a + b\frac{T}{T_c} + \ln J_\mathrm{CNT}. \tag{4.9}$$

4.5.2 Comparison with other measurements and scaled and phenomenological models

Kacker and Heist [100] have used a similar approach as ours to correlate the function $A+B/T$ with the deviation of the nucleation work from its classical value, Eq. (4.2), for ethanol and n- and i-propanol. Their results imply factors corresponding to our $D(T)/k_\mathrm{B}T$ from approximately 240 to −70, which extends the range of our scaling for the same substances by many times. It should be noted that also other researchers have used similar functional forms for the correction factor [75, 92]. However, these results are not directly comparable to ours as the parameters fitted to different

functional forms are not usually comparable. More recently, McGraw ([101], see also [102]) has argued that the form $A + B/T$ can also be retrieved from $\ln(J/J_{\mathrm{CNT}})$, and that this form is consistent with the second nucleation theorem and the Arrhenius-type temperature dependence of J. However, depending on the assumed temperature dependencies of σ, ρ, and p_e in Eq. (4.1), it is also plausible to reach the same conclusion from our analysis. McGraw [101] has also used principal component analysis to estimate $\ln J$ as a function of $1/T$ and $\ln S$. When comparing the quality of these fits to those utilising Eq. (4.6) with the same sets of experimental data, we find that the method presented in this article gives better fits for the water data of Wölk and Strey [27] and the methanol data of Strey et al. [75] ($R^2 = 0.964$ and 0.969 vs. 0.94 and 0.89), but does not fit the n-hexanol data of Strey et al. [75] so well ($R^2 = 0.936$ vs. 0.97).

Also other scaled models of nucleation have been proposed [103]. The most successful one so far has been the scaling relation originally proposed by Hale [104, 105]. We have compared results of Eq. (4.6) to those of Hale [26] and Wölk et al. [92] for water. Results are shown in Table 4.4. The scaling proposed originally by Wölk et al. is in reasonable agreement with the experimental data, especially at the centre of experimental interval. Hale's scaling, on the other hand, seems to overpredict $D(T)$. In other words, the prediction of the temperature dependence of J in Hale's theory (with $\Omega = 1.47$) differs from the measured data to other direction than CNT. Besides water, scaling analyses of other substances are readily available from the literature, for example Rusyniak and El-Shall [106] have given a detailed analysis of the scaling of nucleation rate data of higher n-alkanes according to Hale's [104] theory.

Besides other scaling or correction models, results using two different phenomenological theories of nucleation, the internally consistent theory (ICT) of [93] and "simple correction" (SC) of Nadykto and Yu [94], were compared to the results of the displacement barrier height scaling with respect to CNT. Results for water are again given in Table 4.4. These results show that for water, ICT most closely predicts the nucleation rate when compared to other theories discussed here. However, the agreement is not as perfect as found by Merikanto et al. [23] for simulated water, who noticed that $D(T)$ in their simulations for water was given exactly by the internal consistency correction of Girshick and Chiu [93] for clusters larger than approximately ten molecules. We also confirm that SC gives a sur-

prisingly good estimate for the water nucleation rate despite its somewhat heuristic origins. Further comparisons between different phenomenological theories and experimental data can be found from the literature [e.g. 94].

4.6 Conclusions

According to our results, a theoretically based temperature dependent correction to CNT can be given as a linear function using reduced variables for molecular fluids. Furthermore, the temperature dependence of this correction seems to be of universal nature, as it is affected by the experimental technique to measure the nucleation rate at least as much as the studied substance. These findings suggest a possibility to develop a universal correction for nucleation rates. Future work will be needed to check this theory against other substances besides those used in this study and to check the possibility to extent it to mixtures.

4.A Addendum: $D(T)$-scaling for metals

Besides organic molecular fluids and waters, vapour-to-liquid nucleation experiments have performed also on "simple" fluids, like argon [for a review, see 107, Chap. 10, and also 108] and nitrogen [108–111], and on various metals [see, e.g., Refs. 112, 113, and references therein]. For a comparison, we [114] have performed the displacement barrier height analysis also for the homogeneous nucleation rate measurements of mercury [115] and caesium [116, 117], which results are depicted in Fig. 4.6.[9] Sources of thermodynamic data needed for the analysis are given in Table 4.6.

[9] We have also carried out a similar analysis of argon nucleation rates [118]; however, it turned out that the calculated $D(T)$-values posed too large scatter for a meaningful estimation of parameters a and b. Homogeneous nucleation of bismuth would also be an interesting test for the assumptions of the $D(T)$-scaling, as the bismuth vapour is dominated by dimers [e.g. 119]; unfortunately, the available experimental data [113] are not i) completely independent from the CNT, and ii) cover only J evaluated at two conditions.

Table 4.6. Same as Tables 4.1 and 4.2 but including also T_c for Ce and Hg.

Substance	p_e	ρ	γ_∞	T_c
caesium	[116]	[116]	[116]	[96]
mercury	[120]	[120]	[121]	[122]

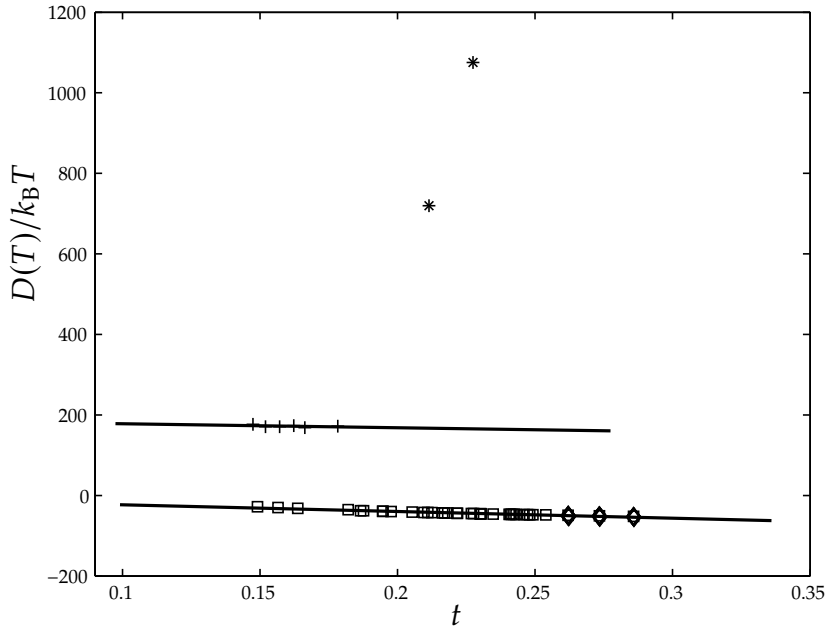

Fig. 4.6. $D(T)$-analysis for mercury (+, $*$) and caesium ($\Box$, $\Diamond$).

For mercury, only data points below $t = 0.2$ (marked with + in Fig. 4.6), which were treated differently already in the original analysis of the raw measurement data [115], were included into analysis: At higher temperatures, a likely explanation for the discrepancy is that larger critical clusters are metallic, whilst smaller critical clusters at lower temperatures are non-metallic [115, 122]. Obviously there is now some inconsistency in the analysis, as thermodynamic properties of bulk, metallic liquid are assumed. The linear scaling of $D(T)/k_\mathrm{B}T$, however, produces a reasonable fit to measurements below $t = 0.2$, yielding $a = 188.162$ and $b = -100.166$ (if all data are included, the resulting coefficients are $a = -1621.29$ and $b = 11265.682$). For caesium, both data sets [116, 117] follow the same linear correlation with $a = -6.289$ and $b = -166.849$. Negative value for a implies that, in contrast to other studied substances, CNT does not predict the nucleation rate of caesium correctly anywhere in the studied temperature range.

References

[1] A. Laaksonen and K. E. J. Lehtinen. Nucleation. In: *Environmental Chemistry of Aerosols*. Ed. by I. Colbeck. Oxford: Blackwell, 2008. Chap. 2.

[2] M. Kulmala, H. Vehkamäki, T. Petäjä, M. Dal Maso, A. Lauri, V.-M. Kerminen, W. Birmili and P. H. McMurry. Formation and growth rates of ultrafine atmospheric particles: a review of observations. *Journal of Aerosol Science* 35 (2004), 143–176.

[3] W. Cantrell and A. Heymsfield. Production of ice in tropospheric clouds: A review. *Bulletin of the American Meteorological Society* 86 (2005), 797–807.

[4] W.-T. Chen, H. Liao and J. H. Seinfeld. Future climate impacts of direct radiative fording of anthropogenic aerosols, tropospheric ozone, and long-lived greenhouse gases. *Journal of Geophysical Research D* 112 (2007), D14209.

[5] U. Lohmann. Aerosol effects on clouds and climate. *Space Science Reviews* 125 (2006), 129–137.

[6] M. Volmer and A. Weber. Keimbildung in übersättigten Gebilden. *Zeitschrift für physikalische Chemie* 119 (1926), 277–301.

[7] R. Becker and W. Döring. Kinetische Behandlung der Keimbildung in übersättigten Dämpfen. *Annalen der Physik* 416 (1935), 719–752.

[8] B. Donn and J. A. Nuth. Does nucleation theory apply to the formation of refractory circumstellar grains? *Astrophysics Journal* 288 (1985), 187–190.

[9] O. Galkin and P. G. Vekilov. Are nucleation kinetics of protein crystals similar to those of liquid droplets? *Journal of the American Chemical Society* 122 (2000), 156–163.

[10] K. K. Sahu, Y. Hazama and K. N. Ishihara. Gushing in canned beer: The effect of ultrasonic vibration. *Journal of Colloid and Interface Science* 302 (2006), 356–362.

[11] R. Zandi, P. van der Schoot, D. Reguera, W. Kegel and H. Reiss. Classical nucleation theory of virus capsids. *Biophysical Journal* 90 (2005), 1939–1948.

[12] P. G. Debenedetti and H. Reiss. Reversible work of formation of an embryo of a new phase within a uniform macroscopic mother phase. *Journal of Chemical Physics* 108 (1998), 5498–5505.

[13] W. G. Courtney. Remarks on homogeneous nucleation. *Journal of Chemical Physics* 35 (1961), 2249–2250.

[14] P. Davidovits, C. E. Kolb, L. R. Williams, J. T. Jayne and D. R. Worsnop. Mass accommodation and chemical reactions at gas-liquid surface. *Chemical Reviews* 106 (2006), 1323–1354.

[15] E. J. Davis. A history and state-of-the-art of accommodation coefficients. *Atmospheric Research* 82 (2006), 561–578.

[16] H. Tammet and M. Kulmala. Simulation tool for atmospheric aerosol nucleation bursts. *Journal of Aerosol Science* 36 (2005), 173–196.

[17] Y. Okada, S. Yamaguchi, Y. Kawai, T. Orii and K. Takeuchi. Incorporation probability of a water molecule into a water cluster. *Chemical Physics* 294 (2003), 37–43.

[18] D. Kashchiev. Forms and applications of the nucleation theorem. *Journal of Chemical Physics* 125 (2006), 014502.

[19] R. McGraw and A. Laaksonen. Scaling properties of the critical nucleus in classical and molecular-based theories of vapor–liquid nucleation. *Physical Review Letters* 76 (1996), 2754–2757.

[20] R. McGraw and A. Laaksonen. Interfacial curvature free energy, the Kelvin relation, and vapor–liquid nucleation rate. *Journal of Chemical Physics* 106 (1997), 5284–5287.

[21] V. Talanquer. A new phenomenological approach to gas-liquid nucleation based on the scaling properties of the critical nucleus. *Journal of Chemical Physics* 106 (1997), 9957–9960.

[22] P. R. ten Wolde and D. Frenkel. Computer simulation study of gas-liquid nucleation in a Lennard-Jones system. *Journal of Chemical Physics* 109 (1998), 9901–9918.

[23] J. Merikanto, E. Zapadinsky, A. Lauri and H. Vehkamäki. Origin of the failure of classical nucleation theory: Incorrect description of the smallest clusters. *Physical Review Letters* 98, 145702 (2007), 145702.

[24] I. Napari and A. Laaksonen. Surface tension and scaling of critical nuclei in diatomic and triatomic fluids. *Journal of Chemical Physics* 126 (2007), 134503.

[25] K. Koga and X. C. Zeng. Thermodynamic expansion of nucleation free-energy barrier and size of critical nucleus near the vapor-liquid coexistence. *Journal of Chemical Physics* 110 (1999), 3466–3471.

[26] B. N. Hale. Temperature dependence of homogeneous nucleation rates for water: Near equivalence of the empirical fit of Wölk and Strey, and the scaled nucleation model. *Journal of Chemical Physics* 122 (2005), 204509.

[27] J. Wölk and R. Strey. Homogeneous nucleation of H_2O and D_2O in comparison: The isotope effect. *Journal of Physical Chemistry B* 105 (2001), 11683–11701.

[28] D. Ambrose and J. Walton. Vapour pressures up to their critical temperatures of normal alkanes and 1-alkanols. *Pure and Applied Chemistry* 61 (1989), 1395–1403.

[29] G. J. Doster, J. L. Schmitt and G. L. Bertrand. Binary nucleation of *n*-octane and *i*-octane. *Journal of Chemical Physics* 113 (2000), 7197–7203.

[30] D. Ambrose and C. Tsonopoulos. Vapor-liquid critical properties of the elements and compounds. 2. Normal alkanes. *Journal of Chemical and Engineering Data* 40 (1995), 531–546.

[31] D. E. Hare and C. M. Sorensen. Densities of supercooled H_2O and D_2O in 25 μm glass capillaries. *Journal of Chemical Physics* 84 (1986), 5085–5089.

[32] D. Liu, Y. Zhang, C.-C. Chen, C.-Y. Mou, P. H. Poole and S.-H. Chen. Observation of the density minimum in deeply supercooled confined water. *Proceedings of the National Academy of Sciences U.S.A.* 104 (2007), 9570–9574.

[33] A. K. Soper. Density minimum in supercooled confined water. *Proceedings of the National Academy of Sciences U.S.A.* 108 (2011), E1192.

[34] Y. Zhang, A. Faraone, W. A. Kamitakahara, K.-H. Liu, C.-Y. Mou, J. B. Leão, S. Chang and S.-H. Chen. Reply to Soper: Density measurement of confined water with neutron scattering. *Proceedings of the National Academy of Sciences U.S.A.* 108 (2011), E1193–E1194.

[35] F. Caupin. Escaping the no man's land: Recent experiments on metastable liquid water. *Journal of Non-Crystalline Solids* 407 (2015), 441–448.

[36] A. I. Gaman, I. Napari, P. M. Winkler, H. Vehkamäki, P. E. Wagner, R. Strey, Y. Viisanen and M. Kulmala. Homogeneous nucleation of *n*-nonane and *n*-propanol mixtures: A comparison of classical nucleation theory and experiments. *Journal of Chemical Physics* 123 (2005), 244502.

[37] C.-H. Hung, M. J. Krasnopoler and J. L. Katz. Condensation of a supersaturated vapor. VIII. The homogeneous nucleation of *n*-nonane. *Journal of Chemical Physics* 90 (1989), 1856–1865.

[38] D. M. Murphy and T. Koop. Review of the vapour pressures of ice and supercooled water for atmospheric applications. *Quarterly Journal of the Royal Meteorological Society* 131 (2005), 1539–1565.

[39] V. Holten, D. G. Labetski and M. E. H. van Dongen. Homogeneous nucleation of water between 200 and 240 K: New wave tube data and estimation of the Tolman length. *Journal of Chemical Physics* 123 (2005), 104505.

[40] T. Schmeling and R. Strey. Equilibrium vapor pressure measurements for ten n-alcohols in the temperature range from −30 °C to +30 °C. *Berichte der Bunsengesellschaft für physikalische Chemie* 87 (1983), 871–874.

[41] W. G. Mallard, ed. *NIST Chemistry WeBbook*. 2007. URL: `http://webbook.nist.gov`.

[42] R. Strey and T. Schmeling. Surface tension measurements for ten n-alcohols in the temperature range from −40 °C to +40 °C. *Berichte der Bunsengesellschaft für physikalische Chemie* 87 (1983), 324–327.

[43] J. W. Kang, ed. *Korea Thermophysical Properties Data Bank*. 2007. URL: `http://www.cheric.org/kdb`.

[44] J. L. Schmitt, G. W. Adams and R. A. Zalabsky. Homogeneous nucleation of ethanol. *Journal of Chemical Physics* 77 (1982), 2089–2097.

[45] M. M. Rudek, J. L. Katz, I. V. Vidensky, V. Ždímal and J. Smolík. Homogeneous nucleation rates of n-pentanol measured in an upward thermal diffusion cloud chamber. *Journal of Chemical Physics* 111 (1999), 3623–3629.

[46] A.-P. Hyvärinen, H. Lihavainen, Y. Viisanen and M. Kulmala. Homogeneous nucleation rates of higher n-alcohols measured in a laminar flow diffusion chamber. *Journal of Chemical Physics* 120 (2004), 11621–11633.

[47] S. Z. Mikhail and W. R. Kimel. Densities and viscosities of methanol-water mixtures. *Journal of Chemical and Engineering Data* 6 (1961), 533–537.

[48] M. M. Rudek, J. A. Fisk, V. M. Chakarov and J. L. Katz. Condensation of a supersaturated vapor. XII. The homogeneous nucleation of the n-alkanes. *Journal of Chemical Physics* 105 (1996), 4707–4713.

[49] M. Rusyniak, V. Abdelsayed, J. Campbell and M. S. El-Shall. Vapor phase homogeneous nucleation of higher alkanes: Docadecane, hexadecane, and octadecane. 1. Critical supersaturation and nucleation rate measuremens. *Journal of Physical Chemistry B* 105 (2001), 11866–11872.

[50] C. T. R. Wilson. Condensation of water vapour in the presence of dust-free air and other gases. *Philosophical Transactions of the Royal Society of London, Series A* 189 (1897), 265–307.

[51] R. H. Heist and H. He. Review of vapor to liquid homogeneous nucleation experiments from 1968 to 1992. *Journal of Physical and Chemical Reference Data* 23 (1994), 781–804.

[52] M. R. A. Pitkänen, S. Mikkonen, K. E. J. Lehtinen, A. Lipponen and A. Arola. Artificial bias typically neglected in comparisons of uncertain atmospheric data. *Geophysical Research Letters* 43 (2016), 10003–10011.

[53] D. Brus, V. Ždímal and F. Stratmann. Homogeneous nucleation rate measurements of 1-propanol in helium: The effect of carrier gas pressure. *Journal of Chemical Physics* 124 (2006), 164306.

[54] D. Brus, A.-P. Hyvärinen, J. Wedekind, Y. Viisanen, M. Kulmala, V. Ždímal, J. Smolík and H. Lihavainen. The homogeneous nucleation of 1-pentanol in a laminar flow diffusion chamber: The effect of pressure and kind of carrier gas. *Journal of Chemical Physics* 128 (2008), 13432.

[55] A.-P. Hyvärinen, D. Brus, V. Ždímal, J. Smolík, M. Kulmala, Y. Viisanen and H. Lihavainen. The carrier gas pressure effect in a laminar flow diffusion chamber, homogeneous nucleation of *n*-butanol in helium. *Journal of Chemical Physics* 124 (2006), 224304.

[56] A. Bertelsman, R. Stuczynski and R. H. Heist. Effects of background gases on the homogeneous nucleation of vapors 3. *Journal of Physical Chemistry* 100 (1996), 9762–9773.

[57] R. H. Heist, A. Bertelsmann, D. Martinez and C. Y. F. Thermal diffusion cloud chamber: New criteria for proper operation. *Atmospheric Research* 65 (2003), 189–209.

[58] Y. Viisanen, R. Strey and H. Reiss. Homogeneous nucleation rates for water. *Journal of Chemical Physics* 99 (1993), 4680–4692.

[59] K. Iland, J. Wedekind, J. Wölk, P. E. Wagner and R. Strey. Homogeneous nucleation rates of 1-pentanol. *Journal of Chemical Physics* 121 (2004), 12259–12264.

[60] M. P. Anisimov, P. K. Hopke, I. N. Shaimordanov, S. D. Shandakov and L.-E. Magnusson. Binary *n*-octanol-sulfur hexafluoride nucleation. *Journal of Chemical Physics* 115 (2001), 810–816.

[61] K. N. H. Looijmans, C. C. M. Luijten and M. E. H. van Dongen. Binary nucleation rate measurements of *n*-nonane/methane at high pressures. *Journal of Chemical Physics* 103 (1995), 1714–1717.

[62] D. Brus, A.-P. Hyvärinen, V. Ždímal and H. Lihavainen. Erratum: "Homogeneous nucleation rate measurements of 1-butanol in helium: A comparative study of a thermal diffusion cloud chamber and a laminar flow diffusion chamber" [J. Chem. Phys. 122, 214506 (2005)]. *Journal of Chemical Physics* 128.7 (2008), 079901.

[63] A.-P. Hyvärinen, D. Brus, V. Ždímal, J. Smolík, M. Kulmala, Y. Viisanen and H. Lihavainen. Erratum: "The carrier gas pressure effect in a laminar flow diffusion chamber, homogeneous nucleation of *n*-butanol in helium" [J. Chem. Phys. 124, 224304 (2006)]. *Journal of Chemical Physics* 128.10 (2008), 109901.

[64] H. Lihavainen, Y. Viisanen and M. Kulmala. Homogeneous nucleation of *n*-pentanol in a laminar flow diffusion chamber. *Journal of Chemical Physics* 114 (2001), 10031–10038.

[65] V. Vohra and R. H. Heist. The flow diffusion nucleation chamber: A quantitative tool for nucleation research. *Journal of Chemical Physics* 104 (1996), 382–395.

[66] M. P. Anisimov, P. K. Hopke, S. D. Shandakov and I. I. Shvets. n-Pentanol–helium homogeneous nucleation rates. *Journal of Chemical Physics* 113 (2000), 1971–1975.

[67] Y. Viisanen and R. Strey. Homogeneous nucleation rates for *n*-butanol. *Journal of Chemical Physics* 101 (1994), 7835–7843.

[68] J. L. Schmitt, K. Van Brunt and G. J. Doster. The homogeneous nucleation of water. *AIP Conference Series* 534 (2000), 51–54.

[69] E. Herrmann, A.-P. Hyvärinen, D. Brus, H. Lihavainen and M. Kulmala. Re-evaluation of the pressure effect for nucleation in laminar flow diffusion chamber experiments with Fluent and the Fine Particle Model. *Journal of Physical Chemistry A* 113 (2009), 1434–1439.

[70] J. Wedekind, A.-P. Hyvärinen, D. Brus and D. Reguera. Unravelling the "pressure effect" in nucleation. *Physical Review Letters* 101 (2008), 125703.

[71] J. Smolík and P. E. Wagner. Joint experiments on homogeneous nucleation. Measurements of nucleation rates in supersaturated *n*-pentanol vapor. In: *Nucleation and Atmospheric Aerosols*. Ed. by M. Kulmala and P. E. Wagner. Oxford: Pergamon, 1996, 58–60.

[72] M. Gharibeh, Y. Kim, U. Dieregsweiler, B. E. Wyslouzil, D. Ghosh and R. Strey. Homogeneous nucleation of *n*-propanol, *n*-butanol, and *n*-pentanol in a supersonic nozzle. *Journal of Chemical Physics* 122 (2005), 094512.

[73] J. Hrubý, Y. Viisanen and R. Strey. Homogeneous nucleation rates for *n*-pentanol in argon: Determination of the critical cluster size. *Journal of Chemical Physics* 104 (1996), 5181–5187.

[74] C. C. M. Luijten, O. D. E. Baas and M. E. H. van Dongen. Homogeneous nucleation rates for n-pentanol from expansion wave tube experiments. *Journal of Chemical Physics* 106 (1997), 4152–4156.

[75] R. Strey, P. E. Wagner and T. Schmeling. Homogeneous nucleation rates for *n*-alcohol vapors measured in a two-piston expansion chamber. *Journal of Chemical Physics* 84 (1986), 2325–2335.

[76] J. L. Schmitt and G. J. Doster. Homogeneous nucleation of *n*-pentanol measured in an expansion cloud chamber. *Journal of Chemical Physics* 116 (2002), 1976–1978.

[77] V. Ždímal and J. Smolík. Homogeneous nucleation rate measurements in 1-pentanol vapor with helium as a buffer gas. *Atmospheric Research* 46 (1998), 391–400.

[78] F. T. Ferguson, R. H. Heist and J. A. Nuth. The effect of carrier gas pressure and wall heating on the operation of the thermal diffusion cloud chamber. *Journal of Chemical Physics* 115 (2001), 10829–10836.

[79] Y. J. Kim, B. E. Wyslouzil, G. Wilemski, J. Wölk and R. Strey. Isothermal nucleation rates in supersonic nozzles and the properties of small water clusters. *Journal of Physical Chemistry A* 108 (2004), 4365–4377.

[80] D. G. Labetski, V. Holten and M. E. H. van Dongen. Comment on "The nucleation behavior of supercooled water vapor in helium" [J. Chem. Phys. 117, 5647 (2002)]. *Journal of Chemical Physics* 120 (2004), 6314–6314.

[81] V. B. Mikheev, P. M. Irving, N. S. Laulainen, S. E. Barlow and V. V. Pervukhin. Laboratory measurement of water nucleation using a laminar flow tube reactor. *Journal of Chemical Physics* 116 (2002), 10772–10786.

[82] C. H. Heath, K. A. Streletzky, B. E. Wyslouzil, J. Wölk and R. Strey. Small angle neutron scattering from D_2O–H_2O nanodroplets and binary nucleation rates in a supersonic nozzle. *Journal of Chemical Physics* 118 (2003), 5465–5473.

[83] A. Khan, C. H. Heath, U. M. Dieregsweiler, B. E. Wyslouzil and R. Strey. Homogeneous nucleation rates for D_2O in a supersonic Laval nozzle. *Journal of Chemical Physics* 119 (2003), 3138–3147.

[84] K. A. Streletzky, Y. Zvinevich, B. E. Wyslouzil and R. Strey. Controlling nucleation and growth of nanodroplets in supersonic nozzles. *Journal of Chemical Physics* 116 (2002), 4058–4070.

[85] Y. Viisanen, R. Strey and H. Reiss. Erratum: "Homogeneous nucleation rates for water" [J. Chem. Phys. 99, 4680 (1993)]. *Journal of Chemical Physics* 112 (2000), 8205–8206.

[86] R. C. Miller, R. J. Anderson, J. L. Kassner Jr. and D. E. Hagen. Homogeneous nucleation rate measurements for water over a wide range of temperature and nucleation rate. *Journal of Chemical Physics* 78 (1983), 3204–3211.

[87] A. Graßmann and F. Peters. Homogeneous nucleation rates of n-propanol in nitrogen measured in a piston-expansion tube. *Journal of Chemical Physics* 116 (2002), 7617–7620.

[88] H. Lihavainen and Y. Viisanen. A laminar flow diffusion chamber for homogeneous nucleation studies. *Journal of Physical Chemistry B* 105 (2001), 11619–11629.

[89] R. Strey and Y. Viisanen. Measurement of the molecular content of binary nuclei. Use of the nucleation rate surface for ethanol–hexanol. *Journal of Chemical Physics* 99 (1993), 4693–4704.

[90] Y. Viisanen, R. Strey, A. Laaksonen and M. Kulmala. Measurement of the molecular content of binary nuclei. II. Use of the nucleation rate surface for water-ethanol. *Journal of Chemical Physics* 100 (1994), 6062–6072.

[91] Y. Viisanen, P. E. Wagner and R. Strey. Measurement of the molecular content of binary nuclei. IV. Use of the nucleation rate surfaces for the *n*-nonane–*n*-alcohol series. *Journal of Chemical Physics* 108 (1998), 4257–4266.

[92] J. Wölk, R. Strey, C. H. Heath and B. E. Wyslouzil. Empirical function for homogeneous water nucleation rates. *Journal of Chemical Physics* 117 (2002), 4954–4960.

[93] S. L. Girshick and C.-P. Chiu. Kinetic nucleation theory: A new expression for the rate of homogeneous nucleation from ideal supersaturated vapor. *Journal of Chemical Physics* 93 (1990), 1273–1277.

[94] A. B. Nadykto and F. Yu. Simple correction to the classical theory of homogeneous nucleation. *Journal of Chemical Physics* 122 (2005), 104511.

[95] K. S. Pitzer, D. Z. Lippmann, R. F. Curl, C. M. Huggins and D. E. Petersen. The volumetric and thermodynamic properties of fluids. II. Compressibility factor, vapor pressure and entropy of vaporization. *Journal of the American Chemical Society* 77 (1955), 3433–3440.

[96] D. R. Lide, ed. *CRC Handbook of Chemistry and Physics*. 86th ed. Boca Raton: CRC Press, 2005.

[97] J.-L. M. Abboud and R. Notario. Critical compilation of scales of solvent parameters. Part I. Pure, non-hydrogen bond donor solvents. *Pure and Applied Chemistry* 71 (1999), 645–718.

[98] M. El-Hefnawy, K. Sameshima, T. Matsushita and R. Tanaka. Apparent dipole moments of 1-alkanols in cyclohexane and *n*-heptane, and excess molar volumes of (1-alkanol + cyclohexane or *n*-heptane) at 298.15 K. *Journal of Solution Chemistry* 34 (2005), 43–69.

[99] R. Estrada-Torres, G. A. Iglesias-Silva, M. Ramos-Estrada and K. R. Hall. Boyle temperatures for pure substances. *Fluid Phase Equilibria* 258 (2007), 148–154.

[100] A. Kacker and R. H. Heist. Homogeneous nucleation rate measurements. I. Ethanol, *n*-propanol, and *i*-propanol. *Journal of Chemical Physics* 82 (1985), 2734–2744.

[101] R. McGraw and R. Zhang. Multivariate analysis of homogeneous nucleation rate measurements. Nucleation in the p-toluic acid/ sulfuric acid/water system. *Journal of Chemical Physics* 128 (2008), 064508.

[102] R. McGraw. Arrhenius temperature dependence of homogeneous nucleation rates. In: *Nucleation and Atmospheric Aerosols: 17th International Conference*. Ed. by C. D. O'Dowd and P. E. Wagner. Dordrecht: Springer, 2007, 144–148.

[103] B. N. Hale. Scaled models for nucleation. *Lecture Notes in Physics* 309 (1988), 323–349.

[104] B. N. Hale. Application of scaled homogeneous nucleation-rate formalism to experimental data at $T << T_c$. *Physical Review A* 33 (1986), 4156–4163.

[105] B. N. Hale. The scaling of nucleation rates. *Metallurgical Transactions A* 23 (1992), 1863–1868.

[106] M. Rusyniak and M. S. El-Shall. Vapor phase homogeneous nucleation of higher alkanes: Docadecane, hexadecane, and octadecane. 1. Corresponding states and scaling law analysis. *Journal of Physical Chemistry B* 105 (2001), 11873–11879.

[107] V. Kalikmanov. *Nucleation Theory*. Dordrecht: Springer, 2013.

[108] L. M. Feldmar, J. Wölk and R. Strey. New measurements of argon and nitrogen nucleation in the cryogenic nucleation pulse chamber. *AIP Conference Proceedings* 1527 (2013), 15–18.

[109] P. P. Wegener. Nucleation of nitrogen: experiment and theory. *Journal of Physical Chemistry* 91 (1987), 2479–2481.

[110] K. Iland, J. Wedekind, J. Wölk and R. Strey. Homogeneous nucleation of nitrogen. *Journal of Chemical Physics* 130 (2009), 114508.

[111] A. Bhabhe and B. Wyslouzil. Nitrogen nucleation in a cryogenic supersonic nozzle. *Journal of Chemical Physics* 135 (2011), 244311.

[112] D. M. Martínez, F. T. Ferguson, R. H. Heist and J. A. Nuth, III. Application of scaled nucleation theory to metallic vapor condensation. *Journal of Chemical Physics* 115 (2001), 310–316.

[113] A. A. Onischuk, S. V. Vosel, O. V. Borovkova, A. M. Baklanov, V. V. Karasev and S. di Stasio. Experimental study of homogeneous nucleation from the bismuth supersaturated vapor: evaluation of the surface tension of critical nucleus. *Journal of Chemical Physics* 136 (2012), 224506.

[114] J. Malila, A.-P. Hyvärinen, Y. Viisanen and A. Laaksonen. Displacement barrier heights from experimental nucleation rate data: Scaling and universality. In: *Nucleation and Atmospheric Aerosols: 17th International Conference*. Ed. by C. D. O'Dowd and P. E. Wagner. Dordrecht: Springer, 2007, 139–143.

[115] J. Martens, H. Uchtmann and F. Hensel. Homogeneous nucleation of mercury vapor. *Journal of Physical Chemistry* 91 (1987), 2489–2492.

[116] J. A. Fisk, M. M. Rudek, J. L. Katz, D. Beiersdorf and H. Uchtmann. The homogeneous nucleation of cesium vapor. *Atmospheric Research* 46 (1998), 211–222.

[117] M. M. Rudek, J. L. Katz and H. Uchtmann. Homogeneous nucleation of supersaturated cesium vapor. *Journal of Chemical Physics* 110 (1999), 11505–11510.

[118] A. Fladerer and R. Strey. Homogeneous nucleation and droplet growth in supersaturated argon vapor: the cryogenic nucleation pulse chamber. *Journal of Chemical Physics* 124 (2006), 164710.

[119] J. L. Katz, H. Saltsburg and H. Reiss. Nucleation in associated vapors. *Journal of Colloid and Interface Science* 21 (1966), 560–568.

[120] A. A. Onischuk, P. A. Purtov, A. M. Baklanov, V. V. Karasev and S. V. Vosel. Evaluation of surface tension and Tolman length as a function of droplet radius from experimental nucleation rate and supersaturation ratio: metal vapor homogeneous nucleation. *Journal of Chemical Physics* 124 (2006), 014506.

[121] V. I. Kalikmanov. Mean-field kinetic nucleation theory. *Journal of Chemical Physics* 124 (2006), 124505.

[122] F. Hensel, M. Stolz, G. Hohl, R. Winter and W. Götzlaff. Critical phenomena and the metal–nonmetal transition in liquid metals. *Journal de Physique IV* C5 (1991), 191–205.

5 Losses of sub-critical clusters and the first nucleation theorem[1]

Despite recent advances in monitoring nucleation from a vapour at close-to-molecular resolution, the identity of the critical cluster, forming the bottleneck for the nucleation process, remains elusive. During past twenty years, the first nucleation theorem has been often used to extract the size of the critical cluster from nucleation rate measurements. However, derivations of the first nucleation theorem invoke certain questionable assumptions that may fail, e.g., in the case of atmospheric new particle formation, including absence of sub-critical cluster losses and heterogeneous nucleation on pre-existing nanoparticles. Here we extend the kinetic derivation of the first nucleation theorem to give a general framework to include such processes, yielding sum rules connecting the size dependent particle formation and loss rates to the corresponding loss-free nucleation rate and the apparent critical size from a naïve application of the first nucleation theorem that neglects them.

[1]This chapter incorporates the article J. Malila, R. McGraw, A. Laaksonen and K. E. J. Lehtinen. Communication: Kinetics of scavenging of small, nucleating clusters: First nucleation theorem and sum rules. *Journal of Chemical Physics* 142 (2015), 011102. Dr. Vitaly Shneidman for discussions and the Magnus Ehrnrooth Foundation for providing the travel grant to visit Brookhaven National Laboratory (BNL) are acknowledged. Work at BNL was supported by the Atmospheric Systems Research (ASR) Program of the US Department of Energy.

5.1 Introduction

First-order phase transformations via nucleation are encountered in a variety of natural and technological processes. The vapour-phase synthesis of nanoparticles with prescribed properties for subsequent assembly into novel nanostructures is one application [1]. In the Earth's atmosphere, the formation of new particles and their growth into cloud condensation nuclei give rise to feedback processes that modulate cloudiness, precipitation, and climate [2, 3]. The reliable modeling of such processes requires going beyond classical phenomenology towards a molecular-level description. To this end the development of so-called nucleation theorems has been particularly effective [for a review, see 4], however, in their current form, these theorems rely on restrictive assumptions that limit their use mainly to interpretation of carefully controlled laboratory measurements. Here we derive extended forms of the first nucleation theorem, and related sum rules, to include loss of molecular clusters from a prescribed nucleation and growth sequence. Loss can be due to scavenging by background aerosol and/or container walls, or removal from the nucleation volume by diffusion or phoretic forces. We also include the possibility that clusters, especially ones of sub-critical size, are lost due to their serving as heterogeneous condensation sites in a way that opens up new off-sequence channels for new particle formation. These results have direct consequences for the interpretation of atmospherically relevant field and laboratory measurements.

5.2 Theory

As demonstrated by Bowles et al. [5], these theorems—with emphasis on the first nucleation theorem,

$$\left(\frac{\partial \Delta W_{g^*}}{\partial \mu_v}\right)_{V,T} = -\Delta g^* + 1 \tag{5.1}$$

—are a direct consequence of the law of mass action for nucleation from an ideal vapour. W_{g^*} is the work needed to form a cluster of critical size, Δg^* is the excess number of molecules in the nucleus over that present in the same

volume of parent phase and μ is the chemical potential of nucleating species present in the parent phase. Under typical laboratory and atmospheric conditions Δg^* can be approximated by the thermodynamic critical size g^*, which is given in the classical nucleation theory by the minimum of the constrained equilibrium distribution of g-mers (clusters containing g monomeric units of condensed phase), $n_g = n_1 e^{-\Delta W_g / k_B T}$, where n_1 is the number concentration of monomers. The connection with nucleation rate measurements is achieved by expressing the nucleation rate in Arrhenius-form, $J = K e^{-\Delta W_{g^*} / k_B T}$, where the prefactor K should take into account the law of mass action. These relations, involving the reversible work of cluster formation, can be described as *thermodynamic nucleation theorems*. Alternatively, *kinetic nucleation theorems* can be derived directly from the master equation approach to nucleation kinetics using the law of mass action and detailed balance [6, 7].

A detailed kinetic treatment of homogeneous nucleation was presented by Farkas [8], following Szilárd's suggestion that clusters grow or decay by absorbing or evaporating a monomer. This simplification does not usually compromise the accuracy of the theory, as in a typical case of vapour–liquid nucleation the collisions with monomers dominate the total number of collisions encountered by g-mers. Letting f_g denote the actual population of g-mers, the net forward flux between adjacent sizes, say g and $g + 1$, is given as

$$J_g = \beta_g f_1 f_g - \alpha_{g+1} f_{g+1} \tag{5.2}$$

where β_g is the addition rate of a monomer to a g-mer, and α_g is the evaporation rate of a monomer from a g-mer. The detailed balance condition, $\beta_g n_g f_1 = \alpha_{g+1} n_{g+1}$, where f_1 is the actual monomer concentration, which we hold as constant equal to n_1, is used to eliminate the evaporation rate:

$$J_g = \beta_g f_1 n_g \left(\frac{f_g}{n_g} - \frac{f_{g+1}}{n_{g+1}} \right) \equiv p_g \left(u_g - u_{g+1} \right). \tag{5.3}$$

The new variables, forward rates p_g and the normalised concentrations u_g, are introduced for subsequent use. Dividing both sides of Eq. (5.3) by p_g and summing for $g = 1, \ldots, G$, where G is a sufficiently large integer with boundary conditions $u_G = 0$ and $u_1 = 1$, and noticing that J_g is constant (J) for all g when no losses are present, we arrive at the Becker–Döring [9]

result

$$J = \left(\sum_{g=1}^{G-1} \frac{1}{p_g} \right)^{-1} . \tag{5.4}$$

The remarkable fact of this well-known result is that it depends only on β_g—determined from kinetic theory—and n_g.

For an ideal vapour, incorporating the law of mass action $\mu_g = g\mu$, or $n_g \propto n_1^g$, the following result is obvious:

$$\left[\frac{\partial \ln(n_1 n_g)}{\partial \ln n_1} \right]_T = g + 1. \tag{5.5}$$

As defined here, β_g does not depend on n_1 [see Eq. (5.3)] and substitution of this last result into Eq. (5.4), with $p_g = \beta_g n_1 n_g$, gives the kinetic version of the first nucleation theorem [6, 7],

$$\left(\frac{\partial \ln J}{\partial \ln n_1} \right)_T = \bar{g} + 1, \tag{5.6}$$

where the kinetic critical size is defined as an expectation value $\bar{g} = \sum_{g=1}^{G-1} P(g) g$ with respect to the normalized $1/p_g$ distribution

$$P(g) = \frac{1}{p_g} \left(\sum_{g=1}^{G-1} \frac{1}{p_g} \right)^{-1} . \tag{5.7}$$

Although the first nucleation theorem has been tested well in cloud chamber studies of single-component and binary nucleation [10], recent atmospherically relevant field [11] and laboratory [12–14] studies of sulphuric acid driven nucleation have produced inconsistent results; suggesting, for example, that new particle formation may occur via activated (with barrier) or purely kinetic (without barrier) mechanisms under nearly identical experimental conditions. Several possible reasons for this behavior have been suggested, including problems related to the experimental detection of freshly nucleated clusters [12] and the influence of other trace vapours [13–17] on the new particle formation rate [18]. Recent simulation studies have underlined the effect of wall and coagulation losses—and alternative

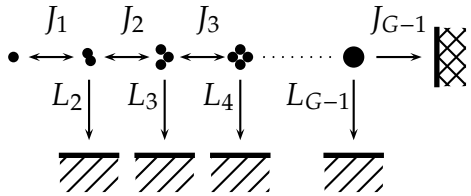

Fig. 5.1. A schematic description of the Szilárd process with losses.

growth paths including addition of clusters containing several H_2SO_4 molecules [19]—on the interpretation of the first nucleation theorem [20, 21], an effect that has not been yet fully accounted for when applying the first nucleation theorem to laboratory or atmospheric measurements [3].

To extend the kinetic nucleation theorem for cases with losses we apply the discrete model of McGraw and Marlow [22], which is more appropriate at small cluster sizes than corresponding continuum presentations [23] and allows cluster growth by condensation, evaporation, and size-dependent cluster losses. Net fluxes between g-mer and $(g+1)$-mers are still given by Eq. (5.3), but each g-mer is additionally scavenged at rate L_g. The assumption of linear dependence of L_g on f_g, $L_g = q_g f_g$, where q_g is the rate coefficient that can apply to each of the loss mechanisms mentioned above, but not to removal by self-coagulation or production of smaller clusters through fragmentation, allows derivation of a closed-form solutions for the relative sensitivities of rates J_g with respect to n_1 (see Sec. 5.A for additional analytic results).[2]

Prior to consideration of more complex systems, it is worthwhile comparing the thermodynamic and kinetic approaches underlying derivation of Eqs. (5.1) and (5.6), respectively. Both approaches are extendable to multicomponent nucleation with the kinetic approach having advantage of working with a directly measurable quantity, nucleation rate. The essential difference is that thermodynamic nucleation theorems focus on extrema

[2]Linear loss term was first introduced into Eq. (5.10) by Becker and Reiss [24], who studied the effect of diffusion loss from the nucleation zone of thermal diffusion cloud chamber. The same correction was also independently considered by Fishman [25] in connection to the crystallisation of glasses and the nucleation of electron–hole liquid from excitons in a semiconductor. Friedlander [26, 27] was first to apply it on coagulation losses of atmospheric clusters, though he continued to assume a kinetic nucleation mechanism before developing theory further.

of the free-energy surface whereas the kinetic approaches work with rate coefficients and the (possibly multiple) pathways over which nucleation can occur [cf. 28]. From the kinetic viewpoint, the overall rate sensitivity for a complex system can often be expressed simply as a flux-weighted average of sensitivities over dominant paths [7].

Using now the model described in Fig. 5.1, we derive two sum rules for the nucleation rates: First, from Eq. (5.3) we get

$$\sum_{g=1}^{G-1} \frac{J_g}{p_g} = \sum_{g=1}^{G-1} (u_g - u_{g+1}) = u_1 - u_G = 1. \tag{5.8}$$

Multiplying both sides by $J = \left(\sum_{g=1}^{G-1} 1/p_g \right)^{-1}$ from Eq. (5.4) yields the first sum rule:

$$\sum_{g=1}^{G-1} P(g) J_g = \bar{J}_g = J, \tag{5.9}$$

that is, at steady state the $P(g)$-averaged transition rate equals the homogeneous nucleation rate without losses. As the fluxes in Fig. 5.1 are conserved, at each size g,

$$J_g = J_{g-1} - L_g. \tag{5.10}$$

Equations (5.9) and (5.10) imply that the net forward rates at small sizes are larger than the corresponding loss-free rates, and smaller at large sizes [29]. The addition of cluster loss tends to promote the assumption of steady state used in the derivation of Eqs. (5.9) and (5.10). This is because cluster losses actually drive the system towards steady state faster than would otherwise happen without the loss [30]. Additionally, it has been shown that background aerosol, which increases scavenging loss, widens the stability range of steady-state conditions in dynamical systems involving coupled nucleation and growth [31].

Taking the derivatives of both sides of Eq. (5.9), completing the logarithms of differentials, and applying Eqs. (5.5)–(5.7) to evaluate the derivatives of p_g, J, and $P(g)$ we get after some algebra the second sum rule:

$$\sum_{g=1}^{G-1} \left[\left(\frac{\partial \ln J_g}{\partial \ln n_1} \right)_{T,\{q_g\}} - g \right] P(g) J_g = J. \tag{5.11}$$

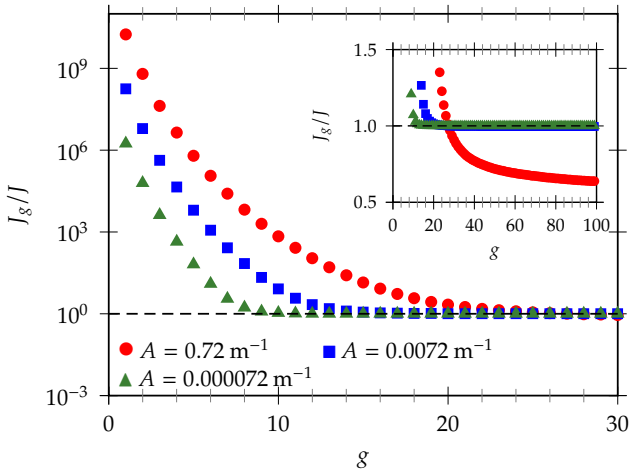

Fig. 5.2. Normalised formation rates of a g-mer as a function of g and A at $S = 10$. Dashed line denotes $J_g = J$. Inset shows in linear scale how in the case of large losses $J_g \leq J$ for large g.

This sum rule involving both rates and rate sensitivities can be seen as a generalization of the kinetic first nucleation theorem, as Eq. (5.11) reduces to Eq. (5.6) for the loss-free case with $J = J_g$. It should be noted that Eqs. (5.9) and (5.11) do not depend on the nature of losses as long as self-coagulation and fragmentation of clusters can be neglected.

5.3 Results and discussion

To illustrate the new sum rules we perform calculations for a model condensable vapour—a proxy to ethanesulfonic acid that facilitates comparison with previous work [22–24, 32, 33]. Table 5.3 lists properties of the model compound. Losses of clusters are taken to be due to Brownian coagulation with background aerosol with specific surface area density A varying from particle-free conditions ($A = 0$ m^2/m^3) to a high value of A typical of a severe duststorm; an intermediate value $A = 0.072$ m^{-1}, which gives a loss rate comparable to the diffusion loss from the nucleation zone in a thermal diffusion cloud chamber [24], was used in earlier work [22]. Fuchs surface areas [34] are implied throughout. Results are shown in Figs. 5.2 and 5.3. Figure 5.2 shows that the net growth rates can be

considerably larger with loss than without for clusters of sub-critical size. This behavior can be rationalized by the fact that the loss channel is more important for clusters that are, in effect, trapped by the thermodynamic barrier and thus have more time to experience loss. Super-critical clusters are able to grow much faster and thus do not get lost that efficiently at any given size. Similar behavior is seen in continuous models for nucleation with loss [32, 33].[3] As can be seen by comparing Figs. 5.2 and 5.3(a), qualitatively similar behavior is observed whether the loss rate is increased by increasing A at fixed S (Fig. 5.2) or the saturation ratio is decreased at fixed A [Fig. 5.3(a)]. This similarity is related to the importance of a non-dimensional loss parameter, $L = A/(A_1 f_1)$, where A_1 is the surface area of a monomer, introduced independently in slightly different contexts in Refs. [22] and [34]. In what follows, only the effect of a varying saturation ratio at fixed background aerosol surface area is considered.

Figure 5.3(b) shows size dependent sensitivities of $\ln J_g$ with respect to $\ln n_1$ at constant T [term in parenthesis in Eq. (5.11)] as a function of g (filled symbols). The result, if naïvely interpreted, would indicate an apparent critical size ($\tilde{g}$) that can differ appreciably from the kinetic critical size determined in the loss-free case ($\bar{g}$), which, in turn, is very close to the actual number of molecules in the critical nucleus, g^*, of homogeneous nucleation theory. For the smallest clusters, the apparent critical size depends linearly from the size at which the rate is determined, i.e. $\tilde{g} \approx g$ (see the supplement for computational details). For clusters larger than $\bar{g}$, slight overestimates are obtained. Thus, it is possible to obtain estimates $\tilde{g}$ biased into either direction, if the effect of loss is neglected. The quantitative deviation depends in a complicated manner on p_g and q_g [Eq. (5.18)].

An interesting feature that is apparent from Figs. 5.2 and 5.3 is that the first nucleation theorem seems to approximately hold if applied to the rate $J_{\bar{g}}$ determined at the loss-free kinetic critical size $\bar{g}$. However, it is premature to say whether this behavior is of general nature, or a consequence of the model system; the effect of losses on the gradient $u_g - u_{g+1}$ is mainly important at sizes smaller than $\bar{g}$ [see, e.g., Fig. 5.4(b)]. It would also be

[3] Perhaps the most obvious physical interpretation for such an apparently counterintuitive result follows from the diffusion analogy: losses of consecutive sub-critical cluster populations increase the gradient $u_g - u_{g+1}$ affecting J_g more at small g than the decrease of the net forward rate p_g that plays the role of the diffusion coefficient.

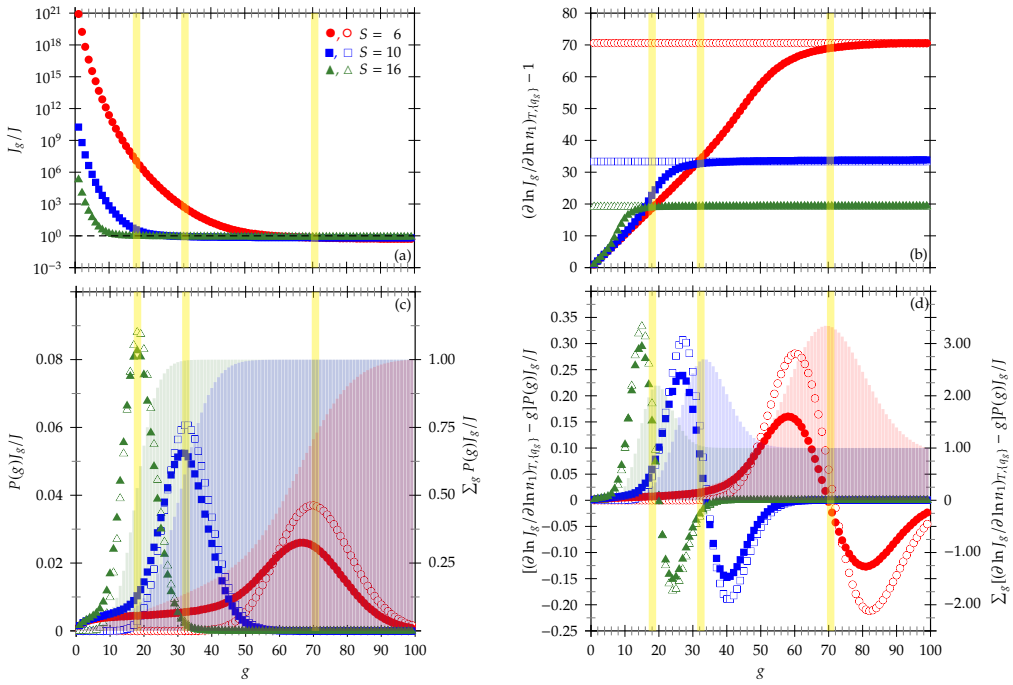

Fig. 5.3. (a) Normalised formation rates of a g-mer as a function of g at different saturation ratios with a fixed $A = 0.0072\ \mathrm{m}^{-1}$. (b) Apparent results $\tilde{g}$ of naïvely applied first nucleation theorem as a function of cluster size g, note the linear regime for small g. Open and filled symbols refer to loss-free and lossy cases, respectively. (c, d) Distributions $P(g)J_g/J$ and $\left[\left(\partial \ln J_g/\partial \ln n_1\right)_{T,\{q_g\}} - g\right] P(g)J_g/J$ (markers and values at left axes) and their cumulative sums (for lossy cases only; histograms and values at right axes). In all panels, yellow vertical lines indicate the locations of the loss-free critical sizes $\bar{g}$ from Eq. (5.6).

possible to define a kinetic critical size for the lossy case, $\hat{g}$, by averaging g with respect to the generalized distribution $P(g)J_g/J$: in such case the second sum rule could be written as (for derivation, see the supplement)

$$\hat{g} + 1 = \sum_{g=1}^{G-1} \frac{J_g P(g)}{J} \left(\frac{\partial \ln J_g}{\partial \ln n_1} \right)_{T,\{q_g\}} . \tag{5.12}$$

As can be interpreted from Fig. 5.3(c), at least for our model cases $\hat{g}$ is well approximated by $\bar{g}$. However, there is no unambiguous physical interpretation of $\hat{g}$, as there is no single rate limiting step corresponding the bottleneck for the observed nucleation rate, though the thermodynamic critical size g^* appears in the theoretical estimates for the transient time scale of nucleation also in such case [30, 35, also V. I. Shneidman, personal communication, 2013.].[4]

Figures 5.3(c) and (d) demonstrate the first and second sum rules, respectively. In Panel (c), the distribution $P(g)J_g/J$, generalizing Eq. (5.7), is given together with its cumulative sum. These cumulative sums are given for the cases with loss only: under loss-free conditions it is clear that the cumulative distributions approach unity as the distribution $P(g)$ is normalized, in the case of Panel (c), and the second sum rule, demonstrated in Panel (d), reduces to Eq. (5.6). These figures show the effect of applying the first nucleation theorem to the formation rates of clusters of different size, and illustrate the validity of Eqs. (5.9) and (5.11) for a realization of the flux network model illustrated in Fig. 5.1.

In a recent simulation study with qualitatively similar findings, Ehrhart and Curtius [21] used the SAWNUC sulphuric acid–water nucleation [37] model to study sensitivity of nucleation rate to changes in vapour phase sulphuric acid concentration as a function of cluster size and scavenging rate. Similar behavior was also seen in simulations of the binary sulphuric acid–ammonia system using another modeling approach (ACDC) [20]. However, for an even more nonideal system of sulphuric acid and dimethylamine, a more complicated behavior was observed [20], which is likely due to kinetic effects and/or breakdown of the Szilárd mechanism.

[4] Many of these conclusions were also obtained in a simultaneous study by Olenius et al. [36], who pointed out the size-dependent effect of losses on cluster growth rates due to changes in the ratio of condensation and evaporation fluxes, as well as the non-existence of a uniquely defined critical size in cases where losses are present.

5.4 Concluding remarks

Yet another loss process that can be approximately cast into linear form is the heterogeneous nucleation on the small sub-critical clusters in the presence of, e.g., an organic vapour [38]. This is essentially a new channel for growth that opens up, thereby effectively removing clusters from the growth sequence illustrated in Fig. 5.1. Conversely, collisions of sub-critical clusters with existing ambient nanoparticles, for which we can also consider single large organic molecules [39], can also result in crossing of the heterogeneous nucleation barrier. Earlier applications of the (kinetic) first nucleation theorem on such cases have produced meaningless estimates for $\bar{g}$ [3, 40]. However, when considering some fraction of each loss rate L_g actually resulting in a channel contributing to the observed new particle formation, an extension of the first kinetic nucleation theorem can be derived [Eq. (5.33)]. In this case the resulting apparent critical size $\tilde{g}$ is smaller than the corresponding $\bar{g}$, being either characteristic size for the heterogeneous nucleus, if only one path is available, or a flux-weighted average over possible homo- and heterogeneous pathways [41]. This mechanism, together with the observation of the linear estimate for the apparent critical size at small sizes, also casts some doubts on the interpretation of measurements from particle size magnifiers when used to detect critical clusters at low nucleation rate [e.g. 12]. In reality the working fluid may be condensing on clusters of sub-critical size leading to too small an estimate of $\bar{g}$.

As demonstrated by our results—as well as recent simulation studies [20, 21]—a naïve application of the first nucleation theorem when sub-critical cluster losses are expected can lead to seriously biased estimates on the critical cluster size, and consequently on the mechanism behind the new particle formation, even if the other known deficiencies [20] of the analysis have been appropriately considered. The fundamental concepts behind nucleation theorems, like mass action and detailed balance, still apply but the theorems themselves need correction to yield physically meaningful results. Here we have provided sum rules that can be used to identify and/or correct these biases. Besides applications to analysis of field and laboratory measurements of new particle formation, derived sum rules can also find applications in control of chemical vapour deposition and

vapour-phase synthesis of nanomaterials in inhomogeneous medium [33], and also in a broader context to other types of nucleation processes that can be described using the Szilárd model.

5.A Appendix

In this Appendix methods to calculate normalized cluster population u_g either analytically using continued fractions or numerically using a mathematically equivalent matrix approach are given. The first mentioned method is applied to calculate the exact form of the first nucleation theorem in a lossy case. We also give details of numerical calculations presented in the main text together with the extended formulae for cases where sub-critical cluster loss results in a new pathway for particle formation.

5.A.1 Calculation of J_g and $\partial \ln J_g / \partial \ln n_1$

From the condition of flux conservation at size g [Eq. (5.10)] we get

$$p_{g-1}(u_{g-1} - u_g) = p_g(u_g - u_{g+1}) + c_g u_g, \tag{5.13}$$

where we have introduced normalized loss rate coefficients $c_g = q_g n_g$, which give the loss rates as $L_g = c_g u_g$, to be consistent with Eq. (5.3); the Szilárd boundary conditions are $u_1 = 1$ and $u_G = 0$.

Closed form solution

Following Ref. [22] (see also Ref. [42]), we derive the analytic solution for u_g in terms of a finite continued fraction. We first rewrite Eq. (5.13) as

$$\begin{aligned}
\frac{u_g}{u_{g+1}} &= a_g + \frac{b_{g+1}}{u_{g+1}/u_{g+2}} \\
&\vdots \\
&= a_g + \cfrac{b_{g+1}}{a_{g+1} + \cfrac{b_{g+2}}{a_{g+2} + \cfrac{b_{g+3}}{a_{g+3} + \cfrac{b_{g+2}}{\ddots \\ a_{G-3} + \cfrac{b_{G-2}}{a_{G-2}}}}}} \\
&= a_g + \underset{j=g+1}{\overset{G-2}{\mathrm{K}}} \left(\frac{b_j}{a_j} \right),
\end{aligned} \tag{5.14}$$

where

$$a_g = \frac{p_{g+1} + p_g + c_{g+1}}{p_g}, \tag{5.15}$$

and

$$b_g = -\frac{p_g}{p_{g-1}} \tag{5.16}$$

(note here the sign difference in sign convention from Ref. [22]). Gauss' symbol for the continued fraction has been used to compact notation, and $\mathrm{K}_{l=j}^{G-2}(b_l/a_l) = \mathrm{K}_{l=j}^{G-1}(b_l/a_l)$ due to boundary condition $u_G = 0$. For diffusion losses, q_g and thus c_g are proportional to $D_g\nabla^2$, where D_g is the diffusion coefficient of a g-mer and ∇ denotes the spatial gradient. Although one could also consider a continued fraction where elements a_g are operators [43], in this context this would lead into a continued fraction defined in terms of a suitable inverse of a non-commutative operator. These considerations would deviate substantially from the scope of this work and are omitted. Thus, the present treatment will be exact only when terms

related to diffusion losses can be neglected or approximated with real-valued functions of g [24, 32, 33].

Since $u_1 = 1$, we have

$$u_g = u_1 \frac{u_2}{u_1}\frac{u_3}{u_2}\cdots\frac{u_g}{u_{g-1}} = \prod_{k=2}^{g} \frac{1}{a_{k-1} + \mathrm{K}_{j=k}^{G-2}\left(\frac{b_j}{a_j}\right)}. \tag{5.17}$$

From u_g we get $J_g = p_g(u_g - u_{g+1})$ and its relative sensitivity to monomer concentration n_1 at each g when expanding the derivatives of continued fractions [44]:

$$\begin{aligned}\left(\frac{\partial \ln J_g}{\partial \ln n_1}\right)_{T,\{c_g\}} &= g + 1 + \sum_{j=2}^{g}\left[\mathrm{K}_{l=j}^{G-2}\left(\frac{b_l}{a_l}\right) - a_{l-1}\right]^{-1} \\ &\quad\times\left(\frac{p_j}{p_{j-1}} + \sum_{m=g+1}^{G-2}\left\{\frac{p_{m+1}}{p_m} - \frac{p_m}{p_{m+1}}\left[\mathrm{K}_{n=m}^{G-2}\left(\frac{b_n}{a_n}\right)\right]^{-1}\right\}\right. \\ &\quad\left.\times\left\{\prod_{l=j}^{m}\frac{p_{l-1}}{p_l}\left[\mathrm{K}_{n=l}^{G-2}\left(\frac{b_n}{a_n}\right)\right]^2\right\}\right) \\ &\quad + \frac{u_{g+1}^2}{u_g^2 - u_g u_{g+1}}\left(\frac{p_{g+1}}{p_g} + \sum_{m=g+1}^{G-2}\left\{\frac{p_{m+1}}{p_m} - \frac{p_m}{p_{m+1}}\left[\mathrm{K}_{n=m}^{G-2}\left(\frac{b_n}{a_n}\right)\right]^{-1}\right\}\right. \\ &\quad\left.\times\left\{\prod_{l=g+1}^{m}\frac{p_{l-1}}{p_l}\left[\mathrm{K}_{n=l}^{G-2}\left(\frac{b_n}{a_n}\right)\right]^2\right\}\right) \qquad (5.18) \\ &\overset{g\to 1}{\to} g + 1. \qquad (5.19)\end{aligned}$$

For small g we see that two last terms both approach zero, due to an empty sum in the first one and the fact that $u_1 >> u_2$ for supersaturated vapour in the second. This behaviour explains, together with the assumption that Eq. (5.18) yields physically sensible behaviour, the linear regime at small g observed in model calculations [Fig. 5.3(b), see also Table 5.1].[5] Unfortunately, Eq. (5.18), from which the complete expression follows after

[5] A more close examination of Fig. 5.3 and Table 5.1 reveals somewhat surprising

substitution of u_g and u_{g+1} from Eq. (5.17), does not provide clear interpretation at large g limit.

An observant reader might have noticed that the derivative above was taken at constant $\{c_g\}$, while in the main text reference was made to a derivative taken at constant $\{q_g\}$. It is easy to see that these conditions are indeed equivalent, since for any ℓ and g ($1 < \ell, g < G$) we have

$$\begin{aligned}
\frac{\left(\frac{\partial \ln J_g}{\partial \ln n_1}\right)_{T,c_\ell}}{\left(\frac{\partial \ln J_g}{\partial \ln n_1}\right)_{T,q_\ell}} &= \frac{\left(\frac{\partial \ln c_\ell}{\partial \ln n_1}\right)_{T,J_g}\left(\frac{\partial \ln J_g}{\partial \ln c_\ell}\right)_{T,n_1}}{\left(\frac{\partial \ln q_\ell}{\partial \ln n_1}\right)_{T,J_g}\left(\frac{\partial \ln J_g}{\partial \ln q_\ell}\right)_{T,n_1}} \\
&= \left(\frac{\partial \ln c_\ell}{\partial \ln q_\ell}\right)_{T,J_g}\left(\frac{\partial \ln q_\ell}{\partial \ln c_\ell}\right)_{T,n_1} \\
&= \left(\frac{\partial \ln q_\ell}{\partial \ln q_\ell}\right)_{T,J_g} + \left(\frac{\partial \ln n_\ell}{\partial \ln q_\ell}\right)_{T,J_g} \\
&= 1,
\end{aligned}$$

where we have used the facts that $\mathrm{d}\ln c_\ell = \mathrm{d}\ln q_\ell + \mathrm{d}\ln n_\ell$, and that n_ℓ is constant at fixed saturation (monomer number density) and temperature and is always independent of q_ℓ.

If one wants to use Eq. (5.18) to compare with experimental measurements, the question arises how to calculate individual $p_g = \beta_g n_1 n_g$ and $c_g = q_g n_g$. Specific loss rate coefficients q_g can be obtained with a reasonable accuracy, if the macroscopic properties of the system (background aerosol or wall surface area, temperature and concentration profiles, or such) are known. Also the kinetic theory estimate for β_g should be reasonable for nucleation from vapours. On the other hand, classical approaches fail to predict n_g for the smallest clusters [45, 46], and one needs an alternative approach such as quantum chemistry-based simulation.

overshooting effect, resulting in larger apparent critical sizes with larger saturation ratios. This effect is rationalised by the second sum rule [Eq. (5.11)] when divided by J: at small sizes, the weight $P(g)J_g/J$ strongly biases slight positive deviations from the $\tilde{g} = g$ line in comparison to large deviations at large g.

Table 5.1. Apparent critical sizes $\tilde{g}$ at small g from the case examined in Fig. 5.3(b) ($A = 0.0072$ m^{-1}). The linear approximation $\tilde{g} \approx g$ holds for $g << \bar{g}$.

g	$\tilde{g}$		
	$S = 6$	$S = 10$	$S = 16$
1	1.02	1.04	1.07
2	2.04	2.08	2.14
3	3.07	3.12	3.25
4	4.09	4.18	4.42
5	5.12	5.24	5.76
⋮			
10	10.29	10.71	15.30
⋮			
15	15.49	17.43	18.44

Matrix approach

The continued fraction method outlined above gives closed-form solutions but is impractical for numerical calculations.Here we recast the solution in a more computationally tractable, but mathematically equivalent, matrix form. Substituting a_g and b_g defined above [Eqs. (5.15) and (5.16)], Eq. (5.13) becomes

$$-u_g + a_g u_{g+1} + b_g u_{g+2} = 0 \tag{5.20}$$

The Szilárd boundary conditions are $u_1 = 1$ and $u_G = 0$ with the result hat at the boundaries Eqs. (5.20) take the form:

$$a_1 u_2 + b_1 u_3 = 1 \tag{5.21}$$

and

$$-u_{G-2} + a_{G-2} u_{G-1} = 0. \tag{5.22}$$

The $G-2$ equations (5.20)–(5.22), in the variables $u_2, u_3, \ldots, u_{G-1}$, can be compactly expressed in a matrix-vector form as

$$\underbrace{\begin{pmatrix} a_1 & -b_1 & 0 & \cdots & 0 & 0 \\ -1 & a_2 & -b_2 & \cdots & 0 & 0 \\ 0 & -1 & a_3 & \cdots & 0 & 0 \\ \vdots & \vdots & \vdots & \ddots & \vdots & \vdots \\ 0 & 0 & 0 & \cdots & a_{G-3} & -b_{G-3} \\ 0 & 0 & 0 & \cdots & -1 & a_{G-2} \end{pmatrix}}_{=\mathbf{B}} \underbrace{\begin{pmatrix} u_2 \\ u_3 \\ u_4 \\ \vdots \\ u_{G-2} \\ u_{G-1} \end{pmatrix}}_{=\mathbf{U}} = \underbrace{\begin{pmatrix} 1 \\ 0 \\ 0 \\ \vdots \\ 0 \\ 0 \end{pmatrix}}_{=\mathbf{1}}. \tag{5.23}$$

Solution for u_g, $g = 2, \ldots, G-1$, follows on inverting the tridiagonal matrix $\mathbf{B}$:

$$\mathbf{U} = \mathbf{B}^{-1}\mathbf{1} \tag{5.24}$$

subject to the boundary conditions. Once these have been obtained, the fluxes J_g follow immediately from Eq. (5.3).

To obtain J_g directly, write $\mathbf{J} = \mathbf{p}\tilde{\mathbf{U}}$, where $\mathbf{J}$ is the vector of elements J_g for $g = 1$ through $G-1$, $\tilde{\mathbf{U}}^{\mathrm{T}} = (1, \mathbf{U}^{\mathrm{T}}, 0)$, and $\mathbf{p}$ is the $G-1$ by G matrix consisting of the diagonal elements $p(g)$, and super-diagonal elements $-p(g)$, along row g, and $\mathbf{p}(G-1, G) = 0$.

The method described above is well suited for numerical calculation, and was used to calculate the results depicted in Figs. 5.2, 5.3, and 5.4, and in Tables 5.1 and 5.2.

To obtain the relative rate sensitivities from the matrix method, it is necessary to differentiate matrices $\mathbf{B}$ and $\mathbf{p}$ defined above. Application of the standard formula for differentiation of the inverse matrix, $\mathrm{d}\mathbf{B}^{-1} = -\mathbf{B}^{-1}(\mathrm{d}\mathbf{B})\mathbf{B}^{-1}$ gives

$$\mathrm{d}\mathbf{U} = -\mathbf{B}^{-1}(\mathrm{d}\mathbf{B})\mathbf{B}^{-1}\mathbf{1}. \tag{5.25}$$

In extended form, including the constant boundary conditions as before, we obtain $\mathrm{d}\tilde{\mathbf{U}} \equiv [0, \mathrm{d}u_2, \ldots, \mathrm{d}u_{G-1}, 0]$ and $\mathrm{d}\mathbf{J} = \mathbf{p}\mathrm{d}\tilde{\mathbf{U}} + \mathrm{d}\mathbf{p}\tilde{\mathbf{U}}$ from the product rule. The vector of relative sensitivities then follows

$$\frac{(\mathrm{d}\mathbf{J})_k / \mathrm{d}\ln n_1}{\mathbf{J}_k} = \left(\frac{\partial \ln J_k}{\partial \ln n_1}\right)_{T,\{c_g\}}, \tag{5.26}$$

where $\mathbf{J}_k = J_k$, etc. These derivatives are readily shown to satisfy the second sum rule.

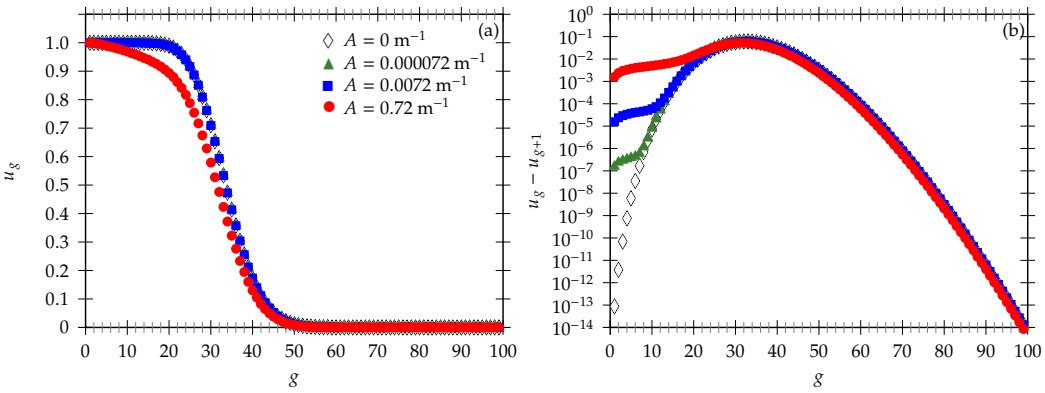

Fig. 5.4. Normalized populations u_g (a) and gradients $u_g - u_{g+1}$ (b) corresponding to Fig. 5.2 ($S = 10$) in the main text.

5.A.2 On the kinetic critical size $\hat{g}$

Using the generalized kinetic distribution $J_g P(g)/J$, we can define kinetic critical size $\hat{g}$ as

$$\hat{g} = \sum_{g=1}^{G-1} g \frac{J_g P(g)}{J}; \tag{5.27}$$

obviously $\hat{g} = \bar{g}$ if there are no cluster losses. From Eq. (5.3) we have $J_g/p_g = u_g - u_{g+1}$, and because $P(g) = J/p_g$ this results in an alternative form:

$$\hat{g} = \sum_{g=1}^{G-1} g(u_g - u_{g+1}). \tag{5.28}$$

Comparison with Fig. 5.4(b) reveals that in the lossy case, small cluster sizes are given more weight when compared to the loss-free case, and thus generally $\hat{g} < \bar{g}$. It is possible to rewrite the second sum rule in terms of $\hat{g}$: dividing both sides of Eq. (5.11) by J, splitting the sum into two and transferring the second term on the other side we get an ostensible generalization of the kinetic first nucleation theorem,

$$\hat{g} + 1 = \sum_{g=1}^{G-1} \frac{J_g P(g)}{J} \left(\frac{\partial \ln J_g}{\partial \ln n_1} \right)_{T,\{q_g\}}. \tag{5.29}$$

Examination of Fig. 5.3(c) suggest that $\hat{g} \lesssim \bar{g}$, as the maxima of the corresponding distributions are close to each other, which is confirmed in Table 5.2.

Table 5.2. Generalized kinetic critical size $\hat{g}$ for various cases as a function of saturation ratio S and the specific surface area of pre-existing particles A (m^{-1}). Note that when $A = 0\ m^{-1}$, $\hat{g} = \bar{g}$.

A \ S	6	10	16
0	70.40	33.35	19.10
0.000072	70.40	33.35	19.10
0.0072	70.25	33.32	19.10
0.72	57.99	30.31	18.16

5.A.3 Flux weighting and sum rules for loss rates

The loss fluxes L_g can represent loss of clusters due to scavenging by background aerosol or laboratory chamber walls (for example), but they can also represent loss of clusters that serve as a heterogeneous nucleation sites that provide alternative pathways to new particle formation (NPF). In that case while the cluster is lost, a new particle is formed. Separating these two contributions we obtain

$$L_g = L_{g,\mathrm{NPF}} + L_{g,S}, \tag{5.30}$$

where the sink term $L_{g,S} = c_g u_g$, as before, and $L_{g,\mathrm{NPF}} = c_{g,\mathrm{NPF}} u_g$. The coefficients $c_{g,\mathrm{NPF}}$ will depend in detail on the heterogeneous nucleation mechanism and is beyond scope of the present study. From flux balance

$$J_1 = J_{G-1} + L_{\mathrm{NPF}} + L_S \equiv J_{G-1} + \sum_{g=2}^{G-1} L_{g,\mathrm{NPF}} + \sum_{g=2}^{G-1} L_{g,S}. \tag{5.31}$$

The first two terms on the right hand side contribute to NPF; these are the contributions from the barrier crossing along the prescribed sequence, J_{G-1}, and alternative paths, L_{NPF}. The remaining term, L_S, includes scavenging loss of clusters to background aerosol, diffusion, and/or walls.

Flux weighting introduced in Refs. [7, 47] can now be applied to the network of Fig. 5.1 in numerous ways. Here we focus on the fluxes that result in new particle formation:

$$J_{\mathrm{NPF}} \equiv J_{G-1} + \sum_{g=2}^{G-1} L_{g,\mathrm{NPF}}. \tag{5.32}$$

Taking the differential of each term gives $\mathrm{d}J_{\mathrm{NPF}} = \mathrm{d}J_{G-1} + \sum_{g=2}^{G-1} \mathrm{d}L_{g,\mathrm{NPF}}$ and

$$\frac{\partial \ln J_{\mathrm{NPF}}}{\partial \ln n_1} = \frac{J_{G-1}}{J_{\mathrm{NPF}}} \left(\frac{\partial \ln J_{G-1}}{\partial \ln n_1} \right) + \sum_{g=2}^{G-1} \frac{L_{g,\mathrm{NPF}}}{J_{\mathrm{NPF}}} \left(\frac{\partial \ln L_{g,\mathrm{NPF}}}{\partial \ln n_1} \right), \tag{5.33}$$

showing the overall relative sensitivity for new particle formation as a flux-weighted sum of the sensitivities for each path.

We can also use the matrix method described above to obtain the relative sensitivities of the loss fluxes from flux weighting:

$$L_k \frac{\partial \ln L_k}{\partial \ln n_1} = J_{k-1} \frac{\partial \ln J_{k-1}}{\partial \ln n_1} - J_k \frac{\partial \ln J_k}{\partial \ln n_1} \tag{5.34}$$

and these may be further apportioned into contributions from scavenging and loss to NPF once the heterogeneous nucleation mechanism(s) or a model for it has been determined.

Finally, we can also present the first sum rule in terms of loss rates L_g: Let $Q(g)$ be a cumulative of $P(g)$, so that $P(g) = Q(g+1) - Q(g)$ and $Q(1) = 0$. Now the first sum rule gives

$$J = \sum_{g=1}^{G-1} P(g) J_g = \sum_{g=1}^{G-1} [Q(g+1) - Q(g)] J_g = J_{G-1} + \sum_{g=2}^{G-1} Q(g) L_g, \tag{5.35}$$

where the condition of flux conservation [Eq. (5.10)] has been used together with $Q(G) = 1$ from normalization of $P(g)$.

5.A.4 Model system

Formation rates J_g in Figs. 5.2 and 5.3 and normalized cluster populations u_g in Fig. 5.4 were calculated using the classical nucleation theory, though

it should be noted that the results and their interpretation are qualitatively independent on the applied nucleation theory: The intensive work to create a g-mer is given as

$$\Delta W_g = -(g-1)k_\mathrm{B}T \ln S + A_1 \gamma_\infty g^{2/3}, \tag{5.36}$$

where $S = k_\mathrm{B}Tn_1/p_e$ is the ideal gas saturation ratio and k_B is the Boltzmann constant; all calculations were made at $T = 293.15$ K and other symbols are given in Table 5.3. It is worth noting that when applying the capillarity approximation, the intensive free energy formulation [5] equals to the Courtney's $1/S$-correction [48]. From the kinetic theory of gasses we have[6]

$$\beta_g = \sqrt{\frac{k_\mathrm{B}T}{2\pi m}} A_1 g^{2/3}. \tag{5.37}$$

In a pure Brownian case coagulation losses are given by

$$q_g = \sqrt{\frac{k_\mathrm{B}T}{2\pi m g}} A. \tag{5.38}$$

Here A is the specific surface area of the pre-existing aerosol particles: If particle diameters are in order of the mean free path in the gas phase, this can be interpreted as a transition regime corrected (Fuchs) surface area density [34]. [49] However, if particles are much larger than the mean free path, the vapour distribution around particles becomes nonuniform, and a further correction for the coagulation coefficient is needed to take diffusophoretic effects into account [50]. For our model system, this limit is reached when the particle size (for an equivalent monodisperse distribution) is approximately 4 μm [23].

Table 5.3 gives the properties of the model compound used in this work. The chosen model compound can be seen as a proxy of ethanesulfonic acid, a potential contributor to new particle formation in polluted air.

[6] In the original article, there was a typo in Eq. (5.37) that contained an extra factor n_1. This erroneous factor was not, however, applied when calculating the results. A more substantial issue is the application of the approximative form instead of the exact formula [Eq. (2.19)] for the collision rate also for the smallest clusters: It turns out, however, that there is no qualitative difference in results obtained using either of the formulae, and also the quantitative differences are minor, at least in our example cases, being an order of 0.1 molecules for both $\tilde{g}$ and $\bar{g}$.

Table 5.3. Properties of the model compound.

Equilibrium vapour pressure p_e (Pa)	$1.33 \cdot 10^{-3}$
Molecular mass m (kg)	$1.60 \cdot 10^{-25}$
Molecular surface area A_1 (m^2)	$1.50 \cdot 10^{-18}$
Surface tension γ_∞ (N/m)	0.030

5.B Addendum: Comparison with results from Ref. [21]

Figure 5.5 depicts results from the SAWNUC-model [51] for binary H_2SO_4–H_2O nucleation, showing the dependence of the apparent critical size ($n_d^* \approx \widetilde{g_{H_2SO_4}}$) on the diameter d where the new particle formation rate J_d is evaluated at as a function of monomer concentration with $T = 248$ K and $q_1^{-1} = 500$ s. At low and moderate H_2SO_4 concentrations, the apparent critical size is found to be larger than the kinetic critical size when J_d is evaluated at sizes larger than the kinetic critical size, whilst when J_d is evaluated below the kinetic critical size (at $d = 1$ nm), a constant apparent critical size is found, indicating the existence of the linear regime also for binary H_2SO_4–H_2O system. Circled area highlights the range of high monomer concentration, where $\widetilde{g_{H_2SO_4}} < \overline{g_{H_2SO_4}}$ due to self-coagulation of clusters.

References

[1] N. E. Motl, A. K. P. Mann and S. E. Skrabalak. Aerosol-assisted synthesis and assembly of nanoscale building blocks. *Journal of Materials Chemistry A* 1 (2013), 5193–5202.

[2] V.-M. Kerminen, M. Paramonov, T. Anttila, I. Riipinen, C. Fountoukis, H. Korhonen, E. Asmi, L. Laakso, H. Lihavainen, E. Swietlicki, B. Svenningsson, A. Asmi, S. N. Pandis, M. Kulmala and T. Petäjä. Cloud condensation nuclei production associated with atmospheric nucleation: a synthesis based on existing literature and new results. *Atmospheric Chemistry and Physics* 12 (2012), 12037–12059.

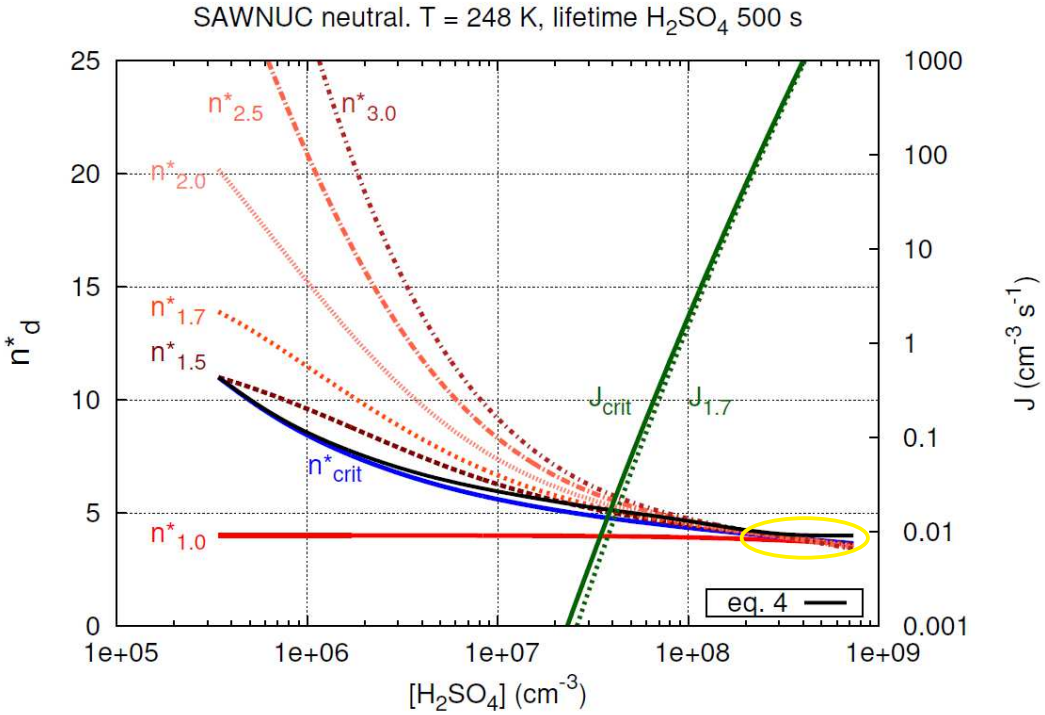

Fig. 5.5. Apparent critical size and formation rate evaluated at different cluster sizes d. Adapted from Ref. [21] under Creative Commons Attribution 3.0 License.

[3] H. Vehkamäki and I. Riipinen. Thermodynamics and kinetics of atmospheric aerosol particle formation and growth. *Chemical Society Reviews* 41 (2012), 5160–5173.

[4] D. Kashchiev. Forms and applications of the nucleation theorem. *Journal of Chemical Physics* 125 (2006), 014502.

[5] R. K. Bowles, R. McGraw, P. Schaaf, B. Senger, J.-C. Voegel and H. Reiss. A molecular based derivation of the nucleation theorem. *Journal of Chemical Physics* 113 (2000), 4524–4532.

[6] I. J. Ford. Nucleation theorems, the statistical mechanics of molecular clusters, and a revision of classical nucleation theory. *Physical Review E* 56 (1997), 5615–5629.

[7] R. McGraw and D. T. Wu. Kinetic extensions of the nucleation theorem. *Journal of Chemical Physics* 118 (2003), 9337–9347.

[8] L. Farkas. Keimbildungsgeschwindigket in übersättigten Dämpfen. *Zeitschrift für physikalische Chemie* 175 (1927), 236–242.

[9] R. Becker and W. Döring. Kinetische Behandlung der Keimbildung in übersättigten Dämpfen. *Annalen der Physik* 416 (1935), 719–752.

[10] R. Strey, P. E. Wagner and Y. Viisanen. The problem of measuring homogeneous nucleation rates and the molecular contents of nuclei: Progress in the form of nucleation pulse measurements. *Journal of Physical Chemistry* 98 (1994), 7748–7758.

[11] M. Kulmala, K. E. J. Lehtinen and A. Laaksonen. Cluster activation theory as an explanation of the linear dependence between formation rate of 3 nm particles and sulphuric acid concentration. *Atmospheric Chemistry and Physics* 6 (2006), 787–793.

[12] M. Sipilä, T. Berndt, T. Petäjä, D. Brus, J. Vanhanen, F. Stratmann, J. Patokoski, R. L. Mauldin, III, A.-P. Hyvärinen, H. Lihavainen and M. Kulmala. The role of sulfuric acid in atmospheric nucleation. *Science* 327 (2010), 1243–1246.

[13] J. Kirkby, J. Curtius, J. Almeida, E. Dunne, J. Duplissy, S. Ehrhart, A. Franchin, S. Gagné, L. Ickes, A. Kürten, A. Kupc, A. Metzger, F. Riccobono, L. Rondo, S. Schobesberger, G. Tsagkogeorgas, D. Wimmer, A. Amorim, F. Bianchi, M. Breitenlechner, A. David, J. Dommen, A. Downard, M. Ehn, R. C. Flagan, S. Haider, A. Hansel, D. Hauser,

W. Jud, H. Junninen, F. Kreissl, A. Kvashin, A. Laaksonen, K. Lehtipalo, J. Lima, E. R. Lovejoy, V. Makhmutov, S. Mathot, J. Mikkilä, P. Minginette, S. Mogo, T. Nieminen, A. Onnela, P. Pereira, T. Petäjä, R. Schnitzhofer, J. H. Seinfeld, M. Sipilä, Y. Stozhkov, F. Stratmann, A. Tomé, J. Vanhanen, Y. Viisanen, A. Vrtala, P. E. Wagner, H. Walther, E. Weingartner, H. Wex, P. M. Winkler, K. S. Carslaw, D. R. Worsnop, U. Baltensperger and M. Kulmala. Role of sulphuric acid, ammonia and galactic cosmic rays in atmospheric aerosol nucleation. *Nature (London)* 476 (2011), 429–433.

[14] J. H. Zollner, W. A. Glasoe, B. Panta, K. K. Carlson, P. H. McMurry and D. R. Hanson. Sulfuric acid nucleation: Power dependencies, variation with relative humidity, and effect of bases. *Atmospheric Chemistry and Physics* 12 (2012), 4399–4411.

[15] R. Zhang, L. Wang, A. Khalizov, J. Zhao, J. Zheng, R. L. McGraw and L. T. Molina. Formation of nanoparticles of blue haze enhanced by anthropogenic pollution. *Proceedings of the National Academy of Sciences U.S.A.* 106 (2009), 17650–17654.

[16] J. Almeida, S. Schobesberger, A. Kürten, I. K. Ortega, O. Kupiainen-Määttä, A. P. Praplan, A. Adamov, A. Amorim, F. Bianchi, M. Breitenlechner, A. David, J. Dommen, N. M. Donahue, A. Downard, E. Dunne, J. Duplissy, S. Ehrhart, R. C. Flagan, A. Franchin, R. Guida, J. Hakala, A. Hansel, M. Heinritzi, H. Henschel, T. Jokinen, H. Junninen, M. Kajos, J. Kangasluoma, H. Keskinen, A. Kupc, T. Kurtén, A. N. Kvashin, A. Laaksonen, K. Lehtipalo, M. Leiminger, J. Leppä, V. Loukonen, V. Makhmutov, S. Mathot, M. J. McGrath, T. Nieminen, T. Olenius, A. Onnela, T. Petäjä, F. Riccobono, I. Riipinen, M. Rissanen, L. Rondo, T. Ruuskanen, F. D. Santos, N. Sarnela, S. Schallhart, R. Schnitzhofer, J. H. Seinfeld, M. Simon, M. Sipilä, Y. Stozhkov, F. Stratmann, A. Tomé, J. Tröstl, G. Tsagkogeorgas, P. Vaattovaara, Y. Viisanen, A. Virtanen, A. Vrtala, P. E. Wagner, E. Weingartner, H. Wex, C. Williamson, D. Wimmer, P. Ye, T. Yli-Juuti, K. S. Carslaw, M. Kulmala, J. Curtius, U. Baltensperger, D. R. Worsnop, H. Vehkamäki and J. Kirkby. Molecular understanding of sulphuric acid-amine particle nucleation in the atmosphere. *Nature (London)* 502 (2013), 359–363.

[17] F. Riccobono, S. Schobesberger, C. E. Scott, J. Dommen, I. K. Ortega, L. Rondo, J. Almeida, A. Amorim, F. Bianchi, M. Breitenlechner, A. David, A. Downard, E. M. Dunne, J. Duplissy, S. Ehrhart, R. C. Flagan, A. Franchin, A. Hansel, H. Junninen, M. Kajos, H. Keskinen, A. Kupc, A. Kürten, A. N. Kvashin, A. Laaksonen, K. Lehtipalo, V. Makhmutov, S. Mathot, T. Nieminen, A. Onnela, T. Petäjä, A. P. Praplan, F. D. Santos, S. Schallhart, J. H. Seinfeld, M. Sipilä, D. V. Spracklen, Y. Stotzhkov, F. Stratmann, A. Tomé, G. Tsagkogeorgas, P. Vaattovaara, Y. Viisanen, A. Vrtala, P. E. Wagner, E. Weingartner, H. Wex, D. Wimmer, K. S. Carslaw, J. Curtius, N. M. Donahue, J. Kirkby, M. Kulmala, D. R. Worsnop and U. Baltensperger. Oxidation products of biogenic emissions contribute to nucleation of atmospheric particles. *Science* 344 (2014), 717–721.

[18] It should be noted that the interpretations from carefully controlled laboratory measurements [e.g. 12–17] are often done at much higher H_2SO_4 concentrations than observed in the atmosphere.

[19] H. Vehkamäki, M. J. McGrath, T. Kurtén, J. Julin, K. E. J. Lehtinen and M. Kulmala. Rethinking the application of the first nucleation theorem to particle formation. *Journal of Chemical Physics* 136 (2012), 094107.

[20] O. Kupiainen-Määttä, T. Olenius, H. Korhonen, J. Malila, M. Dal Maso, K. E. J. Lehtinen and H. Vehkamäki. Critical cluster size cannot in practice be determined by slope analysis in atmospherically relevant applications. *Journal of Aerosol Science* 77 (2014), 127–144.

[21] S. Ehrhart and J. Curtius. Influence of aerosol lifetime on the interpretation of nucleation experiments with respect to the first nucleation theorem. *Atmospheric Chemistry and Physics* 13 (2013), 11465–11471.

[22] R. McGraw and W. H. Marlow. The multistate kinetics of nucleation in the presence of an aerosol. *Journal of Chemical Physics* 78 (1983), 2542–2548.

[23] M. Noppel. Nucleation in the presence of air ions and aerosol particles. In: *Nucleation and Atmospheric Aerosols*. Ed. by M. Kulmala and P. E. Wagner. Oxford: Pergamon, 1996, 208–211.

[24] C. Becker and H. Reiss. Nucleation in a nonuniform vapor. *Journal of Chemical Physics* 65 (1976), 2066–2070.

[25] I. M. Fishman. Steady-state and transient nucleation of a new phase in a first-order transition. *Soviet Physics Uspekhi* 31 (1988), 561–576.

[26] S. K. Friedlander. A note on new particle formation in the presence of an aerosol. *Journal of Colloid and Interface Science* 67 (1978), 387–388.

[27] S. K. Friedlander. Theory of new particle formation in the presence of an aerosol. *Journal of Aerosol Science* 10 (1979), 198–199.

[28] I. Kusaka, Z.-G. Wang and J. H. Seinfeld. Binary nucleation of sulfuric acid and water: Monte Carlo simulation. *Journal of Chemical Physics* 108 (1998), 6829–6848.

[29] In a preliminary account of the current work [J. Malila, R. McGraw, A. Laaksonen and K. E. J. Lehtinen. Repairing the first nucleation theorem: Precritical cluster losses. *AIP Conference Proceedings* 1527 (2013), 31–34], an erroneous assumption $J_1 = J$ was implied. Therefore, the results of that work are quantitative only for a kinetically controlled process, in which case the solution obtained earlier by one of the authors [A. Laaksonen. Application of nucleation theories to atmospheric new particle formation. *AIP Conference Proceedings* 534 (2000), 711–723] is recovered.

[30] G. Shi, J. H. Seinfeld and K. Okuyama. Transient kinetics in nucleation. *Physical Review A* 41 (1990), 2101–2108.

[31] R. McGraw and J. H. Saunders. A condensation feedback mechanism for oscillatory nucleation and growth. *Aerosol Science and Technology* 3 (1984), 367–380.

[32] D. Reguera and J. M. Rubí. Homogeneous nucleation in inhomogeneous media. I. Nucleation in a temperature gradient. *Journal of Chemical Physics* 119 (2003), 9877–9887.

[33] G. Shi, J. H. Seinfeld and K. Okuyama. Homogeneous nucleation in spatially inhomogeneous systems. *Journal of Applied Physics* 68 (1990), 4550–4555.

[34] P. H. McMurry and S. K. Friedlander. New particle formation in the presence of an aerosol. *Atmospheric Environment* 13 (1979), 1635–1651.

[35] V. A. Shneidman and I. M. Fishman. Nucleation of a new phase for particles with finite lifetimes. *Chemical Physics Letters* 173 (1990), 331–336.

[36] T. Olenius, I. Riipinen, K. Lehtipalo and H. Vehkamäki. Growth rates of atmospheric molecular clusters based on appearence times and collision–evaporation fluxes: Growth by monomers. *Journal of Aerosol Science* 78 (2014), 55–70.

[37] Due to orders-of-magnitude difference between water vapour and sulphuric acid monomer concentrations in typical experimental/ atmospheric conditions, this system can be treated as a quasiunary one with respect to the sulfuric acid, and thus our results apply directly also in this case.

[38] J. Wang, R. McGraw and C. Kuang. Growth of atmospheric nanoparticles by heterogeneous nucleation of organic vapor. *Atmospheric Chemistry and Physics* 13 (2013), 6523–6531.

[39] P. M. Winkler, A. Vrtala, G. Steiner, D. Wimmer, H. Vehkamäki, K. E. J. Lehtinen, G. P. Reischl, M. Kulmala and P. E. Wagner. Quantitative characterization of critical nanoclusters nucleated on large single molecules. *Physical Review Letters* 108 (2012), 085701.

[40] D. W. Oxtoby and A. Laaksonen. Some consequences of the nucleation theorem for binary fluids. *Journal of Chemical Physics* 102 (1995), 6846–6850.

[41] R. P. Sear. On the interpretation of quantitative experimental data on nucleation rates using classical nucleation theory. *Journal of Physical Chemistry B* 110 (2006), 21944–21949.

[42] R. B. McClurg. Nucleation rate and primary particle size distribution. *Journal of Chemical Physics* 117 (2002), 5328–5336.

[43] P. Wynn. Continued fractions whose coefficients obey a non-commutative law of multiplication. *Archive for Rational Mechanics and Analysis* 12 (1963), 273–312.

[44] J. Malila. The derivative of a finite continued fraction. *Applied Mathematics E-Notes* 14 (2014), 13–19.

[45] J. Merikanto, E. Zapadinsky, A. Lauri and H. Vehkamäki. Origin of the failure of classical nucleation theory: Incorrect description of the smallest clusters. *Physical Review Letters* 98, 145702 (2007), 145702.

[46] S. L. Girshick. The dependence of homogeneous nucleation rate on supersaturation. *Journal of Chemical Physics* 141 (2014), 024307.

[47] R. McGraw and R. Zhang. Multivariate analysis of homogeneous nucleation rate measurements. Nucleation in the p-toluic acid/ sulfuric acid/water system. *Journal of Chemical Physics* 128 (2008), 064508.

[48] W. G. Courtney. Remarks on homogeneous nucleation. *Journal of Chemical Physics* 35 (1961), 2249–2250.

[49] For coagulation loss, the coefficients q_i are closely related to the concept of coagulation sink (CoagS; M. Kulmala, M. Dal Maso, J. M. Mäkelä, L. Pirjola, M. Väkevä, P. Miikkulainen, K. Hämeri and C. D. O'Dowd. On the formation, growth and composition of nucleation mode particles. *Tellus B* 53 (2001), 479–490) used in the analysis of atmospheric NPF: The main difference is that CoagS is calculated assuming a fixed critical size and continuous distribution of background particles. At the monomer limit ($i \rightarrow 1$), q_i approaches another related concept, condensation sink (CS). Relationship between A, CS, and the parameter L mentioned earlier are described in detail by P. H. McMurry, M. Fink, H. Sakurai, M. R. Stolzenburg, R. L. Mauldin, J. Smith, F. Eisele, K. Moore, S. Sjostedt, D. Tanner, L. G. Huey, J. B. Nowak, E. Edgerton and D. Voisin. A criterion for new particle formation in the sulfur-rich Atlanta atmosphere. *Journal of Geophysical Research: Atmospheres* 110 (2005), D22S02.

[50] R. McGraw and P. H. McMurry. The coupling of nucleation and diffusion near an aerosol particle. *Journal of Colloid and Interface Science* 92 (1983), 584–587.

[51] E. R. Lovejoy, J. Curtius and K. D. Froyd. Atmospheric ion-induced nucleation of sulfuric acid and water. *Journal of Geophysical Research: Atmospheres* 109 (2004), D08204.

6 Critical cluster size cannot in practice be determined by slope analysis in atmospherically relevant applications[1]

The first nucleation theorem is the most widely used method to assess atmospheric new-particle formation mechanisms from particle formation rate measurements. The theorem states that the slope $(\partial \ln J)/(\partial \ln C_i)$ of the nucleation rate J versus the concentration C_i of a nucleating compound gives the number of molecules of that species in the critical cluster. In principle, the derivation of the theorem is solid, but it contains very restrictive assumptions, the validity of which is questionable in realistic situations. It applies only for systems where clusters grow by addition of single molecules, and there are no external losses. In addition, application of the theorem to experimental data requires that the nucleation rate can be determined from particle concentration observations. This work presents sim-

[1]This chapter incorporates the article O. Kupiainen-Määttä, T. Olenius, H. Korhonen, J. Malila, M. Dal Maso, K. E. J. Lehtinen and H. Vehkamäki. Critical cluster size cannot in practice be determined by slope analysis in atmospherically relevant applications. *Journal of Aerosol Science* 77 (2014), 127–144. Drs. Ismael K. Ortega and Theo Kurtén are acknowledged for discussions and the Academy of Finland (Centre of Excellence programme grant #272041, LASTU programme project #135054, Research Fellow position #250348), the European Research Council (project ERC-StG 257360-MOCAPAF), the ACCC doctoral programme, and the Vilho, Yrjö and Kalle Väisälä Foundation for funding.

ulation results on particle formation rates in atmospherically relevant conditions. We show that the slope of the nucleation rate in realistic conditions differs from that in an ideal situation. The slope analysis can easily lead to erroneous conclusions on the critical cluster size, and should therefore not be used to interpret experimental data.

6.1 Introduction

Formation of aerosol particles from precursor vapours is an important and widely studied topic in the field of atmospheric sciences. Numerous experimental and theoretical studies have focused on assessing the formation mechanism of aerosols in varying environments [1–3]. The phenomenon begins with vapour-phase molecules colliding with each other to form small molecular clusters and continues with the clusters growing by further collisions, at the same time also being able to lose molecules by evaporation. While sulphuric acid has been recognized as the key compound of the process in many environments [4, 5], identities and roles of other compounds still remain uncertain.

The gas-to-liquid phase transition related to the particle formation process is in general assumed to proceed via nucleation, where the cluster formation free energy surface exhibits an energy barrier that the growing cluster must overcome in order to become a stable particle. Another option is barrierless condensation, where already the smallest clusters are stable and particle formation is kinetically limited. In case of nucleation, the location of the energy barrier is called the critical cluster size. Clusters that are smaller than the critical size are more likely to evaporate into smaller sizes than to grow further, and clusters that are larger than the critical size are more likely to grow than to decay. A central question concerning the nucleation mechanism is the size and composition of the critical cluster. As cluster energies cannot be measured directly, the critical cluster cannot simply be identified from the energy profile of the nucleating system. A seemingly easy-to-use, and thus very widely employed, method to deduce indirectly the composition of the critical cluster from experimental observations is the first nucleation theorem. According to its most generally used form,

the number of molecules of any compound i in the critical cluster g_i^* is approximately equal to the slope of the logarithm of the nucleation rate J as a function of the logarithm of the gas-phase concentration C_i of the compound i:[2]

$$\frac{\partial \ln J}{\partial \ln C_i} \approx g_i^*, \tag{6.1}$$

where other parameters such as temperature and concentrations of other vapours are assumed to be constant. As sulphuric acid has been identified as the main driving compound of atmospheric new particle formation, several studies have focused on determining the number of sulphuric acid molecules in the critical cluster [6, 7]. In experimental studies, this is normally done by measuring particle concentrations at different sulphuric acid concentrations, determining the particle formation rate at each point, and applying a linear fit to the data presented in a log-log scale. Consequently, the observed formation rate is often reported as a power-law $J \propto [H_2SO_4]^P$ [5, 8, 9].[3] However, different experiments have given values for the exponent P ranging from 1.3 to 12.9 [7, 10–13], and the measured formation rates at similar H_2SO_4 concentrations have varied by several orders of magnitude. The formation rate is normally given at the assumed critical cluster size corresponding to a mobility diameter of 1–2 nm. On the other hand, the detection limit of particle counters is often significantly higher than the assumed critical size, and thus the formation rate at the size of interest must be calculated from the particle concentrations at the observed size by assuming a certain growth rate, and accounting for possible losses between these sizes [14–16].

The nucleation theorem has also been widely used in fundamental nucleation studies not directly related to atmospheric aerosols. Critical cluster sizes determined using the nucleation theorem for measured nucleation rates of various molecular liquids have been compared with theoretical predictions using the classical liquid droplet model. For n-butanol, Viisanen

[2] In this chapter, we continue to use f_g (actual values) and n_g (constrained equilibrium value) for concentrations of g-mers (clusters containing g gas phase monomers that can of same or different species), and in multicomponent case use C_i for the gas-phase concentration of monomers of compound i.

[3] For future reference, it should be noted that assumption of constant P that implies a linear graph in a log-log scale plot is equivalent to assuming a critical size that is independent of environmental conditions.

and Strey [17] found reasonably close agreement between the two approaches, although the slope values were slightly higher than the classical results. On the other hand, Brus et al. [18] found later large discrepancies between critical cluster sizes of n-butanol determined using different measurement set-ups. For the ethanol–hexanol mixture, Strey and Viisanen [19] found qualitative agreement between critical cluster composition determined from measurements and theory, while especially the critical cluster size of pure hexanol deviated by several tens of percent between the slope approach and the liquid drop model. Also in the n- and i-octane mixture, Vehkamäki and Ford [20] found notable differences between slope values and classical theory. Slope values that are considerably lower than classical predictions have been reported for n-propanol [21] and slopes slightly lower than predicted have also been observed for n-pentanol [22]. Also for water, classical predictions may be slightly or even significantly higher than experimental results, especially for larger critical sizes or higher temperatures [23, and references therein, 24], but there are also some discrepancies between different experimental data sets [see 23, 25, and references therein].

Some recent studies [26–28] have pointed out that external losses affect the nucleation rate and thus the applicability of the nucleation theorem. In addition to requiring that there are no losses, the derivation of the nucleation theorem also involves several other assumptions. In this work, we present an overview of the derivation, and examine how breaking each of the assumptions affects the results obtained by applying the theorem. While our examples are related to atmospheric new-particle formation, the problems raised in this study are quite general and may affect the applicability of the nucleation theorem also in other systems.

We use a cluster population dynamics model to simulate the formation rate of sulphuric acid–base clusters at a mobility diameter of approximately 1.5 nm, a size at which experimental particle formation rates are often reported. We present the simulated formation rate and its slope with respect to sulphuric acid and base concentrations as a function of acid concentration, and show that the slope may be altered by various factors.

To study the uncertainties related to calculating the formation rate of sub-2 nm particles from the concentrations of larger particles, we also apply a separate aerosol microphysics model to simulate particle growth from 1.5

nm to larger sizes. In this case, the formation rate at 1.5 nm is assumed to follow a power-law dependence $J \propto [H_2SO_4]^P$. The nucleation rate is then back-calculated from the concentrations of 3–6 nm particles following the procedure used in the analysis of experimental data. We show that the exponent P obtained from the slope of the calculated nucleation rate differs from the actual value used as input in the growth simulation, leading to erroneous conclusions about the critical cluster size.

6.2 The first nucleation theorem

Relation (6.1), usually referred to as the first nucleation theorem, was first developed on the basis of the classical capillary drop model by Nielsen [29], who applied it to crystallization from a melt. Kashchiev [30] gave the result a more general theoretical footing, still in the capillary drop framework, and coined the term "nucleation theorem". Later, other derivations have been constructed which rely less on the formation energy. The most simplified proof for the single-component case is that by McGraw and Wu [31] (see also Ford [32]) which we present below briefly. Let us denote the steady-state concentration of a g-molecule cluster by f_g and its "constrained equilibrium" concentration (that is, the concentration it would have in an equilibrium distribution where the monomer had the supersaturated concentration $f_1 \equiv n_1$) by n_g. Taking into account only monomer additions and evaporations, the net flux between each pair of consecutive cluster sizes is

$$J_g = \beta_{1,g} n_1 f_g - \alpha_{1,g} f_{g+1}, \tag{6.2}$$

where $\beta_{1,g}$ is the collision coefficient between a monomer and a g-molecule cluster and $\alpha_{1,g} = \beta_{1,g} n_1 n_g / n_{g+1}$ is the evaporation rate of a monomer from the $g+1$-molecule cluster, related by detailed balance to the collision rate and the constrained equilibrium distribution. In the absence of external losses, the rate of change of each cluster concentration can be expressed in term of collision and evaporation fluxes as $\mathrm{d}f_g/\mathrm{d}t = J_{g-1} - J_g$. As in steady state the concentrations are time-independent, $\mathrm{d}f_g/\mathrm{d}t = 0$, the flux J_g through the system of clusters is equal for all sizes g. It is also equal to the flux at the critical size, or the nucleation rate, denoted as J. Rearranging the terms, summing the birth-death equations for each cluster size and

assuming that $f_g/n_g \to 0$ as $g \to \infty$, the nucleation rate can be written as

$$J = \left(\sum_{g=1}^{\infty} \frac{1}{\beta_{1,g} n_1 n_g} \right)^{-1}. \tag{6.3}$$

The constrained equilibrium cluster concentrations follow the law of mass action

$$K_g = \frac{n_g}{n_1 n_{g-1}}, \tag{6.4}$$

where K_g is the equilibrium constant, which only depends on temperature and can also be expressed in terms of cluster free energies. Equation (6.4) results in the power law $n_g \propto n_1^g$ for the equilibrium cluster concentrations. From this, it can directly be seen that

$$\frac{\partial(n_1 n_g)}{\partial n_1} = (g+1)\frac{n_1 n_g}{n_1}, \tag{6.5}$$

and the derivative of the nucleation rate (6.3) can be calculated to give

$$\left(\frac{\partial \ln J}{\partial \ln n_1} \right)_T = \frac{\sum_{g=1}^{\infty} \frac{g}{\beta_{1,g} n_g}}{\sum_{g=1}^{\infty} \frac{1}{\beta_{1,g} n_g}} + 1 \equiv \bar{g} + 1. \tag{6.6}$$

If the distribution $1/(\beta_{1,g} n_g)$ has one high maximum at g^* that dominates the sum $\sum_{g=1}^{\infty} g/(\beta_{1,g} n_g)$, the value $\bar{g}$ is approximately equal to g^*. Finally, taking into account the relation between constrained equilibrium concentrations and cluster formation energies, the expression inside the summation becomes

$$\frac{1}{\beta_{1,g} n_g} \propto \frac{1}{\beta_{1,g}} \exp\left(\frac{\Delta G_g}{k_B T} \right),$$

where ΔG_g is the Gibbs free energy of formation of the g-molecule cluster, k_B is the Boltzmann constant and T is the temperature. If the collision rate depends only weakly on cluster size, the maximum of the distribution $1/(\beta_{1,g} n_g)$ likely coincides with the maximum of the energy barrier at the critical cluster size.

Similar arguments relying on the law of mass action and involving some approximations have been used [33] to motivate the multicomponent nucleation theorem

$$\left(\frac{\partial \ln J}{\partial \ln C_i}\right)_{T,C_{j\neq i}} = g_i^* + \epsilon_i, \tag{6.7}$$

where C_i is the monomer concentration of component i, g_i^* is the number of molecules i in the critical cluster and ϵ_i gives the relative fraction of the growth flux out of the critical cluster due to addition of a molecule of type i, $\sum_i \epsilon_i = 1$.

In a case where clusters grow and decay only through additions and removals of single molecules, and all growth and evaporation processes occur along a single pathway, the multicomponent nucleation theorem can also be derived rigorously. The derivation follows closely that of the single-component case, except that each growth step on the formation pathway is associated with the specific molecule type added to the cluster at that step. The net flux between two consecutive cluster sizes is now

$$J_k = \beta_{m_k,k} C_{m_k} f_k - \alpha_{m_k,k} f_{k+1},$$

where f_k and f_{k+1} are the concentrations of the k^{th} and $(k+1)^{\text{th}}$ clusters, respectively, and m_k is the monomer type added to the cluster k to form the cluster $k+1$. Analogously to the one-component case, the birth–death equations can be rearranged as $J_k/\left(\beta_{m_k,k} C_{m_k} n_k\right) = \left(f_k/n_k - f_{k+1}/n_{k+1}\right)$ and summed to give

$$J = \left(\sum_{k=1}^{\infty} \frac{1}{\beta_{m_k,k} C_{m_k} n_k}\right)^{-1}. \tag{6.8}$$

The constrained equilibrium cluster concentrations have again a power law dependence on monomer concentrations, $f_k \propto \prod_{i=1}^{M} {C_i}^{g_{k,i}}$ where M is the number of molecule types and the exponent $g_{k,i}$ is the number of molecules of species i in cluster k. The derivative corresponding to that of Eq. (6.5) depends on whether the monomer concentrations in the numerator and denominator correspond to the same molecule type,

$$\left(\frac{\partial (C_{m_k} n_k)}{\partial C_i}\right)_{C_{j\neq i}} = (g_{k,i} + \delta_{m_k,i}) \frac{C_{m_k} n_k}{C_i},$$

where $\delta_{m_k,i}$ is the Kronecker delta ($\delta_{m_k,i} = 1$ if $m_k = i$ and $\delta_{m_k,i} = 0$ otherwise), and the derivative of the nucleation rate becomes

$$\left(\frac{\partial \ln J}{\partial \ln C_i}\right)_{T,C_{j\neq i}} = \frac{\sum_{k=1}^{\infty} \frac{g_{k,i} + \delta_{m_k,i}}{\beta_{m_k,k} C_{m_k} n_k}}{\sum_{l=1}^{\infty} \frac{1}{\beta_{m_l,l} C_{m_l} n_l}} \equiv \bar{g}_i + \bar{\epsilon}_i, \tag{6.9}$$

where the summations go over the clusters on the formation pathway. Once again, if the sum in the numerator is dominated by a sharp maximum in the distribution $1/\left(\beta_{m_k,k} C_{m_k} n_k\right)$ at one cluster size g^*, $\bar{g}_i$ is close to the number of molecules i in that cluster. Similarly $\bar{\epsilon}_i$ is close to one if the next step on the formation pathway after the cluster g^* is an addition of molecule i and close to zero if it is an addition of some other molecule type. As opposed to the one-component system, however, the monomer concentrations do not cancel out in Eq. (6.9), and they may affect the values of $\bar{g}_i$ and $\bar{\epsilon}_i$ if different monomer types have very different concentrations.

The kinetic derivations presented above for the one-component and multi-component systems are very general in the sense that they do not (explicitly) assume anything about the cluster energies. They do, however, contain several other very restrictive assumptions, both related to their derivation and to their application to experimental data. These assumptions and their validity are summarized in Table 6.1. The widely established conception that the ΔG surface contains one maximum (assumption A) follows from thermodynamic treatment of a bulk liquid droplet, where the formation free energy of a cluster is the energy difference between the liquid and vapour phases minus the energy required to form the surface separating the phases. The birth–death equations are derived assuming that the growth and decay of the clusters occurs via a Szilárd–Farkas scheme, that is solely via monomer collisions and evaporations, and that there are no external loss terms such as deposition of clusters on surfaces or coagulation with larger particles (assumptions B and C). Assumption D (single nucleation pathway) is required for the present derivation of the multi-component nucleation theorem, but is not based on any prior evidence. Assumptions E–H are essentially related to the experimental conditions, measurement accuracy and data analysis. It is assumed that the flux from the critical cluster to larger sizes can be obtained from the observed appearance rate of freshly formed particles at some larger size (assumption E). Concen-

trations of all precursor vapours and clusters, and all ambient conditions such as temperature, must be constant during the particle formation event (assumptions F and G). Finally, the formation free energies ΔG_n, and thus also the composition of the critical cluster, or equivalently the slope of the particle formation rate as a function of the concentration of any component i [right-hand side of Eq. (6.7)], depend on the monomer concentrations. Therefore application of the first nucleation theorem to experimental data also requires the resolution and accuracy of the data to be sufficient for determining the partial derivative [left-hand side of Eq. (6.7)] as a function of the monomer concentration (assumption H).

For a multicomponent system, the nucleation theorem may not be applicable even in the case where all the assumptions of Table 6.1 are valid, if the traditional definition of the critical cluster being located at the saddle point of the ΔG surface is used. As the frequency at which a molecule collides with a cluster depends on the concentration of the molecule, components with a high concentration collide with the clusters more often than components with a lower concentration. As a result, the flux may be distorted from the energetically optimal growth pathway, and does not necessarily proceed via the saddle point of the free energy surface at all. Thus, the energy barriers related to cluster formation may be higher than would be expected based on the saddle point of the formation free energy surface, and can only be solved by taking explicitly into account the actual growth pathway [34–36]. The nucleation rate, on the other hand, is related by Eq. (6.9) to the composition of the cluster(s) on the formation pathway with the highest ΔG value(s). This disparity can, however, easily be resolved by redefining the critical cluster as the highest-energy cluster on the formation pathway, and we use this new definition in the rest of this article.

When ions are present, cluster formation can proceed along three separate ΔG surfaces corresponding to neutral, negatively charged and positively charged clusters. Furthermore, clusters can move from one charging state to another at any size by collisions with ions or charged clusters [37]. In the atmosphere, ions originate from cosmic rays and radon decay, and while their formation rate and total concentration are relatively constant, the concentrations of individual molecular ions vary. For instance, the concentration of the bisulfate ion (HSO_4^-), the ionic monomer relevant for the nucleation theorem, depends on the sulphuric acid concentration [38].

Therefore, if the nucleation rate in the presence of natural ionization is measured at different sulphuric acid concentration, the bisulfate ion concentration is not constant between the measurements, and thus assumption G does not hold and the nucleation theorem cannot be used.

The derivation of the nucleation theorem assumes that evaporation rates

$$\alpha_{1,k} \propto \beta_{1,k} \exp\left(\frac{\Delta G_{k+1} - \Delta G_k}{k_B T}\right) \tag{6.10}$$

are connected to collision rates and cluster formation energies by detailed balance (assumption I). It is also implicitly assumed that each number of molecules (or in the multicomponent case each set of numbers of different molecules) corresponds to exactly one cluster energy and that the configuration corresponding to that energy is reached immediately when the cluster is formed. This simplified view is, however, probably not correct. Especially in the case of large asymmetrical molecules, it is more likely that the colliding molecules or clusters first stick together in a configuration determined by the collision geometry and then gradually rearrange to an energetically more favorable configuration. Evaporation of the cluster would then be more probable shortly after it is formed than once it has found a more stable configuration. The effect of excess energy released when a cluster is formed is also neglected, which is supported by earlier studies suggesting that atmospherically relevant clusters have enough vibrational degrees of freedom to accommodate most of the collision energy [39], and that the corresponding increase in cluster temperature is not likely to increase the evaporation rates to the extent that the derivative $\partial(\ln J)/\partial(\ln C)$ is affected strongly [40]. However, there is at present no other way to obtain cluster evaporation rates than to make these simplifications and use Eq. (6.10), although the first steps toward a more detailed description have recently been taken [41, 42]. Therefore assessing the effect of assumption I on the nucleation theorem is beyond the scope of this study.

Table 6.1. Assumptions used when deriving the nucleation theorem (A–D, I) and applying it to experimental results (E–H), their validity in different situations, and sections of this work where the validity is discussed in detail.

	Assumption	Validity	Discussion
A	The ΔG surface has one high energy barrier.	Unknown	Secs. 6.4.1, 6.4.2
B	Only monomer processes are relevant.	Good (e.g. water nucleation)/ unknown (e.g. acid–base clustering)	Sec. 6.4.2
C	There are no external losses.	Poor	Sec. 6.4.3, Chap. 5
D	Multi-component nucleation proceeds along a single pathway.	Unknown	Secs. 6.4.1, 6.4.5
E	The nucleation rate with respect to vapour concentrations can be obtained from measurements.	Poor (atmosphere) / unknown (experiments)	Secs. 6.4.4, 6.4.7, [43]
F	The system is in steady state.	Unknown (atmosphere) / good (chamber experiments) / poor (flow tube)	Sec. 6.4.6
G	All other conditions are kept constant.	Poor (atmosphere, flow tube) / good (chamber experiments)	Secs. 6.4.5, 6.4.7
H	The partial derivative (Eq. 6.7) can be accurately determined.	Poor	Secs. 6.4.1, 6.4.4, 6.4.7
I	Collision and evaporation rates are connected by detailed balance	Unknown	

6.3 Methods

6.3.1 ACDC

We simulated the formation of sulphuric acid (H_2SO_4)–ammonia (NH_3) and sulphuric acid–dimethylamine ($(CH_3)_2NH$, or shortly DMA) clusters with a dynamic cluster model ACDC (Atmospheric Cluster Dynamics Code; [37, 44]). ACDC generates the time derivatives of the concentrations of a given set of clusters, also called the cluster birth-death equations or Becker–Döring equations, and solves the time evolution of the concentrations by numerical integration using the Matlab ode15s solver [45]. If evaporation is disabled for all cluster sizes, the set of equations solved reduces to the Smoluchowski coagulation equations. In addition to monomer collisions and evaporations, the code enables the inclusion of external sink and source terms for all cluster sizes and all possible cluster–cluster collision and fragmentation processes. If the system contains also electrically charged clusters, the equations include ionization and recombination by generic ionizing species that give their charge to other molecules and clusters upon collisions but do not otherwise participate in cluster formation (see Olenius et al. [37] or Almeida et al. [46] for more details). Vapour (monomer) concentrations can either be set to a predetermined value or solved from the birth–death equations when source terms and initial monomer concentrations are given.

For collisions between electrically neutral clusters, the collision coefficients are calculated as hard-sphere collision rates, and for collisions between a neutral and an ionic cluster, a parameterisation based on the cluster masses and the dipole moment and polarisability of the neutral cluster [47] is used. The evaporation coefficients are calculated from quantum chemical Gibbs free energies of formation according to the condition of detailed balance [Eq. (6.10)] as described by Ortega et al. [48].

The particle formation rate is defined in ACDC as the rate at which clusters grow out of the simulation system. To account for the limited size of the system (the largest clusters are $(H_2SO_4)_4 \cdot ((CH_3)_2NH)_4$ and $(H_2SO_4)_5 \cdot ((NH_3)_5)$, clusters are only allowed to leave the system if they have a favorable composition, or in practice an acid:base ratio of approximately one (neutral

clusters must contain at least 6 H_2SO_4 molecules + 5 NH_3 molecules, 5 H_2SO_4 molecules + 4 DMA molecules, 4 H_2SO_4 molecules + 5 DMA molecules, or in Sec. 6.4.6 5 H_2SO_4 molecules + 4 base molecules or 4 H_2SO_4 molecules + 5 DMA molecules, negatively charged clusters must have at least 1 HSO_4^- ion + 5 H_2SO_4 molecules + 1 NH_3 molecule, and positively charged clusters at least 1 NH_4^+ ion + 5 H_2SO_4 molecules + 5 NH_3 molecules). In the context of ACDC simulations, J refers always to this particle formation rate, not the nucleation rate at the critical size. The time evolution of the cluster concentrations and the particle formation rate are obtained directly as output from the integration of the birth–death equations, and the steady state formation rate can be solved by setting the vapour concentrations or their source terms to a constant value and running the simulation until all concentrations have reached a constant value.

Water vapour and the hydration of clusters are not taken into account in this study due to the lack of thermochemical data for hydrated clusters. The presented formation rates should therefore not be interpreted as quantitative predictions. Instead, the systems of dry clusters should be considered as a simplified test case for examining the performance of the nucleation theorem.

In this study, ACDC was used to solve the particle formation rate in two- and three-component sulphuric acid-base systems, where the base is either ammonia, dimethylamine (DMA) or both. The temperature was 278 K in all simulations. In Secs. 6.4.3 and 6.4.6 we used for all clusters a loss term $-Lf_g$ where L is a size-independent loss constant corresponding to coagulation with larger particles or deposition on walls and f_g is the cluster concentration. The simulation results should again be interpreted as giving a qualitative estimate of the effect of losses. In reality, the loss coefficients depend on cluster size, and in case of coagulational losses to larger particles also on the time evolution of the particle distribution. Detailed information on the clusters included in the systems and on the boundary conditions, and the quantum chemical data can be found in our earlier publications [37, 46]. Both ammonia and DMA have been observed in the atmosphere in various urban and rural areas [49], and our simulations were performed at realistic ambient sulphuric acid and base concentrations that produce particle formation rates comparable to those observed in the atmosphere, both according to ACDC simulations and chamber experiments [46, 50].

To study the dependence of the particle formation rate on precursor concentrations, we ran each simulation at several sulphuric acid concentrations and two base concentrations (or vice versa in the lower panel of Fig. 6.4), and approximated the partial derivative based on the difference between the formation rate at two adjacent simulation points as

$$\left(\frac{\partial \ln J}{\partial \ln C_i}\right)_{T,C_{j\neq i}} \approx \left(\frac{\Delta \ln J}{\Delta \ln C_i}\right)_{T,C_{j\neq i}},$$

where C_i is the acid or base concentration. The step size along the logarithmic concentration axis was set to 20 simulation points per an order of magnitude, and the concentrations of the other compound were set to $1{\cdot}[C_j]$ and $1.01 \cdot [C_j]$, except in Fig. 6.8 we used 10 simulation points per an order of magnitude for the sulphuric acid concentration and a base concentration $1.1 \cdot$ [base]. The Gibbs free energy of formation as a function of cluster growth was determined by tracing the growth pathways as described by Olenius et al. [37]. In the case that the main growth route exhibits one or more energy barriers, the critical cluster was identified as the location of the highest barrier.

6.3.2 UHMA

In addition to the cluster kinetics model, we used an aerosol microphysics model to investigate the applicability of the nucleation theorem to interpret field data. Our aerosol microphysics model UHMA (University of Helsinki Multicomponent Aerosol model; [43, 51]) was used to generate synthetic size distribution evolution data that resembles what is measured during atmospheric particle formation events. A detailed description of the model and the data analysis scheme is given by Korhonen et al. [43] (see also [5]), and we present here only the details that differ from that study.

In the simulations, particles were assumed to nucleate at 1.5 nm and the nucleation rate was assumed proportional to the sulphuric acid concentration squared, i.e. $J_{1.5} = k_2[\mathrm{H_2SO_4}]^2$. The time dependence of the sulphuric acid concentration was set to be parabolic, with a peak concentration of $1.5 \cdot 10^6$ cm^{-3} at noon and zero values before 10 am and after 2 pm, and some random noise was added to mimic rapidly varying atmospheric conditions. (This time interval is somewhat shorter than what is seen in the

atmosphere, and was chosen for computational reasons.) The value of k_2 was taken randomly from a uniform distribution in the range $5 \cdot 10^{-18}$ – $5 \cdot 10^{-17}$ at each time step.

The cluster growth rates were prescribed (i.e. not calculated from simulated vapour concentrations) to be linearly dependent on cluster size, as indicated by recent atmospheric observations [52]. At the beginning of each simulation, the growth rates at 1.5 nm and 3 nm were selected from the ranges 0.4–1.4 and 1.4–2.4 nm/h, respectively, and the same growth rates were used for the length of the simulation. This assumption of sulphuric acid-independent growth rates mimics a situation where the newly formed particles grow mainly by oxidized organic compounds.

The evolution of the particle size distribution was modeled using a fully moving sectional grid. The number of size bins was 20 at the beginning of the simulation, and new bins were created for the freshly nucleated particles, leading to a total of 260 bins at the end of the run. The time step was 0.2 s when sub-4-nm particles were present, and 60 s otherwise. The pre-existing aerosol population at the beginning of the run was modeled as one narrow mode at 200 nm in diameter corresponding to a coagulation sink between $0.04 \cdot 10^{-3}$ and $0.11 \cdot 10^{-3}$ s^{-1}. The sulphuric acid concentration and the particle size distribution above 3 nm diameter were stored for analysis every ten minutes.

6.4 Case studies

In this section we go through the assumptions listed in Table 6.1 and present examples where they may lead to a wrong assignment of the critical cluster. Results from ACDC are presented in Secs. 6.4.1–6.4.6, and results from UHMA in Sec. 6.4.7. Sections 6.4.1, 6.4.2 and 6.4.3 discuss the assumptions used in the derivation of nucleation theorem, while Secs. 6.4.4, 6.4.5 and 6.4.6 consider issues related to precursor vapour concentrations and Sec. 6.4.7 focus on difficulties in extracting the nucleation rate from measurements.

6.4.1 The critical cluster size depends on conditions (assumptions A, D and H)

According to the quantum chemical cluster formation energies used in this study, neutral sulphuric acid-ammonia cluster formation proceeds along a pathway containing three local maxima [37]. Depending on the precursor concentrations, any one of the clusters $(H_2SO_4)_5 \cdot (NH_3)_3$, $(H_2SO_4)_3 \cdot NH_3$ or $(H_2SO_4)_2$ can correspond to the highest maximum, and thus be the rate limiting critical cluster.

Figure 6.1 presents the particle formation rate and its logarithmic partial derivatives over a wide range of sulphuric acid concentrations. The slope of the particle formation rate with respect to the sulphuric acid concentration is high at low $[H_2SO_4]$ and decreases with increasing $[H_2SO_4]$. A comparison to the critical cluster composition shows that the slope $(\partial \ln J)/(\partial \ln[H_2SO_4])$ corresponds closely to the number of sulphuric acid molecules in the critical cluster. However, while the identity of the critical cluster changes in discrete steps, the slope decreases smoothly. This can easily be understood from Eq. (6.6): the nucleation theorem assumes that the critical cluster size alone determines the slope, but in this case the two highest maxima of the ΔG curve both contribute significantly to the summation of Eq. (6.9) near the transition from one critical cluster to the other.

Examining the main growth pathway in this system [37], it can be seen that the next step on the growth pathway after each local maximum is the addition of an ammonia molecule. Therefore, in all conditions considered in Fig. 6.1, the flux across the critical cluster is in the direction of the ammonia coordinate, and the correction terms of Eq. (6.7) are $\epsilon_{H_2SO_4} = 0$ and $\epsilon_{NH_3} = 1$. Taking the correction term into account, the nucleation theorem is also approximately valid for the ammonia derivative. The interpretation and validity of Eq. (6.9) are discussed in more detail in Sec. 6.A.1.

In the case of experimental data, the growth pathway is not known. Since the correction terms ϵ_i depend on what is the next step after passing the critical size, they can at best be guessed based on precursor concentrations but not determined reliably. If the critical cluster is small, this leads to a significant uncertainty in determining its composition, although the total

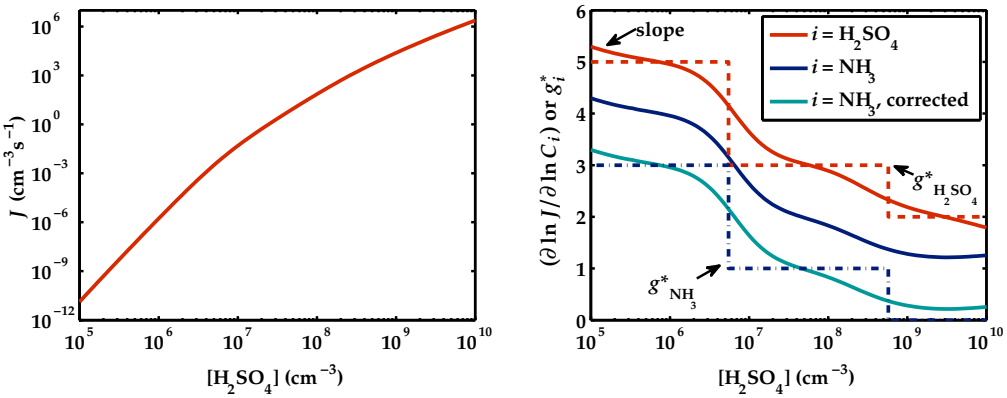

Fig. 6.1. Left panel: Particle formation rate as a function of H_2SO_4 monomer concentration at 278 K and [NH_3] = 10 ppt. Right panel: Logarithmic partial derivatives of the particle formation rate with respect to the sulphuric acid (red solid line) and ammonia (dark blue solid line) monomer concentrations, the ammonia derivative corrected with ϵ_{NH_3} = 1 (light blue solid line), and the number of sulphuric acid (red dashed line) and ammonia (dark blue dash-dotted line) molecules in the critical cluster, defined here as the highest energy barrier on the main growth pathway.

number of molecules can in principle be solved as the sum of the correction terms is always one. Making a single linear fit to a set of measurements where the critical cluster varies from point to point will also lead to an incorrect attribution of the critical cluster.

6.4.2 Cluster-cluster collisions (assumptions A and B)

In the presence of a strong base, such as DMA, small strongly bound acid-base clusters may be abundant enough to contribute significantly to cluster growth [37, see also 53]. Figure 6.2 shows the formation rates and their slopes at [DMA] = 10 ppt both in a simulation where only monomer collisions and evaporations are considered, and in a simulation where cluster–cluster processes are included. Depending on the H_2SO_4 concentration, the formation rate of the case where only monomer processes are included can be either lower or higher than in the case where all possible processes are taken into account: When cluster–cluster collisions are allowed, they contribute significantly to the growth, and as the growth rate

is higher, cluster concentrations are lower (see Sec. 6.A.2). The formation rate of clusters of a certain size depends both on the concentration of smaller clusters and on their growth rate; at low acid concentrations the effect of the growth rate dominates and the formation rate is higher when all collisions are allowed, and at higher acid concentrations the effect of cluster concentrations dominates. It should be noted, however, that forbidding cluster–cluster collisions is only a hypothetical tool for understanding how they affect the formation rate, and that there is no reason to believe that cluster–cluster collisions would not contribute to particle formation in reality if cluster concentrations are significant compared to monomer concentrations. Based on the cluster energies, fragmentation rates of clusters into two smaller clusters may in some cases be comparable to monomer evaporation rates. Fragmentation was allowed when also cluster–cluster collisions were allowed and forbidden when they were not. However, from the simulations, it was observed that the fragmentation processes had little effect on the particle formation rate. In the case where cluster–cluster collisions were enabled, disabling fragmentation changed the particle formation rate at most less than 0.25%.

In situations where small clusters are abundant and cluster–cluster collisions cannot be neglected, the derivation of the nucleation theorem is not valid and the slope of the formation rate does not, even in principle, give information on the critical size. This is the case when formation of the smallest clusters is energetically favorable. If there is no energetic barrier and no critical cluster at larger sizes, the particle formation rate is approximately proportional to the precursor concentrations, and the slopes are close to one in accordance to the nucleation theorem. If, on the other hand, there is a critical cluster at some larger size, the nucleation theorem is not valid [53].

In conditions of Fig. 6.2, cluster formation is barrierless, partly because energy barriers are avoided by collisions with small clusters instead of subsequent additions of monomers. If, on the other hand, only monomer collisions are allowed, the energy profile along the formation pathway has a local maximum at the cluster size $(H_2SO_4)_3 \cdot (DMA)_2$. However, as this is not a global maximum but instead has a negative formation free energy compared to monomers, its location cannot be inferred by slope analysis from Fig. 6.2.

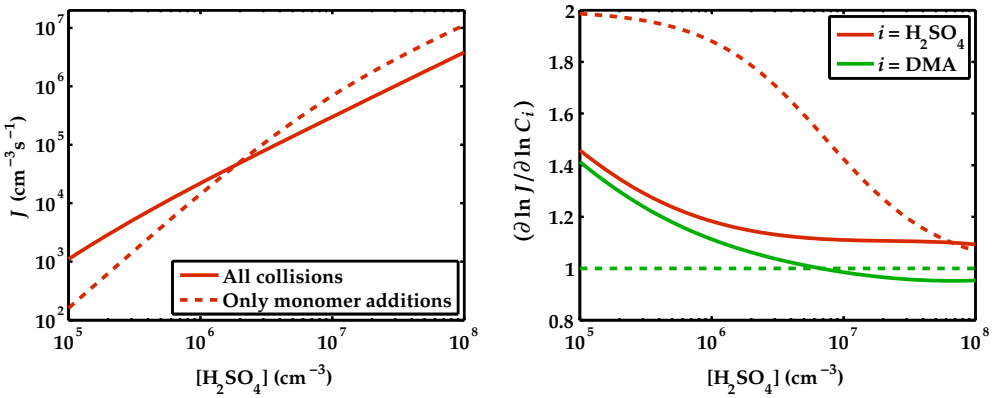

Fig. 6.2. Left panel: Neutral particle formation rate at [DMA] = 10 ppt. Right panel: Logarithmic partial derivatives of the formation rate with respect to the sulphuric acid (red) and DMA (green) monomer concentrations. Cluster–cluster collisions and evaporations are either allowed (solid lines) or disabled (dashed lines).

6.4.3 External losses (assumption C)

When particles are forming, growth and evaporation are usually not the only processes at play as assumed in the nucleation theorem. Instead, the clusters may be lost by coagulating onto larger particles or, in laboratory experiments, by depositing to walls before they reach a detectable size. The effect of these external losses is strongest when cluster formation and early growth are slow compared to the loss rate. The flux between consecutive clusters g and $g+1$ can still be written according to Eq. (6.2) as $J_g = \beta_{1,g} n_1 f_g - \alpha_{1,g} f_{g+1}$, but the steady-state flux is no longer equal for different cluster sizes k as some of the clusters are lost on the way. The cluster concentrations are overall lower than in the absence of losses, and the relative difference increases with cluster size as more clusters are lost at each growth step. Therefore both the forward and backward fluxes are lowered compared to the loss-free case. For each pair of consecutive clusters, the relative decrease in concentration is larger for the the bigger cluster, and thus the backward flux is lowered relatively more than the corresponding forward flux. As a consequence, at small sizes where evaporation is important, the net flux increases, and at larger sizes where evaporation is negligible the net flux decreases.

In experimental studies, formation rates are typically evaluated at a diameter larger than the critical cluster size, and we focus here on such a case. We also assume that the external losses are independent of the precursor concentration and particle formation rate, which is mostly relevant for chamber experiments where deposition to walls is the major loss mechanism. An increase in precursor concentrations then typically increases the particle formation rate both directly and by increasing the growth rate and thus reducing the relative effect of losses, and thus the slope of the formation rate with respect to vapour concentrations is higher than in the absence of losses. In a (pseudo-)one-component case the situation is straightforward, and the effect of losses has been studied previously for binary H_2SO_4-H_2O nucleation [28], and can even be treated analytically [54, note that the earlier version in 26, had an error]. In a multi-component system, on the other hand, the presence of several molecule types with possibly very different monomer concentrations, as well as potential competition between different formation pathways, complicates the situation and the effect of losses on the slope is not as straightforward.

Figure 6.3 shows the effect of external losses on the behavior of the steady-state formation rate in the sulphuric acid–DMA system. The losses were modeled using a size-independent loss constant of either $2.6 \cdot 10^{-3}$ s^{-1} or $2.3 \cdot 10^{-2}$ s^{-1} corresponding to coagulation losses at the Hyytiälä boreal forest station [55] and wall losses the *IfT*-LFT flow tube [56], respectively. It should be noted that the simulations do not aim to mimic atmospheric conditions or a flow tube experiment, but only to probe the effect of losses of different magnitudes in an otherwise ideal system.

As stated above, at $T = 278$ K and [DMA] = 10 ppt there is no critical cluster in the acid–DMA system. However, in the presence of wall losses, the slopes can be close to four for both sulphuric acid and DMA, which the nucleation theorem would interpret as a critical cluster of seven molecules in total, taking into account the correction terms ϵ_i which sum up to one. Corresponding results for the sulphuric acid–ammonia system are presented in the upper panel of Fig. 6.4. Also in this case the losses lower the formation rate and increase its slope with respect to sulphuric acid. However, at low sulphuric acid concentrations when the ammonia concentration is substantially higher than the acid monomer concentration, the relative effect of losses increases with increasing ammonia concentration and the slope of the formation rate with respect to ammonia is lower than in a loss-free

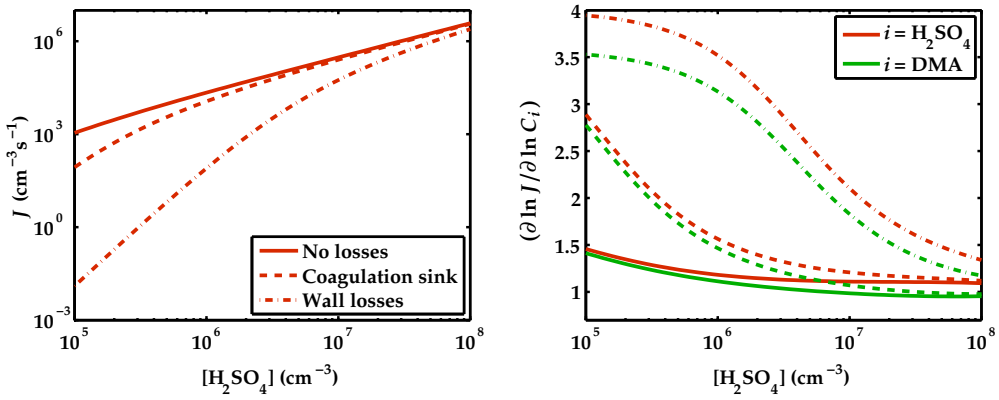

Fig. 6.3. Left panel: Neutral particle formation rate at [DMA] = 10 ppt with no external losses (solid line), with a coagulation loss coefficient $2.6 \cdot 10^{-3}$ s^{-1} corresponding to the Hyytiälä boreal forest station [55] (dashed line) and with a wall loss coefficient $2.3 \cdot 10^{-2}$ s^{-1} corresponding to the *IfT*-LFT flow tube [56] (dash-dotted line). Right panel: Logarithmic partial derivatives of the formation rate with respect to the sulphuric acid (red) and DMA (green) monomer concentrations.

case. At lower ammonia concentrations when $[H_2SO_4] \gg [NH_3]$ (lower panel of Fig. 6.4) losses reduce the slope of the formation rate with respect to both sulphuric acid and ammonia concentrations. External losses do not affect the cluster energetics, and in both of these examples also the main growth pathway remains unaltered. Therefore the identity of the critical cluster is not affected by losses while the slopes change considerably, implying that the nucleation theorem is no longer applicable when loss terms are allowed. In a multi-component system, the slope determined from formation rates measured above the critical size can be either increased or decreased by losses, and the nucleation theorem does not even give an upper or lower limit to the critical cluster size. In field observations, the coagulation sink varies between measurements, and no general conclusions about losses can be made. Clusters can also coagulate with freshly formed particles, complicating the situation further, and the effect of this process on the slope of the formation rate is discussed in Sec. 6.4.7.

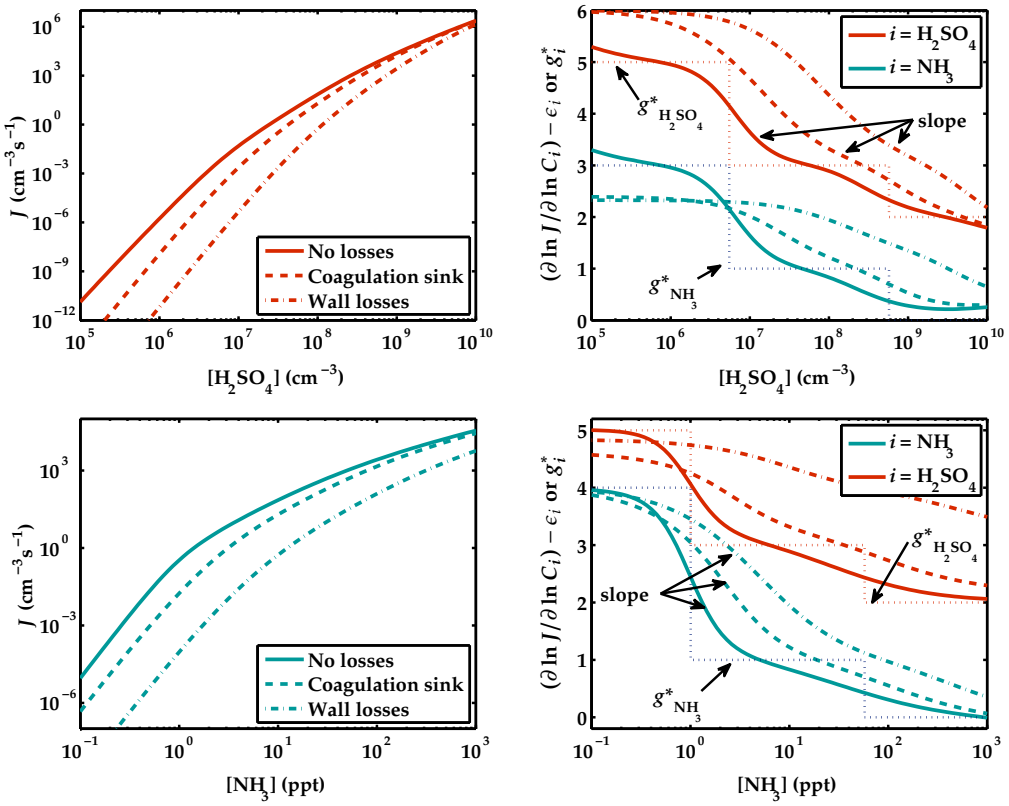

Fig. 6.4. Upper left panel: Neutral particle formation rate at [NH_3] = 10 ppt with no external losses (solid line), with a coagulation loss coefficient $2.6 \cdot 10^{-3}$ s^{-1} corresponding to the Hyytiälä boreal forest station [55] (dashed line) and with a wall loss coefficient $2.3 \cdot 10^{-2}$ s^{-1} corresponding to the *IfT*-LFT flow tube [56] (dash-dotted line). Upper right panel: Logarithmic partial derivatives of the formation rate with respect to the sulphuric acid (red solid, dashed and dash-dotted lines) and ammonia (light blue lines) monomer concentrations, where the ammonia derivative is corrected by subtracting $\epsilon_{NH_3} = 1$. Lower panels: same as the upper panels but with a constant sulphuric acid concentration of 10^7 cm^{-3} and a varying ammonia concentration.

6.4.4 Definition of the precursor concentration (assumptions E and H)

The sulphuric acid concentration is usually measured with a chemical ionization mass spectrometer (CIMS), which charges sulphuric acid molecules with nitrate ions and then detects them by mass spectrometry. However, the CIMS most probably also ionizes acid hydrates $H_2SO_4 \cdot (H_2O)_n$, acid–base clusters $H_2SO_4 \cdot \text{base})_m$ and hydrated acid–base clusters $H_2SO_4 \cdot (\text{base})_m \cdot (H_2O)_n$ [57–59], and after ionization the water and/or base molecules are lost. Consequently, the signal due to pure H_2SO_4 monomers is indistinguishable from the signal due to other clusters containing one sulphuric acid molecule, and the measured sulphuric acid concentration is not equal to the monomer concentration relevant to the nucleation theorem if cluster concentrations are non-negligible. Our quantum-chemical calculations indicate that $H_2SO_4 \cdot$ DMA clusters are very strongly bound and have significant concentrations even at ppt-level base concentrations, but some other theoretical studies have predicted significantly weaker binding [60, 61]. Experiments have not yet provided conclusive results regarding the abundance of $H_2SO_4 \cdot$ base dimers, but the recent results of Almeida et al. [46] show that presence of DMA increases substantially the concentration of clusters containing two H_2SO_4 molecules. On the other hand, it is well-known that H_2SO_4 molecules form hydrates at ambient relative humidities [58], and the CIMS is assumed also to detect $H_2SO_4 \cdot (H_2O)_n$ clusters as pure H_2SO_4 vapour. Therefore the conclusions of this section are also relevant for all sulphuric acid nucleation measurements in the presence of water.

The effect of the "definition" (whether only monomers or also acid molecules bound to other compounds are counted) of the sulphuric acid concentration is illustrated in Fig. 6.5 for the sulphuric acid–DMA system. In the left panel, the solid line presents the particle formation rate as a function of sulphuric acid monomer concentration, and the dashed line as a function of the CIMS-measurable sulphuric acid concentration $[H_2SO_4]$ + $[H_2SO_4 \cdot \text{DMA}]$. At low sulphuric acid concentrations, most of the sulphuric acid is bound to DMA, but as the overall concentration increases, the fraction bound to DMA decreases. Consequently, the dashed line is shifted strongly to the right at low concentrations and somewhat less at higher concentrations, and its slope is therefore higher than for the solid

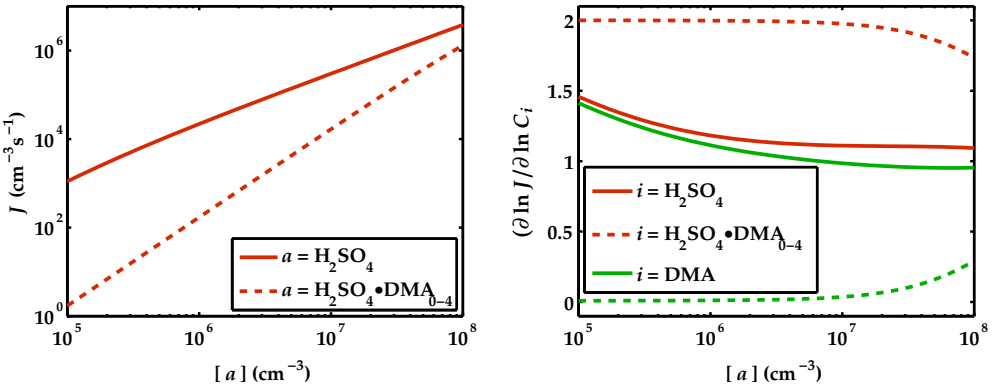

Fig. 6.5. Left panel: Neutral particle formation rate at [DMA] = 10 ppt. Right panel: Logarithmic partial derivatives of the formation rate with respect to the sulphuric acid (red) and DMA (green) monomer concentrations. The sulphuric acid concentration is either the monomer concentration (solid lines) or the measurable concentration $\sum_{d=0}^{4}[H_2SO_4 \cdot (DMA)_d]$ (dashed lines).

line. After the formation of the $H_2SO_4 \cdot DMA$ cluster, the next few steps proceed by collisions with other $H_2SO_4 \cdot DMA$ clusters, and the process is in practice kinetically limited barrierless one-component condensation of $H_2SO_4 \cdot DMA$ with a particle formation rate corresponding to the collision rate of two such units. Since the CIMS-measurable sulphuric acid concentration $[H_2SO_4] + [H_2SO_4 \cdot DMA]$ is dominated by the cluster concentration $[H_2SO_4 \cdot DMA]$ except at very high H_2SO_4 concentrations, the slope of the particle formation rate with respect to this concentration is 2 and there is no DMA dependence. This is in agreement with the nucleation theorem if the critical cluster in barrierless coagulation is defined to be the monomer (as is usually done), but the correct interpretation is only possible if it is known that all measured H_2SO_4 molecules are bound to DMA. In practice, the distribution of H_2SO_4 monomers and different clusters containing one H_2SO_4 molecule is not known, and thus the application and interpretation of the nucleation theorem, is not possible.

6.4.5 Presence of ions (assumptions B, D and G)

Electrically charged molecules and clusters are produced in the atmosphere by ionization due to galactic cosmic rays and radon decay. Ionic clusters are able to enhance particle formation as they are strongly bound by electrostatic forces. In the presence of other enhancing species, such as bases, the contribution of ions to the particle formation rate depends on the relative enhancement due to these other species. In the sulphuric acid–DMA system at [DMA] = 10 ppt (not shown) the effect of ions on the particle formation rate (and thus its slope) in the studied [H_2SO_4] range is negligible, as DMA has a significant enhancing effect on the binding and growth of neutral sulphuric acid clusters, resulting in the role of ions being minor overall [46].

In the sulphuric acid–ammonia system, on the other hand, ions have a strong enhancing effect on particle formation at low sulphuric acid concentrations [50]. The effect of an ion production rate of 3 ion pairs cm^{-3} s^{-1}, approximately the ionization rate in the atmospheric boundary layer [50], is shown in Fig. 6.6. The corresponding HSO_4^- and NH_4^+ ion concentrations are presented in Fig. 6.13 of the Appendix. In this case, particle formation proceeds along numerous different pathways, but at low sulphuric acid concentrations the most important routes start by the formation of small positive and/or negative clusters, which then recombine to form larger neutral clusters and continue to grow by addition of H_2SO_4 and NH_3 monomers. An increase in the concentration of sulphuric acid or ammonia molecules leads to an increase in cluster formation, and therefore the logarithmic derivatives of J with respect to both monomer concentrations are positive.

The contribution of ions to particle formation can, however, never exceed the ion formation rate, and when this limit is approached, an increase in monomer concentrations no longer increases the ion mediated particle formation rate. This is seen as a flattening of the J curve and a dip in the derivatives in Fig. 6.6. When the sulphuric acid concentration is further increased, neutral cluster formation starts to dominate over the ion induced pathways, and the derivatives of J increase again to join those of the purely neutral case.

All clusters along the growth pathways within the negative and positive

charging states have a negative formation free energy with respect to the HSO_4^- and NH_4^+ ions, respectively, but both formation pathways have local energy barriers at larger sizes. It is, however, impossible to extract the absence of barrier in charged cluster formation or the size and composition of the neutral critical cluster from the slope of the formation rate. This results from the violation of three of assumptions of the nucleation theorem: the ion monomer concentrations are not constant (G), particle formation proceeds along several pathways (D) and cluster–cluster collisions are non-negligible (B). As a comparison, Fig. 6.6 presents also the particle formation rate in a case where only negative clusters are present and the bisulfate ion concentration is set to a constant value corresponding to the maximum bisulfate ion concentration in the case with a constant ion pair production rate. In this case, particle formation starts by the collision of a HSO_4^- ion and a H_2SO_4 molecule and proceeds along a single pathway by additions of H_2SO_4 and NH_3 monomers. Accordingly, the logarithmic derivatives of J with respect to monomer concentrations are equal to one for sulphuric acid and the bisulfate ion and zero for ammonia, as the first collision is the rate limiting step and its product $H_2SO_4 \cdot HSO_4^-$ has a negligible evaporation rate.

6.4.6 Experiments where concentrations are not constant (assumption F)

The nucleation rate appearing in the nucleation theorem is a steady-state nucleation rate. Steady-state nucleation may indeed be achieved in a chamber experiment, although the nucleation rate is typically evaluated before the steady state is reached. Atmospheric nucleation might also, at least in some cases, be close to a steady state. For flow tube experiments, however, a perfectly steady state cannot be achieved. Precursor gasses can be introduced into the flow tube in two ways: either they are mixed into the carrier gas or they can be produced in situ inside the tube. The former method is used for water vapour, bases and organic compounds as well as impurities of the carrier air, while sulphuric acid is often produced in the tube from SO_2. In any case, the vapour concentrations are not constant along the length of the tube, and thus a parcel of gas traveling through the tube does not experience time-independent vapour concentrations implying that the

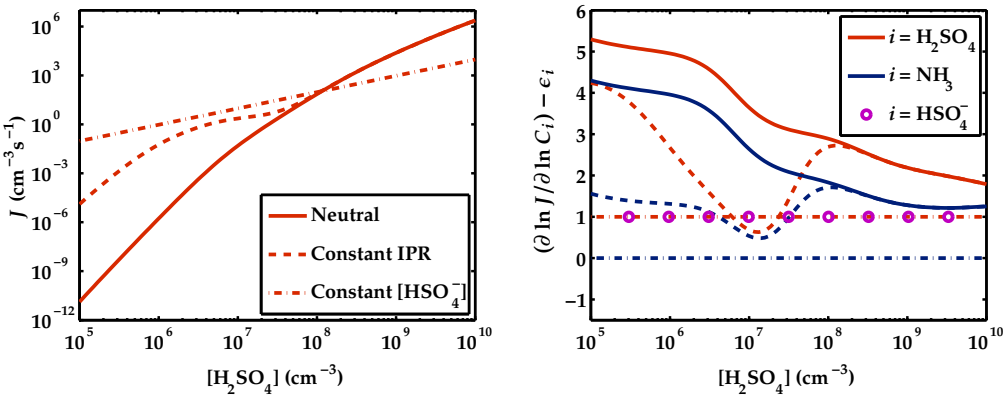

Fig. 6.6. Left panel: Total particle formation rate at $[NH_3]$ = 10 ppt in systems containing only neutral clusters (solid line), neutral as well as positively and negatively charged clusters with an ion pair production rate IPR = 3 $cm^{-3}s^{-1}$ (dashed line) and only neutral molecules and negatively charged clusters with a constant HSO_4^- ion concentration of 427 cm^{-3} (dash-dotted line). Right panel: Logarithmic partial derivatives of the formation rate with respect to the sulphuric acid (red), ammonia (blue) and, for the system with only negative clusters, bisulfate ion (purple circles) concentrations.

cluster formation is not in a steady-state.

An example of a flow tube experiment is presented in Fig. 6.7. The zero-dimensional simulation assumes that gasses are locally well-mixed and concentrations depend only on the position along the length of the flow tube, or equivalently the time that it takes for the flow to reach that point. In reality, the concentrations also have radial gradients, but the zero-dimensional approach can be seen as an approximation for the situation at the axis of the flow tube [62].[4] At the beginning of the tube, sulphuric acid, ammonia and DMA concentrations are set to 10^6 cm^{-3}, 10 pptv and 1 pptv, respectively. sulphuric acid is produced at a constant rate and its concentration increases as a function of time, but the increase gradually levels off because of wall losses. The ammonia concentration decreases along the length of the tube due to wall losses, and the DMA monomer concentration decrease even more rapidly through the formation of sulphuric acid–DMA clusters. The particle formation rate increases at first as

[4]However, even here one should actually include also a loss term, as described in Sec. 6.4.3, due to diffusion loss of clusters in radial direction.

small clusters form and gradually grow to larger sizes, but starts then to decrease as DMA is depleted. Near the end of the flow tube the concentration of formed particles starts also to decrease as losses dominate over the formation rate. As a result, the measured apparent particle formation rate J_{app}, defined as the particle concentration at the end of the tube divided by the residence time, depends strongly on the time evolution of the system. Since the nucleation theorem requires the system to be in steady state, it should not be used for determining the critical cluster composition in a case such as this. The critical cluster can not even be defined for a whole experiment, because its identity changes along the tube with the precursor concentrations. The left panel of Fig. 6.8 shows the apparent particle formation rate as a function of sulphuric acid concentration at the end of the tube. The right panel shows the slope of J_{app} with respect to the end sulphuric acid concentration and the initial base concentrations. At low acid concentrations, the particle formation rate is mostly limited by the DMA being lost on walls, and therefore the formation rate has a high slope with respect to the DMA concentration. At higher acid concentrations, more particles have time to form before the DMA is lost to the walls, and the slope with respect to sulphuric acid increases. Finally, at very high sulphuric acid concentrations, practically all DMA is used up in particle formation and the slopes with respect to both sulphuric acid and DMA decrease. On the other hand, the role of ammonia becomes more important at high sulphuric acid concentrations as there is a lot of excess sulphuric acid compared to DMA.

6.4.7 Practical problems related to analyzing field observations of particle formation events (assumptions E, G and H)

The nucleation rate is not a directly observable quantity, but needs in practice to be calculated from cluster or particle concentration and size distribution measurements. Since clusters are lost by coagulation and deposition during their growth from the critical cluster to detectable particles, formation rate determinations at different cut-off sizes give different results. In order to minimize the effect of losses, the particle formation rate determined at the instrument cut-off size (for instance 3 nm) is often converted to

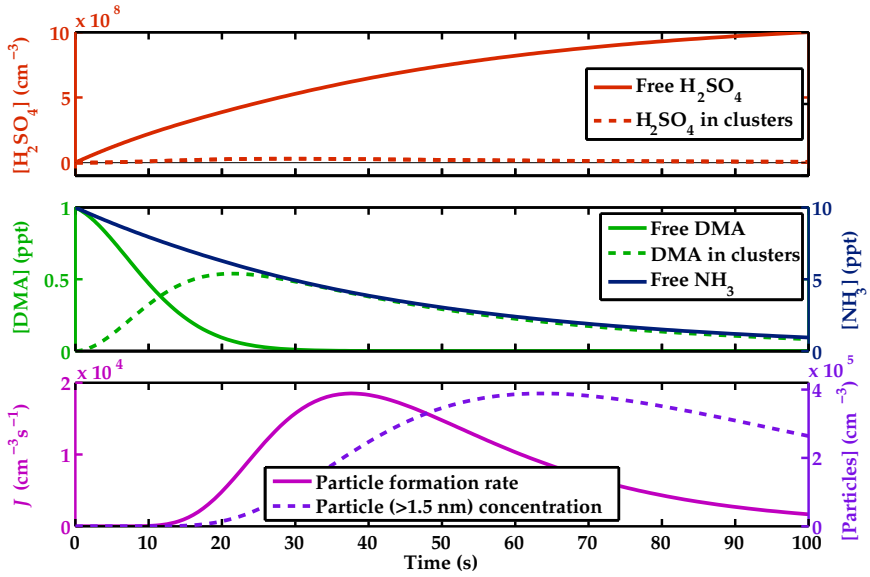

Fig. 6.7. Modelled precursor gas, cluster and particle concentrations in a flow tube experiment where sulphuric acid is produced in situ and the wall loss coefficient is $2.3 \cdot 10^{-2}$ s^{-1}.

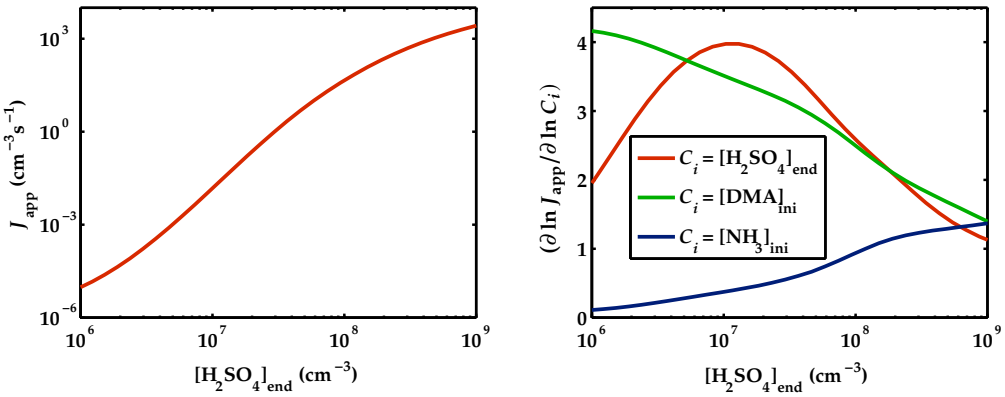

Fig. 6.8. Left panel: Apparent particle formation rate in a flow tube, defined as the particle concentration at the end of the tube divided by the residence time, as a function of end sulphuric acid concentration keeping the initial ammonia and DMA concentrations constant. Right panel: logarithmic partial derivatives of the particle formation rate with respect to the final sulphuric acid concentration and the initial ammonia and DMA concentrations.

the nucleation rate at the assumed critical cluster size (1 or 1.5 nm) using the formulation of Kerminen and Kulmala [14].

One critical step when applying this procedure to atmospheric data is determining the cluster growth rate since the coagulation loss rate depends strongly on cluster size. The growth rate also determines how long the clusters spend in any particular size range, affecting the overall effect of losses. The growth rate has typically been determined from the time shift between the appearance of sulphuric acid and of small particles, which has been interpreted as the time required for freshly nucleated clusters to grow to a detectable size. Using the same aerosol microphysics model as in this study (UHMA), Korhonen et al. [43] have studied the effect of inaccuracies in determining the cluster growth rate on the estimation of the nucleation rate at the critical size.[5]

In the case of a strong nucleation burst, coagulation losses increase significantly during the event due to the large number of nucleation mode particles, reducing the concentration of the smallest particles. This alters the time profile of the particle concentration compared to cases where losses are dominated by the fairly constant background particle population, and skews the growth time determination resulting systematically in too high values for the growth rate. This, in turn, leads to an underestimation of the nucleation rate, which is most prominent at high nucleation rates, corresponding in general to high sulphuric acid concentrations. Finally, the sulphuric acid dependent bias in the calculated nucleation rate leads to an incorrect estimate of the exponent in the nucleation rate power law and thus an erroneous interpretation of the nucleation mechanism.

We simulated eight events with the UHMA aerosol microphysics model assuming a particle formation rate of the form $J_{1.5,\,\mathrm{input}} = k_2[\mathrm{H_2SO_4}]^2$. The background particle concentration and the cluster growth rate were varied between the simulations, which corresponds to what happens also in measurement campaigns where events on different days exhibit different conditions. As in [5], the particle formation rate J_3 at 3 nm was obtained directly from the time evolution of the particle size distribution and the average growth rate below 3 nm was solved from the time shift between $[\mathrm{H_2SO_4}]$ and N_{3-6}. The formation rate $J_{1.5}$ at 1.5 nm was then estimated using the Kerminen–Kulmala [14] formulation. A detailed description of

[5] Actually, at the estimated, or assumed, critical size.

the methodology was presented by Korhonen et al. [43].

Figure 6.9 presents the synthetic measurement campaign of eight events generated with UHMA. Each data point represents a single 'measurement' of [H_2SO_4] and the corresponding estimate of $J_{1.5}$. The spread in the $J_{1.5}$ values is due to several factors: each of the eight events represent different conditions with different growth rates and coagulation sinks, the prefactor k_2 varies with time during each event, and finally the analysis method is sensitive to the conditions of the event and does not always reproduce the input formation rate even in more idealized conditions.

Fitting a least-squares line to the estimated nucleation rates gives a slope of 0.92, which is clearly lower than the input exponent 2. Another set of nucleation events with slightly different growth rates or coagulation sinks would have lead to a different exponent. Many previous studies of atmospheric new particle formation have applied the first nucleation theorem to extensive field data by combining nucleation rate data inferred from a large number of events, some [e.g. 63] even acknowledging that the conditions for the validity of the nucleation theorem are not met. Our example shows, however, that applying slope analysis to a collection of several independent data sets corresponding to randomly varying atmospheric conditions may lead to a wrong conclusion about the dependence of $J_{1.5}$ on [H_2SO_4]. One approach for avoiding the difficulties related to varying conditions was proposed by Laaksonen et al. [64], who applied multivariate regression analysis to nucleation rates measured in the atmosphere. However, this method requires prior knowledge about all compounds involved in particle formation, and their concentrations must be measured with a sufficient time resolution during the events.

6.5 Summary and conclusions

Numerous studies have used the first nucleation theorem to assess atmospheric new particle formation mechanisms. According to the theorem, derived for ideal conditions, the slope of the nucleation rate as a function of the concentration of a nucleating compound is approximately equal to the number of molecules of the compound in the critical cluster. In this work, the sensitivity of the slope to various non-idealities was examined.

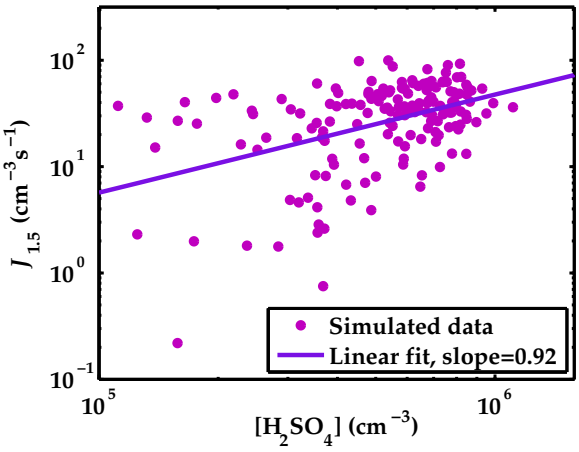

Fig. 6.9. Particle formation rates at 1.5 nm determined every ten minutes for eight model runs of new particle formation events as a function of sulphuric acid concentration. The linear least-squares fit to the data points has a slope of 0.92, while the input nucleation rate is of the form $J_{1.5} = k_2[H_2SO_4]^2$ corresponding to a slope of 2. Only data points for which the simulated sulphuric acid concentration was higher than 10^5 cm^{-3} are included (approximately the detection limit for atmospheric sulphuric acid measurements). If data points below this limit were included, the slope of the fitted line would be 0.33.

We used a cluster kinetics model to simulate the formation rate of stable small clusters consisting of sulphuric acid and base molecules. The simulations were performed both in ideal conditions and in realistic conditions where the assumptions related to the nucleation theorem are not valid. Even in otherwise ideal conditions, the ΔG surfaces taken from quantum chemical calculations did not comply to the assumptions made in the derivation of the nucleation theorem. However, in the sulphuric acid–ammonia system where the formation free energy curve has several local maxima along the formation pathway, the nucleation theorem was shown to be very closely valid. On the other hand, any other nonidealities such as external losses of clusters or not reaching a steady-state, were seen to destroy the applicability of the theorem. For instance, in the presence of wall losses, slope analysis can indicate the presence of a large critical cluster even when cluster formation is in fact barrierless.

Furthermore, the so-called nucleation rate is in practice calculated from the measured concentrations at larger, experimentally detectable sizes. To assess uncertainties related to the calculation, an aerosol microphysics model was used to simulate the growth of freshly formed particles to detectable sizes. The slope of the calculated nucleation rate as a function of sulphuric acid concentration was found to differ from that of the actual formation rate used as input in the simulation.

The derivation of the nucleation theorem requires that there are no external losses, which is never perfectly true in reality. However, with high enough precursor concentrations and a suitable setup, the effect of losses on the particle formation rate may become negligible. On the other hand, a high precursor concentration may lead to a non-negligible contribution of cluster-cluster collisions, which also breaks the applicability of the nucleation theorem. Even the less restrictive assumptions that the nucleation is in steady state and that all conditions except for one concentration are kept constant between different measurement points are often not fulfilled. Thus the first nucleation theorem cannot be used to determine the critical cluster size in most realistic situations.

6.A Appendix

6.A.1 Validity of the multicomponent nucleation theorem Eq. (6.9)

Figure 6.10 presents the derivatives from Fig. 6.1 together with the terms $\bar{g}_i$ and $\bar{\epsilon}_i$ of Eq. (6.9). The derivatives with respect to both sulphuric acid and ammonia are very closely equal to $\bar{g}_i + \bar{\epsilon}_i$, in agreement with the multicomponent nucleation theorem. The small discrepancy can be explained by a fraction of the particle formation proceeding along an alternative pathway [see 37, for more details]. However, while Eq. (6.9) is approximately valid, it does not give a direct link between the slope of the particle formation rate and the critical cluster size. This can be understood by examining the distribution (shown in Fig. 6.11) over which the weighted average of cluster compositions is calculated to give $\bar{g}_i$. It is traditionally assumed that the term $1/n_k \propto \exp\left(\frac{\Delta G_k}{k_B T}\right)$ has such a high peak at the location of the energy barrier that this one term dominates the whole sum and $\bar{g}_i \approx g_i^*$, but the example of Fig. 6.11 shows that several terms, some of which do not even correspond to local maxima of the formation energy curve, may have a non-negligible contribution to the sum. In Fig. 6.11, the sum in the denominator of Eq. (6.9) is only computed over the monomer and the nine smallest clusters on the formation pathway, but adding more terms would affect merely the normalization, not the shape, of the distribution.

6.A.2 Cluster concentrations in the sulphuric acid–DMA system

The cluster concentrations corresponding to Fig. 6.2 are presented in Fig. 6.12. Cluster concentrations are overall higher in the hypothetical case where cluster–cluster collisions are forbidden, compared to the case where all collisions are allowed.

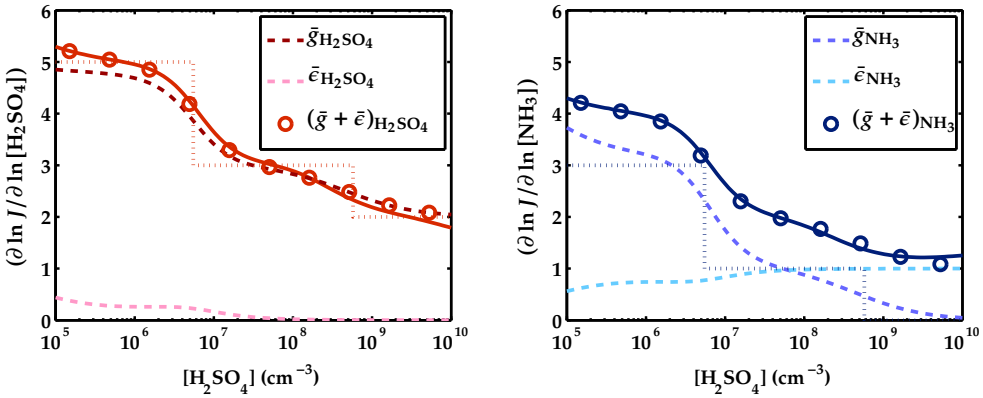

Fig. 6.10. Logarithmic partial derivatives of the particle formation rate with respect to sulphuric acid and ammonia concentrations (bright red and dark blue solid lines, respectively) at $[NH_3] = 10$ ppt compared to the prediction of the nucleation theorem (circles). The dotted lines correspond to the number of H_2SO_4 and NH_3 molecules in the critical cluster, and the dashed lines refer to the terms on the right-hand side of Eq. (6.9).

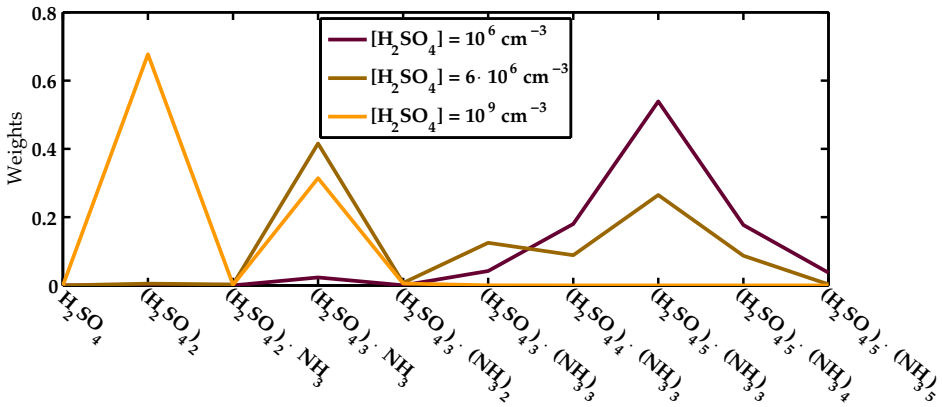

Fig. 6.11. The distribution $\frac{1}{\beta_{m_k,k} C_{m_k} n_k} / \left(\sum_{l=1}^{10} \frac{1}{\beta_{m_l,l} C_{m_l} n_l} \right)$ appearing in Eq. (6.9) computed at different H_2SO_4 monomer concentrations and $[NH_3] = 10$ ppt for the neutral sulphuric acid–ammonia system.

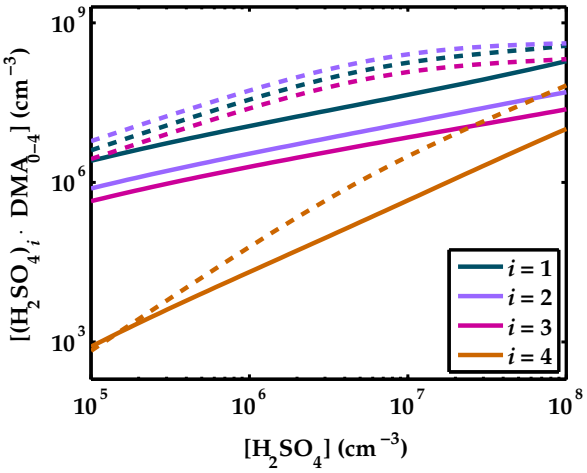

Fig. 6.12. Concentrations of neutral clusters containing 1, 2, 3 and 4 sulphuric acid molecules and any number of DMA molecules at [DMA] = 10 ppt. The solid lines correspond to the case where all collisions are allowed, and the dashed lines correspond to a hypothetical situation where cluster–cluster collisions and fragmentations are forbidden.

6.A.3 Ion concentrations when the ion production rate is fixed

Figure 6.13 presents the HSO_4^- and NH_4^+ concentrations corresponding to the constant ion production rate of Fig. 6.6. At low sulphuric acid concentrations the bisulfate ion concentration increases with increasing sulphuric acid concentration as there are more H_2SO_4 molecules available to get ionized by the charger ions. The NH_4^+ ion concentration, on the other hand, has practically no dependence on the sulphuric acid concentration at low acid concentrations, as the ammonium ions are formed when an ammonia molecule is charged positively, and lost mainly by colliding with a second ammonia molecule and forming an $NH_3 \cdot NH_4^+$ cluster. At higher sulphuric acid concentrations, collisions with H_2SO_4 molecules become an important loss mechanism for both HSO_4^- and NH_4^+ ions, and their concentrations therefore decrease with increasing sulphuric acid concentration.

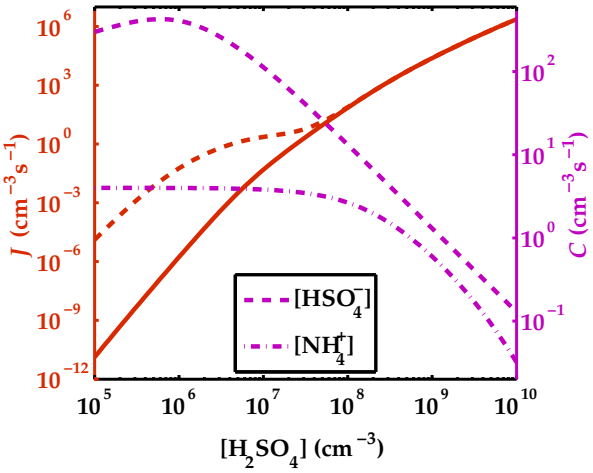

Fig. 6.13. Particle formation rate at [NH_3] = 10 ppt with no ions (solid red line) and with an ion production rate IPR = 3 ion pairs cm^{-3} s^{-1} (red dashed line), and the bisulfate and ammonium ion concentrations (purple) corresponding to the same ion production rate.

References

[1] M. Kulmala, H. Vehkamäki, T. Petäjä, M. Dal Maso, A. Lauri, V.-M. Kerminen, W. Birmili and P. H. McMurry. Formation and growth rates of ultrafine atmospheric particles: a review of observations. *Journal of Aerosol Science* 35 (2004), 143–176.

[2] L. H. Young, D. R. Benson, F. R. Kameel, J. R. Pierce, H. Junninen, M. Kulmala and S.-H. Lee. Laboratory studies of H_2SO_4/H_2O binary homogeneous nucleation from the SO_2 + OH reaction: evaluation of the experimental setup and preliminary results. *Atmospheric Chemistry and Physics* 8 (2008), 4997–5016.

[3] R. Zhang, A. Khalizov, L. Wang, M. Hu and W. Xu. Nucleation and growth of nanoparticles in the atmosphere. *Chemical Reviews* 112 (2012), 1957–2011.

[4] R. J. Weber, J. J. Marti, P. H. McMurry, F. L. Eisele, D. J. Tanner and A. Jefferson. Measured atmospheric new particle formation rates: Implications for nucleation mechanisms. *Chemical Engineering Communications* 151 (1996), 53–64.

[5] S.-L. Sihto, M. Kulmala, V.-M. Kerminen, M. Dal Maso, T. Petäjä, I. Riipinen, H. Korhonen, F. Arnold, R. Janson, M. Boy, A. Laaksonen and K. E. J. Lehtinen. Atmospheric sulphuric acid and aerosol formation: Implications from atmospheric measurements for nucleation and early growth mechanisms. *Atmospheric Chemistry and Physics* 6 (2006), 4079–4091.

[6] R. Zhang. Getting to the critical nucleus of aerosol formation. *Science* 328 (2010), 1366–1367.

[7] J. H. Zollner, W. A. Glasoe, B. Panta, K. K. Carlson, P. H. McMurry and D. R. Hanson. Sulfuric acid nucleation: Power dependencies, variation with relative humidity, and effect of bases. *Atmospheric Chemistry and Physics* 12 (2012), 4399–4411.

[8] I. Riipinen, S.-L. Sihto, M. Kulmala, F. Arnold, M. Dal Maso, W. Birmili, K. Saarnio, K. Teinilä, V.-M. Kerminen, A. Laaksonen and K. E. J. Lehtinen. Connections between atmospheric sulphuric acid and new particle formation during QUEST III-IV campaigns in Heidelberg and Hyytiälä. *Atmospheric Chemistry and Physics* 7 (2007), 1899–1914.

[9] C. Kuang, P. H. McMurry, A. V. McCormick and F. L. Eisele. Dependence of nucleation rates on sulfuric acid vapor concentration in diverse atmospheric locations. *Journal of Geophysical Research: Atmospheres* 113 (2008), D10209.

[10] S. M. Ball, D. R. Hanson, F. L. Eisele and P. H. McMurry. Laboratory studies of particle nucleation: Initial results for H_2SO_4, H_2O, and NH_3 vapors. *Journal of Geophysical Research* 104(D19) (1999), 32709–23718.

[11] D. R. Benson, L.-H. Young, F. R. Kameel and S.-H. Lee. Laboratory-measured nucleation rates of sulfuric acid and water binary homogeneous nucleation from the $SO_2 + OH$ reaction. *Geophysical Research Letters* 35 (2008), L11801.

[12] M. Sipilä, T. Berndt, T. Petäjä, D. Brus, J. Vanhanen, F. Stratmann, J. Patokoski, R. L. Mauldin, III, A.-P. Hyvärinen, H. Lihavainen and M. Kulmala. The role of sulfuric acid in atmospheric nucleation. *Science* 327 (2010), 1243–1246.

[13] D. Brus, A.-P. Hyvärinen, Y. Viisanen, M. Kulmala and H. Lihavainen. Homogeneous nucleation of sulfuric acid and water mixture: experimental setup and first results. *Atmospheric Chemistry and Physics* 10 (2010), 2631–2641.

[14] V.-M. Kerminen and M. Kulmala. Analytical formulae connecting the "real" and the "apparent" nucleation rate and the nuclei number concentration for atmospheric nucleation events. *Journal of Aerosol Science* 33 (2002), 609–622.

[15] K. E. J. Lehtinen, M. Dal Maso, M. Kulmala and V.-M. Kerminen. Estimating nucleation rates from apparent particle formation rates and vice versa: Revised formulation of the Kerminen–Kulmala equation. *Journal of Aerosol Science* 38 (2007), 988–994.

[16] H. Korhonen, V.-M. Kerminen, H. Kokkola and K. E. J. Lehtinen. Estimating atmospheric nucleation rates from size distribution measurements: Analytical equations for the case of size dependent growth rates. *Journal of Aerosol Science* 69 (2014), 13–20.

[17] Y. Viisanen and R. Strey. Homogeneous nucleation rates for *n*-butanol. *Journal of Chemical Physics* 101 (1994), 7835–7843.

[18] D. Brus, A.-P. Hyvärinen, V. Ždímal and H. Lihavainen. Homogeneous nucleation rate measurements of 1-butanol in helium: A comparative study of a thermal diffusion cloud chamber and a laminar flow diffusion chamber. *Journal of Chemical Physics* 122 (2005), 214506.

[19] R. Strey and Y. Viisanen. Measurement of the molecular content of binary nuclei. Use of the nucleation rate surface for ethanol–hexanol. *Journal of Chemical Physics* 99 (1993), 4693–4704.

[20] H. Vehkamäki and I. J. Ford. Excess energies of *n*-and *i*-octane molecular clusters. *Journal of Chemical Physics* 114 (2001), 5509–5513.

[21] D. Brus, V. Ždímal and F. Stratmann. Homogeneous nucleation rate measurements of 1-propanol in helium: The effect of carrier gas pressure. *Journal of Chemical Physics* 124 (2006), 164306.

[22] J. Hrubý, Y. Viisanen and R. Strey. Homogeneous nucleation rates for *n*-pentanol in argon: Determination of the critical cluster size. *Journal of Chemical Physics* 104 (1996), 5181–5187.

[23] A. A. Manka, D. Brus, A. P. Hyvärinen, H. Lihavainen, J. Wölk and R. Strey. Homogeneous water nucleation in a laminar flow diffusion chamber. *Journal of Chemical Physics* 132 (2010), 244505.

[24] M. A. L. J. Fransen, E. Sachteleben, J. Hrubý and D. M. J. Smeulders. Homogeneous nucleation of water in synthetic air. *AIP Conference Proceedings* 1527 (2013), 124–127.

[25] Y. J. Kim, B. E. Wyslouzil, G. Wilemski, J. Wölk and R. Strey. Isothermal nucleation rates in supersonic nozzles and the properties of small water clusters. *Journal of Physical Chemistry A* 108 (2004), 4365–4377.

[26] J. Malila, R. McGraw, A. Laaksonen and K. E. J. Lehtinen. Repairing the first nucleation theorem: Precritical cluster losses. *AIP Conference Proceedings* 1527 (2013), 31–34.

[27] O. Kupiainen, T. Olenius and H. Vehkamäki. Experimental setup affects the particle formation rate and its slope d(log J)/d(log C). AIP Conference Proceedings 1527 (2013), 246–249.

[28] S. Ehrhart and J. Curtius. Influence of aerosol lifetime on the interpretation of nucleation experiments with respect to the first nucleation theorem. *Atmospheric Chemistry and Physics* 13 (2013), 11465–11471.

[29] A. E. Nielsen. *Kinetics of Precipitation*. Oxford: Pergamon, 1964.

[30] D. Kashchiev. On the relation between nucleation work, nucleus size, and nucleation rate. *Journal of Chemical Physics* 76 (1982), 5098–5102.

[31] R. McGraw and D. T. Wu. Kinetic extensions of the nucleation theorem. *Journal of Chemical Physics* 118 (2003), 9337–9347.

[32] I. J. Ford. Nucleation theorems, the statistical mechanics of molecular clusters, and a revision of classical nucleation theory. *Physical Review E* 56 (1997), 5615–5629.

[33] R. McGraw and R. Zhang. Multivariate analysis of homogeneous nucleation rate measurements. Nucleation in the p-toluic acid/sulfuric acid/water system. *Journal of Chemical Physics* 128 (2008), 064508.

[34] B. E. Wyslouzil and G. Wilemski. Binary nucleation kinetics. II. Numerical solution of the birth-death equations. *Journal of Chemical Physics* 103 (1995), 1137–1151.

[35] B. E. Wyslouzil and G. Wilemski. Binary nucleation kinetics. III. Transient behavior and time lags. *Journal of Chemical Physics* 105 (1996), 1090–1100.

[36] J.-S. Li, I. L. Maksimov and G. Wilemski. Genuine saddle point and nucleation potential for binary systems. *Physical Review E* 61 (2000), R4710–R4713.

[37] T. Olenius, O. Kupiainen-Määttä, I. K. Ortega, T. Kurtén and H. Vehkamäki. Free energy barrier in the growth of sulfuric acid–ammonia and sulfuric acid–dimethylamine clusters. *Journal of Chemical Physics* 139 (2013), 084312.

[38] T. Olenius, S. Schobesberger, O. Kupiainen-Määttä, A. Franchin, H. Junninen, I. K. Ortega, T. Kurtén, V. Loukonen, D. R. Worsnop, M. Kulmala and H. Vehkamäki. Comparing simulated and experimental molecular cluster distributions. *Faraday Discussions* 165 (2013), 75–89.

[39] T. Kurtén, C. Kuang, P. Gómez, P. H. McMurry, H. Vehkamäki, I. K. Ortega, M. Noppel and M. Kulmala. The role of cluster energy nonaccommodation in atmospheric sulfuric acid nucleation. *Journal of Chemical Physics* 132 (2010), 024304.

[40] J. C. Barrett. A stochastic simulation of nonisothermal nucleation. *Journal of Chemical Physics* 128 (2008), 164519.

[41] V. Loukonen, I.-F. W. Kuo, M. J. McGrath and H. Vehkamäki. On the stability and dynamics of (sulfuric acid) (ammonia) and (sulfuric acid) (dimethylamine) clusters: A first-principles molecular dynamics investigation. *Chemical Physics* 428 (2014), 164–174.

[42] V. Loukonen, N. Bork and H. Vehkamäki. From collisions to clusters: First steps of sulfuric acid nanocluster formation dynamics. *Molecular Physics* 112 (2014), 1979–1986.

[43] H. Korhonen, S.-L. Sihto, V.-M. Kerminen and K. E. J. Lehtinen. Evaluation of the accuracy of analysis tools for atmospheric new particle formation. *Atmospheric Chemistry and Physics* 11 (2011), 3051–3066.

[44] M. J. McGrath, T. Olenius, I. K. Ortega, V. Loukonen, P. Paasonen, T. Kurtén, M. Kulmala and H. Vehkamäki. Atmospheric Cluster Dynamics Code: A flexible method for solution of the birth–death equations. *Atmospheric Chemistry and Physics* 12 (2012), 2345–2355.

[45] L. Shampine and M. Reichelt. The MATLAB ODE suite. *SIAM Journal of Scientific Computing* 18 (1997), 1–22.

[46] J. Almeida, S. Schobesberger, A. Kürten, I. K. Ortega, O. Kupiainen-Määttä, A. P. Praplan, A. Adamov, A. Amorim, F. Bianchi, M. Breitenlechner, A. David, J. Dommen, N. M. Donahue, A. Downard, E. Dunne, J. Duplissy, S. Ehrhart, R. C. Flagan, A. Franchin, R. Guida, J. Hakala, A. Hansel, M. Heinritzi, H. Henschel, T. Jokinen, H. Junninen, M. Kajos, J. Kangasluoma, H. Keskinen, A. Kupc, T. Kurtén, A. N. Kvashin, A. Laaksonen, K. Lehtipalo, M. Leiminger, J. Leppä, V. Loukonen, V. Makhmutov, S. Mathot, M. J. McGrath, T. Nieminen, T. Olenius, A. Onnela, T. Petäjä, F. Riccobono, I. Riipinen, M. Rissanen, L. Rondo, T. Ruuskanen, F. D. Santos, N. Sarnela, S. Schallhart, R. Schnitzhofer, J. H. Seinfeld, M. Simon, M. Sipilä, Y. Stozhkov, F. Stratmann, A. Tomé, J. Tröstl, G. Tsagkogeorgas, P. Vaattovaara, Y. Viisanen, A. Virtanen, A. Vrtala, P. E. Wagner, E. Weingartner, H. Wex, C. Williamson, D. Wimmer, P. Ye, T. Yli-Juuti, K. S. Carslaw, M. Kulmala, J. Curtius, U. Baltensperger, D. R. Worsnop, H. Vehkamäki and J. Kirkby. Molecular understanding of sulphuric acid-amine particle nucleation in the atmosphere. *Nature (London)* 502 (2013), 359–363.

[47] T. Su and W. J. Chesnavich. Parametrization of the ion-polar molecule collision rate constant by trajectory calculations. *Journal of Chemical Physics* 76 (1982), 5183–5185.

[48] I. K. Ortega, O. Kupiainen, T. Kurtén, T. Olenius, O. Wilkman, M. J. McGrath, V. Loukonen and H. Vehkamäki. From quantum chemical formation free energies to evaporation rates. *Atmospheric Chemistry and Physics* 12 (2012), 225–235.

[49] X. Ge, A. S. Wexler and S. L. Clegg. Atmospheric amines – Part I. A review. *Atmospheric Environment* 45 (2011), 524–546.

[50] J. Kirkby, J. Curtius, J. Almeida, E. Dunne, J. Duplissy, S. Ehrhart, A. Franchin, S. Gagné, L. Ickes, A. Kürten, A. Kupc, A. Metzger, F. Riccobono, L. Rondo, S. Schobesberger, G. Tsagkogeorgas, D. Wimmer,

A. Amorim, F. Bianchi, M. Breitenlechner, A. David, J. Dommen, A. Downard, M. Ehn, R. C. Flagan, S. Haider, A. Hansel, D. Hauser, W. Jud, H. Junninen, F. Kreissl, A. Kvashin, A. Laaksonen, K. Lehtipalo, J. Lima, E. R. Lovejoy, V. Makhmutov, S. Mathot, J. Mikkilä, P. Minginette, S. Mogo, T. Nieminen, A. Onnela, P. Pereira, T. Petäjä, R. Schnitzhofer, J. H. Seinfeld, M. Sipilä, Y. Stozhkov, F. Stratmann, A. Tomé, J. Vanhanen, Y. Viisanen, A. Vrtala, P. E. Wagner, H. Walther, E. Weingartner, H. Wex, P. M. Winkler, K. S. Carslaw, D. R. Worsnop, U. Baltensperger and M. Kulmala. Role of sulphuric acid, ammonia and galactic cosmic rays in atmospheric aerosol nucleation. *Nature (London)* 476 (2011), 429–433.

[51] H. Korhonen, K. E. J. Lehtinen and M. Kulmala. Multicomponent aerosol dynamics model UHMA: Model development and validation. *Atmospheric Chemistry and Physics* 4 (2004), 757–771.

[52] C. Kuang, M. Chen, J. Zhao, J. Smith, P. H. McMurry and J. Wang. Size and time-resolved growth rate measurements of 1 to 5 nm freshly formed atmospheric nuclei. *Atmospheric Chemistry and Physics* 12 (2012), 3575–3589.

[53] H. Vehkamäki, M. J. McGrath, T. Kurtén, J. Julin, K. E. J. Lehtinen and M. Kulmala. Rethinking the application of the first nucleation theorem to particle formation. *Journal of Chemical Physics* 136 (2012), 094107.

[54] J. Malila, R. McGraw, A. Laaksonen and K. E. J. Lehtinen. Communication: Kinetics of scavenging of small, nucleating clusters: First nucleation theorem and sum rules. *Journal of Chemical Physics* 142 (2015), 011102.

[55] M. Dal Maso, A. Hyvärinen, M. Komppula, P. Tunved, V.-M. Kerminen, H. Lihavainen, Y. Viisanen, H.-C. Hansson and M. Kulmala. Annual and interannual variation in boreal forest aerosol particle number and volume concentration and their connection to particle formation. *Tellus B* 60 (2008), 495–508.

[56] T. Berndt and S. Richters. Products of the reaction of OH radicals with dimethyl sulphide in the absence of NO_x: Experiment and simulation. *Atmospheric Environment* (2012), 316–322.

[57] F. Eisele and D. Tanner. Measurement of the gas phase concentration of H_2SO_4 and methane sulfonic acid and estimates of H_2SO_4 production and loss in the atmosphere. *Journal of Geophysical Research: Atmospheres* 98 (1993), 9001–9010.

[58] D. R. Hanson and F. Eisele. Diffusion of H_2SO_4 in uhmidified nitrogen: Hydrated H_2SO_4. *Journal of Physical Chemistry A* 104 (2000), 1715–1719.

[59] O. Kupiainen-Määttä, T. Olenius, T. Kurtén and H. Vehkamäki. CIMS sulfuric acid detection efficiency enhanced by amines due to higher dipole moments—a computational study. *Journal of Physical Chemistry A* 117 (2013), 14109–14119.

[60] A. Nadykto, F. Yu, M. Jakovleva, J. Herb and Y. Xu. Amines in the Earth's atmosphere: A density functional theory study of the thermochemistry of pre-nucleation clusters. *Entropy* 13 (2011), 554–569.

[61] H. R. Leverentz, J. I. Siepmann, D. G. Truhlar, V. Loukonen and H. Vehkamäki. Energetics of atmospherically implicated clusters made of sulfuric acid, ammonia, and dimethyl amine. *Journal of Physical Chemistry A* 117 (2013), 3819–3825.

[62] C. Becker and H. Reiss. Nucleation in a nonuniform vapor. *Journal of Chemical Physics* 65 (1976), 2066–2070.

[63] A. Metzger, B. Verheggen, J. Dommen, J. Duplissy, A. S. H. Prevot, E. Weingartner, I. Riipinen, M. Kulmala, D. V. Spracklen, K. S. Carslaw and U. Baltensperger. Evidence for the role of organics in aerosol particle formation under atmospheric conditions. *Proceedings of the National Academy of Sciences U. S. A.* 107 (2010), 6646–6651.

[64] A. Laaksonen, M. Kulmala, T. Berndt, F. Stratmann, S. Mikkonen, A. Ruuskanen, K. E. J. Lehtinen, M. Dal Maso, P. Aalto, T. Petäjä, I. Riipinen, S.-L. Sihto, R. Janson, F. Arnold, M. Hanke, J. Ücker, B. Umann, K. Sellegri, C. D. O'Dowd and Y. Viisanen. SO_2 oxidation products other than H_2SO_4 as a trigger of new particle formation. Part 2: Comparison of ambient and laboratory measurements, and atmospheric implications. *Atmospheric Chemistry and Physics* 8 (2008), 7255–7264.

7 Discussion and reflections

> Where you can measure what you are speaking about and express it in numbers, you know something about it, and when you cannot measure it, when you cannot express it in numbers, your knowledge is of a meagre and unsatisfactory kind.
>
> – Lord Kelvin

This manifesto of positivism in physical sciences was used as an epigraph by Strey et al. [1] in the article that featured the first nucleation theorem as a quantitative tool to analyse nucleation rate measurements, and the correspondence between the critical sizes obtained using the first nucleation theorem and estimated from the Kelvin equation.[1] However, other viewpoints to physical realism, different to the one advocated by Kelvin and Mach, were also emerging in the late 19th century: In his treatise of mechanics [3], Hertz emphasised the role of physical theories and concepts as representations, or images (*Bilder*), depicting the object at hand from a certain perspective while neglecting some other aspects and possibly containing unnecessary, irrelevant information, true or false.[2] Now clearly the

[1] There is actually a small error in the citation. The original passage from Kelvin's published lecture *Electrical units of measurement* reads in it as "In physical science a first essential step in the direction of learning any subject is to find principles of numerical reckoning and practicable methods for is measuring some quality connected with it. I often say that when you can measure what you are speaking about and express it in numbers you know something about it; but when you cannot measure it, when you cannot express it in numbers, your knowledge is of a meagre and unsatisfactory kind: it may be the beginning of knowledge, but you have scarcely, in your thoughts, advanced to the stage of *science*, whatever the matter may be." [2, p. 73].

[2] For influences of Hertz's philosophy on further development of epistemology, especially to Wittgenstein, see [4, Chap. 17].

nucleation theorems, especially different manifestations of the first nucleation theorem, are influenced by the representation of reality that is taken as a basis when writing down the equations describing the nucleation process, together with explicit or implicit assumptions involved considering e.g. vapour–cluster interactions and cluster mobility. As such, depicting the critical cluster as a stationary and incompressible object surrounded by ideal gas, as done in the thermodynamic derivation of the first nucleation theorem, can be seen as a misapplication of the Ockham's Razor [cf. 5], where the perceived image of the problem ignores some potentially relevant physical parameters for the sake of simplicity.

7.1 How to interpret the first nucleation theorem?

Let us look Eq. (1.3) again:

$$\left(\frac{\partial \ln J}{\partial \ln S}\right)_T \approx \Delta g^*(+1).$$

Leaving aside the most obvious source of error, data corresponding to different temperatures (and pressures; cf. Sec. 6.4.7 and assumptions G and H in Table 6.1), there are three terms that need to be defined for any meaningful interpretation of this relation: what is understood with (steady-state) nucleation rate J, saturation ratio S, and the excess critical number of molecules Δg^*? Considering first the second of these, statistical mechanic, and thermodynamic derivations for the first nucleation theorem agree only when vapour is assumed to behave as an ideal gas, when also the approximation in Eq. (1.3) turns into an equality. In this case we can also replace $\mathrm{d}\ln n_1$ with $\mathrm{d}\ln S$ for isothermal (and isobaric) changes and recover the kinetic form of the first nucleation theorem with g^* replaced by $\bar{g}$. On the other hand, derivations using both conventional and small system thermodynamics, together with statistical mechanic derivations with a loose definition of what comprises the cluster [6], allow also inclusion of nonideal vapour effects (Sec. 3.5.2); the thermodynamic derivation neglects the translation and rotation of the cluster as whole, while it is implicitly

included in the statistical mechanic derivation via dependence of the partition function on the thermal de Broglie wavelength (Sec. 3.A.1); and possible other neglected physical processes.[3] Consequently, even when neglecting effects due to nonisothermality and -ideality, compressibility, and the Poynting effect (Sec. 3.5.2), cluster loss (Chap. 5), and other factors listed in Table 6.1, the resulting excess critical sizes Δg^*_{td}, Δg^*_{sm}, $\bar{g}$, $\langle \Delta g \rangle$ and the nucleation exponent P differ from each other due to different assumptions used to derive such quantities.

- A rate expression not fulfilling the law of mass action, i.e. the incorrect identification of the intensive work of formation ΔW^* [see Eq. (2.25] and the work of formation W^* can either lead to the omission of the correction term $\sum_i \epsilon_i$ (= 1 in single-component case), or into opposite situation, where $\sum_i \epsilon_i = 2$.
- The above-mentioned omission of sub-critical cluster losses from the physical description may also result due to lack of rigour or treatment based on chemical kinetics, where it, however, can be seen as a usable approximation when g^*_i is large, but leads to serious misinterpretations when the critical cluster is small (cf. Figs. 6.4 and 6.10).
- Thermodynamic derivations together with those based on mean-field theories neglect the movement of the cluster as whole, which leads to conclusion that $g^*_{\mathrm{td}} < g^*_{\mathrm{sm}}$ at identical conditions (Sec. 7.A).
- Nishioka [8] has shown that even in the framework of CNT, kinetic and thermodynamic critical sizes generally differ from each other, with the kinetic critical size being smaller than the thermodynamic one. This conclusion pertains also to $\bar{g}$ and g^*_{td}, which are supposed to differ slighty from each other even for nucleation from isothermal vapour for a system that strictly follows Szilárd–Farkas description.[4] An example of this phenomenon can actually be seen in Fig. 2 of McGraw and Wu [10], where the $1/n_g$ distribution (note that $1/n_g = e^{\Delta W^*/k_{\mathrm{B}}T}/n_1$) peaks at slightly larger cluster sizes than the $1/\beta_g n_g$ distribution.

[3] Yet another dividing line can be drawn between *atomistic*, i.e. kinetic, statistical mechanic, and "chemical" derivations, and those based on continuum thermodynamics [7].

[4] For discussion on a similar effect in solid solutions and its relation to the principle of detailed balance, see [9].

- In the case of the nucleation exponent P, it is obvious from the derivation (Sec. 3.A.2) that one has to assume some constant P (approximating g^*) that does not depend on the monomer concentration n_1 (or saturation ratio S), which limits the validity of the slope analysis to small intervals in n_1. This point was already acknowledged by Nielsen [11, p. 18]. Furthermore, as already noted, there is no kinetic contribution due to Zel'dovich factor, i.e. returning flux crossing the nucleation barrier, in derivation based on chemical reaction-rate analysis.

The first two items on the list above have clearly the biggest influence on the interpretation of the first nucleation theorem, as the last two contribute, in most conditions, less than one molecule into obtained Δg^*. Thus, based on considerations above it seems safe to identify Δg^* obtained from the first nucleation theorem with the excess number of molecules in the critical cluster, if there are no precritical cluster losses, if both J and S (or n_1) can be accurately determined, if the system is in steady-state, and if the system follows the Szilárd–Farkas description, i.e. collision–fragmentation processes that do not include monomers can be neglected [12, for another computational example, see also 13].

Nucleation processes that do not follow Szilárd–Farkas kinetics have recently obtained a lot of attention in condensed matter studies, where those have been titled as "nonclassical nucleation" [14–17], while similar processes have also postulated for the atmospheric NPF [18]. Overview of thermodynamics and kinetics of nonclassical nucleation [19] suggests that the apparent barrier for the nucleation can range from nonexisting to very large, depending on the stability and the size distribution of sub-critical clusters. Furthermore, clusters with different sizes may interact directly via coagulation, or indirectly via Ostwald ripening [20]. As a result, both the height of the effective nucleation barrier, and its location with respect to the energy minimum corresponding to stable, sub-critical clusters varies. Both of these effects play down the applicability of nucleation theorems for nonclassical nucleation processes.

To overcome the effects of varying apparent critical sizes, Laxson and Finke [21, see also 22] have argued that one should differentiate the critical nucleus, defined in a manner similar to CNT, *kinetically effective nucleus* (KEN), and *the first observable cluster* (FOC). KEN is defined as "the observed re-

action order in a kinetically demonstrated nucleation step, specifically the reaction order, n, in the assembling monomeric precursor A, in a kinetically demonstrated nucleation step, [A]^n", and can be seen equivalent to the nucleation exponent P resulting from the slope analysis. Laxson and Finke propose that one should identify KEN as 2 (sulphuric acid molecules) in atmospheric NPF, as well as in other strongly-bonded systems (i.e. systems where molecules form multiple hydrogen bonds or other bonds stronger than a hydrogen bond, e.g. metal–metal bonds).[5] In this sense, KEN corresponds to the apparent kinetic critical size $\tilde{g}$. FOC, on the other hand, is defined as the smallest cluster size available for direct observations that, depending on the instrumentation used, would generally be much larger than the "true" critical size in vapour–liquid nucleation. Their model, although based on noteworthy philosophical considerations concerning the limitations of the scientific method to study nucleation processes, neglects most of the other uncertainties listed in Table 6.1, and thus may not be applicable into nucleation from vapour (especially in the atmosphere): For example, it has been noted that also models where critical clusters are known to contain more than two sulphuric acid molecules [24] can result in $P = 2$, if cluster losses are accounted for (see also Fig. 5.3). Also, relatively stable sub-critical clusters contributing to the nonclassical pathway for nucleation may fulfil this definition of KEN, although those are not thermodynamically stable (in the sense that these clusters have not crossed the nucleation barrier). On the other hand, FOC can also be smaller than the critical cluster size: An example would be an application of a particle size magnifier [25] typically using vapour of glycol or some other liquid with very low equilibrium vapour pressure condensing on small, sub-critical clusters, composed e.g. of hydrated sulphuric acid, leading to the stabilisation of these clusters and effectively opening up a new channel for NPF. For the corresponding interpretation of resulting $\tilde{g}$ based on the kinetic nucleation theorem, see Chap. 5.

[5]Results of Laxson and Finke are supported by results on studies of the formation of iridium nanoparticles [21], where KEN of 2 was deduced. On the contrary, Chang et al. [23] have recently observed a precritical cluster population in accordance with the CNT-description for platinum nanoparticle formation.

7.2 Correspondence of the Kelvin equation and the first nucleation theorem

In Chap. 4, experimental data was evaluated within the assumption that the size predicted by the first nucleation theorem coincides with the prediction of the Kelvin equation, leading to the displacement barrier height analysis (Sec. 3.2.1). Since the original publication of Chap. 4, several studies reporting homogeneous nucleation rate measurements of waters [26–30], alkanols [31–36], and alkanes [29, 37, 38] have been reported. Results of these studies do not, in general, change the conclusions presented in Chap. 4, though there are some anomalies that require a more detailed inspection.

Girshick [39] has pointed out that based on recent experimental and computational results, CNT does not predict the saturation ratio dependence of nucleation rate correctly after all, resulting in a deviation of the prediction of the Kelvin equation from the first nucleation theorem.[6] Especially interesting here are the recent results on water nucleation [26, 27, see also, 41], which show anomalous correlation between g^* and g^*_{CNT}: At small critical cluster sizes, corresponding to high nucleation rates, experimentally detected g^* from the first nucleation theorem and g^*_{CNT} are in a good agreement with each other. On the other hand, at large critical cluster sizes, $g^* < g^*_{\mathrm{CNT}}$, a result that seems counterintuitive. As a recent computational study [42] suggests that the Kelvin equation is valid for all clusters large enough to reach uniform density at the centre (corresponding to ca. 40 molecules, which coincidentally agrees with the size where the observed correspondence between the Kelvin equation and the first nucleation theorem ceases to hold),[7] the observed deviation of g^*_{CNT} from g^* might be attributed to problems related to the application of the first nucleation theorem. The observed size-dependence is well in line with the effect of sub-critical cluster loss on the first nucleation theorem, though further work is required for a quantitative analysis, as numerical modelling of sub-critical cluster dy-

[6] The connection to problems with proper application of the first nucleation theorem was first noted Hansen [40], referring to the original publication of Chap. 6.

[7] In Ref. [42], indirect MD calculations with a simple monoatomic water model [43] were performed and the obtained density profiles were validated using first principles simulations.

namics inside a cloud chamber or a flow tube is needed to calculate the loss rates L_g.

Systematic studies of n-alkanols using nucleation chambers [34] and supersonic nozzles [36] have resulted in a similar phenomenon for ethanol and n-butanol, though the effect here is less significant. As there is likely a smaller diffusion loss in these expansion-based setups, the result is in agreement with possible precritical cluster loss effects on $\tilde{g}$. It was also found that the self-coagulation rate of nucleated droplets was enhanced from that of pure Brownian motion, which causes some extra uncertainty on the analysis of data from supersonic nozzles [36]. Also the nonideal behaviour of ethanol in these experiments [34] is remarkable.

7.3 Implications and perspectives

Although the application of the first nucleation theorem into laboratory measurements of vapour–liquid nucleation and atmospheric new particle formation, as discussed in Sec. 1.2, fulfils Kuhn's definition of *normal science*, failure of nucleation theorems to provide truly model-independent information on the nucleation process—if one is actually taking place—can hardly be considered as a shift of paradigm.[8] Instead, it remains within the boundaries of a broader paradigm consisting of the liquid-drop

[8]It should be noted that the whole context here differs remarkably from other issues related to phase transitions [44], where discourse has mainly revolved around singularities of the partition function, which, from the statistical mechanic point of view, are impossible for systems away from the thermodynamic limit, as it is not possible for a finite sum of continuous exponentials to have discontinuities.[9] In fact, for the nucleation phenomena, a more fruitful and natural starting point would be the original atomism of Leucippus and Democritus [see, for example, 45, Chap. 16], where molecules (atoms) of different species move in vacuum and interact with each other depending on their nature, for example molecules binding strongly to others can be described having hooks on them. This imagery can be seen in some current representations of the first stages of atmospheric NPF, where e.g. sulphuric [46] or methanesulphonic [47] acid molecules form strong hydrogen bonds into certain directions, effectively binding other molecules. Again, small system thermodynamics provides tools for rationalising such approach [48, Sec. 5.4].

[9]This issue has also been tackled by the *microcanonical thermodynamics* [49] that provides an alternative description for small, nonextensive systems, which, to a large extent, is analogous to small system thermodynamics.

model and activated process dynamics [cf. 50, Secs. III and V]. Indeed, the (negative) criticism to nucleation theorems discussed in Sec. 3.6 supports this view of nucleation theorems inside this larger, shared paradigm. Sociology of science may provide a further explanation of the perceived approval (and recent disapproval) of nucleation theorems, as the active research community in partially overlapping fields of vapour–liquid nucleation and atmospheric new particle formation is relatively small. In such circumstances, the probability that a novel idea akin to nucleation theorems becomes widely accepted in the research community increases significantly if it is supported, and propagated, by few influential researchers or studies.[10] Thus, the relative popularity of nucleation theorems during the past decades may well have been a result of the finite-size dynamics of the nucleation community itself.

Development of cluster and nucleation measurement techniques [e.g. 32, 38, 52–55] has led us at the verge of direct measurements of critical clusters. At least in laboratory environment, such measurements would allow direct evaluation of nucleation theorems and assumptions therein. However, as discussed by Ferreiro et al. [38], even with such direct observations of the cluster distribution, identification of g^*, or even the existence of an unambiguous critical size, is not immediately obvious.

In an atmospheric setting, direct measurements are still hindered by the requirement of charging and subsequent exposure of clusters to low pressures that distort cluster composition especially when it comes to the existence of water in such clusters [56]. Further applications of the nucleation theorems cannot be recommended before such direct experimental confirmation is possible (if ever), although they remain as one of the few available alternatives to extract molecular-level information from the nucleation processes. Meanwhile, parameterisations based on "activation" and "kinetic" nucleation descriptions used in various atmospheric models retain some pragmatic value, but interpretations of such studies should be done with care, as there is no theoretical basis to expect such dependencies. From philosophical point of view, however, inapplicability of the first nucleation theorem to atmospheric NPF does not pose any significant chal-

[10] A complementary viewpoint is provided by the memetic theory [51, Chap. 11] considering ideas and models as independent agents, Darwinian replicators radiating from one mind to another. The only difference between these views is whether we consider scientists as conscious beings on their own right or not.

lenge for the modelling studies, as in general it is not possible to completely verify or validate any numerical model that describes natural phenomena [57]. Hoffmann et al. [5] propose that to describe real chemical systems in the atmosphere, simple models may be valuable for the *understanding* the driving factors of underlying dynamics, while for the *predictability*, a more detailed description is required. For nucleation/atmospheric NPF, although closely resembling atmospheric chemical reaction dynamics, I have to arrive with an opposite conclusion: simple models may have some power to predict observed trends, but for mechanistic understanding of cluster processes behind atmospheric NPF, more detailed description of the processes is required to avoid caveats of naïve simplifications. Simple models may, however, be useful when provoking new research questions. Thus, further applications of nucleation theorems in atmospheric sciences into other cases than NPF, such as heterogeneous nucleation [58–60] that generally requires lower supersaturations when compared to NPF, should be developed. However, also here one can expect complications due to non-classical nucleation processes [15], adsorption effects [61], etc.

7.A Appendix: Effect of cluster translation and rotation on g^*

Thermodynamic derivation of the first nucleation theorem yielding thermodynamic critical size g^*_{td} [62] considers only clusters that are immobile in the laboratory (or corresponding) frame of reference. However, clusters undergo Brownian motion due to collisions with vapour and carrier gas molecules. Using nonequilibrium thermodynamics, Reguera and Rubí [63] have pointed out that if both translation and rotation of the cluster at whole are taken into account,[11] the total free energy barrier for nucleation

[11]Such a correction to the W^* was first derived by Volmer [64, Sec. 4.A], and applied into analysis of experimental data by Sander and Damköhler [65], whilst slightly different estimates for the same correction to the Kelvin equation were independently derived by Kuhrt [66] and Rodebush [67]. Further theoretical work along these tracks—how to account for the missing degrees of freedom when condensing g vapour molecules, each having their own set of translational and rotational degrees of freedom, into a single cluster—was done by Lothe and Pound [68], who argued that this results in a gross underestimation of the partition function of the cluster, and consequently introduces *a*

becomes

$$\Delta G(g) = \Delta G_{\mathrm{td}}(g) + 4k_{\mathrm{B}}T \ln g, \tag{7.1}$$

where the thermodynamic free energy barrier $\Delta G_{\mathrm{td}}(g)$ is given by Eq. (2.2). If one approximates $\Delta G_{\mathrm{td}}(g)$ using Eq. (2.8), setting $(\partial \Delta G^*/\partial g)_{g=g^*} = 0$ results in a cubic equation for the theoretical g^*, which suggests that there should be a corresponding analytic amendment for the first nucleation theorem as well. Differentiating both sides of Eq. (7.1) with respect to $\Delta\mu$ while keeping T constant gives

$$\begin{aligned}\left(\frac{\partial \Delta G}{\partial \Delta \mu}\right)_T &= \left(\frac{\partial \Delta G_{\mathrm{td}}}{\partial \Delta \mu}\right)_T + \left(\frac{\partial 4k_{\mathrm{B}}T \ln g}{\partial \Delta \mu}\right)_T \\ &= g^*_{\mathrm{td}} + \frac{4k_{\mathrm{B}}T}{g}\left(\frac{\partial g}{\partial \Delta \mu}\right)_T.\end{aligned}$$

Applying the W-form of the first nucleation theorem, rearranging and evaluating the obtained expression at $g = g^*$ results in

$$\left(\frac{\partial^2 \Delta G}{\partial \Delta \mu^2}\right)_{T;g=g^*} - \frac{g^*}{4k_{\mathrm{B}}T}\left(g^* - g^*_{\mathrm{td}}\right) = 0, \tag{7.2}$$

which gives the deviation of g^*_{td} from g^* in terms of the curvature of $\Delta G(\Delta\mu)$.[12] Assuming the validity of the first nucleation theorem this curvature can be expressed as $(\partial^2 \Delta G/\partial \Delta \mu^2)_{T,P} = (\partial g^*/\partial \Delta\mu)_{T,P} > 0$, since increasing supersaturation[13] implies decreasing critical size. Hence Eq. (7.2)

replacement free energy into the expression of the nucleation rate that increases J up to 17 orders of magnitude. Reiss and coauthors [e.g. 69–71] have argued that the replacement free energy should be substantially smaller, owing to the overcounting of available partitions of the phase space by Lothe and Pound, and that the application of the capillarity approximation and a proper accounting of the mixing entropy reintroduce some of the ostensible missing degrees of freedom. However, the issue continues to be debated [see, for example, 72]. It should be noted, though, that the effect of the translational–rotational correction to ΔG discussed here arises via different physical mechanism than the correction leading to the replacement free energy [63]: the first one is an entropic nonequilibrium effect due to cluster diffusion [see also 73], while the latter one is due to improper description of the equilibrium properties of the cluster.

[12] Kashchiev [74] has proposed a more approximative treatment writing $W^* = \Delta G_{\mathrm{td}}(g^*_{\mathrm{td}}) + 4k_{\mathrm{B}}T \ln g^*_{\mathrm{td}}$, where the critical size g^*_{td} (i.e. critical size without translational and rotational correction) is used. If the reasoning above is followed, Kashchiev's treatment leads to the conclusion that there is no critical size at all, since Eq. (7.2) implies now that derivatives are evaluated at an inflection point instead of a maximum in ΔW, or, equivalently, a critical size that is independent of supersaturation.

[13] $\Delta\mu < 0$ for supersaturated vapour.

results in that $g^* > g^*_{\mathrm{td}}$, which is intuitively clear directly from Eq. (7.1), as monotonously increasing perturbation to $\Delta G_{\mathrm{td}}(g)$ shifts the location of the maximum towards larger g.

In their statistical mechanic derivation of the first nucleation theorem, Bowles et al. [75] explicitly included the effect of translation on their cluster description. In such case, the correction term to ΔG_{td} reads as $3k_{\mathrm{B}}T \ln g/2$ [76], which results in a correspondingly smaller correction to g^*. On the other hand, for molecular clusters in typical temperatures for nucleation experiments, rotational degrees of freedom are not frozen out, so one can argue that these are implicitly included in canonical ensemble description through the equipartition of energy, leading to some ambiguity in the actual meaning of g^*_{sm}. This inconsistency arises through description of (ideal) vapour molecules as point masses that pose no angular momentum.

References

[1] R. Strey, P. E. Wagner and Y. Viisanen. The problem of measuring homogeneous nucleation rates and the molecular contents of nuclei: Progress in the form of nucleation pulse measurements. *Journal of Physical Chemistry* 98 (1994), 7748–7758.

[2] W. Thomson (lord Kelvin). *Popular Lectures and Addresses*. Vol. 1. London and New York: MacMillan and Co., 1889.

[3] H. Hertz. *Die Prinzipien der Mechanik in neuem Zusammenhange dargestellt*. Leipzig: Johan Ambrosius Barth, 1894.

[4] R. Juti. *Tiedon filosofia*. Helsinki: Gaudeamus, 2013.

[5] R. Hoffmann, V. I. Minkin and B. K. Carpenter. Ockham's razor and chemistry. *HYLE – An International Journal for the Philosophy of Chemistry* 3 (1997), 3–28.

[6] Y. Viisanen, R. Strey and H. Reiss. Homogeneous nucleation rates for water. *Journal of Chemical Physics* 99 (1993), 4680–4692.

[7] J. R. Bursten, M. J. Hartmann and J. E. Millstone. Concenptual analysis for nanoscience. *Journal of Physical Chemistry Letters* 7 (2016), 1917–1918.

[8] K. Nishioka. Kinetic and thermodynamic definitions of the critical nucleus in nucleation theory. *Physical Review E* 52 (1995), 3263–3265.

[9] M. Leitner. Absence of a trapping effect on the kinetic critical radius in nucleation and growth processes. *Acta Materialia* 60 (2012), 6779–6783.

[10] R. McGraw and D. T. Wu. Kinetic extensions of the nucleation theorem. *Journal of Chemical Physics* 118 (2003), 9337–9347.

[11] A. E. Nielsen. *Kinetics of Precipitation*. Oxford: Pergamon, 1964.

[12] H. Vehkamäki, M. J. McGrath, T. Kurtén, J. Julin, K. E. J. Lehtinen and M. Kulmala. Rethinking the application of the first nucleation theorem to particle formation. *Journal of Chemical Physics* 136 (2012), 094107.

[13] R. Kumar, C. Knight, C. D. Wick and B. Chen. Bringing reactivity to the aggregation-volume-bias Monte Carlo based simulation framework: Water nucleation induced by a reactive proton. *Journal of Physical Chemistry B* 119 (2015), 9068–9075.

[14] D. Gebauer and H. Cölfen. Prenucleation clusters and non-classical nucleation. *Nano Today* 6 (2011), 564–584.

[15] R. P. Sear. The non-classical nucleation of crystals: Microscopic mechanisms and applications to molecular crystals, ice and calcium carbonate. *International Materials Reviews* 57 (2012), 328–356.

[16] M. Sleutel and A. E. S. Van Driesche. Role of clusters in nonclassical nucleation and growth of protein crystals. *Proceedings of the National Academy of Sciences U.S.A.* 111 (2014), E546–E553.

[17] S. Price, S. Veesler, H. Pan, K. Lewtas, M. Smets, B. Rimez, A. Myerson, C. Hughes, A. Hare, F. Zhang, H. Meekes, M. Mazzotti, I. Rosbottom, D. Khamar, J. van den Ende, L. Fabian, S. Black, F. Taulelle, M. Gich, P. Vekilov, D. Toroz, C. A. Bertran, J. Sefcik, S. Schroeder, S. Booth, A. Rasmuson, E. Breynaert, E. Simone, R. Hammond, R. Sear, J. de Yoreo, R. Davey, J. Anwar, R. Ristic, D. M. Camacho Corzo, K. Roberts, K. Harris, H. Cölfen and T. Turner. Molecular self-assembly and clustering in nucleation processes: general discussion. *Faraday Discussions* 179 (2015), 155–197.

[18] M. Kulmala, J. Kontkanen, H. Junninen, K. Lehtipalo, H. E. Manninen, T. Nieminen, T. Petäjä, M. Sipilä, S. Schobesberger, P. Rantala, A. Franchin, T. Jokinen, E. Järvinen, M. Äijälä, J. Kangasluoma, J. Hakala, P. P. Aalto, P. Paasonen, J. Mikkilä, J. Vanhanen, J. Aalto, H. Hakola, U. Makkonen, T. Ruuskanen, R. L. Mauldin III, J. Duplissy, H. Vehkamäki, J. Bäck, A. Kortelainen, I. Riipinen, T. Kurtén, M. V. Johnston, J. N. Smith, M. Ehn, T. F. Mentel, K. E. J. Lehtinen, A. Laaksonen, V.-M. Kerminen and D. R. Worsnop. Direct observations of atmospheric aerosol nucleation. *Science* 339 (2013), 943–946.

[19] D. Zahn. Thermodynamics and kinetics of prenucleation clusters, classical and non-classical nucleation. *ChemPhysChem* 16 (2015), 2069–2075.

[20] W. Ostwald. Studien über die Bildung um Umwandlung fester Körper. *Zeitschrift für physikalische Chemie* 22 (1879), 289–330.

[21] W. W. Laxson and R. G. Finke. Nucleation is second order: An apparent kinetically effective nucleus of two for $Ir(0)_n$ nanoparticle formation from $[(1,5\text{-COD})Ir^{I}\cdot P_2W_{15}Nb_3O_{62}]^{8-}$ plus hydrogen. *Journal of the American Chemical Society* 136 (2014), 17601–17615.

[22] E. E. Finney and R. G. Finke. Fitting and interpreting transition-metal nanocluster formation and other sigmoidal-appearing kinetic data: A more thorough testing of dispersive kinetic vs chemical-mechanism-based equations and treatments for 4-step type kinetic data. *Chemistry of Materials* 21 (2009), 4468–4479.

[23] S.-Y. Chang, Y. Gründer, S. G. Booth, L. B. Molleta, A. Uehara, J. F. W. Mosselmans, G. Cibin, V.-T. Pham, L. Nataf, R. A. W. Dryfe and S. L. M. Schroeder. Detection and characterisation of sub-critical nuclei during reactive Pd metal nucleation by X-ray absorption spectroscopy. *CrystEngCom* 18 (2016), 674–682.

[24] M. Chen, M. Titcombe, J. Jiang, C. Jen, C. Kuang, M. L. Fischer, F. L. Eisele, J. I. Siepmann, D. R. Hanson, J. Zhao and P. H. McMurry. Acid–base chemical reaction model for nucleation rates in the polluted atmospheric boundary layer. *Proceedings of the National Academy of Sciences U.S.A.* 109 (2012), 18713–18718.

[25] J. F. de la Mora. Electrical classification and condensation detection of sub-3-nm aerosols. In: *Aerosol Measurement: Principles, Techniques, and Applications*. Ed. by P. Kulkarni, P. A. Baron and K. Willeke. 3rd ed. Hoboken, N.J.: Wiley, 2011. Chap. 32.

[26] D. Brus, V. Ždímal and H. Uchtmann. Homogeneous nucleation rate measurements in supersaturated water vapor II. *Journal of Chemical Physics* 131 (2009), 074507.

[27] A. A. Manka, D. Brus, A. P. Hyvärinen, H. Lihavainen, J. Wölk and R. Strey. Homogeneous water nucleation in a laminar flow diffusion chamber. *Journal of Chemical Physics* 132 (2010), 244505.

[28] A.-P. Hyvärinen, D. Brus, J. Wedekind and H. Lihavainen. How ambient pressure influences water droplet nucleation at tropospheric conditions. *Geophysical Research Letters* 37 (2010), L21802.

[29] H. Pathak, J. Wölk, R. Strey and B. E. Wyslouzil. Co-condensation of nonane and D_2O in a supersonic nozzle. *Journal of Chemical Physics* 140 (2014), 034034.

[30] M. A. L. J. Fransen, J. Hrubý, D. M. J. Smeulders and M. E. H. van Dongen. On the effect of pressure and carrier gas on homogeneous water nucleation. *Journal of Chemical Physics* 142 (2015), 164307.

[31] F. Rütten, I. Alxneit and H. R. Tschudi. Kinetics of homogeneous nucleation and condensation of *n*-butanol at high supersaturation. *Atmospheric Research* 92 (2009), 124–130.

[32] H. Laksmono, S. Tanimura, H. C. Allen, G. Wilemski, M. S. Zahniser, J. H. Shorter, D. D. Nelson, J. B. McManus and B. E. Wyslouzil. Monomer, clusters, liquids: An integrated spectroscopic study of methanol condensation. *Physical Chemistry Chemical Physics* 13 (2011), 5855–5871.

[33] H. Laksmono, S. Tanimura and B. E. Wyslouzil. Methanol nucleation in supersonic nozzle. *Journal of Chemical Physics* 135 (2011), 074305.

[34] A. A. Manka, J. Wedekind, D. Ghosh, K. Höhler, J. Wölk and R. Strey. Nucleation of ethanol, propanol, butanol and pentanol: A systematic experimental study along the homologous series. *Journal of Chemical Physics* 137 (2012), 054316.

[35] H. Görke, K. Neitola, A.-P. Hyvärinen, H. Lihavainen, J. Wölk, R. Strey and D. Brus. Homogeneous nucleation rates of n-propanol measured in the laminar flow diffusion chamber at different pressures. *Journal of Chemical Physics* 140 (2014), 174301.

[36] K. Mullick, A. Bhabhe, A. Manka, J. Wölk, R. Strey and B. E. Wyslouzil. Isothermal nucleation rates of n-propanol, n-butanol, and n-pentanol in supersonic nozzles: Critical cluster sizes and the role of coagulation. *Journal of Physical Chemistry B* 119 (2015), 9009–9019.

[37] D. Ghosh, D. Bergmann, R. Schwering, J. Wölk, R. Strey, S. Tanimura and B. E. Wyslouzil. Homogeneous nucleation of a homologous series of n-alkanes (C_iH_{2i+2}, $i = 7$–10) in a supersonic nozzle. *Journal of Chemical Physics* 132 (2010), 024307.

[38] J. J. Ferreiro, T. E. Gartmann, B. Schläppi and R. Signorell. Can we observe gas phase nucleation at the molecular level? *Zeitschrift für physikalische Chemie* 229 (2015), 1765–1780.

[39] S. L. Girshick. The dependence of homogeneous nucleation rate on supersaturation. *Journal of Chemical Physics* 141 (2014), 024307.

[40] K. Hansen. Comment on "The dependence of homogeneous nucleation rate on supersaturation". *Journal of Chemical Physics* 141 (2014), 157101.

[41] A. Afzalizar, T. Turunen-Saaresti and A. Grönman. Origin of droplet size underprediction in modeling of low pressure nucleating flows of steam. *International Journal of Multiphase Flow* 86 (2016), 86–98.

[42] M. H. Factorovich, V. Molinero and D. A. Scherlis. Vapor pressure of water nanodroplets. *Journal of the American Chemical Society* 136 (2014), 4508–4514.

[43] V. Molinero and E. B. Moore. Water modeled as an intermediate element between carbon and silicon. *Journal of Physical Chemistry B* 113 (2009), 4008–4016.

[44] T. Menon and C. Callender. Turn and face the strange... Ch-ch-changes: Philosophical questions raised by phase transitions. In: *The Oxford Handbook of Philosophy of Physics*. Ed. by R. Batteman. Oxford: Oxford University Press, 2013. Chap. 6.

[45] R. D. McKiharan. *Philosophy Before Socrates: An Introduction with Texts and Commentary*. 2nd ed. Indianapolis: Hackett Publishing Company, 2010.

[46] T. Kurtén, C. Kuang, P. Gómez, P. H. McMurry, H. Vehkamäki, I. K. Ortega, M. Noppel and M. Kulmala. The role of cluster energy nonaccommodation in atmospheric sulfuric acid nucleation. *Journal of Chemical Physics* 132 (2010), 024304.

[47] M. L. Dawson, M. E. Varner, V. Perraud, M. J. Ezell, R. B. Gerber and B. J. Finlayson-Pitts. Simplified mechanism for new particle formation from methanesulfonic acid, amines, and water via experiments and ab initio calculations. *Proceedings of the National Academy of Sciences U.S.A.* 109 (2012), 18719–18724.

[48] T. L. Hill. *Thermodynamics of Small Systems*. Parts I and II. New York: W. A. Benjamin, 1963–1964.

[49] D. H. E. Gross. *Microcanonical Thermodynamics: Phase Transitions in "Small" Systems*. Singapore: World Scientific, 2001.

[50] T. S. Kuhn. *The Structure of Scientific Revolutions*. 2nd, enlarged ed. Chicago: University of Chicago Press, 1970.

[51] R. Dawkins. *The Selfish Gene*. Oxford: Oxford University Press, 1976.

[52] O. Björneholm, G. Öhrwall and M. Tchaplyguine. Free clusters studied by core-level spectroscopies. *Nuclear Instruments and Methods in Physics Research A* 601 (2009), 161–181.

[53] U. Buck, C. C. Pradzynski, T. Zeuch, J. M. Dieterich and B. Hartke. A size resolved investigation of large water clusters. *Physical Chemistry Chemical Physics* 16 (2014), 6859–6871.

[54] B. Schläppi, J. H. Litman, J. J. Ferreiro, D. Stapfer and R. Signorell. A pulsed uniform Laval expansion coupled with single photon ionization and mass spectrometric determination for the study of large molecular aggregates. *Physical Chemistry Chemical Physics* 17 (2015), 25761–25771.

[55] L. Hautala, K. Jänkälä, M.-H. Mikkelä, M. Tchaplyguine and M. Huttula. Surface site coordination dependent responses resolved in free clusters: applications for neutral sub-nanometer cluster studies. *Physical Chemistry Chemical Physics* 17 (2015), 7012–7022.

[56] H. Junninen, M. Ehn, T. Petäjä, L. Luosujärvi, T. Kotiaho, R. Kostiainen, U. Rohner, M. Gonin, K. Fuhrer, M. Kulmala and D. R. Worsnop. A high-resolution mass spectrometer to measure atmospheric ion composition. *Atmospheric Measurement Techniques* 3 (2010), 1039–1053.

[57] N. Oreskes, K. Schrader-Frechette and K. Belitz. Verification, validation, and confirmation of numerical models in the Earth Sciences. *Science* 263 (1994), 641–646.

[58] R. P. Sear. Nucleation: Theory and applications to protein solutions and colloidal suspensions. *Journal of Physics: Condensed Matter* 19 (2007), 033101.

[59] H. Vehkamäki, A. Määttänen, A. Lauri, M. Kulmala, P. Winkler, A. Vrtala and P. E. Wagner. Heterogeneous multicomponent nucleation theorems for the analysis of nanoclusters. *Journal of Chemical Physics* 126 (2007), 174707.

[60] R. McGraw, J. Wang and C. Kuang. Kinetics of heterogeneous nucleation in supersaturated vapor: fundamental limits to neutral particle detection revisited. *Aerosol Science and Technology* 46 (2012), 1053–1064.

[61] A. Laaksonen and J. Malila. An adsorption theory of heterogeneous nucleation of water vapour on nanoparticles. *Atmospheric Chemistry and Physics* 16 (2016), 135–143.

[62] D. W. Oxtoby and D. Kashchiev. A general relation between the nucleation work and the size of the nucleus in multicomponent nucleation. *Journal of Chemical Physics* 100 (1994), 7665–7671.

[63] D. Reguera and J. M. Rubí. Nonequilibrium translational-rotational effects in nucleation. *Journal of Chemical Physics* 115 (2001), 7100–7106.

[64] M. Volmer. *Kinetik der Phasenbildung*. Dresden und Leipzig: Verlag von Theodor Steinkopff, 1939.

[65] A. Sander and G. Damköhler. Übersättigung bei der spontane Keimbildung in Wasserdampf. *Naturwissenschaften* 39 (1943), 460–465.

[66] F. Kuhrt. Das Tröpchenmodell übersättigter realer Gase. *Zeitschrift für Physik* 131 (1952), 205–214.

[67] W. H. Rodebush. The vapor pressure of small drops. *Proceedings of the National Academy of Sciences U. S. A.* 40 (1954), 789–794.

[68] J. Lothe and G. M. Pound. Reconsiderations of nucleation theory. *Journal of Chemical Physics* 36 (1962), 2080–2085.

[69] H. Reiss, J. L. Katz and E. R. Cohen. Translation–rotation paradox in the theory of nucleation. *Journal of Chemical Physics* 48 (1968), 5553–5560.

[70] H. Reiss. The replacement free energy in nucleation theory. *Advances in Colloid and Interface Science* 7 (1977), 1–66.

[71] H. Reiss, W. K. Kegel and J. L. Katz. Resolution of the problems of replacement free energy, $1/S$, and internal consistency in nucleation theory by consideration of the length scale for mixing entropy. *Physical Review Letters* 78 (1997), 4506–4509.

[72] I. Kusaka. Statistical mechanics of nucleation: Incorporating translational and rotational free energy into thermodynamics of a microdroplet. *Physical Review E* 73 (2006), 031607.

[73] M. Schweizer and L. M. C. Sagis. Nonequilibrium thermodynamics of nucleation. *Journal of Chemical Physics* 141 (2014), 224102.

[74] D. Kashchiev. Analysis of experimental data for the nucleation rate of water droplets. *Journal of Chemical Physics* 125 (2006), 044505.

[75] R. K. Bowles, R. McGraw, P. Schaaf, B. Senger, J.-C. Voegel and H. Reiss. A molecular based derivation of the nucleation theorem. *Journal of Chemical Physics* 113 (2000), 4524–4532.

[76] D. Reguera and J. M. Rubí. Homogeneous nucleation in inhomogeneous media. I. Nucleation in a temperature gradient. *Journal of Chemical Physics* 119 (2003), 9877–9887.

Appendix On continued fractions

In this Appendix a very short introduction to continued fractions is given, and a theorem concerning the derivative of a finite continued fraction—applied in Chapter 5—is proven. The derivative of a finite continued fraction of a complex variable (the most natural domain to study analytic theory of continued fractions is the Riemann sphere $\hat{\mathbb{C}}$) is derived by presenting the continued fraction as a component of a finite composition of $\hat{\mathbb{C}}^2 \to \hat{\mathbb{C}}^2$ linear fractional transformations of analytic functions. Connections to previous work and possible applications of the deduced formula are briefly discussed.

A.1 Continued fractions

Numbers in form

$$a_0 + \cfrac{a_1}{b_1 + \cfrac{a_2}{b_2 + \cfrac{a_3}{\ddots}}}$$

with real or complex elements a_k and b_k, $k = (0), 1, 2, \ldots$, are known as continued fractions (a more elaborate definition is given in the next section). A beautiful example of such expression is given by the golden

ratio,

$$\frac{1+\sqrt{5}}{2} = 1 + \cfrac{1}{1 + \cfrac{1}{1 + \cfrac{1}{1 + \cfrac{1}{\ddots}}}}$$

If we have $a_N = 0$ or $|b_{N+1}| = \infty$ for some N, the continued fraction truncates after N levels and is thus a finite one. Much work involving continued fractions has been done by number theorists, whereas analytical work and applications have played smaller but still noticeable role [1]. In analytical theory, properties of sequences $\{a_k\}_{k\geq 0}$ and $\{b_k\}_{k\geq 1}$ are studied from the viewpoints of convergence, correspondence and classification of continued fractions, as well as truncation-error analysis and algorithmic properties, which arise from computational uses of continued fractions for approximation and inter- and extrapolation of functions. In this context, notation[1]

$$\mathop{\mathrm{K}}_{k=1}^{\infty}\left(\frac{a_k}{b_k}\right) = a_0 + \cfrac{a_1}{b_1 + \cfrac{a_2}{b_2 + \cfrac{a_3}{\ddots}}}, \tag{A.1}$$

analogous to $\sum$- and $\prod$-notations for sums and products, respectively, is customarily used. Part of the motivation for the analytical work stems from the fact that several special functions have also a continued fraction presentation in addition to series and/or integral one [2]. In fact, it is possible to expand any continued fraction formally into a rational function or power series form, although the domain of convergence of these various presentations may be different. A further generalisation into continued fraction function is now obvious in analogy to function series and products, if sequences $a_k(z)$ and $b_k(z)$ are functions of a (complex) argument z. As

[1]This notation was introduced by Gauss after *Kettenbruch*.

an example, we can consider the exponential function,

$$e^z = 1 + \cfrac{2z}{2 - z + \cfrac{z^2/6}{1 + \cfrac{z^2/60}{1 + \cfrac{z^2/140}{1 + \ddots}}}}$$

It should be noted that such continued fraction expansions are not unique, though.

An immediate application of functional continued fractions follows from the solution of second-order difference equations; the specific example motivating the work described in the next section is Eq. (5.13).

A.2 Applications of continued fractions to vapour–liquid nucleation studies; or, the absence of those

Despite being a well-known tool in nonequilibrium statistical mechanics and fluctuation theory [3, 4], continued fraction methods have only been marginally utilised in vapour-to-liquid nucleation studies so far (in contrast to studies of other phase transitions): A straightforward application of the general theory occurs in [5]. Wilemski [6] has derived an algorithm for the efficient calculation of the Becker–Döring sum that can be classified as a continued fraction algorithm. The continued fraction solution for the generalised Szilárd–Farkas kinetics applied in Chap. 5 was first obtained by McGraw and Marlow [7], and later independently by McClurg [8]; the corresponding recurrence relation was also obtained and used by Warren and Seinfeld [9].[2] The third equivalent formulation—that of a rational function—was derived by Laaksonen [11], who, however, only considered supercritical clusters neglecting evaporation terms.

[2] Also McGraw's [10] quadrature method of moments uses continued fraction -based algorithms to compute the numerical solution for the general dynamic equation describing simultaneous nucleation, condensation and coagulation.

One can only wonder why continued fractions have not been utilised more efficiently in nucleation studies. A possible reason is that continued fractions are awkward to deal with when applying the standard operations of calculus, i.e. differentiation and integration. In fact, prior to the work leading to this thesis, there was apparently no publication giving the general formula for the derivative of a continued fraction function with respect to its argument even in the finite case, which is actually trivial as one could always expand the continued fraction into a form of rational function.

A.3 Derivative of a continued fraction[3]

A.3.1 Introduction

Continued fractions

$$\mathop{\mathrm{K}}_{k=n}^{\infty}\left(\frac{a_k}{b_k}\right) = b_{n-1} + \cfrac{a_n}{b_n + \cfrac{a_{n+1}}{b_{n+1} + \cfrac{a_{n+2}}{\ddots}}} \tag{A.2}$$

occur frequently in applications due to close connections between continued fractions and second-order difference and differential equations [12]. Although it has been known since the pioneering work of Euler that one can convert a continued fraction into a power series, implying analyticity in the whole domain of definition as long as the elements a_k and b_k are analytic, it is difficult to give general formulae for the derivatives of a continued fraction with respect to its argument. In some cases this can be accomplished by utilising a connection between a given continued fraction and a special function (e.g. [13], see [2] for further possibilities). So far most studies have concentrated on the more mathematically interesting case of an infinite continued fraction. In applications, however, boundary

[3]This Section incorporates material from the article J. Malila. The derivative of a finite continued fraction. *Applied Mathematics E-Notes* 14 (2014), 13–19. I warmly thank Dr. Eimear Dunne for her critical reading and comments on the manuscript of the original article.

conditions—or computational limitations—lead to the truncation of the continued fraction (A.2) after a finite number of levels, resulting in a finite continued fraction $\mathop{\mathrm{K}}_{k=n}^{N}(a_k/b_k)$. Here we derive a general formula for the derivative of this finite continued fraction by presenting it as a finite composition of linear fractional transformation of analytic functions. We then briefly discuss the connections between the deduced formula and partial derivatives with respect to elements a_k and b_k.

A.3.2 Preliminaries and the main result

We consider a finite continued fraction

$$\mathop{\mathrm{K}}_{k=n}^{N}\left(\frac{a_k}{b_k}\right) = \cfrac{a_n}{b_n + \cfrac{a_{n+1}}{b_{n+1} + \cfrac{a_{n+2}}{\ddots \\ b_{N-1} + \cfrac{a_N}{b_N}}}}, \tag{A.3}$$

where a_k and b_k are functions of a complex argument z that we suppress for brevity. This finite continued fraction is also known as the *Nth approximant* of the infinite continued fraction (A.2). (We neglect the term b_{n-1} for simplicity, which does not affect the generality of our results.) For $N - n > \ell \geq 1$, the expression $\mathop{\mathrm{K}}_{k=n+\ell}^{N}(a_k/b_k)$ is known as the *ℓth tail* of the finite continued fraction (A.3).

Now let $\{a_k\}_{k\geq n}$ and $\{b_k\}_{k\geq n}$ be two sequences of complex-valued analytic functions with domains Ψ and $\Omega \subset \mathbb{C}$, respectively. We define a third sequence of functions $\{g_k\}_{k\geq n}$ as

$$g_k(z,\zeta) = \big(g_{k,1}(z), g_{k,2}(z,\zeta)\big) = \left(z, \frac{a_k(z)}{b_k(z)+\zeta}\right), \tag{A.4}$$

with domain $G \subset \Psi \cap \Omega \times B(0, R_G) \subset \hat{\mathbb{C}}^2$ such that $g_k(G) \subseteq G$ for all $k = n, \ldots, N$; here $B(0, R_G)$ is an open disk with radius $R_G < \infty$ and $\hat{\mathbb{C}} = \mathbb{C} \cup \{\infty\}$. We set the (finite) $G \to G$ composite function

$$f_{n\to N}(z,\zeta) = (f_{n\to N,1}, f_{n\to N,2}) := g_n \circ g_{n+1} \circ \cdots \circ g_N(z,\zeta), \tag{A.5}$$

where subscript $n \to N$ indicates the extent of the composition.

THEOREM 1. Assuming that $a_\ell(z)$, $b_\ell(z)+g_{\ell+1,2}(z,\zeta) \neq 0$ for $\ell = n, \ldots, N-1$ and $b_N(z) \neq 0$ for all $(z,\zeta) \in G$, it follows that

(i) $f_{n\to N}$ is analytic

(ii) $f_{n\to N,2}$ evaluated at $(z,0)$ equals the finite continued fraction (A.3).

PROOF. Claim (i) follows since $g_{k,1}$ and $g_{k,2}$ are $\mathbb{C} \to \mathbb{C}$ linear fractional transformations of analytic functions that are bounded and continuous for every $(z,\zeta) \in G$ and $k = n, \ldots, N$. Thus $f_{n\to N}$ is also analytic as a finite composition of analytic functions [14, Sec. 2.1].

Now $f_{n\to N,2}(z,0) = \mathrm{K}_{k=n}^{N}(a_k/b_k)$ is a well-defined $G \to \mathbb{C}$ function corresponding to the standard definition of the (nth tail of a) continued fraction [12, Sec. I.1], thus satisfying claim (ii). □

LEMMA (Chain rule). The chain rule for $f_{n\to N,2}$ reads as

$$\frac{\partial f_{n\to N,2}}{\partial z} = \sum_{j=n}^{N}\left(\prod_{m=n+1}^{j}\frac{\partial g_{m-1,2}}{\partial g_{m,2}}\right)\frac{\partial g_{j,2}}{\partial z}. \tag{A.6}$$

PROOF. From Theorem 1 all $g_{k,2}$ are analytic and $\partial g_k/\partial(\bar{z},\bar{\zeta}) = \left(\begin{smallmatrix}0&0\\0&0\end{smallmatrix}\right)$. Equation (A.6) is most conveniently proven by induction; the argument is essentially the same as that of Gill [15], but is repeated here for the convenience of the reader. First, letting $N = n+1$, the result follows directly from the usual chain rule:

$$\begin{aligned} P_1 : \frac{\partial f_{n\to N,2}}{\partial z} &= \frac{\partial g_{n,2}}{\partial g_{n+1,1}}\frac{\partial g_{n+1,1}}{\partial z} + \frac{\partial g_{n,2}}{\partial g_{n+1,2}}\frac{\partial g_{n+1,2}}{\partial z} \\ &= \frac{\partial g_{n,2}}{\partial z} + \frac{\partial g_{n,2}}{\partial g_{n+1,2}}\frac{\partial g_{n+1,2}}{\partial z} \\ &= \sum_{j=n}^{n+1}\left(\prod_{m=n+1}^{j}\frac{\partial g_{m-1,2}}{\partial g_{m,2}}\right)\frac{\partial g_{j,2}}{\partial z}, \end{aligned}$$

where $\prod_{m=n+1}^{n}\cdots = 1$. We now assume that Eq. (A.6) holds for $N = n+k$,

i.e.

$$P_k : \frac{\partial f_{n\to N,2}}{\partial z} = \sum_{j=n}^{n+k}\left(\prod_{m=n+1}^{j}\frac{\partial g_{m-1,2}}{\partial g_{m,2}}\right)\frac{\partial g_{j,2}}{\partial z}.$$

To show that this implies P_{k+1}, we first write $f_{n\to N}(z,\zeta) = g_n(f_{n+1\to N}(z,\zeta))$. Now with a simple change in indexing of P_k we have

$$\frac{\partial f_{n+1\to N,2}}{\partial z} = \sum_{j=n+1}^{n+k+1}\left(\prod_{m=n+2}^{j}\frac{\partial g_{m-1,2}}{\partial g_{m,2}}\right)\frac{\partial g_{j,2}}{\partial z},$$

so that

$$\begin{aligned} P_{k+1} : \frac{\partial f_{n\to N,2}}{\partial z} &= \frac{\partial g_{n,2}}{\partial f_{n+1\to N,1}}\frac{\partial f_{n+1\to N,1}}{\partial z} + \frac{\partial g_{n,2}}{\partial f_{n+1\to N,2}}\frac{\partial f_{n+1\to N,2}}{\partial z} \\ &= \frac{\partial g_{n,2}}{\partial z} + \frac{\partial g_{n,2}}{\partial g_{n+1,2}}\sum_{j=n+1}^{n+k+1}\left(\prod_{m=n+2}^{j}\frac{\partial g_{m-1,2}}{\partial g_{m,2}}\right)\frac{\partial g_{j,2}}{\partial z} \\ &= \sum_{j=n}^{n+k+1}\left(\prod_{m=n+1}^{j}\frac{\partial g_{m-1,2}}{\partial g_{m,2}}\right)\frac{\partial g_{j,2}}{\partial z}, \end{aligned}$$

which completes the proof. □

We can now present our main result:

THEOREM 2. Under the assumptions of Theorem 1, $\mathrm{d}\,\mathrm{K}_{k=n}^{N}(a_k/b_k)/\mathrm{d}z$ is an analytic function for all z, $(z,0) \in G$, and

$$\begin{aligned} \frac{\mathrm{d}}{\mathrm{d}z}\mathop{\mathrm{K}}_{k=n}^{N}\left(\frac{a_k}{b_k}\right) = \sum_{j=n}^{N}(-1)^{j-n+1}&\left\{\prod_{k=n}^{j}\frac{1}{a_k}\left[\mathop{\mathrm{K}}_{\ell=k}^{N}\left(\frac{a_\ell}{b_\ell}\right)\right]^2\right\} \\ &\times\left\{\left[\mathop{\mathrm{K}}_{\ell=j}^{N}\left(\frac{a_\ell}{b_\ell}\right)\right]^{-1}\frac{\mathrm{d}a_j}{\mathrm{d}z} - \frac{\mathrm{d}b_j}{\mathrm{d}z}\right\}. \end{aligned} \tag{A.7}$$

PROOF. Applying substitutions

$$\frac{\partial g_{k,2}}{\partial z} = \left.\frac{\frac{\mathrm{d}a_k}{\mathrm{d}z}(b_k+\zeta) - a_k\frac{\mathrm{d}b_k}{\mathrm{d}z}}{(b_k+\zeta)^2}\right|_{\zeta=\zeta_k}$$

and

$$\frac{\partial g_{k,2}}{\partial \zeta} = -\frac{a_k}{(b_k+\zeta)^2}\bigg|_{\zeta=\zeta_k}$$

with $\zeta_k = f_{k+1\to N,2} = \mathrm{K}_{m=k+1}^{N}(a_m/b_m)$ for $k = n, \ldots, N-1$; $\zeta_N = 0$, to the previous Lemma gives for the derivative

$$\sum_{j=n}^{N}\left\{\prod_{k=n+1}^{j}\frac{-a_{k-1}}{\left[b_{k-1}+\mathop{\mathrm{K}}_{\ell=k}^{N}\left(\frac{a_\ell}{b_\ell}\right)\right]^2}\right\}\frac{\left[b_j+\mathop{\mathrm{K}}_{\ell=j+1}^{N}\left(\frac{a_\ell}{b_\ell}\right)\right]\frac{\mathrm{d}a_j}{\mathrm{d}z}-a_j\frac{\mathrm{d}b_j}{\mathrm{d}z}}{\left[b_j+\mathop{\mathrm{K}}_{\ell=j+1}^{N}\left(\frac{a_\ell}{b_\ell}\right)\right]^2},$$

from which we obtain the final result [Eq. (A.7)] after factoring out continued fractions. We can now replace the partial derivative with a total one as $\mathrm{K}_{k=n}^{N}(a_k/b_k)$ is an analytic function of z only. □

It should be noted that if a_k and b_k are unknown analytic functions, conditions in Theorem 1 are sufficient to guarantee that the undetermined cases $0/0$ or $0\cdot\infty$ are not possible to occur when evaluating $\mathrm{d}\,\mathrm{K}_{k=n}^{N}(a_k/b_k)/\mathrm{d}z$. However, if a_k and b_k are known, it might be possible to relax these conditions: for example, if either $a_\ell \equiv 0$ or $b_{\ell+1} \equiv -\mathrm{K}_{k=\ell+2}^{N}(a_k/b_k)$ for some $N-1 > \ell > n$, the original continued fraction simply terminates after $\ell - n$ levels and we can reset $N = \ell$.

A.3.3 Partial derivatives with respect to a_ℓ and b_ℓ

As an example of the application of Eq. (A.7), we turn our attention to two special cases presented in earlier literature which give partial derivatives of continued fractions with respect to their elements. In accordance with the standard practice in the literature, we consider only $n = 1$.

The Nth modified approximant of the continued fraction (A.2) can be now defined in our notation as $f_{1\to N,2}(z,\zeta)$ for arbitrary ζ [cf. 12, Sec. I.5]. This allows us to extend preceding results for infinite continued fractions:

OBSERVATION. The previous Lemma holds for all $\zeta \in B(0, R_G)$ that are independent of z as well as for $\zeta = 0$. Now if we consider sequences $\{a_k\}_{k\geq 1}$, $a_k \neq 0$ for $k < N$, and $\{b_k\}_{k\geq 1}$, which are constants except for subsequences $\{a_\ell(z)\}_{\ell\in I}$ and $\{b_\ell(z)\}_{\ell\in J}$, $I, J \subseteq \{1, 2, \ldots, N\}$ for some N, which are analytic functions of z so that $\mathrm{K}_{k=N+1}^{\infty}(a_k/b_k)$ is defined and converges into $\zeta_\infty \in \hat{\mathbb{C}}$, the Theorem 2 also holds for $\zeta = \zeta_\infty$, i.e. for $\mathrm{K}_{k=1}^{\infty}(a_k/b_k)$.

The rationale behind this observation is that, as long as the $(\ell+1)$st tail, $\ell \leq N$, is constant, the Nth modified approximant of (A.2) given by the finite composition $f_{1\to N}(z, \zeta_\infty)$ results $f_{1\to N,2}(z, \zeta_\infty) = \mathrm{K}_{k=1}^{\infty}(a_k/b_k)$. For the extension to an infinite composition, see [15].

Let us first consider the case where all b_k and $a_{k\neq\ell}$ are constants. Assuming that neither a_ℓ nor $\mathrm{d}a_\ell/\mathrm{d}z$ vanishes, only the term with index ℓ remains from the sum, and applying $\mathrm{d}z = (\partial a_\ell/\partial z)^{-1}\mathrm{d}a_\ell$ on Eq. (A.7) gives

$$\begin{aligned}
\frac{\partial}{\partial a_\ell}\mathop{\mathrm{K}}_{k=1}^{\infty}\left(\frac{a_k}{b_k}\right) &= (-1)^\ell \prod_{k=1}^{\ell}\frac{1}{a_k}\left[\mathop{\mathrm{K}}_{j=k}^{\infty}\left(\frac{a_j}{b_j}\right)\right]^2\left[\mathop{\mathrm{K}}_{j=\ell}^{\infty}\left(\frac{a_j}{b_j}\right)\right]^{-1} \\
&= (-1)^{\ell-2}\prod_{k=2}^{\ell-1}\frac{1}{a_k}\left[\mathop{\mathrm{K}}_{j=k}^{\infty}\left(\frac{a_j}{b_j}\right)\right]^2\frac{1}{a_1}\left[\mathop{\mathrm{K}}_{j=1}^{\infty}\left(\frac{a_j}{b_j}\right)\right]^2\frac{1}{a_\ell}\mathop{\mathrm{K}}_{j=\ell}^{\infty}\left(\frac{a_j}{b_j}\right) \\
&= \frac{1}{a_\ell}\mathop{\mathrm{K}}_{j=1}^{\infty}\left(\frac{a_j}{b_j}\right)\prod_{k=2}^{\ell-1}\frac{-\mathop{\mathrm{K}}_{j=k}^{\infty}\left(\frac{a_j}{b_j}\right)}{b_k+\mathop{\mathrm{K}}_{j=k+1}^{\infty}\left(\frac{a_j}{b_j}\right)}\frac{\mathop{\mathrm{K}}_{j=\ell}^{\infty}\left(\frac{a_j}{b_j}\right)}{b_1+\mathop{\mathrm{K}}_{j=2}^{\infty}\left(\frac{a_j}{b_j}\right)} \\
&= \frac{1}{a_\ell}\mathop{\mathrm{K}}_{j=1}^{\infty}\left(\frac{a_j}{b_j}\right)\prod_{k=2}^{\ell}\frac{-\mathop{\mathrm{K}}_{j=k}^{\infty}\left(\frac{a_j}{b_j}\right)}{b_{k-1}+\mathop{\mathrm{K}}_{j=k}^{\infty}\left(\frac{a_j}{b_j}\right)},
\end{aligned} \tag{A.8}$$

which is the generalisation of Waadeland's [16] formula by Levrie and Bultheel [17]; the original formula follows if $b_k \equiv 1$ and $\ell \geq 2$. Note that if $\ell = 1$, the minus sign cannot be taken inside the (empty) product.

Next we turn to the opposite case, and set all a_k and $b_{k\neq\ell}$ constants and assume that neither b_ℓ nor $\mathrm{d}b_\ell/\mathrm{d}z$ vanishes. Considering first the finite case, Eq. (A.7) reduces to

$$\frac{\partial}{\partial b_\ell}\operatorname*{\mathbb{K}}_{k=1}^{N}\left(\frac{a_k}{b_k}\right) = (-1)^\ell \prod_{k=1}^{\ell}\frac{1}{a_k}\left[\operatorname*{\mathbb{K}}_{j=k}^{N}\left(\frac{a_j}{b_j}\right)\right]^2 . \tag{A.9}$$

Using the determinant formula [12, Eq. (1.2.10)], we can write

$$(-1)^{\ell-1}\prod_{k=1}^{\ell} a_k = B_\ell B_{\ell-1}\left[\operatorname*{\mathbb{K}}_{k=1}^{\ell}\left(\frac{a_k}{b_k}\right) - \operatorname*{\mathbb{K}}_{k=1}^{\ell-1}\left(\frac{a_k}{b_k}\right)\right], \tag{A.10}$$

where the mth canonical denominator B_m is given by the Wallis–Euler recurrence relation $B_m = b_m B_{m-1} + a_m B_{m-2}$ with initial conditions $B_{-1} = 0$ and $B_0 = 1$ and satisfies the relation $A_m/B_m = \mathbb{K}_{k=1}^{m}(a_k/b_k)$. On the other hand, Dudley [18, Corollary 1.10 that also holds in the complex case] has shown that

$$\frac{\partial}{\partial b_\ell}\operatorname*{\mathbb{K}}_{k=1}^{N}\left(\frac{a_k}{b_k}\right) = -\frac{\left[\operatorname*{\mathbb{K}}_{k=1}^{\ell-1}\left(\frac{a_k}{b_k}\right) - \operatorname*{\mathbb{K}}_{k=1}^{N}\left(\frac{a_k}{b_k}\right)\right]^2 B_{\ell-1}}{\left[\operatorname*{\mathbb{K}}_{k=1}^{\ell}\left(\frac{a_k}{b_k}\right) - \operatorname*{\mathbb{K}}_{k=1}^{\ell-1}\left(\frac{a_k}{b_k}\right)\right] B_\ell}. \tag{A.11}$$

Together Eqs. (A.9)–(A.11) give

$$\prod_{k=1}^{\ell}\left[\operatorname*{\mathbb{K}}_{j=k}^{N}\left(\frac{a_j}{b_j}\right)\right]^2 = B_{\ell-1}^2\left[\operatorname*{\mathbb{K}}_{k=1}^{N}\left(\frac{a_k}{b_k}\right) - \operatorname*{\mathbb{K}}_{k=1}^{\ell-1}\left(\frac{a_k}{b_k}\right)\right]^2 , \tag{A.12}$$

which seems to be a new result, though it can be likely obtained independently from the basic properties of continued fractions. Using the Observation above and Theorem 1.11 in [18], we can extend the previous result:

CONJECTURE. If $\mathbb{K}_{k=1}^{\infty}(a_k/b_k)$ converges in $\hat{\mathbb{C}}$,

$$\prod_{k=1}^{\ell}\left[\operatorname*{\mathbb{K}}_{j=k}^{\infty}\left(\frac{a_j}{b_j}\right)\right]^2 = B_{\ell-1}^2\left[\operatorname*{\mathbb{K}}_{k=1}^{\infty}\left(\frac{a_k}{b_k}\right) - \operatorname*{\mathbb{K}}_{k=1}^{\ell-1}\left(\frac{a_k}{b_k}\right)\right]^2 . \tag{A.13}$$

We remark that although the derivation leading to Eqs. (A.12) and (A.13) was based on the assumption of analytic sequences $\{a_k\}_{k\geq 1}$ and $\{b_k\}_{k\geq 1}$, this is not necessary for the proposed Conjecture to hold, as we can always expand $\mathrm{K}_{k=1}^{\infty}(a_k/b_k)$ into a series whose elements are rational functions of a_k and b_k [2, Sec. 1.7], and are therefore analytic with respect to a_ℓ or b_ℓ for all $\ell < \infty$.

A.3.4 Concluding remarks

Despite its simplicity, the main result of this short note, Theorem 2, has not apparently been published before: As only intermediate complex analysis is needed to prove the result, it might have some instructional use besides being relevant for scientists working in adjacent fields. It should be noted that in practical applications, a_k and b_k are typically relatively simple functions, such as low-degree polynomials or rational functions, so that the relevant domain for the problem D, $D \times B(0, R_G) \subseteq G$, can often be inferred directly from the context.

The fact that the obtained formula contains the original continued fraction and its tails yields some useful corollaries: First, for relatively simple a_k and b_k the computational cost of numerical evaluation of the analytic expression [Eq. (A.7)] for the derivative is not much higher than that of the original continued fraction if a vector containing computed tails/approximants is updated during each iteration step, and can be lower than that of the evaluation of the corresponding finite difference that involves two evaluations of $\mathrm{K}_{k=n}^{N}(a_k/b_k)$ at different points. Secondly, the obtained result can be applied iteratively to calculate higher order derivatives of the finite continued fraction if needed. However, expressions for these higher derivatives become increasingly impractical with increasing order, and we make no attempt to present those here; we are unaware of any suitable generalisation of the Faá di Bruno's formula that could simplify this treatment.

References

[1] W. B. Jones and W. J. Thron. *Continued Fractions: Analytic Theory and Applications*. Addison–Wesley, 1980.

[2] A. Cuyt, V. Brevik Pedersen, B. Verdonk, H. Waadeland and W. B. Jones. *A Handbook of Continued Fractions for Special Functions*. Berlin: Springer, 2008.

[3] P. Hänggi, F. Rösel and D. Trautmann. Continued fraction expansions in scattering theory and statistical non-equilibrium mechanics. *Zeitschrift für Naturforschning* 33a (1978), 402–417.

[4] Y. T. Millev. Answer to question #4. "Is there physics application that is best analyzed in terms of continued fractions?" *American Journal of Physics* 66 (1998), 655–656.

[5] R. McGraw. Dynamics of barrier crossing in classical nucleation theory. *Journal of Physical Chemistry B* 105 (2001), 11838–11848.

[6] G. Wilemski. The Kelvin equation and self-consistent nucleation theory. *Journal of Chemical Physics* 103 (1995), 1119–1126.

[7] R. McGraw and W. H. Marlow. The multistate kinetics of nucleation in the presence of an aerosol. *Journal of Chemical Physics* 78 (1983), 2542–2548.

[8] R. B. McClurg. Nucleation rate and primary particle size distribution. *Journal of Chemical Physics* 117 (2002), 5328–5336.

[9] D. R. Warren and J. H. Seinfeld. Nucleation and growth of aerosol from a continuously reinforced vapor. *Aerosol Science and Technology* 3 (1984), 135–153.

[10] R. McGraw. Description of aerosol dynamics by the quadrature method of moments. *Aerosol Science and Technology* 27 (1997), 255–265.

[11] A. Laaksonen. Application of nucleation theories to atmospheric new particle formation. *AIP Conference Proceedings* 534 (2000), 711–723.

[12] L. Lorentzen and H. Waadeland. *Continued Fractions with Applications*. Amsterdam: North-Holland, 1992.

[13] L. R. Shenton and K. O. Bowman. Continued fractions for the Psi function and its derivatives. *SIAM Journal of Applied Mathematics* 20 (1971), 547–554.

[14] L. Hörmander. *An Introduction to Complex Analysis in Several Variables*. 3rd rev. ed. Amsterdam: North-Holland, 1990.

[15] J. Gill. A note on bounds for the derivatives of continued fractions. *Journal of Computational and Applied Mathematics* 72 (1996), 301–307.

[16] H. Waadeland. A note on partial derivatives of continued fractions. *Lecture Notes in Mathematics* 1199 (1986), 294–299.

[17] P. Levrie and A. Bultheel. A note on the relation between two convergence acceleration methods for continued fractions. *Journal of Computational and Applied Mathematics* 101 (1999), 167–175.

[18] R. M. Dudley. Some inequalities for continued fractions. *Mathematics of Computation* 49 (1987), 585–593.